Alma Mater Studiorum – Università di Bologna

DOTTORATO DI RICERCA IN

IL FUTURO DELLA TERRA, CAMBIAMENTI CLIMATICI E SFIDE SOCIALI

Ciclo 35

Settore Concorsuale: 04/A2 - GEOLOGIA STRUTTURALE, GEOLOGIA STRATIGRAFICA, SEDIMENTOLOGIA E PALEONTOLOGIA

Settore Scientifico Disciplinare: GEO/02 - GEOLOGIA STRATIGRAFICA E SEDIMENTOLOGICA

ASSESSMENT OF SEA-LEVEL VARIABILITY FOR THE EMILIA-ROMAGNA COASTAL AREA IN THE FRAMEWORK OF THE MEDITERRANEAN SEA

Presentata da: Dr. Matteo Meli

Coordinatore Dottorato

Prof. Dr. Silvana Di Sabatino

Supervisore

Prof. Dr. Claudia Romagnoli

Co-supervisore

Dr. Marco Olivieri

Esame finale anno 2023

Acknowledgments

I would like to express my gratitude to the external reviewers, Prof. Dr. Velibor Spalevic and Prof. Dr. Davide Zanchettin, for their kind and valuable evaluation of this thesis. I will always be grateful to Dr. Aimée B.A. Slangen for giving me the opportunity to work and collaborate with the sea level research group at NIOZ in Yerseke during my time abroad, and I would like to thank all people there for their warm welcome and kindness towards me. Lastly, my deepest appreciation goes to my supervisor, Prof. Dr. Claudia Romagnoli, and co-supervisor, Dr. Marco Olivieri, for their unwavering support throughout these arduous years, for standing by me despite my personal hardships and the pandemic, and for believing in me. I would like to dedicate this work to my daughter, and tell her to always persevere in life and to keep moving forward, even in the darkest moments.

Abstract

Sea–level change is one of the ocean characteristics closely connected to climate change. Understanding its variation is essential since a large portion of the world's population is located in low–lying locations. Two main techniques are employed to measure sea level: satellite altimetry and tide gauges. Satellite altimetry monitors sea–level relative to a geocentric reference, is unaffected by crustal processes and covers nearly the entire surface of the oceans since 1993. Conversely, tide gauges measure sea level at specific coastal locations and relative to a local ground benchmark, therefore are impacted by vertical land movements. In this study, the linear and non–linear geocentric and relative sea–level trends along the Emilia–Romagna coast (Northern Italy) have been analyzed over different periods. In order to assess the local sea–level variability, data from satellite altimetry and tide gauges have been compared over a common time interval (1993–2019), hence disentangling the contribute of vertical land movements. Non–linearity has been also evaluated at the broader scale of the Mediterranean Sea, in order to depict the main variability in geocentric sea–level trends from regional to sub–basin scale. Furthermore, the anthropogenic and natural influence at the river basin scale has been addressed, in order to shed light on the factors inducing the drastic reduction of riverine sediment supply to the Emilia–Romagna coast over the period 1920–2020. The findings of this analysis indicate that the sediment delivery reduction to the coast by rivers has been driven by several anthropogenic processes, acting on various spatiotemporal scales. Moreover, the local absolute sea–level trend is far from linear and appear "contaminated" by the presence of natural oscillations that act at the multi–decadal, quasi–decadal and inter–annual scale, mainly driven by both large–scale climatic modes and variations in local oceanography.

Contents

List of acronyms	
ADT	Absolute Dynamic Topography
AMO	Atlantic Multidecadal Oscillation
ARPAE	Agenzia Regionale per la Protezione Ambientale, Emilia–Romagna
ASL	absolute sea level
C3S	Copernicus Climate Change Service
CMEMS	Copernicus Marine Service
DAC	Dynamic Atmospheric Correction
ECV	Essential Climate Variable
ER	Emilia–Romagna
ERF	effective radiative forcing
GCOS	Global Climate Observing System
GIA	glacial isostatic adjustment
GMSL	Global Mean Sea Level
GNSS	Global Navigation Satellite System
GRD	Earth Gravity, Earth Rotation and viscoelastic solid Earth deformation
IB	inverse barometer
IPCC	Intergovernmental Panel on Climate Change
LECZ	low–elevation coastal zone
MDT	Mean Dynamic Topography
MSS	mean sea surface
N	absolute sea level variation
NAO	North Atlantic Oscillation
PSMSL	Permanent Service for Mean Sea Level
RLR	Revised Local Reference
RSL	relative sea level
S	relative sea level variation
SA	satellite altimetry
SLA	sea level anomaly
SLE	sea level equation
SSH	sea surface height
SST	sea surface temperature
TG	tide gauge
U	vertical displacement
UNFCCC	United Nations Framework Convention on Climate Change
VLM	vertical land motion

1 Introduction

Sea level is one of the Essential Climate Variables (ECVs) that represent the key parameters of the Earth system, as defined and evaluated on a regular basis by the Global Climate Observing System (GCOS) in support of the United Nations Framework Convention on Climate Change (UNFCCC) and the Intergovernmental Panel on Climate Change (IPCC). It is represented by the position of the sea surface after it has been time–averaged to remove high–frequency signals caused by factors such as wind–waves (Pugh and Woodworth, 2014) and short–term meteorological impacts (Gregory et al., 2019). However, over interannual, decadal, and longer time intervals, there is substantial geographical variability (Figure 1) (Meyssignac et al., 2017).

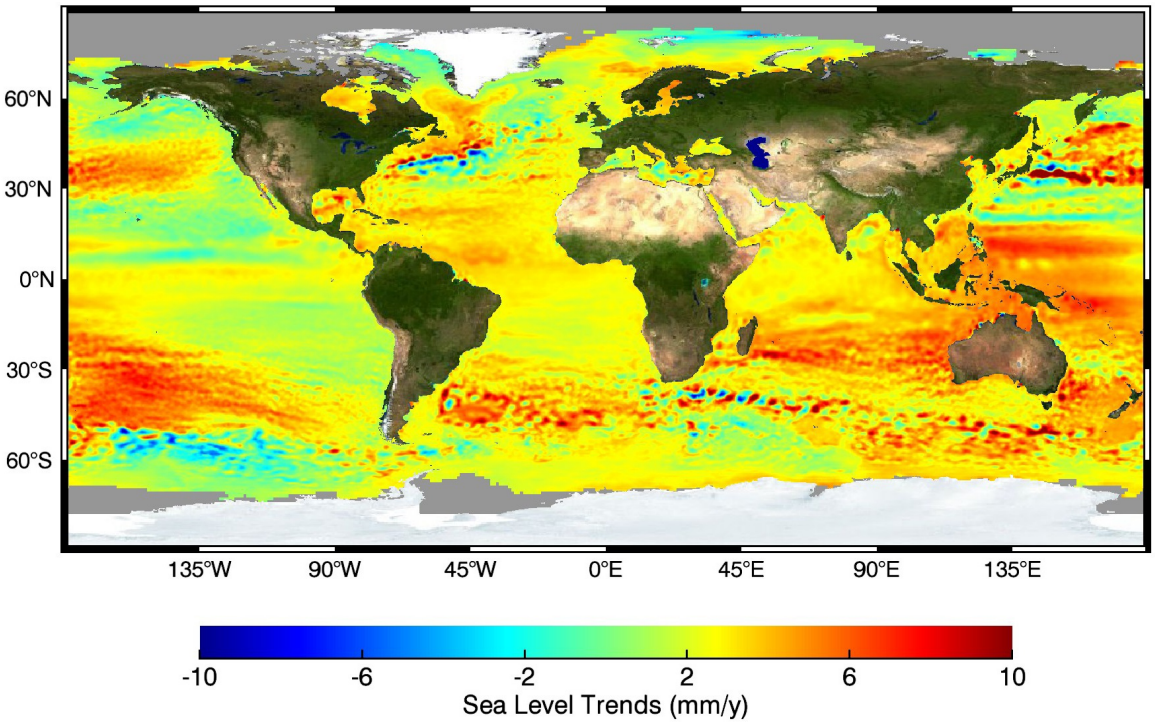

Figure 1: Sea–level trends and their variability across the globe over the period 1993–2016. From NASA/JPL–Caltech.

It is widely acknowledged that the rise in anthropogenic greenhouse gas emissions in the atmosphere, along with a slight increase in natural solar irradiance, has resulted in a cumulative increase in effective radiative forcing (ERF) since the 1970s (IPCC, 2021), and therefore in global warming. Since the early 20th century, there has been persuasive evidence from observational records that Global Mean Sea Level (GMSL) has been increasing in response to growing atmospheric concentrations of greenhouse gasses emitted

by human activities (Oppenheimer et al., 2019). Indeed, over the last 60 years the ocean has stored more than 90% of the heat gain in the climate system caused by the ERF (Levitus et al., 2012), resulting in thermal expansion and sea–level rise.

Sea level has continuously changed on all time spans, in response to a continuously changing Earth's climate over time. On a worldwide basis, there is general agreement that sea level has risen at a rate of 1.7 ± 0.2 mm·year^{-1} over the 20th century (IPCC, 2021), and at a rate of 3.3 ± 0.5 mm·year^{-1} over the period 1993–2015 (Legeais et al., 2018). This is not a constant process as a positive acceleration (0.084 ± 0.025 mm·year^{-2}) was also found at different temporal scales (Nerem et al., 2018; Dangendorf et al., 2019). However, analyses on paleoclimate data showed that current sea–level rates are unprecedented in the whole upper Holocene (Kopp et al., 2016), highlighting how this process has been impacted by anthropogenic activities.

Nowadays, it is certain that sea–level rise and climate change will have significant social and environmental consequences, especially in low–elevation coastal zones (LECZs) where more than 620 million people are currently inhabited, and this number is expected to double by 2060 (Nicholls et al., 2011; Neumann et al., 2015). LECZs are, above all, impacted by the aforementioned processes, producing a constant increasing risk for coastal populations and ecosystems living there. This raises global generalized concern about the sea–level rise impact at large scales and along coasts. LECZs globally have reached a key tipping point, transitioning from a natural pseudo–stable state to a state dominated by human dynamics (Tessler et al., 2015) as a result of land–use changes throughout their catchment regions (Milliman and Syvitski, 1992; Darby et al., 2016). Despite the fact that climate–driven changes continue to have an impact, they may be of secondary relevance locally (Darby et al., 2015) because human factors may interact more significantly with hydrological processes. Anthropogenic changes across catchment regions, as well as hydrological and climatic changes and their links to atmospheric dynamics, should thus be considered in order to better understand which factors are most likely to drive the evolution of coastal areas.

1.1 The sea–level components

Sea–level change is the result of a constant, changeable, and complex interplay between several components that act across the whole Earth system, i.e. between the ocean, solid Earth, atmosphere, and cryosphere, also mixing nowadays anthropogenic and natural factors. Furthermore, all these components act on a wide range of spatial and temporal scales (Oppenheimer et al., 2019; Fox-Kemper et al., 2021). Indeed, some components represent the major drivers of sea–level change at the global scale, while others are critical at regional and/or local scale (Figure 2), which might locally overwhelm global drivers and alter the sea–level rate.

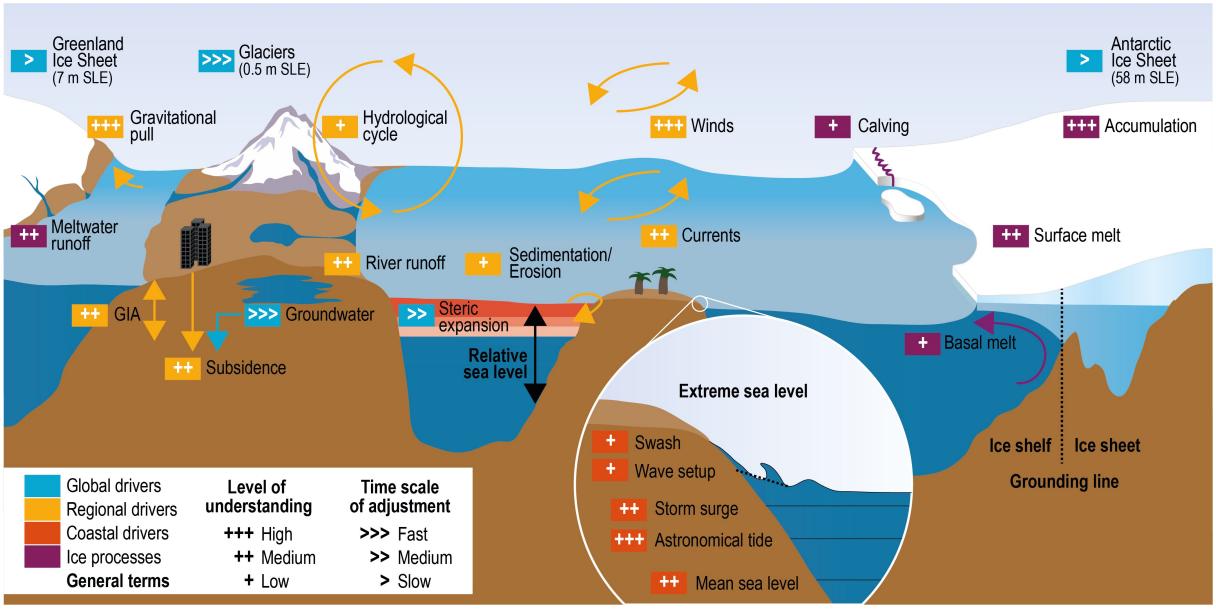

Figure 2: Processes that influence sea level at the global (blue), regional (orange) and local/coastal (red) scale, and their related current level of understanding. From Oppenheimer et al. (2019).

As shown in Figure 2, different processes are characterized by different time scale of adjustment, further highlighting the complexity of the phenomenon. Furthermore, not all processes have a high (nor medium) level of understanding, pointing out the need for a constant effort in order to reach a highest level of comprehension.

1.1.1 Global processes

The main components causing GMSL change at present are the change in density of seawater, i.e., the effect induced by variations in water temperature and salinity, and the water mass exchange between ocean and continents, that is linked to the growth/decrease

of terrestrial glaciers, ice sheets and amount of water stored on land. These contributors vary in response to both anthropogenic global climate change and natural climate variability (Rhein et al., 2013). According to the standard terminology (Gregory et al., 2019), the GMSL change induced by density variations is referred as the steric component (Mellor and Ezer, 1995; Levitus et al., 2012), while the mass component (or barystatic sea level) is the result of ocean/continental mass exchange (Ngo-Duc et al., 2005; Meier et al., 2007) which, from a specific source, propagates around the globe, such that all regions experience a sea–level change (Lorbacher et al., 2012). The amount of sea–level change driven by the addition/removal of water mass is called sea–level equivalent, i.e. the conversion of a continental water mass (liquid, ice or vapor) into a sea–level amount. For instance, by considering the current volume of the ocean and a density value of 1000 $kg \cdot m^{-3}$, a water mass addiction (removal) of $362.5 \cdot 10^{12}$ kg would be necessary to generate 1 mm of GMSL rise (fall). The bulk of sea–level rise throughout the twentieth century is explained by mass components (Slangen et al., 2017), although thermal expansion contribution has progressively grown since 1910 and especially from the 1970s (Levitus et al., 2012), when the anthropogenic forcing (linked to ERF modification) become dominant (Slangen et al., 2016).

Steric sea–level change is driven by variations in ocean density and is made up of thermosteric and halosteric sea–level changes. Thermosteric sea–level change occurs as a result of changes in ocean temperature: rising (declining) temperatures decrease (increase) ocean density while increasing (lowering) volume per unit mass, thus leading to thermal expansion (contraction). According to estimates (Church et al., 2010), a temperature increase of about 0.1 °C leads to an expansion of a 1000 meters water column by around 1 to 2 cm. Salinity changes, conversely, cause halosteric sea–level change: increased salinity leads to higher density and decreased volume per unit of mass, and vice–versa. Both processes are significant also on regional to local scales (Durack and Wijffels, 2010; Church et al., 2010); however, thermosteric changes substantially contribute to GMSL change, whereas halosteric influence is minimal (Gregory et al., 2019; IPCC, 2021).

The largest freshwater reservoirs on Earth are currently represented by the Antarctic and Greenland ice sheets, which are the major contributors to the GMSL change linked

to the mass component. The imbalance between accumulation and loss from melting, sublimation, and iceberg calving causes fluctuations in ice sheet volume. Furthermore, changes in the thickness and extent of the ice sheets as a consequence of melt from below, calving, or disintegration, as a result of surface meltwater infiltrating crevasses, can have an impact on the flow of inland ice streams. Little is known about the mass balance of ice sheets, due to insufficient and fragmentary observations prior to the 1990s. Indeed, since that period several remote sensing observations, e.g., airborne and satellite radar and laser altimetry, interferometric synthetic aperture radar InSAR, space gravimetry from the GRACE mission (Velicogna, 2009), have provided critical observations of the ice sheets' mass balance, indicating a mass loss at an accelerated rate (Rignot et al., 2011). Nowadays, SLE estimates about ice sheets provide values of ca. 7 m, 3.2 m and 60 m of GMSL rise if Greenland, West Antarctica (the unstable part of the continent) and East Antarctica would totally melt, respectively (Lemke et al., 2007; Bamber et al., 2009; Ivins, 2009; Joughin and Alley, 2011).

Also mountain glaciers and small ice caps give their contribution to GMSL change through the imbalance between mass gain/loss processes. Since the early 1990s, continental glaciers have been subjected to persistent retreat (Meier et al., 2007), as they are very sensitive to global warming and climate change. Indeed, geodetic and glaciological observations enlighten that, during the decade 2010 to 2019, the rates of early 21st–century mass loss are, since 1850, the highest (Zemp et al., 2015). However, the melted water from glaciers usually does not always flow directly into the ocean and, along the path, can evaporate, feed rivers or lakes (then might be anthropogenically exploited), or refreeze.

A further contribution to changing GMSL, as part of the mass component, arises from the storage of water on land. The so–called "land water storage" term accounts for rivers, lakes, dams, wetlands, soil moisture, groundwater storage, permafrost and snow cover. Thus, the variability of this term is influenced by both climate variations and human activities (e.g., aquifers exploitation and mining for irrigation and consumption, dams construction, deforestation, urbanization). The latter, directly induced a lowering of GMSL by about -0.5 mm·year^{-1} during the second half of the twentieth century (Chao et al., 2008), and especially during the 1970s (Frederikse et al., 2020), due to a sharp

increase of dam building and water impoundments. Conversely, over the same period, a few tenths of mm·year^{-1} sea level rise have been associated with groundwater extraction and crop irrigation (Wada et al., 2012).

1.1.2 Regional and local processes

At regional (e.g. Mediterranean Sea) and local scales sea level changes could be amplified or mitigated by several factors (Stammer et al., 2013; Palmer et al., 2020), with respect to the global ocean.

The change in mean sea level associated with the circulation is referred to as the ocean dynamic sea–level change. By definition, this component of sea level has a zero global mean but varies at the regional scale, especially in semi–enclosed basins (Pinardi et al., 2015; Bilbao et al., 2015). The rise or depression of the sea surface due to atmospheric pressure is usually included in this component.

Regionally, the contemporary redistribution of mass between terrestrial ice and water reservoirs and the ocean lead to changes in sea–level due to the so–called GRD component (Larour et al., 2017; Mitrovica et al., 2018), i.e. sea–level variations induced by Earth Gravity, Earth Rotation and viscoelastic solid Earth Deformation. In detail, terrestrial mass loss generates a localized elastic solid Earth uplift and relative sea–level fall near the source (within 2000 km), while farther away (>7000 km from the source) the relative sea level rises due to gravitational effects. Furthermore, the effect of Earth's rotation increases the spatial variability of sea level pattern globally, while further changes are induced by loading effects and self–attraction linked to the redistribution of ocean water within the ocean itself.

The ongoing GRD in response to past changes in the redistribution of water and ice on the Earth's surface is defined as the Glacial Isostatic Adjustment (GIA). GIA is commonly referred to as the viscoelastic Earth's crust and mantle rebound to last deglaciation, causing geoid changes and movements of the solid Earth following mass redistribution, on a timescale of decades to tens of millennia. GIA induced land motion is described by global geodynamic models (Lambeck et al., 2014; Peltier et al., 2015), which related uncertainties underlie in the complexity of the rheological structure of the solid

Earth that drives the long–term viscoelastic deformation (Whitehouse, 2018).

At the coastal scale, GIA and GRD effects on relative sea level might be strongly overwhelmed by the influence of local vertical land motion (VLM) processes, impacting the reliability of sea–level rates assessment (King et al., 2012; Wöppelmann et al., 2013). VLM is the variability in height of both the land surface and sea floor, induced by the concurrent effect of several causes, of natural and anthropogenic origins, or just some of them. In detail, terrain subsidence is driven by compaction of alluvial sediments, local tectonic activity (also linked to possible volcanic activities and earthquakes), drainage of peatlands, and groundwater mining and fluids exploitation by removal of water, oil, and gas.

The combination of short–term phenomena, like storm surges, tides and waves, can lead to exceptional high or low local sea–surface height commonly referred to as extreme sea level (Figure 2). Extreme sea levels can be influenced by changes in the frequency, tracks, or strength of weather systems, or anthropogenic modifications. Wind–waves contribute as well to changing coastal sea level. Extreme Total Water Level is the extreme still water level plus wave setup (time–mean sea level elevation due to wave energy dissipation). When considering coastal impacts, swash (vertical displacement up the shore–face induced by individual waves) is also important and included in Extreme Coastal Water Level.

At last, another component of coastal sea level is represented by sediment supply delivered to the coast by rivers, which can drive the shoreline evolution in terms of retreat or progradation trends. Riverine sediment discharge, that represents the primary feeding source for LECZs (Nicholls et al., 2007; Syvitski et al., 2009), has decreased dramatically over the 20th century (Llorens et al., 1997; Walling, 2006; Syvitski and Kettner, 2011; Weston, 2014; Buendia et al., 2016) and is expected to fall further (Zarfl et al., 2015; Dunn et al., 2019). Its role is largely variable due to the climatic condition and human impacts within a specific area, the lithologies of river basins and the dimension of the catchment area (Milliman, 2001; Vörösmarty et al., 2003; Syvitski et al., 2005).

1.2 Techniques for measuring sea level

Currently, sea level change is mainly measured over time through the use of two instruments: satellite altimetry (SA) and tide gauges (TG) (Figure 3). The former acquires sea level data relative to a geocentric reference, usually referred as the absolute sea level (ASL, even if the term "geocentric" should be preferred (Gregory et al., 2019)), with a quasi–global spatial coverage, while the latter measures sea level in relation to a local ground benchmark, referred as relative sea level (RSL), thus directly affected by VLMs and providing punctiform information in space.

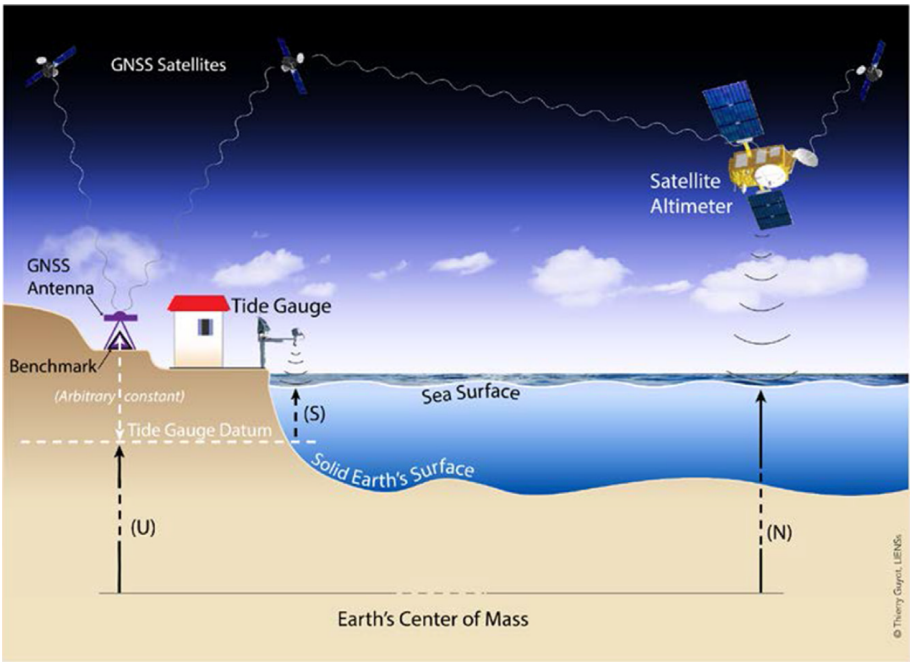

Figure 3: In–situ (tide gauge) and space–borne (satellite altimeter) sea level measurement techniques. GNSS allows the connection of relative (S) and absolute (N) sea level by monitoring the tide gauge benchmark vertical variation (U). From Marcos et al. (2023).

Although the lack of contamination of VLMs in SA, the reliability of these measurements decrease towards the coast preventing accurate assessments in coastal areas. Furthermore, SA missions started only in the early 1990s, thereby preventing long–term sea level assessments, conversely to the TGs which in some cases started recording in the 1800s. Therefore, the existence of these spatial and temporal divergences requires an integrated approach, especially when a high–detail local–scale evaluation is needed.

Despite the fact that the SA and TG time series are presently the two major sources of information for sea level, the disparity in their observational capacity remains an unsolved issue. Furthermore, SA and TG data sets had low and high collection rates, respectively

(Cipollini et al., 2017). Only SA measurement allows for the observation of fluctuation in sea level from the open ocean to the coastal area, and therefore is regarded as critical for providing perspective at the regional and global scales without clarifying some fundamental coastal processes, which are instead recorded by TGs. RSL and ASL fluctuation, as well as VLM, are connected by the Sea Level Equation (SLE), which reads in its simplest form (Farrell and Clark, 1976):

$$S = N - U$$

where S denotes the RSL variation, N the ASL variation, and U the vertical displacement (see also Figure 3). According to this equation, the sea–level change at the pier is the combination of the absolute seal level variation in a geocentric reference frame minus the vertical displacement at the TG coastal site.

Depending on the scope of a specific study or assessment, VLMs must be eliminated if one is interested in the climate–related components of sea level rise. Conversely, relative sea level rise (including VLM as recorded by tide gauges) is of importance for understanding the coastal implications of sea level rise.

1.2.1 Satellite altimetry

The first SA missions occurred in the 1970s and 1980s, however, the high–precision (centimeter–level) satellite altimetry era did not begin until 1992, with the launch of the TOPEX/POSEIDON satellite. SA missions began with the intention of giving, among other things, an assessment of quasi–global coverage sea level in the Earth's mass center reference system. ASL is the difference between the satellite's altitude over the reference ellipsoid and its height above the immediate sea surface (Figure 4), as determined by emitting microwave radiations toward the sea surface that are partially reflected to the satellite (Chelton et al., 2001; Andersen and Scharroo, 2011).

As a result of this configuration, sea level measurement from altimetry is influenced by a number of sources of uncertainty. Radar altimeters transmit more than 1700 pulses per second toward the Earth then receiving back echoes from the sea surface. The electromagnetic radiation transmitted by the satellite is attenuated as it travels through the atmosphere and eventually hits the sea surface. As the signal travels back to the satellite,

it is further attenuated passing by the atmosphere (see below). Furthermore, surfaces with steep slopes, as in the case of rough seas, make proper interpretation more challenging. Indeed, the pulse might impact the peak of a wave, as well as a sequence of additional crests, bringing the reflected wave amplitude to increase more gradually than in the flat ocean case (Brown, 1977). The return signal's strength is also proportional to sea surface roughness, that is closely connected with near–surface winds (Chelton and McCabe, 1985; Nerem and Mitchum, 2001).

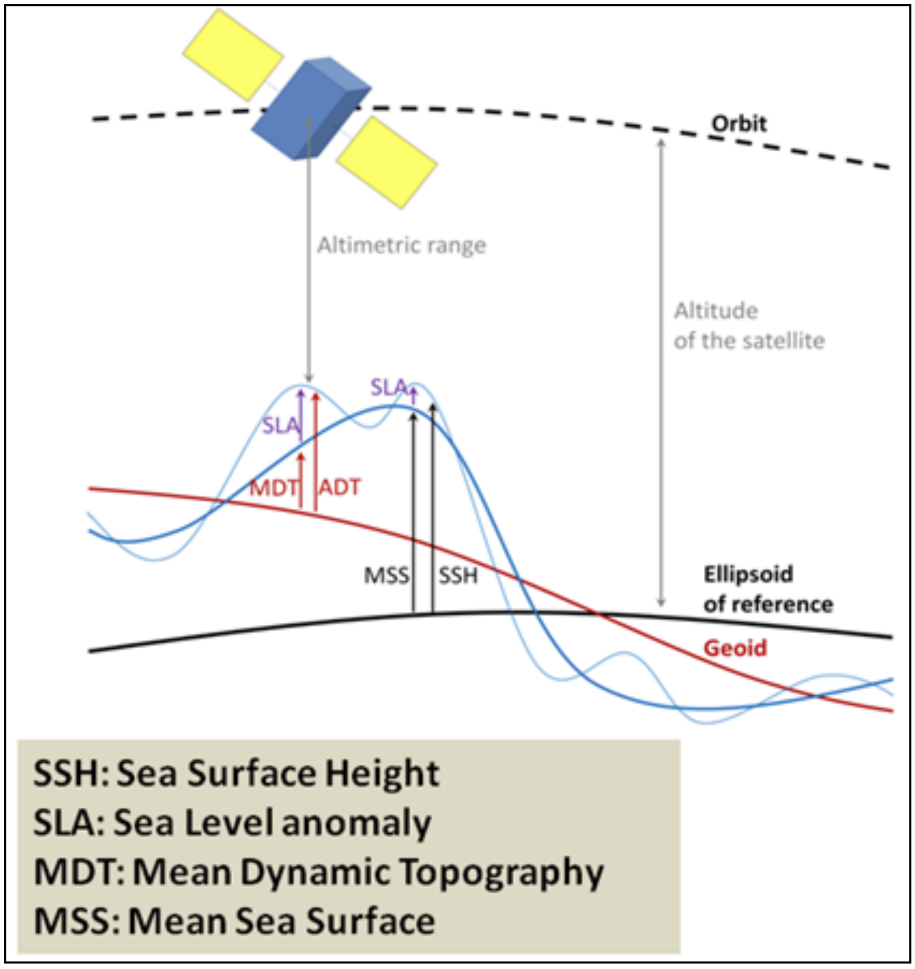

Figure 4: Altimetry heights naming convention (from DUACS).

In detail, SA uncertainties and errors are addressed by accounting for several corrections. Sources of error are usually grouped in four main categories, namely the instrumental errors, satellite position errors, signal propagation errors, and geophysical errors.

Instrumental errors are related to the oscillator drift, pointing angle errors, altimeter calibration, and Doppler shift effect. All of these (among others) must be properly accounted for in order to achieve accurate measurements (see e.g. Chelton et al. (2001)).

The satellite position errors arise from the perturbation that a number of forces

cause on the motion of a near Earth satellite, i.e. Earth gravity field, perturbations linked to the Sun and Moon, Earth and solar albedo radiation pressure, and atmospheric drag; since the beginning of the satellite altimetry era, many attempts have been made to create techniques capable of decreasing orbit errors, as high accuracy is essential for oceanographic applications (Tapley et al., 1994; Le Traon and Ogor, 1998; Rudenko et al., 2012; Couhert et al., 2015). The ability to identify the satellite orbit (Figure 4) with high precision is a critical aspect in satellite altimetry, as any inaccuracy in the satellite orbit radial component would directly influence the measurement.

The signal propagation errors account for two distinct sources of error, that is the sea–state bias and atmospheric refraction. The former is linked to the state of the sea surface (i.e., the roughness) at the moment of the measurement and its related effect on the reflected signal, commonly corrected employing ocean waves models (Tran et al., 2010). Signal's path delay is a common way to represent the effects of atmospheric refraction. The existence of the atmosphere slows the altimeter signal's propagation, increasing the recorded two–way travel time. If atmospheric refraction is not corrected, the range estimate is longer than the real range. Tropospheric and ionospheric (Imel, 1994) refraction corrections are accounted individually; tropospheric correction is further subdivided into wet (Keihm et al., 1995; Fernandes et al., 2015) and dry (Chelton et al., 2001) tropospheric delay.

As long as altimetry detects the instantaneous sea surface height, each measurement is inevitably influenced by time–dependent geophysical processes such as ocean, solid earth and polar tides, ocean loading, and high and low frequency sea surface reaction to air pressure and wind stress. The latter effects are both accounted in the so called Dynamic Atmospheric Correction (DAC; Carrere and Lyard (2003)). Reanalysis of hydrodynamic ocean models, forced with atmospheric data, are usually considered to account for the direct dynamic response of the ocean to pressure variations at high frequencies (<20 days; Carrere and Lyard (2003)), which also consider the wind effect that prevails around the 10 days period (Fukumori et al., 1998; Ponte and Gaspar, 1999). For period >20 days, only atmospheric pressure impacts are generally eliminated, typically by assuming an inverse barometer (IB) adjustment, i.e. an increase (decrease) of 1 mbar in atmospheric

loading locally pull down (push up) the sea surface of about 1 cm (Dorandeu and Traon, 1999).

Because the travel time must be precisely known, i.e. a precision of 30 picoseconds is necessary to attain a height accuracy of 1 cm, the actual measurements are generated by averaging a large number of individual radar echoes. After calculating the range, the sea surface height (SSH; see also Figure 4), i.e. the sea surface above a reference ellipsoid, may be estimated. The reference ellipsoid is a theoretical surface that is easier to deal with than the geoid. The latter is an equipotential surface of the Earth's gravity field and can be described as the sea surface's static portion (Gregory et al., 2019); in absence of external forces (Pugh and Woodworth, 2014), this surface would be equivalent to mean sea surface (MSS; Figure 4). Actually, due to ocean currents and other perturbing processes, sea level might diverge from the geoid by a few meters in what is known as Absolute Dynamic Topography (ADT; Figure 4) and its temporal mean (called Mean Dynamic Topography, MDT; Figure 4). The latter represents a quasi–stationary part of the ocean topography which measurements are difficult to achieve, partly due to limited knowledge of the geoid, especially at small spatial scales (on the order of km to tens of km). Thus, sea level changes from SA are computed as sea level anomalies (SLA; Figure 4) with respect to the MSS over a temporal reference (currently 1993–2012).

Consecutive and ongoing high–precision SA missions have been compared and calibrated since 1992, to give a consistent and uniform quasi–global coverage of sea level record. Each satellite mission is validated with in–situ TG data (Mitchum, 2000), improving the uncertainty characterisation of global and regional mean sea level trends with an accuracy of ca. 0.5 and 2 mm·year^{-1}, respectively (Ablain et al., 2017, 2019). However, it should be pointed out that SA observations in shallow water and close to shorelines (<20 km within the coast), with respect to the open ocean, are impacted by both the contamination of land in the satellite footprint and the less accurate geophysical corrections (Cipollini et al., 2017; Vignudelli et al., 2019). The necessity for accurate coastal altimetry data has resulted in the development of sophisticated altimetry products in recent years within international projects (e.g. ESA–CCI, COASTALT), with enhanced reprocessing and specific adjustments aiming to extend valid measurements towards the

coast (e.g., X–TRACK/ALES; Passaro et al. (2014); Birol et al. (2021)).

Various national and international agencies and projects make multi–mission satellite altimetry measurements nowadays available in standardized formats. In addition to along–track data for each particular satellite mission, gridded sea level fields, particularly valuable for regional and local sea level assessments, are generated considering measurements from simultaneous missions (Le Traon et al., 1998; Legeais et al., 2018). Along–track and gridded global and regional products are both distributed with different spatial resolution via data repositories such as the Copernicus Climate Change Service (C3S, `https://climate.copernicus.eu/`), Copernicus Marine Service (CMEMS, `https://marine.copernicus.eu/it`), AVISO (`https://www.aviso.altimetry.fr/en/home.html`) or international programs such as the ESA–CCI (`https://climate.esa.int/en/`).

1.2.2 Tide gauges

Due to their relevance for maritime navigation and harbor operation and safety, direct monitoring of RSL through TGs extends back to the 18th Century (Matthäus, 1972; Wöppelmann et al., 2008), making credible models of sea–level fluctuation and its relationship to climate change conceivable. TGs offer a measure of the sea level in relation to the pier to which the TG is attached, and hence it is frequently referred to as RSL.

In detail, RSL measurement is referred to a benchmark on land ideally located on a stable surface, in order to provide a reliable local height reference level. The stability and maintenance of the benchmark, hence the continuity of the TG datum, is critical to achieve a consistent RSL time series. However, this stability in time cannot always be guaranteed and unidentified or unreported variations in the vertical position of the datum might seriously compromise the interpretation of RSL changes (Zerbini et al., 2017). Thus, the elevation of the benchmark should be measured and checked periodically in relation to a group of other local benchmarks. Furthermore, also the vertical position of the TG itself should be periodically monitored through space techniques and high–precision leveling (Wöppelmann and Marcos, 2016; Woodworth et al., 2017).

National and subnational authorities, as well as research institutes, deploy, maintain, and operate tide gauges. Most institutions currently offer their tidal gauge network

observations via their own website and data servers, with varied formats, quality criteria, and restrictions. Furthermore, there are a number of international data assembly centers that gather, store, regulate, standardize, and disseminate tidal gauge data and metadata. One of the most outstanding worldwide is the Permanent Service for Mean Sea Level (PSMSL), founded in 1933 and hosted by the National Oceanography Center in Liverpool. The PSMSL has the biggest TG database where more than 2300 TG time series are collected (Figure 5a), updated on a regular basis, reduced to a common datum, i.e. the Revised Local Reference (RLR) (Holgate et al., 2013; PSMSL, 2022), and distributed through the website (www.psmsl.org) as monthly and annual mean time series. Prior to generating the monthly and annual averages, low–frequency data are generated by filtering high–frequency readings to hourly values and these to daily means.

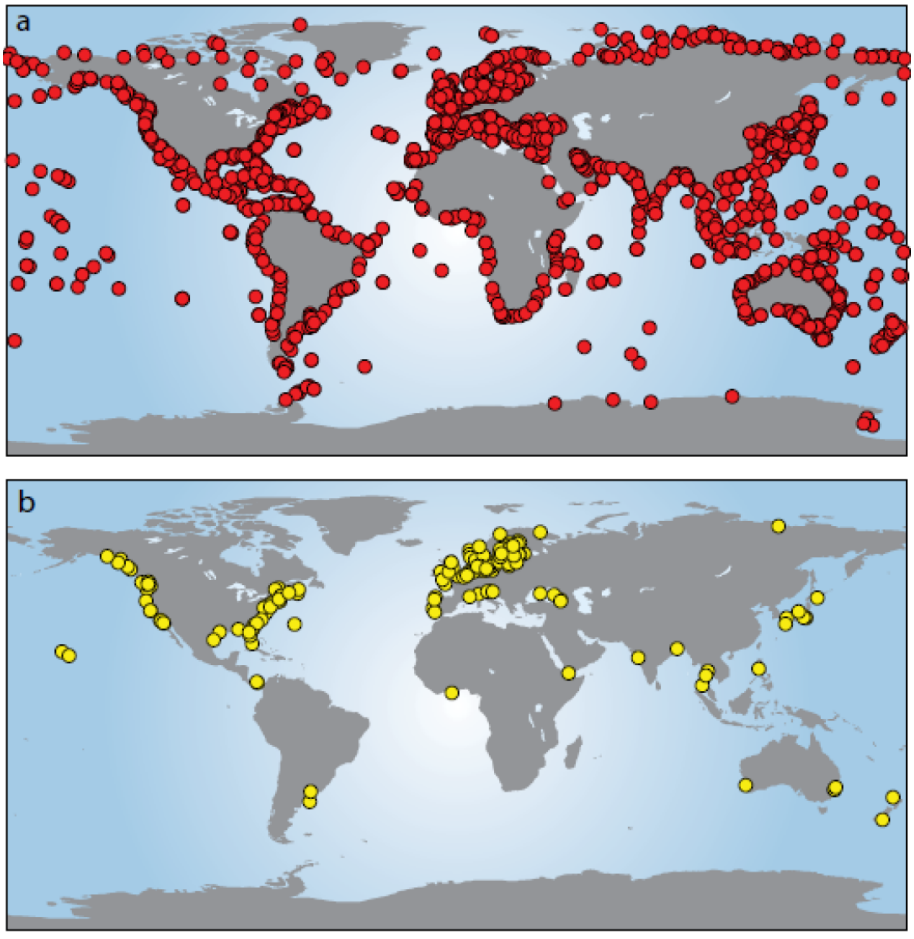

Figure 5: Permanent Service for Mean Sea Level (PSMSL) TG database overview. (a) The complete database; (b) stations with a record of >60 years of data. From Woodworth et al. (2011).

Despite their extended coverage (with more than 60 years of data in several cases, Figure 5b), TGs data are spatially constrained due to their diverse geographical distri-

bution. Since the 1950s, TGs measurements have grown, particularly in the Northern Hemisphere (Gröger and Plag, 1993). This constraint creates a bias that may impede accurate and reliable global sea level estimation.

Developed for distinct objectives, such as observing the tide within harbors, TG data used for long–term sea–level studies are inevitably contaminated by the pier's VLM. Several studies (Douglas, 1991, 1997, 2001; Church and White, 2011) dealt with this problem only accounting for GIA, as it can be described by global physical models; however, as previously stated in Section 1.1.2, local VLMs might overwhelm any other sea–level contributor, as in the case of the Mediterranean Sea, where GIA can be irrelevant or negligible. This issue was been partially solved by the co–location of GNSS (Global Navigation Satellite System) at the TG site. However, because this approach just began in the late 1990s (Zerbini et al., 1996; Bouin and Wöppelmann, 2010), GNSS installations do not cover neither the whole time period nor most TG sites (Santamarìa-Gòmez et al., 2012).

1.3 Overview of own research

Coastal environment represents the land–ocean transition and its dynamics is intensively driven by the interaction of both natural and anthropogenic influences, subjected to non–linear oscillations over time. Climate change, sea–level rise and human impact have led over the last century to a generalized increase in coastal erosion worldwide (Church et al., 2013). Shoreline erosion was observed in many areas of the world during the twentieth century (Bird, 1987), but it is unclear how much this is due to climate–related sea level rise (Vellinga and Leatherman, 1989) or to more local non–climatic factors such as ground subsidence due to underground fluids exploitation, decrease in sediment supply, coastal management, waves and currents. Thus, the purpose of this PhD project is to understand some of the processes that governed the complex, non–linear evolution of sea level over different temporal and spatial scales. In detail, the main focus is on the sea–level change occurred at the scale of the Emilia–Romagna (ER) coastal stretch (Figure 6) over both the satellite altimetry era (1993–2019) and the last century (1920–2020).

The ER coast is a 130–kilometer–long stretch of highly urbanized LECZ (1.45 m

maximum average elevation) located on the eastern edge of the Po Plain in Northern Italy (Figure 6). Coastal anthropization of the whole ER coast began in the 1950s (Lorito et al., 2010) becoming, over the next few decades, one of the most popular tourist sites in Italy, as well as a major source of revenue for the region's economy.

A significant amount of the ER coastline area is now below sea level, which would increase the impact of future sea–level rise. According to Perini et al. (2017), the combined effect of the IPCC's worst scenario (Church et al., 2013) and present local subsidence would result in a further expansion (346 km^2) of the regions below mean sea level in 2100 compared to 2012. As a result, determining the relative sea–level (RSL, i.e., the local sea level relative to a benchmark on land) change at the local scale for the ER coast is critical for the territory's and its delicate environment's management.

The main question that drives this work is: **Which is the sea–level variability for the Emilia–Romagna coastal area in the framework of the Mediterranean Sea?** To answer this question, three sub–questions were formulated:

1. How sea level has changed at the Emilia–Romagna coastal scale as resulting from different observative approaches?

2. How natural and anthropogenic footprints impacted dynamics of the catchment areas and, indirectly, the coast?

3. What is the main variability of sea–level trends in the Mediterranean Sea?

In order to do that, data from available local TGs and up to date SA products, as well as climatic parameters (e.g. air temperature, rainfall, river discharge) representative of the ER inland territory, have been considered. Furthermore, water temperature and salinity profiles from a regional reanalysis are considered for the whole Mediterranean Sea domain. Indeed, different analyses in this study focus on different spatiotemporal scales: the local sea–level change at the decadal scale (1993–2019, Section 3.1), the modification occurred at the river basin scale over the last century (1920–2020, Section 3.2), and the non–linearity in sea level across the Mediterranean Sea over the altimetry era (1993–2019, Section 3.3).

The study area is described in Section 2, while the results achieved for each analysis

have been documented in three published research papers, presented in Section 3. Each sub–section (3.1, 3.2 and 3.3) consists of a manuscript, together with an introductory page with information about the paper and the open question to which the manuscript aims to address. At last, Section 4 reports the conclusion of this dissertation, along with answers to the formulated questions and outlook perspectives, in order to highlight the still open issues that deserve to be addressed.

2 Study area

2.1 The Emilia–Romagna coast

The ER coast (Figure 6) is microtidal, characterized by sandy, mostly dissipative beaches, and generally impacted by low–energy wave climate (Ciavola et al., 2007; Gaeta et al., 2018) with the significant wave height tipically below 1.25 m. However, storm surge levels due to water piling by prevailing winds ('Bora' with ENE provenance, and 'Scirocco' from the SE) and low barometric pressure may almost double the tidal range, with extreme levels in the order of 1 m in the 1– to 10–year return period, causing extensive inundation and erosion at the coast when associated with storm waves (Armaroli et al., 2012). At the geological scale, the Po coastal plain is a foredeep basin, characterized by transgressive–regressive cyclicity of coastal and alluvial deposits overlain by a Holocene coastal succession, made up of a prograding delta front/beach–ridge sands, typical of a shallow–marine depositional environment, in a laterally continuous, wedge–shaped body (Amorosi et al., 1999; Correggiari et al., 2005).

Figure 6: Satellite overview of the ER coast location. Modified from Map Data ©2023 Google.

A critical factor for the morphological evolution of the area is the effect of land subsidence. The coastal area under study suffers from natural and anthropogenic subsidence, the latter showing higher rates during the period 1950–1980 due to an intense overpumping of underground fluids (Carbognin et al., 1984; Gambolati et al., 1999; Zerbini et al., 2007). Since the second half of the 20th century, in fact, the rate of subsidence in the area has been considerably increased by the groundwater and gas extraction (Teatini et al., 2005),

with rates locally exceeding natural subsidence by an order of magnitude. This resulted in local land settlement surpassing 100 cm in a few decades (Aguzzi et al., 2016), while a following steady decrease in subsidence, reported across the entire ER coast, is widely attributed to groundwater extraction stoppage, which has forced since the 1970s (Teatini et al., 2005; Pirazzoli, 1986). VLM estimates based on the regional high–precision levelling network, which has been regularly monitored since 1983 by the ER Regional Agency for Prevention, Environment, and Energy (ARPAE), show average subsidence rates in the order of 5 mm·year^{-1} for the last 15 years, decreasing to 3–4 mm·year^{-1} in the period 2011–2016 (Aguzzi et al., 2016), with peak values in the order of about 20 mm·year^{-1} still observed in some areas. Land subsidence has been estimated to have indirectly subtracted a volume of about 20 millions m^3 in the ER littoral area from 1984 to 1993 (IDROSER, 1996) and this has marked consequences on coastal erosion.

The anthropogenic sprawl, and related processes as the underground fluids exploitation, widespread use of coastal defense structure, land–use changes, and modifications occurred throughout catchment areas, seriously stiffened the ER coastal plain by deteriorating its reliability to cope with environmental changes (Carbognin et al., 1984; Gambolati et al., 1999; Teatini et al., 2005; Elfrink et al., 1998). Indeed, the heavy, anthropogenically driven reduction in sediment delivery by rivers (mainly due to sediment digging and river regulation), mostly occurred between the 1940s and 1980s, has led to generalized erosion and shoreline retreat. Although safeguard policies for riverbed excavation, introduced by the ER regional government during the early 1980s, were expected to gradually reverse this, only the amount of suspended material has slowly increased, whereas fluvial bedload has never recovered (Preti et al., 2008; Aguzzi et al., 2016, 2020).

The combined effects of subsidence, sediment supply shortfall due to river regulation, dune ridge destruction, the widespread use of coastal defense structures, and increased anthropogenic pressure (Teatini et al., 2005; Elfrink et al., 1998; Billi et al., 2017; Aguzzi et al., 2020) make the ER coastal tract especially vulnerable to coastal flooding caused by storm surges and sea–level rise (Marsico et al., 2017; Antonioli et al., 2017).

2.2 The river basin scale

The dynamics within a river basin behind a coastal stretch significantly influence the shoreline evolution. Solid transport by rivers is inevitably linked to soil erosion, primarily due to agricultural use, and enhanced by local climate, anthropization, morphology and lithologies. Due to this, we have selected a particularly critical stretch of the ER coast, located in the northern littoral belt, south of the Po River Delta, receiving inputs from the Reno and Lamone drainage basins (Figure 7a) for a holistic approach.

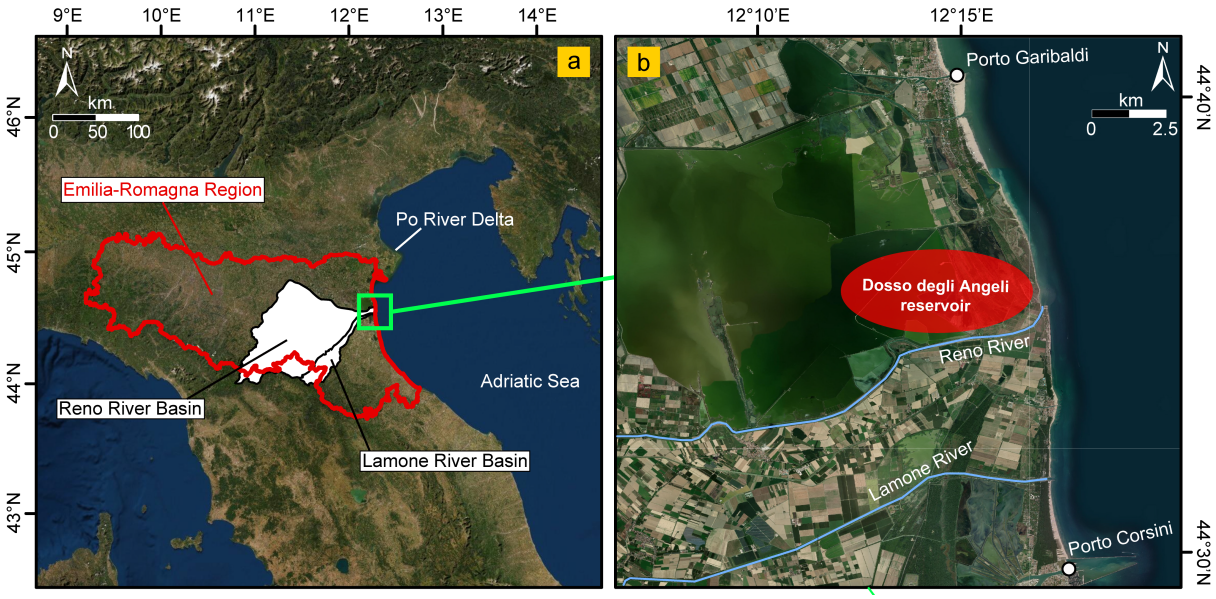

Figure 7: (a) Location of the Lamone and Reno river basins in the ER Region and (b) the ER coastal stretch that receives inputs from both river basins. Modified from Meli and Romagnoli (2022).

The Reno River, with a length of 210 km and basin area of 4628 km^2 (Figure 7a), constitutes the main river of the ER Region after the Po River, and the sixth nationwide. It drains both mountains and plain terrains, and it receives as affluents (see Chapter 3.2 for location) a number of natural streams from the Apennines (e.g. Samoggia, Idice, Sillaro, Santerno and Senio) and artificial channels in the plain (e.g. Navile and Savena Abbandonato). Its fluvial regime is mainly controlled by rainfall (1000 mm·year^{-1} on average), with river floods mainly in Spring and Autumn (ARPA, 2002; Toreti et al., 2009; Crespi et al., 2018). The Reno River was initially merged in the 18th century to the main paleo–Po branch at that time (called Primaro) and developed in a northward oriented mouth (Figure 8). Since the beginning of the 20th century, the Reno river delta underwent further natural shifting and geomorphological evolution (Bondesan et al., 1978)

to its gradual dismantling (Aguzzi et al., 2020).

The Lamone river basin (ca. 520 km^2, Figure 7a) is much smaller than that of the Reno river; its sediment supply provides an input source to the coastal budget of this area. However, the marked subsidence affecting the river mouth area partly nullifies this contribution (Preti et al., 2008).

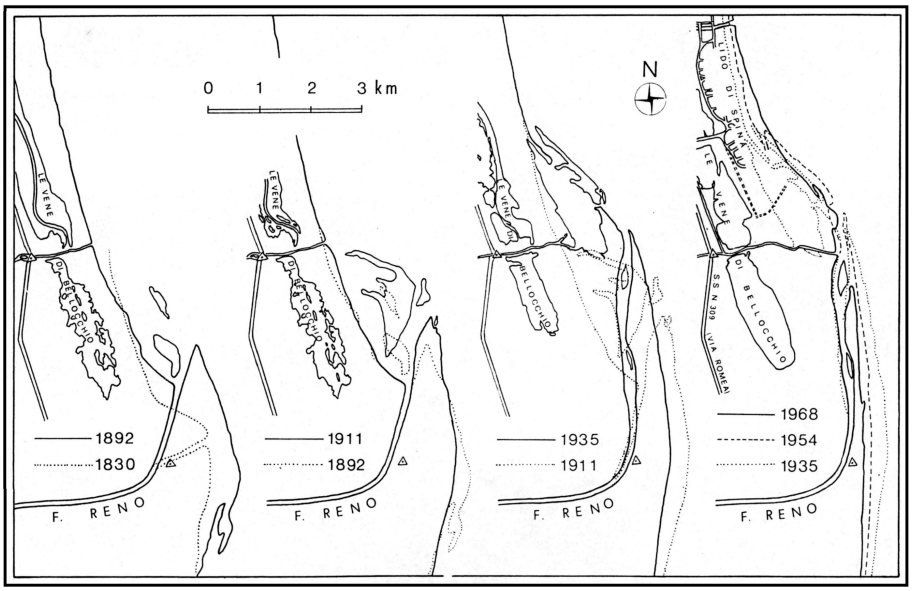

Figure 8: Planimetric evolution of the Reno River mouth between 1830 and 1968. Modified from Bondesan et al. (1978).

The most drastic shoreline erosion occurred north of the Reno River mouth during the periods 1954–1988 (Figure 8), was mainly due to extensive groundwater pumping from the regional multi–aquifer systems as a response to growing demand for domestic, agricultural and industrial uses (Teatini et al., 2005). Furthermore, the location in this very critical coastal sector of the two gas reservoirs exploited by ENI S.p.A. in the wells Agosta 1 and Dosso degli Angeli is considered to have had a marked impact on the ground lowering (Comerci and Vittori, 2019).

In particular, at Dosso degli Angeli gas extraction site (Figure 7b), active between 1971 and 2004, about 40 cm of ground lowering have been estimated for the period 1984–2015 (Aguzzi et al., 2020). In the last two decades, a decay of ground lowering was observed, although estimated rates are not always coherent among different data sources and observative techniques (Simeoni et al., 2017; Comerci and Vittori, 2019; Aguzzi et al., 2020). However, production at this gas field resumed in 2011 and is expected to continue until 2023. This should result in a renewed high anthropogenic subsidence, possibly not

evident yet in recent data (Aguzzi et al., 2016, 2020) but to be taken into account in the overall subsidence affecting the area (Simeoni et al., 2017). According to Comerci and Vittori (2019), the simulation of the total expected subsidence by 2060 due to gas production exceeds 30 cm at Dosso degli Angeli site; whatever the amount of subsidence will be in the next years, this should have important consequences in terms of coastal vulnerability in this area, where the very low height of the beach (less than 1–1.5 metres) causes its susceptibility to flooding and extreme events.

In terms of coastal dynamics and sedimentary budgets, the coastal area under study corresponds to the so–called "Macrocell 5" (ca. 20 km long), as delineated by Preti et al. (2008), bounded by the Porto Garibaldi and Porto Corsini harbors (Figure 7b). The main drivers of coastal dynamics in this area are the predominant longshore current, diverging at Reno River mouth (Figure 7b), i.e. north ward directed in the area north of the river mouth and South–ward directed to the south of it (IDROSER, 1983). Due to this, a wide stretch of the surrounding coast was previously fed by river sediment.

In the Macrocell 5, sediment is mostly composed of medium and fine sand (mean grain size: 0.500–0.250 and 0.250–0.125 mm, respectively) in the emerged beach and in the foreshore, while in the submerged beach the percentage of very fine sands (mean grain size 0.063–0.125 mm) increases with depth (Aguzzi et al., 2016, 2020). Granulometric fining seaward is common, and silt is present in significant percentages only below the depth of 4/6 meters. Clay is locally present in relatively small amounts, being found in the submerged beach especially in the northern part of the Macrocell, but also at the Lamone River mouth. In proximity of the Reno River mouth the sediment is relatively coarser–grained (average size up to 250 mm) with respect to most part of the ER coast, also in part of the submerged beach (Aguzzi et al., 2020). This is likely due to the gradual cannibalization of the river mouth sediment and not to present–day fluvial supply, as also observed by Bondesan et al. (1978) which carried out a sampling of the emerged and submerged beach in 1971–1972.

When the Reno River sediment supply decreased and the river delta migrated southward being gradually reworked (Bondesan et al., 1978; Aguzzi et al., 2020), the central portion of this coastal tract (about 13 km from the Lamone river mouth to Lido di Spina)

underwent erosion, while the northern and southern tracts, lying up–drift with respect to the Porto Garibaldi and Porto Corsini jetties, still gradually advanced (Aguzzi et al., 2016). Overall, between 1982 and 2006, in a 5–km long coastal stretch between the Reno River delta and Lido di Spina 75 hectares of land were lost, with a 200 m coastline retreat (Preti et al., 2008).

Hard defense structures (e.g. groynes, breakwaters, revetments, sandbag barriers, etc.) placed in the last decades to protect the coast from erosion, were not effective in reducing the problem and also interfered with the coastal dynamics and longshore drift in the Macrocell (Aguzzi et al., 2016). Periodic nourishment interventions have also been carried out since 1995 by the ER Region at Lido di Spina, north of the Reno River mouth, although subsequent monitoring showed that the interventions were insufficient for stabilizing the coastline (Aguzzi et al., 2020).

2.3 The Mediterranean Basin oceanography

Sea level variability at a specific location, as in the case of the ER coast, is inevitably the response to changes occurred on a sub–basin scale (in this case the Adriatic Sea, Figure 9), driven by processes that act within the sub–basin or elsewhere across the region (i.e., the Mediterranean Sea). Indeed, changes and non–linearity in the Mediterranean Sea oceanography might modify sea–level trends at the local scale, due to a chain of changes which propagate among the sub–basins through the thermohaline circulation and mass redistribution (Robinson et al., 2001; Von Schuckmann et al., 2019). For this reason, the study of the sea level at a local scale must always take into consideration the regional framework.

The Mediterranean Sea (Figure 9) is a semi–enclosed, mid–latitude sea linked to the North Atlantic Ocean by the Gibraltar Strait, where water, heat, and salt are exchanged. Its articulated physiography defines different sub–basins as the Western Mediterranean, Tyrrhenian, Ionian, Southern Central Mediterranean, Southern Crete, Levantine, and two peripheral seas known as the Adriatic and Aegean, all connected by channels and straits (Figure 9).

The Mediterranean receives mass from the Atlantic Ocean to compensate for per-

sistent surface water loss, which is primarily caused by evaporation processes (due to rising sea surface temperature) and a persistent freshwater deficit (Romanou et al., 2010; Tanhua et al., 2013; Pastor et al., 2018), resulting in basin–scale salinification (Grodsky et al., 2019), that is, an increase in sea surface salinity. Changes in thermohaline properties have been revealed for surface (0–100 m) and intermediate (100–400 m) layers, with the Levantine water salinity and temperature characterized by rising trends stronger than those observed at intermediate layers in the world ocean (Schroeder et al., 2017; Fedele et al., 2021).

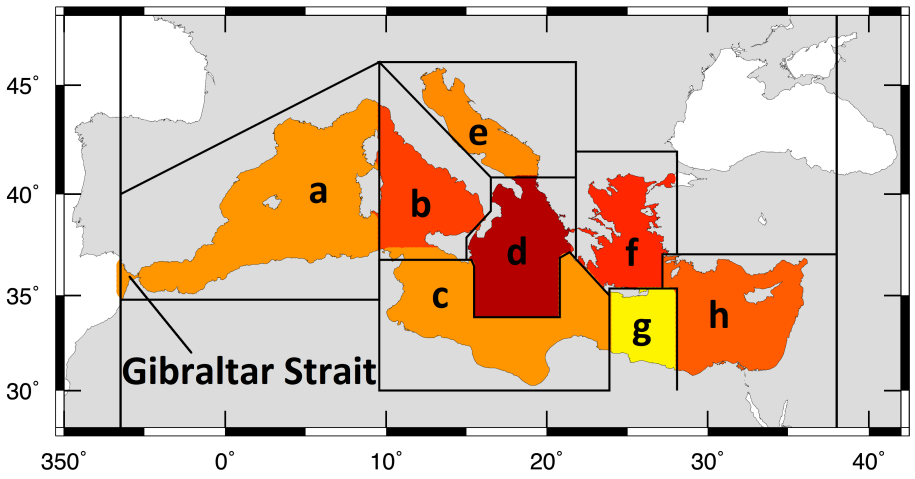

Figure 9: The Mediterranean Sea and related sub–basins: (a) Western Mediterranean, (b) Tyrrhenian, (c) Southern Central Mediterranean, (d) Ionian, (e) Adriatic, (f) Aegean, (g) Southern Crete, and (h) Levantine. Modified from Galassi and Spada (2014).

Excess evaporation over precipitation produces high–salinity waters that drive and maintain the thermohaline circulation in the Mediterranean Sea via a large salinity contrast that forms between the Levantine waters and the inflowing waters at Gibraltar (Lascaratos et al., 1993; Robinson et al., 2001). Basinwide, the thermohaline circulation is limited to the surface and intermediate layers, while the deep circulation is mainly controlled by a north–south temperature gradient, where winter air–sea heat losses and vertical convection are the primary forces (Gačić et al., 2013). Circulation within the basin (Pinardi et al., 2015) reflects its complexity, with cyclonic (anticyclonic) gyres dominating the northern (southern) regions, with the exception of the northern Ionian Sea, where reversal episodes of surface circulation were observed at the quasi–decadal time scale (Gačić et al., 2013; Menna et al., 2019).

The semi–enclosed conditions characterizing the Mediterranean Sea often lead to di-

vergences among global sea–level trends and those measured within the basin, even without matching the values observed for the nearby Atlantic Ocean (Tsimplis and Baker, 2000). The mass component is considered the dominant contributor to the mean sea level tendency in the Mediterranean Sea (Calafat et al., 2010; Pinardi et al., 2014), while the steric component accounts for approximately 20% of the total variance (Calafat et al., 2012). This contrasts with the steric influence at the global scale, which explains approximately 50%–70% of the total sea level variability (Storto et al., 2019). However, this is not the case for both the Aegean and Levantine, as a steric contribution of approximately 52% has been found by Mohamed and Skliris (2022), mainly due to the thermosteric effect (Vera et al., 2009).

Strong differences in sea–level trends at the sub–basin scale are a well–known aspect of the Mediterranean (Bonaduce et al., 2016; Skliris et al., 2018; Mohamed et al., 2019), in which variability and complexity arise from thermohaline changes and local circulation (Menna et al., 2012, 2019, 2021; Mauri et al., 2019; Poulain et al., 2021). For instance, the Ionian is considered a falling sea level sub–basin (Cazenave et al., 2002; Fenoglio-Marc, 2002), in contrast to other sub–basins, primarily because of complexities and changes in the local circulation pattern (Pinardi et al., 1997; Malanotte-Rizzoli et al., 1997, 1999).

A direct relationship between sea surface temperature and sea level in the Mediterranean has been demonstrated in previous studies (Cazenave et al., 2001, 2002; Fenoglio-Marc, 2002), highlighting a continuous and fast–rising trend associated with SST from 1992 to 1999 and for all sub–basins, except for the Ionian. Large–scale climatic modes also influence long–term and inter–annual variability of the Mediterranean sea level (Vigo et al., 2011; Calafat et al., 2012; Landerer and Volkov, 2013; Tsimplis et al., 2013), such as the North Atlantic Oscillation (NAO) and Atlantic Multidecadal Oscillation (AMO). The NAO, in particular, affects variations in atmospheric sea–level pressure in the Mediterranean (Tsimplis and Josey, 2001) and modulates wind and oceanic circulation near Gibraltar, impacting net water flow exchange with the Atlantic Ocean (Menemenlis et al., 2007; Tsimplis et al., 2013). Instead, AMO has a strong relationship with heat and salt content (Iona et al., 2018), impacting SST and sea evaporation (Marullo et al., 2011).

3 Manuscripts

3.1 Manuscripts I

Title:

Sea–Level Change along the Emilia–Romagna Coast from Tide Gauge and Satellite Altimetry

Authors:

Matteo Meli (Department of Biological, Geological and Environmental Sciences (BiGeA), University of Bologna, Bologna, Italy)

Marco Olivieri (Istituto Nazionale di Geofisica e Vulcanologia (INGV), Bologna, Italy)

Claudia Romagnoli (Department of Biological, Geological and Environmental Sciences (BiGeA), University of Bologna, Bologna, Italy)

Status:

Published in *Remote Sensing (2021), vol. 13, 97.* `https://doi.org/10.3390/rs13010097`

Overview:

In this study, we analyze the sea–level variation for the Emilia–Romagna coastal area by selecting three sites along the coast: Porto Garibaldi, Marina di Ravenna, and Rimini. These are the only sites where a tide gauge in operation currently exists, although recording on different time intervals. For each site we also identify the closest satellite altimetry cell to put the relative sea level observed at tide gauges in the framework of the ongoing geocentric sea level for the region.

Open question:

How sea level has changed at the Emilia–Romagna coastal scale as resulting from different observative approaches?

remote sensing

MDPI

Article

Sea-Level Change along the Emilia-Romagna Coast from Tide Gauge and Satellite Altimetry

Matteo Meli [1,*], Marco Olivieri [2] and Claudia Romagnoli [1]

[1] Department of Biological, Geological and Environmental Sciences, University of Bologna, 40126 Bologna, Italy; claudia.romagnoli@unibo.it
[2] Istituto Nazionale di Geofisica e Vulcanologia, Sezione di Bologna, 40128 Bologna, Italy; marco.olivieri@ingv.it
* Correspondence: matteo.meli7@unibo.it

Abstract: Coastal flooding and retreat are markedly enhanced by sea-level rise. Thus, it is crucial to determine the sea-level variation at the local scale to support coastal hazard assessment and related management policies. In this work we focus on sea-level change along the Emilia-Romagna coast, a highly urbanized, 130 km-long belt facing the northern Adriatic Sea, by analyzing data from three tide gauges (with data records in the last 25–10 years) and related closest grid points from CMEMS monthly gridded satellite altimetry. The results reveal that the rate of sea-level rise observed by altimetry is coherent along the coast (2.8 ± 0.5 mm/year) for the period 1993–2019 and that a negative acceleration of -0.3 ± 0.1 mm/year is present, in contrast with the global scale. Rates resulting from tide gauge time series analysis diverge from these values mainly as a consequence of a large and heterogeneous rate of subsidence in the region. Over the common timespan, altimetry and tide gauge data show very high correlation, although their comparison suffers from the short overlapping period between the two data sets. Nevertheless, their combined use allows assessment of the recent (last 25 years) sea-level change along the Emilia-Romagna coast and to discuss the role of different interacting processes in the determination of the local sea level.

Keywords: sea level; Adriatic Sea; satellite altimetry; tide gauges; vertical land movements; climate change

Citation: Meli, M.; Olivieri, M.; Romagnoli, C. Sea-Level Change along the Emilia-Romagna Coast from Tide Gauge and Satellite Altimetry. *Remote Sens.* **2021**, *13*, 97. https://doi.org/10.3390/rs13010097

Received: 26 November 2020
Accepted: 25 December 2020
Published: 30 December 2020

1. Introduction

Sea level lies among the 54 Essential Climate Variables (ECVs) that represent the Earth system's key parameters, as defined and periodically assessed by the Global Climate Observing System (GCOS), in support of the United Nations Framework Convention on Climate Change (UNFCCC) and of the Intergovernmental Panel on Climate Change (IPCC). Direct observation of the sea level dates back to the 18th century [1] and this made possible realistic models for the sea-level variation and its interconnection with climate change. The ongoing sea-level change is the product of a continuous, mutable, and complex interaction among several components through the whole Earth system, combining natural and anthropic causes. It is commonly recognized that the increase in anthropogenic greenhouse gasses emission in the atmosphere, plus a small increment of natural solar irradiance, has led to a progressive effective radiative forcing (ERF) growth since the 1970s [2], hence to climate warming. More than 90% of the heat increase in the climate system, derived from the ERF, has been stored by the ocean, with the consequential thermal expansion and sea-level rise. At global scale, there is a general consensus that sea level has been rising at 1.7 ± 0.2 mm/year over the last century [2], and at 3.3 ± 0.5 mm/year over the last 25 years [3]. This is not a steady process since at both temporal scales, a positive acceleration (0.084 ± 0.025 mm/year^2) was also confirmed [4,5]. Presently, there is the virtual certainty that sea-level rise and climate change will bring to society and the environment significant consequences, especially in low-elevation coastal zones where more than 620 million people live presently, a number that is expected to double

by 2060 [6,7]. This enhances the climate-related concern about the sea-level rise impact at global scale and at coasts.

Satellite radar altimetry (SA) missions started in the early 1990s with the goal of providing, among other data, a fortnightly measure for the global sea surface height (SSH) in the reference system of the Earth's mass center. Given its reference frame, this is commonly referred to as the absolute sea level (ASL). SSH represents the difference between the satellite altitude above the reference ellipsoid and the height of the satellite above the instantaneous sea surface, measured by transmitting microwave radiations toward the surface which are partly reflected to the satellite [8]. As a consequence of this configuration, SSH measurements are affected by several sources of uncertainties. Such uncertainties are resolved by compensating for the effect of instrumental drift, signal refraction passing through the atmosphere, Glacial Isostatic Adjustment (GIA), tides and atmospheric pressure influence whose correction is commonly known as the Dynamic Atmospheric Correction (DAC). However, in shallow water and at the coast SA data are influenced and contaminated by both the presence of land in the satellite footprint and the spatio-temporal scale reduction of atmospheric and oceanographic processes with respect to the open ocean [8–10]. The need for reliable coastal altimetry data has led over recent years to the development of new sophisticated altimetry products, where the improved reprocessing and dedicated corrections aim to extend valid measurement to within < 20 km from the coast [11–13].

On the contrary, tide gauges (TGs) provide a measure of the sea level with respect to the pier at which the TG is attached and for this reason it is commonly referred to as relative sea level (RSL). The largest TG database is the Permanent Service for Mean Sea Level (PSMSL), where almost two thousand TG time series are collected, periodically updated, and reduced to a common datum, producing the Revised Local Reference (RLR) dataset [14–16]. Developed for different purposes, i.e., the observation of the harbor tide, currently TG data used for long-term sea-level studies suffer from the contamination by the vertical land movement (VLM) of the pier itself. This problem was sorted out in the recent past by the co-location of GNSS (Global Navigation Satellite System) at the TG site. However, this practice only started since the late 1990s [17,18] and for this reason it does not cover the whole time series at most of the TG sites. Despite the long period coverage (since 19th century for some specific cases) TGs data are geographically limited because of their heterogeneous spatial distribution. TGs measurement has increased since the 1950s, primarily throughout the Northern Hemisphere [19]. This limitation generates a bias that may hinder accurate and reliable sea level consideration at global scale.

Despite SA and TG time series currently represent the two main source of information for the sea level, the contrast between their observational ability remains an unresolved point. RSL, measured by the TGs, reflects the local variations in sea level and it is influenced by the VLM effect and the coastal processes, differently from the SA ASL records that provide geocentric sea-level variations. SA and TG data sets are, moreover, characterized by low and high acquisition rate, respectively [11]. Only SA measurement allows observation of the variability on sea level from the open ocean towards the coastal area and it is considered essential for giving perspective at regional and global scale without resolving, however, some key coastal processes, which instead are recorded by TGs. RSL and ASL variation and VLM are linked by means of the Sea Level Equation (SLE) that, in its simplest form, reads [20]:

$$S = N - U \tag{1}$$

where S is the RSL variation, N represents the ASL variation and U is vertical displacement [21,22]. This equation tells that the sea-level change at the pier is the combination of the absolute seal level variation in a geocentric reference frame minus the vertical displacement at the TG coastal location.

At global scale, the drivers of sea-level change are primarily related to variations in steric contribution [23,24] and ocean mass component [25–27]. By contrast, at regional (e.g., the Mediterranean Sea) and local scale the sea-level change could be amplified or

mitigated by several other drivers [28,29] such as VLMs, ocean dynamics (which become significant in semi- enclosed basins [30,31]) and the GIA (i.e., the visco-elastic crustal response to the inhomogeneous loading redistribution of ice melted water throughout continents and ocean [32–34]). The sea-level variability observed in the Mediterranean Sea is the consequence of several factors among which the circulation forced by heat and buoyancy flux at the surface, wind stress, and water exchange through the Strait of Gibraltar, varying periodically the water mass amount within the entire domain [30,35,36]. Regional sea-level variations are, in fact, influenced also by the balance between evaporation processes and precipitation–river runoff in the basin [37,38]. Wind stress can also lead to large Mediterranean sea level, generating periodic non-steric fluctuations due to mass transportation through Gibraltar from Atlantic [39,40]. A critical role of atmospheric forcing on sea-level change since the 1960s, not constant in time, has been documented for the Mediterranean Sea [41]. Indeed, several studies found a direct influence of inter-annual, decadal, and multidecadal climate fluctuations on sea level, corresponding to several tenths of mm/year [42,43]. This non-stationary variability is correlated with natural modes of the coupled ocean–atmosphere system such as El Niño Southern Oscillation (ENSO), North Atlantic Oscillation (NAO) and the Atlantic Multidecadal Oscillation (AMO) [44,45].

The Emilia-Romagna (E-R) coast is a highly urbanized, 130 km-long belt of low-elevated area (1.45 m maximum average elevation), located at the eastern margin of the Po Plain in Northern Italy (Figure 1). Coastal anthropization started in the 1950s [46], in the following decades the E-R coast became one of the most attractive tourist destinations in Italy and an important source for the regional economy. The combined effect of subsidence, sediment supply deficit due to the marked decrease in fluvial transport, removal of the dune ridge and increased anthropic pressure, cause the E-R coastal tract to be extremely sensitive to coastal flooding due to storm surges and sea-level rise [47]. In particular, a considerable portion of the E-R coastal area is currently below sea level and this would exacerbate the impact of future sea-level rise. As shown by Perini et al. [48] the combined effect of the IPCC worst scenario [2] and of the current local subsidence would cause, at 2100 with respect to 2012, a further extension (346 km^2) of the areas below mean sea level. Also, for this reason, the determination of the relative sea-level (RSL, i.e., the local sea level relative to a benchmark on land) variation at local scale for the E-R coast is paramount for the management of the territory and of its fragile environment.

In this paper, we analyze the sea-level variation for the E-R coastal area by selecting three sites along the E-R coast: Porto Garibaldi, Marina di Ravenna, and Rimini (Figure 1). These are the only sites where a TG in operation currently exists. For each site we also identify the closest SA altimetry cell to put the RSL observed at TGs in the framework of the ongoing ASL for the region. TG times series cover different time spans, and this complicates the analysis. The main objectives are: (i) to verify the consistency of different instrumental sea-level records (TG/SA) at each site, by comparing in situ data with the latest CMEMS (Copernicus Marine Environment Monitoring Service) altimetry products (see Section 3); (ii) to observe and analyze differences among obtained sea-level data at the three sites, i.e., at the coastal scale, with a focus on the local variability, heavily influenced here by VLM; (iii) to assess the recent (last 25 years) sea-level change and if it can be assumed as a reference for the E-R region, also highlighting the variability of sea-level rates which strongly depends on the records length and (iv) to discuss this figure in the framework of similar studies at the basin-scale (Adriatic/Mediterranean), and of climate change-related processes. The determination of current sea-level rise at regional scale remains a complex task especially when only short time series are available. However, since this remains a crucial point in support of coastal hazard evaluation and related management/adaptation policies, efforts should be made to understand sea-level variability and to describe its intricacy from the coastal and basin perspective. The paper is organized as follows: Section 2 introduces the study area, Sections 3 and 4 are dedicated to the description of data and analysis, respectively. Results are presented in Section 5 and discussed in Section 6. Finally, in Section 7, conclusions are drawn.

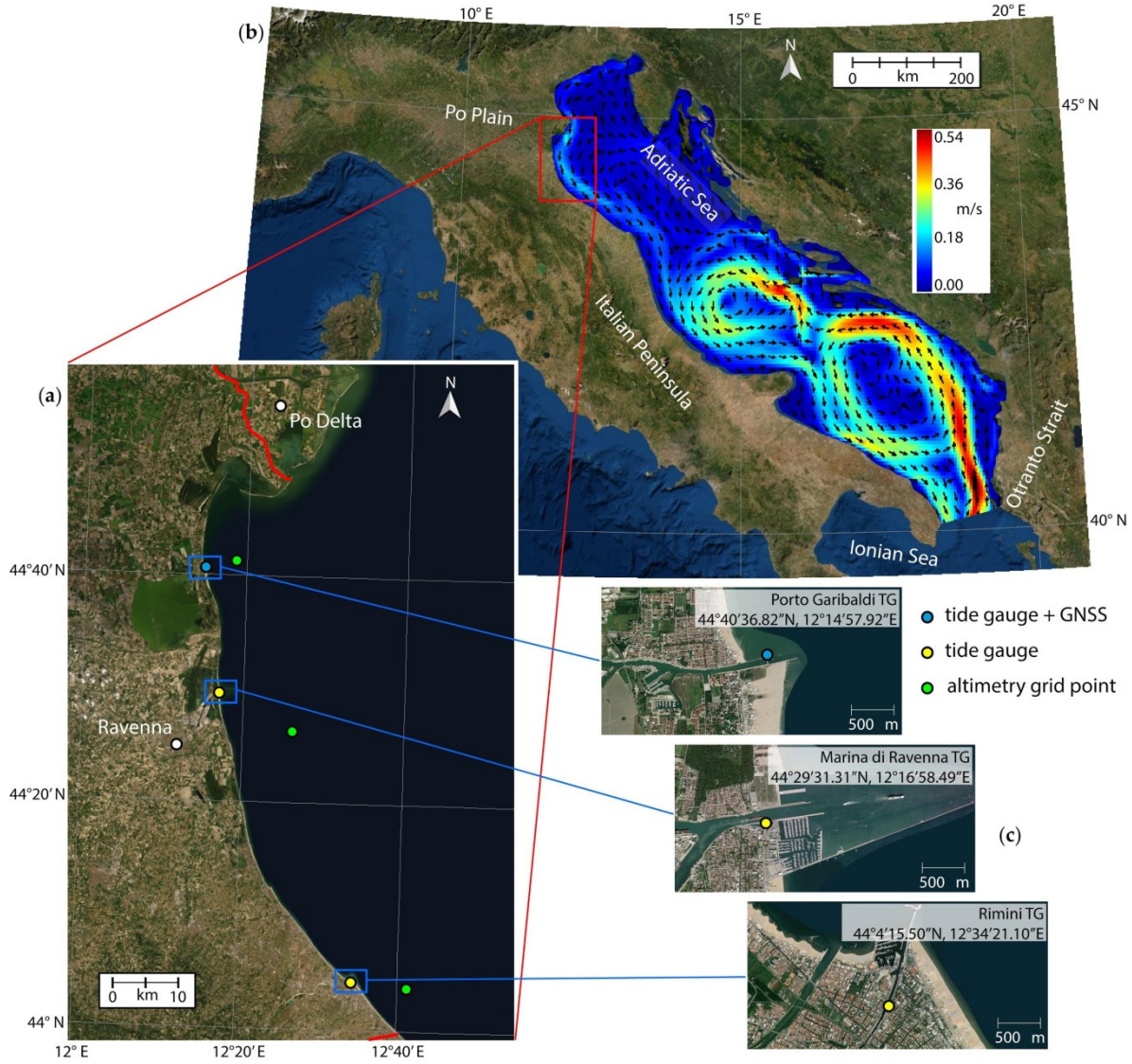

Figure 1. Satellite overview of the study site. (**a**) The E-R coast with northern and southern limits marked by red lines, the location of the selected tide gauges (blue and yellow circles) and their nearest satellite altimetry grid points (green circles). The blue circle at Porto Garibaldi remarks that, differently from the other two, the TG site is co-located with a GNSS antenna. (**b**) map of the surficial (upper 10 m layer) Adriatic current directions and velocity vectors (November 2018 monthly average, based on the MEDSEA_REANALYSIS_PHYS_006_004 model) [49]. (**c**) Detailed location of the three tide gauges considered in this work.

2. Study Area

The coastal belt of E-R is located in the eastern part of the Po Plain, south of the Po Delta (Figure 1). In geological terms, the Po Plain represents a foredeep basin suffering from natural subsidence. VLMs are mainly due to the consolidation of Quaternary alluvial deposits, with estimated rates along the coastal area of about -1 mm/year and -2.5 mm/year to the south and north of Ravenna municipality respectively, and twice as much at the Po river Delta [50]. Long-term VLMs due to tectonic component have been taken into account by Ferranti et al. [51] and Antonioli et al. [52,53] with rates in the order of -0.95 mm/year since the Last Interglacial (last 125 kyrs) for the northern E-R coast, while -0.22 ± 0.05 mm/year represents the glacio-hydro-isostatic contribution estimated by different GIA models [48]. Since the second half of the 20th century, the subsidence rate in the area has been markedly enhanced by the withdrawal of groundwater and gas extrac-

tion [54], with rates locally exceeding the natural subsidence by one order of magnitude. This caused land settlement locally exceeding 100 cm in a few decades [55]. The following gradual decrease in subsidence observed for almost the whole E-R coast is commonly attributed to the groundwater withdrawal cessation, occurred since the 1970s e.g., [54,56], and it has become more evident in the last two decades [55,57]. Current estimates of VLM based on the regional high-precision levelling network, regularly monitored since 1983 by the Regional Agency for Prevention, Environment and Energy of the E-R region (ARPAE), indicate average subsidence rates in the order of 5 mm/year for the last 15 years, decreasing to 3–4 mm/year in the period 2011–2016 [55]; however, peak values in the order of about 20 mm/year are still locally observed in the Ravenna coastal tract. The Coastal Geodetic Network is now the base for the definition of the orthometric heights along the E-R coast [58], integrated with InSAR techniques and GNSS measurements. Recently, Montuori et al. [59] integrating GNSS and multitemporal DInSAR techniques for the monitoring of land subsidence processes along the coastal plain, obtained average rates >3 mm/year, increasing to over 5 mm/year for Ravenna and some tracts along the SE coast. Rates of land subsidence for the Marina di Ravenna dock (from 1970 to present) based on geometric levelling, InSAR techniques and GNSS measurements, are compared by Cerenzia et al. [60].

From a morphological point of view, the E-R coast is represented by fine to medium-sand low-gradient dissipative beaches, 60% of which is the seat of hard protection structures [55]. The E-R coast is in general affected by low-energy waves, with Hs commonly below 1.25 m and microtidal regime [61,62]. The main storms come from the Bora (northeast) and Scirocco (southeast) winds, resulting in storm surge levels >1 m on a 100-year return period [48]. This is a huge concern for such low-elevation coastal zones, exacerbated by forthcoming climate change effects.

The E-R coast faces the northern Adriatic basin (Figure 1), a shallow sub-basin (a few tens of m of depth) with a low topographic gradient. The Adriatic is a narrow epicontinental shelf (800 by 200 km), communicating with the Ionian Sea through the Otranto Strait (Figure 1). The sea-level variability in the Adriatic Sea significantly differs from the other Mediterranean Sea sub-basins because of its setting [63–65]. It is dominated by cyclonic circulation driven by wind and thermohaline currents, mainly represented by three gyres centered in the southern, middle, and northern sector of the basin; northerly and southerly currents flow along the eastern (Eastern Adriatic Current, EAC) and western (Western Adriatic Current, WAC) coast, respectively (Figure 1) [64–67]. Previous analyses of sea-level rise in the altimetry era found an average rate of 3.2 ± 0.3 mm/year over the 1993–2008 for the Adriatic Sea, not uniform on the whole period, but positive (9 ± 0.5 mm/year) between 1993 and 2000 and negative (-2.5 ± 0.5 mm/year) between 2001 and 2008 [68]. Similar positive and negative rates before and after 2001 result for the (basin-average) steric component of sea level, which is correlated with Adriatic Sea level. For the northern sector of the Adriatic, rates of 4.25 ± 1.25 mm/year for the period 1993–2015 [69] and of 3.00 ± 0.53 mm/year for the period 1993–2018 [70] have been recently estimated.

3. Data

In situ sea-level signals are achieved from the three TGs currently operational along the E-R coast (Figure 1). These are installed at Porto Garibaldi (TG_{PG}), Marina di Ravenna, also known as Porto Corsini (TG_{RA}), and Rimini (TG_{RN}). In particular:

TG_{PG} has been operational since July 2009 and it is co-located with a permanent GNSS (Figure 1) station (GARI) that provides VLM information for this site. Different sources are freely available for geocentric surface velocity data at GARI [71]. In this work we considered the GARI time series produced with the INGV (Istituto Nazionale di Geofisica e Vulcanologia) solution by employing the GAMIT/GLOBK software and expressed in the IGS14 (International GPS Service) reference frame [72]. Only TG_{PG} and a portion of TG_{RA} are RLR data retrieved from the PSMSL.

At Marina di Ravenna, different TGs almost continuously collected relative sea-level data since 1873 [73,74], with a main gap from 1922 to 1933. Presently, data are managed

by the Italian National Tide Gauge Network (Rete Mareografica Nazionale, RMN) which refers TG data to a local benchmark, located at the lighthouse, 150 m apart. TG_{RA} has a large gap between 2016 and 2019 and, for this reason, the time series considered in this work terminates in December 2015. A permanent GNSS station has operated since 1996 close to TG_{RA} [73] and is currently managed by the Department of Physics and Astronomy of the University of Bologna (no open data).

TG_{RN} has been in operation since July 2012, it is managed by Hera Group corporation, and it is not equipped with a GNSS antenna. Despite the shortness of the data and the lack of a co-located GNSS antenna, TG_{RN} is valuable since it provides the only datum for the southern portion of the E-R coast.

Both TG_{PG} and TG_{RA} operate with radar systems technology (the former coupled with a float system sensor, following the Intergovernmental Oceanographic Commission (IOC) directives [75]) while TG_{RN} operates with a differential pressure transducer. Since only float systems directly provide a SSH measurement, seawater density and gravitational acceleration are considered to convert pressure measured by TG_{RN} into sea level, while radar systems are supplied with dedicated hardware and software that directly convert the measures [76]. Regarding the SA, in this study we use the CMEMS daily gridded dataset (SEALEVEL_MED_PHY_L4_REP_OBSERVATIONS_008_051), having a spatial resolution of 0.125 degree x 0.125 degree [77]. This product is processed by the DUACS (Data Unification and Altimeter Combinations System) multi-mission altimeter data processing system, merging data from all the satellites available at a given time [77–81]. We selected the three closest pixels (SA_{PG}, SA_{RA}, SA_{RN}) to each of the TG (Figure 1), located at about 5, 13, and 9 km from Porto Garibaldi, Marina di Ravenna, and Rimini TGs, respectively. Each time series was downsampled from daily to monthly by computing the average for the whole samples of each month.

4. Analysis

To minimize the contrast between SA and TG time series, some procedures need to be considered, depending on the purpose of the study. DAC correction in SA (see Section 1) accounts for the low-frequency response of the sea surface to the atmospheric loading, known as the Inverse Barometer (IB) effect [82], and for the high-frequency (HF) response to wind and pressure forcing effect [83]. Since CMEMS products data are corrected by the DAC, the IB and HF effects must be subtracted from TG data for comparison purposes. However, the HF effect is negligible on periods longer than 10 days, hence no correction is needed when monthly averaged data are used [23]. The correction for the IB effect allows the subtraction of the atmospheric loading contribution from the observed RSL at TG. The IB effect correction considered in this work is based on the Wunsch and Stammer [82] formula:

$$IB(\theta,\lambda,t) = -9.948\ (\Delta rdry(\theta,\lambda,t) - 1013.3) \quad (2)$$

where $\Delta rdry(\theta,\lambda,t)$ and -1013.3 are the local and global (standard) atmospheric pressure (in millibar) respectively, and -9.948 a constant that accounts for the water density and gravitational acceleration. The monthly mean time series of atmospheric loading at each TG was recovered from the ERA5 reanalysis [84] developed by the European Centre for Medium-Range Weather Forecasts (ECMWF). Furthermore, the application of the GIA correction on TG time series is considered of great importance when reconstructing the ASL, since no worldwide TG record can be assumed to be completely unaffected from the GIA effect [85]. However, since we are interested in studying the local RSL change with respect to the ASL change, and since we are considering short-lived time series, we can neglect to apply this correction.

Assessing the rate of sea-level variations is a complicated task exacerbated when time series are short and possibly affected by multi-annual and decadal oscillations, difficult to determine on the short term. However, we stick on standard trend assessment by means of ordinary least squares (using NumPy's Python library [86]) to ease the comparison with previous results even though we are conscious that more sophisticated analysis could

provide different results and that this approach neglects the autocorrelation of the time series. This weakness is compensated by the characterization of the periodic signals using two separate approaches, first we compute the Lomb–Scargle periodogram [87,88] (LSP) for each time series to provide a complete description of the frequency content by using the Lomb package [89] implemented in R [90]. Then, we apply the Empirical Mode Decomposition (EMD) method [91,92], a standard method for splitting non-linear and non-stationary time series into a limited sequence of empirically orthogonal "intrinsic mode functions" (IMFs) that describe cyclic modes not necessarily characterized by a constant amplitude nor phase. Differently from traditional spectral methods, the EMD is not requiring assumptions on the functional expression of the regression model. This allows us to decompose each time series in sequence of IMFs plus a residual. The latter, normally monotonic, helps to define how a linear trend is a good model for the non-periodic component of each time series. The significance of the resulting trends is discerned by means of standard test [93] that checks the probability of the null hypothesis to be true. This test is reported beside each trend with its significance code: *** $p < 0.001$; ** $p < 0.01$; * $p < 0.05$; ° $p < 0.1$; ' ' (blank) $p < 1$.

5. Results

5.1. Sea-Level Assessment

Satellite altimetry time series (SA_{PG}, SA_{RA}, SA_{RN}) are shown in Figure 2a. The visual comparison among the three SA time series highlights excellent coherence that is confirmed by the correlation coefficient [94] r = 0.98. To better characterize the frequency content of these time series we compute the Lomb–Scargle periodogram (LSP; Figure 2b) for each of them [87,88]. The time series are dominated by the annual and semi-annual oscillation, both related to the seasonality, with peak-to-peak amplitude varying in the order of 150–300 mm (Figure 2a). The resulting LSPs (Figure 2b) also confirm the coherence between the three sites and demonstrate the presence of multi-annual oscillation whose most relevant periods are about 4 and 12 years (see Section 6.1 for detail). LSP significance analysis indicates a small probability (<10%) for the peak at about 12 years to be artefact even though the large sample spacing prevents an accurate definition of the period itself. Conversely, the random peak probability is larger than 10% for the one at about 4 years.

Standard linear regression provides a coherent rate of 2.8 ± 0.5 mm/year over the timespan January 1993–May 2019 (details in Table 1). These values are smaller but comparable to the global average (in the range of 3.1–3.4 mm/year [95]) over the same timespan. The rate assessed in our analysis is smaller than what observed for the northern sector of the Adriatic for the period 1993–2015 (4.25 ± 1.25 mm/year) by Vignudelli et al. [69] even though the two error bars partly overlap, and consistent with what observed for the period 1993–2018 (3.00 ± 0.53 mm/year) by Mohamed et al. [70]. We in fact observe that when fitting the same time series with a second-order model (quadratic, Figure 2a), we get a slight but statistically significant negative acceleration of -0.3 ± 0.1 mm/year^2. This local negative acceleration, in contrast with that at the global scale for which a slight positive acceleration (0.084 ± 0.025 mm/year^2) has been observed [4], is discussed in Section 6.3.

As summarized in Section 3, the three TG time series do not cover the same timespan and are shorter than SA (Figures 3 and A1). This limits the comparison between different sites and, for the shorter one, the reliability of the RSL rate assessment. The longest time series is TG_{RA} (January 1993–December 2015), showing a RSL rate of 5.8 ± 0.8 mm/year (Table 2). This value is consistent with previous studies e.g., [60,68] and significantly higher than the ASL rate observed offshore (January 1993–May 2019, Table 1), as a consequence of the strong vertical land motion expected in this coastal sector. The rate from TG_{PG} has a large uncertainty that leaves the null hypothesis (absence of trend) likely, while from TG_{RN} it is largely negative. Despite the large disparity in the resulting RSL rate is also a consequence of the different time spans, we note that the correlation coefficient, restricted to the overlapping periods, is 0.80 between Porto Garibaldi and Marina di

Ravenna, 0.94 between Porto Garibaldi and Rimini, and 0.77 between Rimini and Marina di Ravenna.

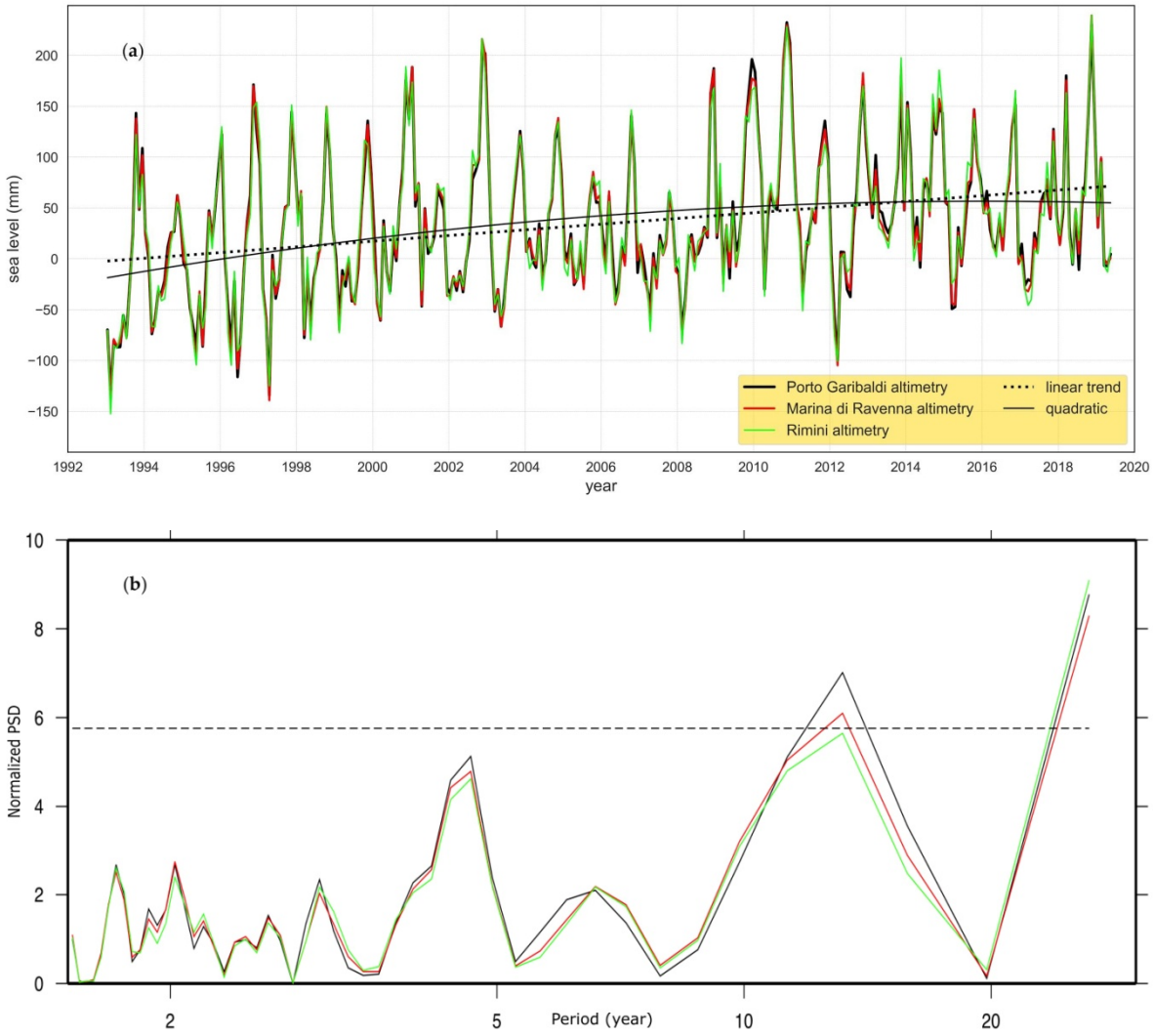

Figure 2. (**a**) SA_{PG}, SA_{RA}, SA_{RN} time series with superimposed linear and quadratic model for the sole case of SA_{PG}. (**b**) Lomb–Scargle periodograms for the three time series. Color coding is black for SA_{PG}, red for SA_{RA}, and green for SA_{RN}. Measure unit is normalized power spectral density (PSD). At small periods, the periodograms are limited to 1.5 years to enhance the readability at long periods. The dashed line represents the significance (90%) of the periodogram.

Table 1. Linear trend rate and acceleration estimated in this work from SA data. Symbol *** indicates that the model is strongly significant with $p < 0.001$ and symbol * refers to $p < 0.05$.

	SA Rate (mm/year)	**SA Acceleration (mm/year^2)**
Porto Garibaldi (January 1993–May 2019)	2.8 ± 0.5 ***	-0.3 ± 0.1 *
Marina di Ravenna (January 1993–May 2019)	2.8 ± 0.5 ***	-0.3 ± 0.1 *
Rimini (January 1993–May 2019)	2.9 ± 0.5 ***	-0.3 ± 0.1 *

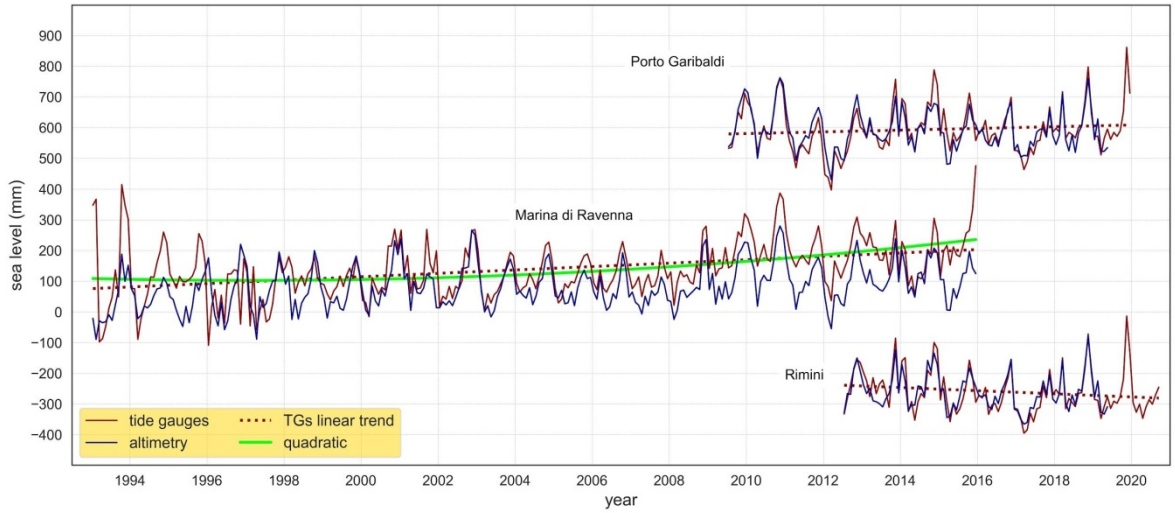

Figure 3. The three TG time series (IB-corrected) compared with their SA closest grid point data. Associated TGs linear and quadratic models are represented by dotted and solid lines, respectively, and their values summarized in Table 2. The time series are displayed with random offsets for readability purposes.

Table 2. Linear trend rate (for raw data and IB-corrected data) for the tide gauges considered in this work. The significance of the resulting trend varies according to the symbol beside each rate (significance code: *** $p < 0.001$; * $p < 0.05$; ° $p < 0.1$; ' ' $p < 1$).

	TG Rate (mm/year)	TG (IB-Corrected) Rate (mm/year)
Porto Garibaldi (July 2009–December 2019)	1.4 ± 2.8	2.8 ± 2.2
Marina di Ravenna (January 1993–December 2015)	5.8 ± 0.8 ***	5.5 ± 0.8 ***
Rimini (July 2012–September 2020)	-7.7 ± 3.6 *	-5.1 ± 3.0 °

Since one of the goals of this study is the comparison between RSL and ASL to better understand the different governing mechanisms and observational approaches, we apply the IB correction to the raw TG data to compare them with SA time series (corrected for DAC). This correction gives a valid reprocessing of the sea-level variability without the meteorological effect influence [96]. We can observe that the IB correction leads to a reduction, in amplitude, for most of the extrema (Figures 3 and A1) and this reflects in smaller variance for the residual of the OLS regression and, indeed, in a smaller error associated with the trend (Table 2). As expected, the IB-corrected TG time series result in different RSL rates and smaller uncertainties. We also note that the quadratic fit for TG_{RA} returns a positive acceleration (0.7 ± 0.3 mm/year^2), not present in the ASL data (Figure 3).

The SA time series have been shortened to match each of the three TG time series (Figure 3). Also in this case the correlation coefficient is high (0.89) for Porto Garibaldi e Rimini and moderate for Marina di Ravenna (0.66). We notice that the rates for the shortened SA time series (Table 3) differ from what observed for the complete time series (January 1993–May 2019). In particular, in the case of SA_{PG} and SA_{RN}, for which we consider only the last part of the time series, rates turn negative. In details, for SA_{PG} (timespan July 2009–May 2019) the trend is negative, while the corresponding rate of RSL is positive (Table 3). This result for SA linear trends is not unexpected since it is consistent with the observed negative acceleration (Table 1) that suggests a decrease in ASL rate of about -5 mm/year over the removed 16 years (1993–2009). For the same reason, at SA_{RA} the trend for the period January 1993–December 2015 is larger than the one computed

for the whole SA timespan, and lower than the RSL rate (Table 3). Finally, for the case of Rimini, SA_{RN} trend is negative (Table 3) but the large error bar demonstrates that the null hypothesis (no trend) could not be rejected with $0.1 < p < 1$. In other words, the large error bar demonstrates the low significance of the linear model and that the rate could also be null or even positive. As in the case of altimetry, the analysis of shorter-term time series also modifies the TG trend values (compare Tables 2 and 3), except for TG_{RA} whose time series is fully covered by the altimetry and therefore does not need to be cut. Furthermore, an important contribution to the local sea-level variation at different sites is represented by the vertical movements (VLM) component included in the TG data. This will be taken into account and discussed in Section 6.2.

Table 3. Linear trend rate comparison between SA and TG for the common timespan covered. The significance of the resulting trend varies according to the symbol beside each rate (significance code: *** $p < 0.001$; * $p < 0.05$; ' ' $p < 1$).

	SA Rate (mm/year)	**TG (IB-Corrected) Rate (mm/year)**
Porto Garibaldi (July 2009–May 2019)	-3.1 ± 2.0	1.2 ± 2.3
Marina di Ravenna (January 1993–December 2015)	3.5 ± 0.6 ***	5.5 ± 0.8 ***
Rimini (July 2012–May 2019)	-3.3 ± 3.2	-7.6 ± 3.7 *

5.2. Periodic Signals

The large uncertainty in estimated rates, and in their variation over different time spans, suggests analyzing the periodic components of the time series and to define their relevance in terms of amplitude and frequency to better constrain the characteristics of the sea-level change. With an approach similar to that used in Section 5.1 for SA, we analyze the TG time series by means of LSP and EMD.

Results are shown in Figure 4. LSP analysis (Figure 4a) for the whole period range confirms the prominence of the oscillation at 1 year (especially for longer time series), while at shorter periods (below 1 year) different peaks emerge between 0.2 and 0.5 years (i.e., between 2 and 6 months). For the case of Porto Garibaldi and Rimini we notice that the IB correction enhances the signal for the annual oscillation and that a clear peak emerges at 0.85 years (10 months). This partly contrasts with what observed for the LSPs computed for the SA time series in which the semi-annual oscillation emerges more clearly. The ascending termination of the periodograms at the longest period (right side) for the case of TG_{RN} and TG_{RA} could reflect the presence of periodic signals at periods longer than the timespan covered by this (very short) time series. We also notice that IB correction reduces the power amplitude at longer periods.

To better discern the periodic signals from the long-term trend, we also applied the EMD analysis to each IB-corrected time series. From Figure 4b, we note that at high frequency (IMF1–2), large non-sinusoidal oscillations exist, and these show an overall coherence between the three sites. This suggests a regional scale origin. IMF3, whose periodic signals range between 1.5 and 3 years, is not coherent during the overlapping timespan, pointing to a site-related effect. IMF4 exists only for Marina di Ravenna and Rimini but these time series overlap for a very short timespan and this prevents any comparison. IMF5 at even longer periods emerges only for Ravenna and it demonstrates an almost sinusoidal oscillation with a period of about 10.7 years. Residuals confirm what observed from linear regression (Table 3) and introduce some more complexity: Marina di Ravenna shows short-lived positive acceleration around year 2000, Porto Garibaldi is almost linear with two minor inflections, while Rimini shows a parabolic shape contrasting with a linear model. For Rimini, the shortness of this time series limits the distinction

between a branch of a parabola or of a sinusoid with period of about twice the length of the time series.

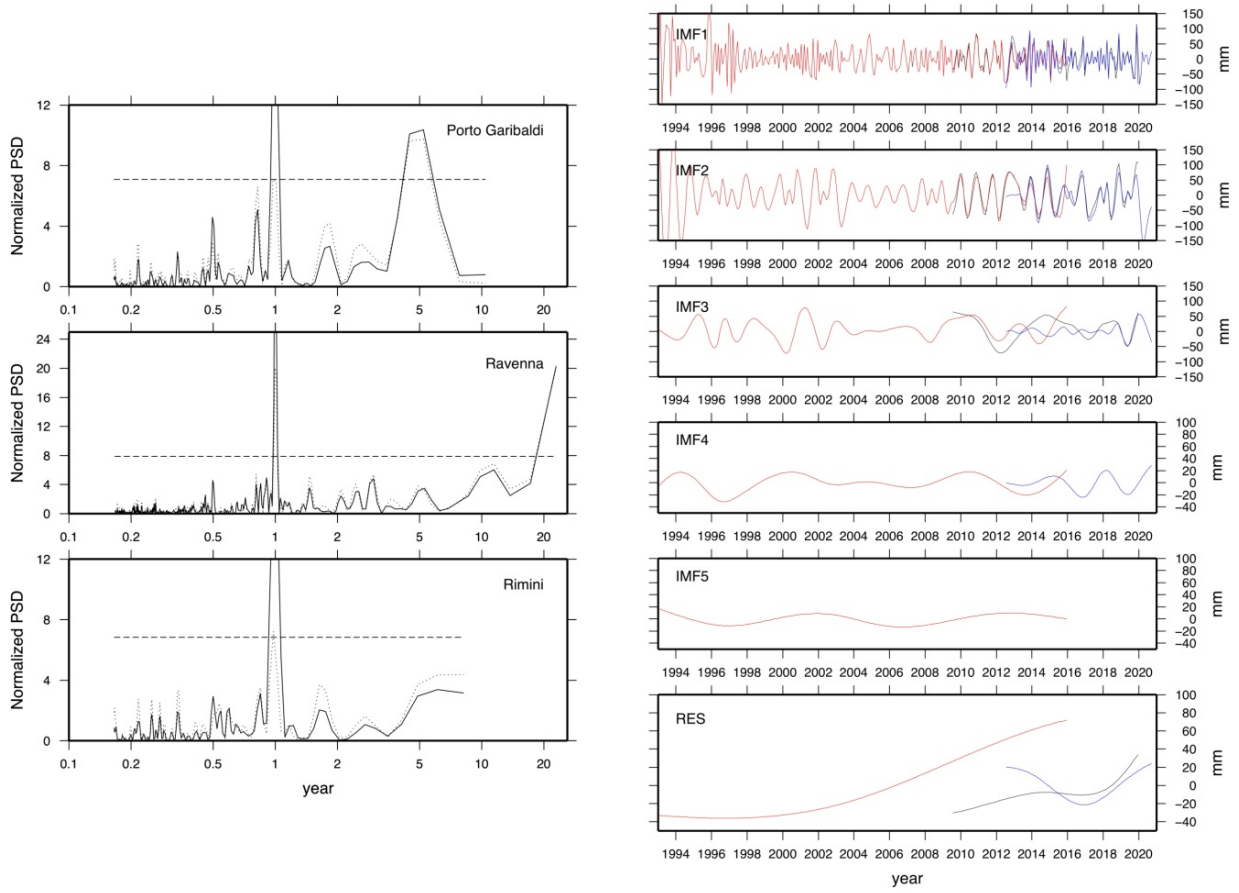

(**a**) (**b**)

Figure 4. (**a**) Normalized power spectral density (PSD) periodogram resulting from the LSP analysis for TG_{PG}, TG_{RA}, TG_{RN} time series. In each frame, the dotted line represents the periodogram for raw data while the solid line is the periodogram for IB-corrected time series. The dashed horizontal line represents the significance (90%); (**b**) EMD for IB-corrected data. Red for Ravenna, black for Porto Garibaldi, and blue for Rimini. The Y axis of the two bottom frames have been enlarged to better visualize the small amplitude signals.

6. Discussion

The above data analyses provide a complex picture for the sea-level variation along the E-R coast. Actually, different data and processing, and the large literature available for the region suggest several perspectives for discussing and interpreting such complexity. In this section, we propose a comprehensive interpretation of our results, also in the framework of previous studies. We focus on factors affecting sea-level variability, on the role of the VLM in the E-R coast, and on the difficulties of providing a figure for the current or recent rate of sea level for the area.

6.1. Sea-Level Time Series and Rates for the E-R Coast

To verify the consistency of different instrumental sea-level records at the coastal scale, TG and satellite altimetry time series were analyzed at three sites along the E-R coast. Altimetry time series at the three sites turn out to be very consistent, showing basically the same rate of sea-level rise (Figure 2a; Table 1) and variability in the last 25 years, also denoted by a perfect correlation among them (r = 0.98). On the other hand, the results provided by the three TGs are more variable in terms of trend and variability

both among them and with respect to the altimetry. This can be the consequence of some critical factors. First, the TG time series cover different time spans (Figure 3), and this can cause discrepancies in the observed rates (Tables 2 and 3). Indeed, the timespan for which the three TG time series overlap is very short, thus preventing a reliable comparison. Secondly, rate assessments based on short records are particularly sensitive to oscillations especially at their extremes, thus they are not suitable for deriving climatological-related information in the long term [2].

It is a common practice to reproduce the sea-level variation over time by a linear model. However, this approach sometimes forces the observed phenomenon into a model that is too simple, neglecting periodic and aperiodic variations of different time scale and size that can bias the resulting trend. The addition or subtraction of a few samples at the time series extrema can cause considerable variations of the trend rate as recognizable by comparing values listed in Tables 1 and 2 with those of Table 3. For the case of the Adriatic Sea, the rate of sea-level rise strongly varies with time because of the chosen record length [68,85,97,98], and by the contamination of seasonal and inter-annual variability [99]. To constrain this, we combined EMD analysis and LSP periodograms. LSP, among the expected annual and semi-annual oscillations, demonstrates two oscillations at about 4 and about 12 years for SA data, while the interpretation of TG data is more complex given the short timespan for TG_{PG} and TG_{RN}. TG_{RA} shows a more complex periodogram in this band, suggesting that several events contribute to hinder the SA peaks; however, EMD analysis returns a period signal at about 10.7 years. We can speculate that this oscillation and the SA peak at about 12 years are comparable with the 10 years-oscillation at Mediterranean scale observed by Bonaduce et al. [100].

The oscillations that influence the Adriatic Sea are mainly due to cycles that act at annual (stronger energy signal), semi-annual (6 months) and inter-annual (5 years and higher) scales [101], as also demonstrated in our data (Figures 2a and 4a). The whole Mediterranean basin is also influenced by oscillations at lower frequencies driven by natural modes, which produce intermittent anomalies in the long-term rate. As analyzed by Galassi and Spada [45] the NAO and AMO power are mainly concentrated at a period of about 8 and 9 years respectively; they also pointed out that the AMO strongest signal is found at multidecadal periodicities, i.e., between 50 and 70 years. Moreover, one of the most energetic modes of variability in the Adriatic basin is linked to the periodic occurrence (approximately 20 years) of opposite phases of the NAO and AMO [45] which produce a large scale zonal atmospheric gradient [102] and a sea-level non-steric fluctuation directly linked to mass transport through the Strait of Gibraltar driven by wind [39,103]. The last occurrence of this phenomenon was determined as the cause of the large positive anomaly recorded in sea-level signal during 2010–2011 [40,70] by all Mediterranean TG stations [100]. Indeed, the right site upgoing termination of the LSPs (Figures 2b and 4a) could be an indicator of a longer period oscillation that could not be quantified here because of the length of the time series.

One further cause of the variability in SL rate and corresponding uncertainties is the different data processing and different corrections applied. An example of the above cited complexity is the Marina di Ravenna site for which several previous studies exist, based on the same TG time series but using different methodologies and adopted corrections, as shown in Figure 5 where the results of some of the most representative studies conducted on TG_{RA} are summarized (see also Table A1). There is a relation between the time series length and the error size of the trend resulting from OLS regression, i.e., the error scales inversely with the number of samples of the analyzed time series [104]. Rate for longest datasets generally agree, but only when similar data corrections are applied: Zerbini et al. [73] and Bruni et al. [74] removed from data the non-linear VLM resulting from GNSS data, while Cerenzia et al. [60] accounted for the linear VLM (from various geodetic data), and Tsimplis et al. [41] normalized the data with respect to the TG time series of Trieste (considered to be a tectonic stable site). Rates computed from long time series without VLM correction are significantly higher [41,60,105] but still relatively grouped. By contrast,

rates from short time series (i.e., less than 20 years, see [60,68,105,106]) denote extreme variability and inconsistency between them regardless of the corrections applied, e.g., IB correction and deseasoning, whose influence is relatively low here with respect to the crustal movements corrections. This highlights how the natural variability and the contribution of VLMs strongly influences the RSL signal at the TGs, preventing the estimate of a univocal sea-level trend valid at the short-, middle-, and long-term scales. Given the short time spans and the described complexities, we thus cannot establish if and how the observed trends could be representative of the long-term rate of RSL rise. Also, the time series analyzed in this work (Figure 3; Table 2) suggest that a not constant rate of subsidence might play a crucial role in the observed RSL change at this time scale.

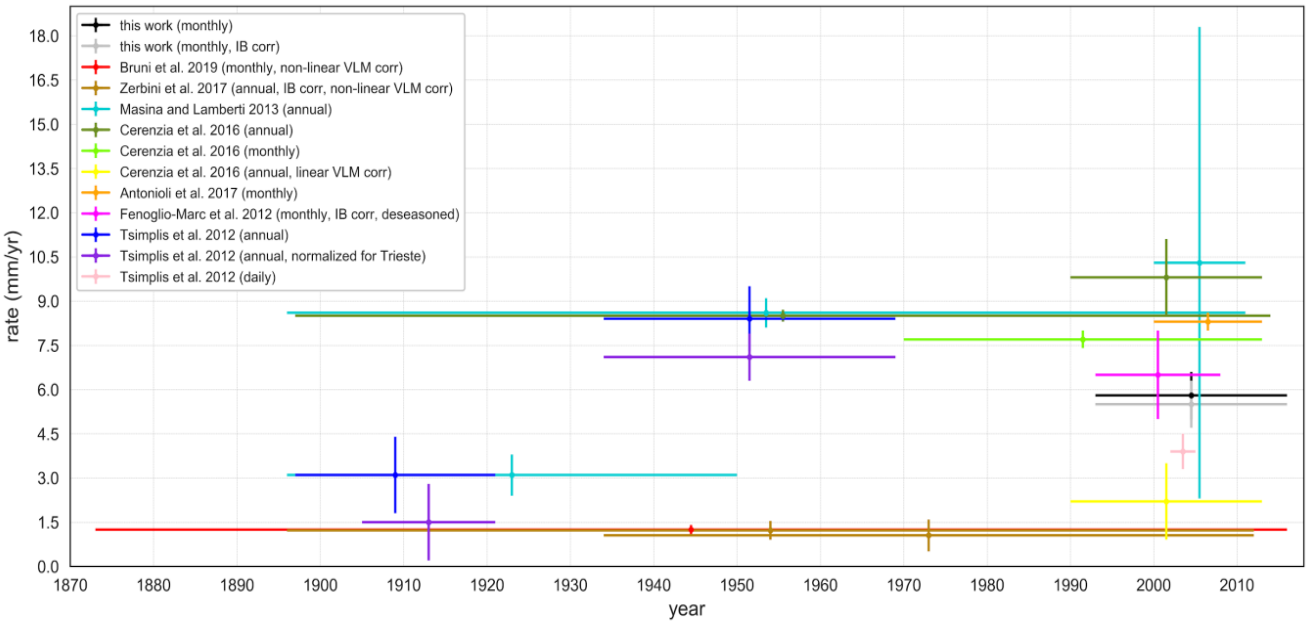

Figure 5. Rates of sea-level change obtained by some of the most representative studies on TG_{RA}. Vertical bars represent error associated with the rate, while horizontal bars reflect the considered timespan.

Regarding the comparison between the two different techniques, the analyzed SA and TG records have been downsized to cover only the overlapping timespan at each site and this causes differences in the estimated rates at the three sites (Tables 2 and 3). The results of this comparison are thus expected to improve in the next years/decades when the available time series will be longer for the analyzed sites. An 18-year- [107] or 15-year-long [108] recording is needed to obtain a good correlation. It has been shown, in fact, that over intervals shorter than 10 years the inter-annual variability affects more the rate of global mean sea level from TG than from altimetry [68]. However, despite these considerations, we obtain very high correlation between SA and TG sea-level time series at the three studied coastal sites. In particular, the three downsized SA time series show a strong correlation with the IB-corrected TG time series (Figure 3), especially at Porto Garibaldi and Rimini ($r = 0.98$). This confirms the good quality of the chosen SA product that, as suggested by Vignudelli et al. [69] for the northern Adriatic Sea, is less affected by degradation at the coast than previous SA data. As a matter of fact, different linear rates result for TG and SA at each of three study sites (Table 3). Since SA provides a coherent rate along the E-R coastal area (Table 1), an important contribution to the spatial variability of RSL at different sites should derive from the VLM component included in the TG data, and this is the focus of the next section.

6.2. The Role of Vertical Movements in Sea-Level Determination

In the E-R coastal area (and on a great portion of the Northern Adriatic coast, Italian side) subsidence is widespread and occurs at high rates [109], while vertical deformations caused by other phenomena as GIA are more than one order of magnitude smaller than subsidence that here dominates the VLM affecting RSL change [60,68,69,105,106,109]. Presently, different integrated techniques, such as high-resolution levelling, e.g., GNSS and InSAR, provide data on VLM with increasing accuracy [57,58]. However, the small size and short-lived variation of vertical deformation processes causes this information to be not always comparable/homogeneous. Furthermore, the common practice of co-locating a GNSS station at the TG site is relatively recent and many TGs do not have associated VLM data with the necessary precision.

As mentioned in Section 3, TG_{PG} has co-located GNSS station (coded name GARI) since Jul. 2009. GARI station provides well constrained VLM data well reproduced by a linear trend with rate equal to -2.8 ± 0.1 mm/year. At Marina di Ravenna, the VLM rate estimated for the GNSS station located close to TG_{RA}, estimated through the Gipsy software over the timespan July 1996–December 2015, is -5.6 ± 0.2 mm/year [110]. These VLM rates, when compared with rates of RSL at each site well explain a relevant portion of the sea-level change in the considered time frames (Table 2) while the ASL contribution seems low or negligible. At Rimini, the rate of RSL in the time frame Jul. 2012–Sep. 2020 (the only one available at TG_{RN}) is negative (-5.1 ± 3.0 mm/year; Table 2), in contrast with what observed for TG_{RA} and TG_{PG}. Here, a GNSS station (ITRN) operated by the Coastal Geodetic Network [57] (located at 2.6 km from the tide gauge, at 44°2′54″N 12°34′55.4″E) shows a VLM rate almost null (0.00 ± 0.8 mm/year) for the period 2011–2016 (for further details see [111] and references therein).

Integrated data on vertical deformations (topographic levelling, GNSS and InSAR) of selected benchmarks of the E-R Coastal Geodetic Network and data previously acquired in the framework of the Regional Network for subsidence monitoring [112], provide gradually decreasing subsidence rates for all the coastal sites under study in the last 25 years [55,57] (Table 4). These data are gridded at 100 m × 100 m and reproduced as isokinetics of VLM at the regional scale; associated error is estimated as ±2 mm/year [57]. For the area that contains the TG data, rates summarized in Table 4 can be considered representative of the subsidence. Actually, these data agree with the rate observed by GNSS at Porto Garibaldi and Marina di Ravenna. For Rimini, subsidence data suggest that this phenomenon is gradually decreasing but not inverted, as the negative rate of RSL rise might suggest.

Table 4. Ranges for the rate of subsidence estimated over different time frames for each of the study sites from selected benchmarks of the E-R Coastal Geodetic Network [111].

	1992–2000 (mm/year)	2002–2006 (mm/year)	2006–2011 (mm/year)	2011–2016 (mm/year)
Porto Garibaldi	7.5–10	7.5–10	2.5–5	2.5–5
Marina di Ravenna	7.5–10	7.5–10	5–7.5	2.5–5
Rimini	5–7.5	5–7.5	5–7.5	0–2.5

As a parallel approach, we use the SLE (Equation (1)) to compare the observed sea level or ground variation with the one obtained by the combination of the over two data. It must be pointed out, however, that the accuracy of this method is frequently larger than 1 mm/year whatever its application [113–115]. Despite the coarseness of this method (20 years of data should be required to yield a high-precision estimate, [115]) several authors have applied it to regional studies, since understanding VLM for sea-level research is of farthest significance e.g., [21,116–124].

For the case of Porto Garibaldi, the three variables that form Equation (1) are available from the different observables considered for this work over the common period July

2009–May 2019. This allows us to evaluate the different estimates obtained through the two approaches, i.e., by comparing the rate obtained from the linear regression of the direct observation (Table 3) with those computed by using Equation (1) (hereafter computed). Visual inspection of Figure 6 suggests a strong correlation between the pairs (SA, *U*+*S*) and (TG, *N*-*U*), this confirmed by r = 0.90. By contrast, the correlation between (*N*-*S*) and the GNSS is low (r = 0.37). This follows the different accuracy of GNSS data (below 0.1 mm/year) with respect to TG data contained in *N*-*S*. The trend values related to the computed time series (Table 5) slightly differ from those of the observed one (Table 3). We note that only for *U* the null hypothesis (no trend) could be rejected. Figure 7 shows that the observed and computed trends match within their error bars, despite the differences between their central values, suggesting a good coherence between the different observations. In particular, the trend observed for *N* (from *U*+*S*) is lower in value than the ASL derived from SA_{PG} (-3.1 ± 2.0 mm/year) even though their error bars overlap (Figure 7). The trend for *S* is almost null and its error bar shows good overlap with the rate of RSL given from TG_{PG} (1.2 ± 2.3 mm/year; Figure 3, Figure 6, and Figure 7). *U* is affected by larger uncertainties with respect to the GNSS time series, with uncertainties lower in value (-2.9 ± 0.1 mm/year in the time frame Jul. 2009–May 2019) and completely contained in the *U* error bar (Figure 7).

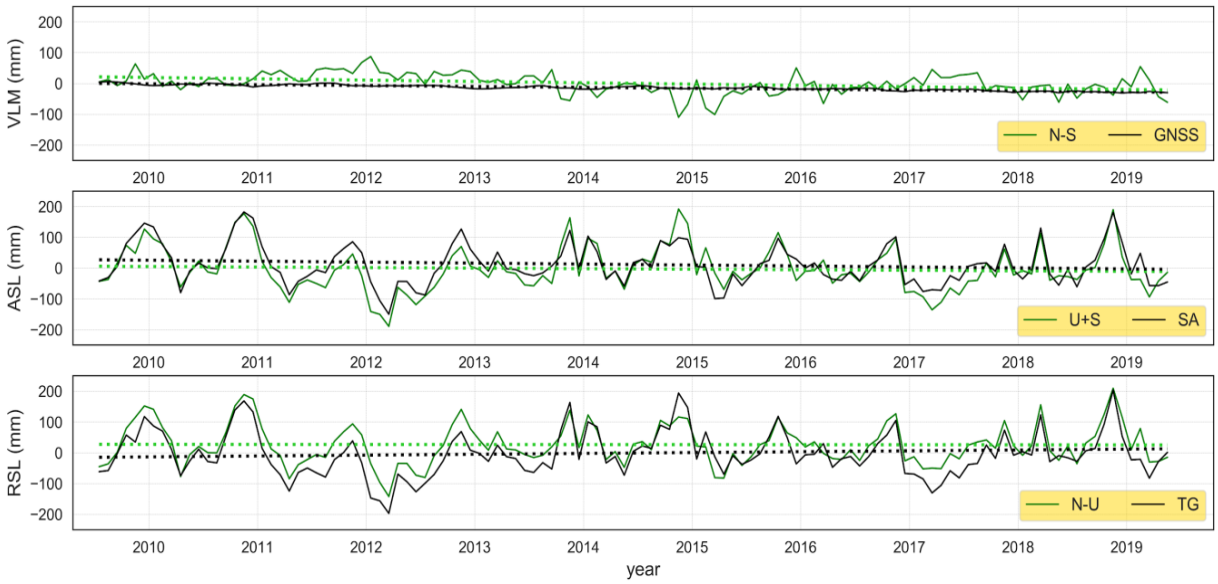

Figure 6. The comparison of observed (black) data (from GNSS, SA e TG) and those computed, i.e., indirectly derived from direct observations (green) at the Porto Garibaldi site. Associated linear trends are represented by dotted lines with the same color code of the time series.

Table 5. *U*, *N* and *S* resulting from the SLE (Equation (1)) where *N* is the ASL variation, *U* is vertical displacement and *S* is the RSL variation (values in mm/year). NA = not available. The significance of the resulting trend varies according to the symbol beside each rate (significance code: *** $p < 0.001$).

	U	***N***	***S***
Porto Garibaldi (July 2009–May 2019)	-4.3 ± 3.1 ***	-1.7 ± 2.3	-0.2 ± 2.1
Marina di Ravenna (January 1993–December 2015)	-2 ± 1	NA	NA
Rimini (July 2012–May 2019)	4.3 ± 4.9	NA	NA

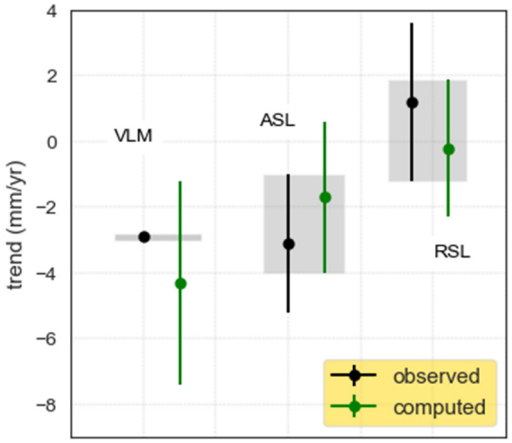

Figure 7. The comparison of linear trend estimates from observed data (black) and those computed (green) at Porto Garibaldi. Dots represent the central values with their standard deviation depicted by the line. Grey areas show the common interval between the different datasets trend values. It can be noted that the values of the observed and computed trends match within their error bars.

For the case of Marina di Ravenna and Rimini, only *S* and *N* can be directly determined, since GNSS instruments are not co-located at these TGs. Then, Equation (1) can be applied to indirectly estimate *U*. Figure 8 shows the time series (SA-TG) for Marina di Ravenna and Rimini (with their related errors) whose rate (Table 5), according to Equation (1), should represent ($U = N - S$). These values are quite unexpected since subsidence at Marina di Ravenna is known to be larger (see Table 4); at Rimini this contrasts with the observed subsidence (Table 4). However, if *U* for Marina di Ravenna is computed on the reduced timespan for which GNSS data exist (July 1996–December 2015) the rate of VLM is -4.7 ± 0.6 mm/year, smaller than that provided by the GNSS located near TG_{RA} (-5.6 ± 0.2 mm/year). The two results do not match within their error bar for only 0.1 mm/year. As mentioned above, this GNSS is in the vicinity of TG_{RA} and, the larger the distance between GNSS and TG, the smaller the representativeness of the real VLM at the TG. It has been observed that, when large heterogeneities exist, a few hundred meters of distance between TG and GNSS stations can cause decoupled movements [18]. This seems to be the case for the Marina di Ravenna harbor where Cerenzia et al. [60] found different rates of subsidence at very short distances, likely due to the weight effect of the structures themselves (e.g., the embankment with respect to the dock and the lighthouse). Fenoglio-Marc et al. [68] reports similar results for the Marina di Ravenna site, where GNSS observations provide a higher VLM rate with respect to the one computed from SA and TG difference, attributing it to anthropogenic causes, to the distance between the TG and the closest SA grid point and to the corrections applied on the RSL time series.

At Rimini, the context appears completely different with respect to Marina di Ravenna and Porto Garibaldi. Despite the high correlation between TG_{RN} with SA_{RN}, at Rimini the RSL shows a negative trend (Figure 3), although the small timespan covered by TG_{RN} time series gives at this data very low statistical significance (Tables 2 and 3). The time series (SA-TG) shows a positive trend for *U* (Table 5) indicating a "proxy-derived" local effect of land uplift (Figure 8), in contrast with the VLM rates (0.00 ± 0.8 for the timespan 2011–2016) provided by the ITRN station. GNSS values agree with recent subsidence monitoring activities using InSAR (Table 4). The error associated with InSAR measure is 2 mm/year, suggesting that for the period 2011–2016, some portion of the Rimini area that includes the GNSS and TG stations may undergo opposite VLMs (uplift) with respect to other sectors of the E-R coastal belt. At Rimini, the GNSS station is located 2.6 km apart from the TG and this makes the data comparison even less effective than for the case of Marina di Ravenna [18]. Measured subsidence at Rimini has markedly decreased in the last two decades [57] and it cannot be excluded that VLM could reverse in the next decades;

unfortunately, to date there is not enough data to support this hypothesis and more years of data acquisition are required.

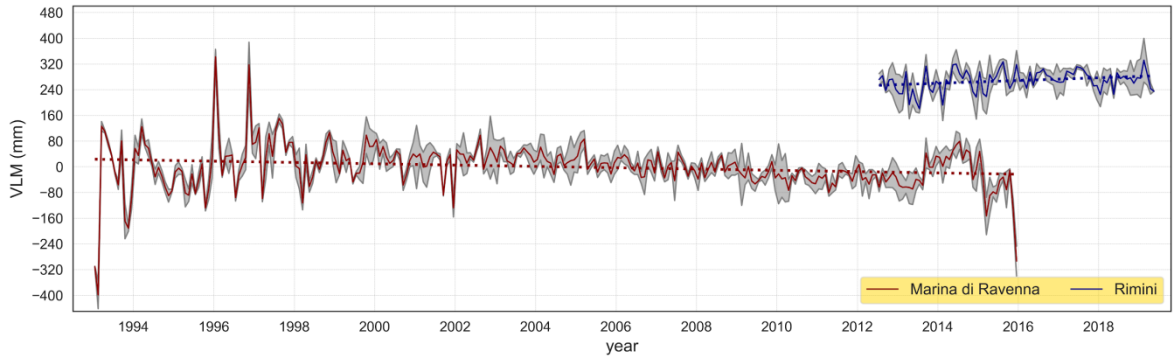

Figure 8. Time series of the $N - S = U$ term at Marina di Ravenna (red) and Rimini (blue) computed by using Equation (1). Gray area represents data error range. The time series are shifted in the vertical scale for presentation purposes.

6.3. The Sea-Level Trend Acceleration Issue

As anticipated in the introduction, at global scale the sea level has been rising at a rate of 3.3 ± 0.5 mm/year [3], with a positive acceleration of 0.084 ± 0.025 mm/year^2 [4] over the altimetric era (1993–present). Global maps show that the sea-level rise is not spatially uniform, with a diffused pattern of null rate and even showing a sea-level fall, see [125]. Then, it is not surprising that this heterogeneity also reflects in different local sea-level acceleration as for the case of the small spot target of this study in which we observe, for the same period, a negative acceleration of –0.3 mm/year^2. Acceleration could be the consequence of global short-lived phenomena, as for the case of the Pinatubo eruption in 1991 [126] or of climatological events. Moreover, given the length of the SA time series, accelerations could be also a consequence of the contribution of multidecadal oscillations for which only a portion of it is sampled. Because of this consideration, the observation of a full cycle (at least) is required to properly model the oscillation itself, determine its origin, and its plausible relation with climate change. Unfortunately, since the satellite altimeter era only started in 1993, and long-term TG observations are contaminated by an unknown non-linear VLM (measured only since co-located GNSS acquisition started, i.e., in the late 1990s), it is currently complicate to properly attribute to the ongoing observed regional sea-level variations to climatological origin. In our case, we observe a localized negative acceleration for the E-R coast, whose interpretation should be put in the broader context of the Mediterranean Sea in which a marked spatial variability of sea-level trend is observed, for instance, by Bonaduce et al. [100]. The ASL negative acceleration observed at the E-R coast in recent decades (Figure 2a; Table 1) has been previously noted by other authors. After a positive acceleration of sea-level rise observed in the Mediterranean Sea during the 1990s [127] since the early 2000s, in fact, the sea level stopped rising [128–130]; this seems to match well with the quadratic fit shown for SA in Figure 2a. As previously explained in Section 6.1, ocean–atmosphere oscillations are responsible for inter-annual and interdecadal cyclic sea-level variations in the Mediterranean; the main engine of these phenomena has been associated, at a global scale, with natural modes (e.g., the NAO and the AMO) inducing temporary reductions or magnification of sea-level trend amplitude at the basin to regional scale [103]. Besides this inter-annual variability, changes in sea-level acceleration on multidecadal time scales have been documented by several authors for the whole 20th century which is generally characterized by a greater rate in the first half, followed by an overall negative acceleration [43,131–133]; however, the processes causing this variability, and their link to climate change, are not completely understood yet.

We showed in Section 5.1 that the SA time series, shortened for matching with the TG time series (Figure 3), provide rates differing from what observed for the complete SA time

series (January 1993–May 2019, Figure 2a). In particular, in the case of SA_{PG} and SA_{RN}, rates turn negative (Table 3; although for Rimini the hypothesis of no trend could not be rejected), consistently with the observed negative acceleration (Table 1). For the Marina di Ravenna site, the overlapping timespan (1993–2015) is long enough to obtain, from the quadratic regression, a significant acceleration in the time series (Figure 3). Namely we get 0.7 ± 0.3 mm/year^2 for TG_{RA} and -0.2 ± 0.2 mm/year^2 for SA_{RA}. The opposite signs suggest that two different phenomena govern the two accelerations and a good candidate could be VLM that, as mentioned above, is governed here by subsidence. From Equation (1), the VLM acceleration is the difference between those of the two terms mentioned above, and it results equal to -0.9 ± 0.4 mm/year^2. Actually, subsidence is slowing down in the region and locally in the surrounding of TG_{RA} as resulting from Table 1, and this should reflect in a positive acceleration in the ongoing negative VLM. We can then argue that what we are observing at TG_{RA} is something different from the effects of the local subsidence or, more likely, other phenomena are governing the acceleration at TG_{RA}.

At the regional scale, the decrease of subsidence measured by the E-R Coastal Geodetic Network over recent decades (see Table 4) is a favorable indication in terms of reducing future flooding vulnerability for this area. However, as already pointed out by Cerenzia et al. [60] and Fenoglio-Marc et al. [68], and discussed at Section 6.2, different rates of VLM are available, depending on the precise site of measurement and not necessarily representative of the VLM at the TG location. We thus remark the need for local and repeated VLM measurements at the TG site to correctly interpret RSL series and for detecting possible ASL positive or negative accelerations.

7. Conclusions

In this paper, we have studied the sea-level variation along the E-R coast by focusing on monthly sea-level observations from the three available TGs located at Porto Garibaldi, Marina di Ravenna, and Rimini. Data are compared with CMEMS SA data from the three grid points closer to each of the TGs; The combined use of altimetry and tide gauge data (supplemented by GNSS acquisition) is considered, in fact, a promising approach, in terms of precision and cost-effective implementation, to better define various physical processes in the coastal domains and to anticipate the impacts of future rise in sea levels [10,11,22,69,134–137].

Our results show that the ASL time series (from SA) are coherent along the coastal tract, providing a rate of 2.8 ± 0.5 mm/year for the timespan Jan 1993–May 2019, smaller but comparable to the global average (3.3 ± 0.5 mm/year). Moreover, we note in the E-R coast a negative acceleration of $-0.3 \pm 0{,}1$ mm/year^2 that contrasts with the positive global acceleration. The comparison with the IB-corrected TG time series suffers from the short overlapping period between the two different datasets (Jul. 2009–May 2019 at Porto Garibaldi; Jan 1993–Dec 2015 at Marina di Ravenna; Jul. 2012–May 2019 at Rimini). Despite their shortness, the SA and TG time series show high correlation coefficient (0.89) at Porto Garibaldi and Rimini, and a moderate one (0.66) at Marina di Ravenna. The lower correspondence achieved at Marina di Ravenna, as well as the difference between ASL and RSL rates for this site (Table 3), are mostly associated with the local rate of VLM. Actually, VLM can hamper the detection of signals associated with sea-level change and related spatial variations [22]. For all the three analyzed sites, this remains an important contribution to quantify. It is remarked the need for co-located monitoring of the ground motions at the TG sites, since the determination of VLM is a key element in understanding how sea level has changed over the past century and how future sea levels may impact coastal areas [22].

Finally, as already observed for other coastal areas [11,13,69], the good match between altimetry and in situ observation confirms that high-standard satellite product can provide consistent data even at short distance from the coast. Linking satellite altimetry measurements with tide gauge, by bridging the open-ocean measurements with those in proximity of the coast [12] is part of a new challenge in monitoring sea-level rise along coastal tracts. In this view, the maintenance and implementation of observation stations for continuous

monitoring of sea level in the coastal zone is a fundamental tool for coastal management and defense strategies.

Author Contributions: Conceptualization, M.M., M.O. and C.R.; Formal analysis, M.M. and M.O.; Investigation, M.M., M.O. and C.R.; Methodology, M.M. and M.O.; Visualization, M.M. and M.O.; Writing—original draft, M.M., M.O. and C.R.; Writing—review & editing, M.M., M.O. and C.R. All authors have read and agreed to the published version of the manuscript.

Funding: This research received no external funding. Ph.D. fellowship of M.M. is financed through the Strategic Development Project of the BiGeA Department, University of Bologna. M.O. research was partly funded by the Istituto Nazionale di Geofisica e Vulcanologia departmental project MACMAP.

Institutional Review Board Statement: Not applicable.

Informed Consent Statement: Not applicable.

Acknowledgments: The authors would like to thank the Hera Group corporation, the PSMSL and the CMEMS for their support and for making data available. We thank Susanna Zerbini, Enrico Serpelloni, Stefano Gandolfi, Fabio Raicich, Davide Putero, Giorgio Spada, Luciana Fenoglio-Marc, Marcello Passaro and ARPAE-SIMC for helpful feedback on technical and scientific aspects. Marco Anzidei and three anonymous reviewers are acknowledged for their fruitful comments and suggestions that helped improving the paper. This work was supported by the University of Bologna, Ph.D. course in *Future Earth, Climate Change and Societal Challenges*.

Conflicts of Interest: The authors declare no conflict of interest.

Abbreviations

AMO	Atlantic Multidecadal Oscillation
ARPAE	Regional Agency for Prevention, Environment, and Energy of the Emilia-Romagna region
ASL	Absolute Sea Level
CMEMS	Copernicus Marine Environment Service
DAC	Dynamic Atmospheric Corrections
DInSAR	Differential Synthetic-Aperture Radar Interferometry
DUACS	Data Unification and Altimeter Combinations System
E-R	Emilia-Romagna
EAC	Eastern Adriatic Current
ECMWF	European Centre for Medium-Range Weather Forecasts
ECV	Essential Climate Variable
EMD	Empirical Mode Decomposition
ENSO	El Niño Southern Oscillation
ERF	Effective Radiative Forcing
GARI	Permanent GNSS station co-located at Porto Garibaldi tide gauge
GCOS	Global Climate Observing System
GIA	Glacial Isostatic Adjustment
GNSS	Global Navigation Satellite System
HF	High Frequencies response of sea level to wind and pressure forcing effects
Hs	Significant wave Height
IB	Inverse Barometer effect
IGS	International GPS Service
IMF	Intrinsic Mode Function
InSAR	Interferometric Synthetic-Aperture Radar
INGV	Istituto Nazionale di Geofisica e Vulcanologia
IOC	Intergovernmental Oceanographic Commission of UNESCO
IPCC	Intergovernmental Panel on Climate Change

GCOS	Global Climate Observing System
LSP	Lomb–Scargle Periodogram
NAO	North Atlantic Oscillation
NGL	Nevada Geodetic Laboratory
OLS	Ordinary Least Square regression
PSMSL	Permanent Service for Mean Sea Level
RLR	Revised Local Reference
RMN	Italian National Tide Gauge Network
RSL	Relative Sea Level
SA	Satellite Altimetry
SA_{PG}	Closest altimetry pixel to Porto Garibaldi tide gauge
SA_{RA}	Closest altimetry pixel to Marina di Ravenna tide gauge
SA_{RN}	Closest altimetry pixel to Rimini tide gauge
SLE	Sea-Level Equation
SSH	Sea Surface Height
TG	Tide Gauge
TG_{PG}	Tide Gauge at Porto Corsini
TG_{RA}	Tide Gauge at Marina di Ravenna
TG_{RN}	Tide Gauge at Rimini
UNFCCC	United Nations Framework Convention on Climate Change
VLM	Vertical Land Movement
WAC	Western Adriatic Current

Appendix A

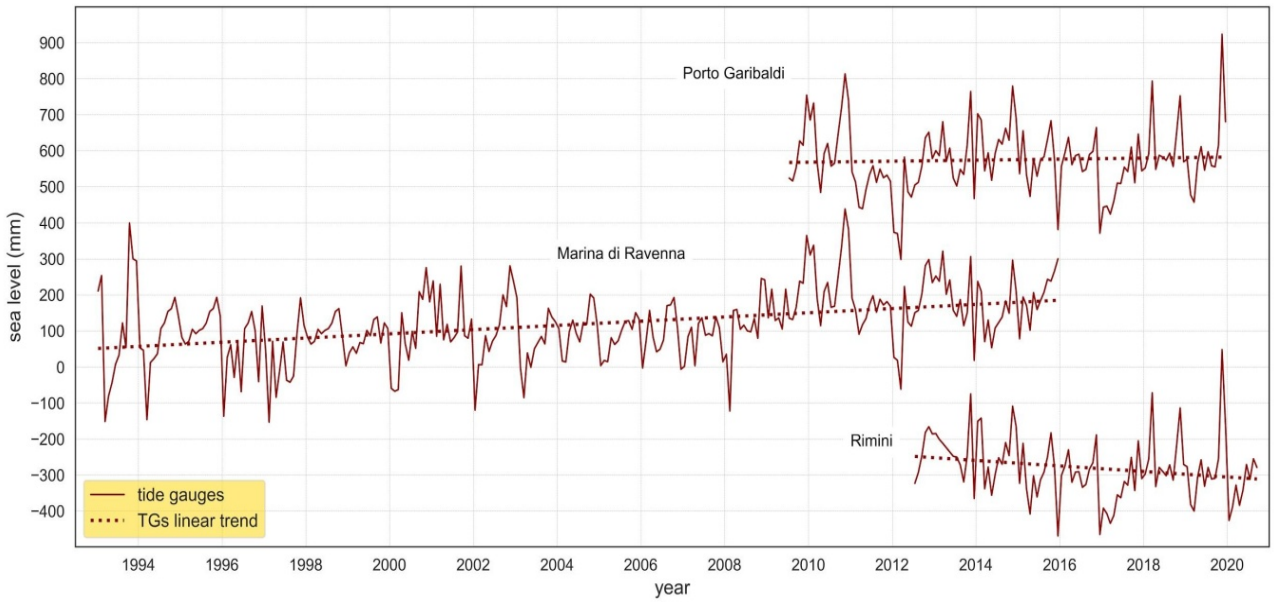

Figure A1. Raw TG time series. Dotted lines represent estimated linear models resulting from OLS regression. The offsets between the time series are arbitrary for better readability.

Table A1. Linear sea-level trend estimates (and related corrections applied) from some of the most representative studies conducted on the Marina di Ravenna TG time series. Time frames considered by various authors are indicated in brackets.

	Rate (mm/year)	Type of Data Considered
Antonioli et al., 2017	8.3 ± 0.3	monthly mean (2000–2013)
Bruni et al., 2019	1.25 ± 0.16	monthly mean (1873–2016), detrended for non-linear VLM
Cerenzia et al., 2016	8.5 ± 0.2	annual mean (1897–2014)
	7.7 ± 0.3	monthly mean (1970–2013)
	9.8 ± 1.3	annual mean (1990–2013)
	(2.2 ± 1.3)	(detrended for linear VLM)
Fenoglio-Marc et al., 2012	6.5 ± 1.5	monthly mean (1993–2008), IB correction, deseasoning
Masina and Lamberti, 2013	8.6 ± 0.5	annual mean (1896–2011)
	3.1 ± 0.7	annual mean (1896–1950)
	10.3 ± 8.0	annual mean (2000–2011)
Tsimplis et al., 2012	3.1 ± 1.3	annual mean (1897–1921)
	1.5 ± 1.3	annual mean (1905–1921), normalized for Trieste
	8.4 ± 1.1	annual mean (1937–1972)
	(7.1 ± 0.8)	(normalized for Trieste)
	3.9 ± 0.6	daily mean
Zerbini et al., 2017	1.22 ± 0.32	annual mean (1896–2012), IB correction, detrended for non-linear VLM
	1.05 ± 0.54	annual mean (1934–2012), IB correction, detrended for non-linear VLM

References

1. Matthäus, W. On the History of Recording Tide Gauges. *Proc. R. Soc. Edinb. Sect. B Biol.* **1972**, *73*, 26–34. [CrossRef]
2. Church, J.A.; Clark, P.U.; Cazenave, A.; Gregory, J.M.; Jevrejeva, S.; Levermann, A.; Merrifield, M.A.; Milne, G.A.; Nerem, R.S.; Nunn, P.D.; et al. Sea level change. In *Climate Change 2013: The Physical Science Basis. Contribution of Working Group I to the Fifth Assessment Report of the Intergovernmental Panel on Climate Change*; Stocker, T.F., Qin, D., Plattner, G.-K., Tignor, M., Allen, S.K., Boschung, J., Nauels, A., Xia, Y., Bex, V., Midgley, P.M., Eds.; Cambridge University Press: Cambridge, UK; New York, NY, USA, 2013; pp. 1139–1216.
3. Legeais, J.-F.; Ablain, M.; Zawadzki, L.; Zuo, H.; Johannessen, J.A.; Scharffenberg, M.G.; Fenoglio-Marc, L.; Fernandes, M.J.; Andersen, O.B.; Rudenko, S.; et al. An improved and homogeneous altimeter sea level record from the ESA Climate Change Initiative. *Earth Syst. Sci. Data* **2018**, *10*, 281–301. [CrossRef]
4. Nerem, R.S.; Beckley, B.D.; Fasullo, J.T.; Hamlington, B.D.; Masters, D.; Mitchum, G.T. Climate-change–driven accelerated sea-level rise detected in the altimeter era. *Proc. Natl. Acad. Sci. USA* **2018**, *115*, 2022–2025. [CrossRef] [PubMed]
5. Dangendorf, S.; Hay, C.; Calafat, F.M.; Marcos, M.; Piecuch, C.G.; Berk, K.; Jensen, J. Persistent acceleration in global sea-level rise since the 1960s. *Nat. Clim. Chang.* **2019**, *9*, 705–710. [CrossRef]
6. Nicholls, R.J.; Marinova, N.; Lowe, J.A.; Brown, S.; Vellinga, P.; de Gusmão, D.; Hinkel, J.; Tol, R.S.J. Sea-level rise and its possible impacts given a 'beyond 4 °C world' in the twenty-first century. *Phil. Trans. Soc. A* **2011**, *369*, 161–181. [CrossRef]
7. Neumann, B.; Vafeidis, A.T.; Zimmermann, J.; Nicholls, R.J. Future Coastal Population Growth and Exposure to Sea-Level Rise and Coastal Flooding—A Global Assessment. *PLoS ONE* **2015**, *10*, e0118571. [CrossRef]
8. Andersen, O.B.; Scharroo, R. Range and geophysical corrections in coastal regions: And implications for mean sea surface determination. In *Coastal Altimetry*; Vignudelli, S., Kostianoy, A., Cipollini, P., Benveniste, J., Eds.; Springer: Berlin, Germany, 2011; pp. 103–146. [CrossRef]
9. Roblou, L.; Lamouroux, J.; Bouffard, J.; Lyard, F.; Le Hénaff, M.; Lombard, A.; Marsaleix, P.; De Mey, P.; Birol, F. Post-processing altimeter data towards coastal applications and integration into coastal models. In *Coastal Altimetry*; Vignudelli, S., Kostianoy, A., Cipollini, P., Benveniste, J., Eds.; Springer: Berlin, Germany, 2011; pp. 217–246. [CrossRef]

10. Vignudelli, S.; Birol, F.; Benveniste, J.; Fu, L.-L.; Picot, N.; Raynal, M.; Roinarn, H. Satellite Altimetry Measurements of Sea Level in the Coastal Zone. *Surv. Geophys.* **2019**, *40*, 1319–1349. [CrossRef]
11. Cipollini, P.; Calafat, F.M.; Jevrejeva, S.; Melet, A.; Prandi, P. Monitoring sea level in the coastal zone with satellite altimetry and tide gauges. *Surv. Geophys.* **2017**, *38*, 33–57. [CrossRef]
12. Cipollini, P.; Benveniste, J.; Birol, F.; Fernandes, M.J.; Obligis, E.; Passaro, M.; Strub, P.T.; Valladeau, G.; Vignudelli, S.; Wilkin, J. Satellite altimetry in coastal regions. In *Satellite Altimetry over the Oceans and Land Surfaces*; Stammer, D., Cazenave, A., Eds.; CRC Press: Boca Raton, FL, USA, 2017; pp. 343–380.
13. Marti, F.; Cazenave, A.; Birol, F.; Passaro, M.; Léger, F.; Niño, F.; Almar, R.; Benveniste, J.; Legeais, J.F. Altimetry-based sea level trends along the coasts of Western Africa. *Adv. Space Res.* **2019**. [CrossRef]
14. Woodworth, P.L.; Player, R. The permanent service for mean sea level: An update to the 21st century. *J. Coast. Res.* **2003**, *19*, 287–295.
15. Holgate, S.J.; Matthews, A.; Woodworth, P.L.; Rickards, L.J.; Tamisiea, M.E.; Bradshaw, E.; Foden, P.R.; Gordon, K.M.; Jevrejeva, S.; Pugh, J. New Data System and Products at the Permanent Service for Mean Sea Level. *J. Coast. Res.* **2013**, *29*, 493–504. [CrossRef]
16. Permanent Service for Mean Sea Level (PSMSL). Tide Gauge Data. Available online: http://www.psmsl.org/data/obtaining/ (accessed on 1 June 2020).
17. Zerbini, S.; Plag, H.-P.; Baker, T.; Becker, M.; Billiris, H.; Burki, B.; Kahle, H.-G.; Marsone, I.; Pezzoli, L.; Richter, B.; et al. Sea level in the Mediterranean: A first step towards separating crustal movements and absolute sea-level variations. *Glob. Planet Chang.* **1996**, *14*, 1–48. [CrossRef]
18. Bouin, M.-N.; Wöppelmann, G. Land motion estimates from GPS at tide gauges: A geophysical evaluation. *Geophys. J. Int.* **2010**, *180*, 193–209. [CrossRef]
19. Gröger, M.; Plag, H.-P. Estimations of a global sea level trend: Limitations from the structure of the PSMSL global sea level data set. *Glob. Planet. Chang.* **1993**, *8*, 161–179. [CrossRef]
20. Farrell, W.E.; Clark, J.A. On Postglacial Sea Level. *Geophys. J. R. Astr. Soc.* **1976**, *46*, 647–667. [CrossRef]
21. Ostanciaux, E.; Husson, L.; Choblet, G.; Robin, C.; Pedoja, K. Present-day trends of vertical ground motion along the coast lines. *Earth Sci. Rev.* **2012**, *110*, 74–92. [CrossRef]
22. Wöppelmann, G.; Marcos, M. Vertical land motion as a key to understanding sea level change and variability. *Rev. Geophys.* **2016**, *54*, 64–92. [CrossRef]
23. Mellor, G.L.; Ezer, T. Sea level variations induced by heating and cooling: An evaluation of the Boussinesq approximation in ocean models. *J. Geophys. Res.* **1995**, *100*, 20565–20577. [CrossRef]
24. Levitus, S.; Antonov, J.I.; Boyer, T.P.; Baranova, O.K.; Garcia, H.E.; Locarnini, R.A.; Mishonov, J.R.; Reagan, J.R.; Seidov, D.; Yarosh, E.S.; et al. World ocean heat content and thermosteric sea level change (0–2000 m), 1955–2010. *Geophys. Res. Lett.* **2012**, *39*. [CrossRef]
25. Milly, P.C.D.; Cazenave, A.; Gennero, C. Contribution of climate-driven change in continental water storage to recent sea-level rise. *Proc. Natl. Acad. Sci. USA* **2003**, *100*, 13158–13161. [CrossRef]
26. Ngo-Duc, T.; Laval, K.; Polcher, J.; Lombard, A.; Cazenave, A. Effects of land water storage on global mean sea level over the past half century. *Geophys. Res. Lett.* **2005**, *32*, L09704. [CrossRef]
27. Meier, M.F.; Dyurgerov, M.B.; Rick, U.K.; O'Neel, S.; Pfeffer, W.T.; Anderson, R.S.; Anderson, S.P.; Glazovsky, A.F. Glaciers dominate Eustatic sea-level rise in the 21st century. *Science* **2007**, *317*, 1064–1067. [CrossRef] [PubMed]
28. Stammer, D.; Cazenave, A.; Ponte, R.M.; Tamisiea, M.E. Causes for contemporary regional sea level changes. In *Annual Review of Marine Science*; Carlson, C.A., Giovannoni, S.J., Eds.; Annual Reviews: Palo Alto, CA, USA, 2013; Volume 5, pp. 21–46.
29. Oppenheimer, M.; Glavovic, B.C.; Hinkel, J.; van de Wal, R.; Magnan, A.K.; Abd-Elgawad, A.; Cai, R.; Cifuentes-Jara, M.; DeConto, R.M.; Ghosh, T.; et al. Sea Level Rise and Implications for Low-Lying Islands, Coasts and Communities. In *IPCC Special Report on the Ocean and Cryosphere in a Changing Climate*; Pörtner, H.-O., Roberts, D.C., Masson-Delmotte, V., Zhai, P., Tignor, M., Poloczanska, E., Mintenbeck, K., Alegrìa, A., Nicolai, M., Okem, A., et al., Eds.; in press; Available online: https://www.ipcc.ch/srocc/chapter/chapter-4-sea-level-rise-and-implications-for-low-lying-islands-coasts-and-communities/ (accessed on 25 December 2020).
30. Pinardi, N.; Bonaduce, A.; Navarra, A.; Dobricic, S.; Oddo, P. The Mean Sea Level Equation and Its Application to the Mediterranean Sea. *J. Clim.* **2014**, *27*, 442–447. [CrossRef]
31. Bilbao, R.A.F.; Gregory, J.M.; Bouttes, N. Analysis of the regional pattern of sea level change due to ocean dynamics and density change for 1993-2099 in observations and CMIP5 AOGCMs. *Clim. Dyn.* **2015**, *45*, 2647–2666. [CrossRef]
32. Lambeck, K.; Smither, K.; Johnston, P. Sea-level change, glacial rebound and mantle viscosity for northern Europe. *Geophys. J. Int.* **1998**, *134*, 102–144. [CrossRef]
33. Peltier, W.R. Global glacial isostasy and the surface of the ice-age Earth: The ICE-5G (VM2) model and GRACE. *Annu. Rev. Earth Planet. Sci.* **2004**, *32*, 111–149. [CrossRef]
34. Chambers, D.P.; Wahr, J.; Tamisiea, M.E.; Nerem, R.S. Ocean mass from GRACE and glacial isostatic adjustment. *J. Geophys. Res.* **2010**, *115*, B11415. [CrossRef]
35. Marcos, M.; Tsimplis, M. Forcing of coastal sea-level rise patterns in the North Atlantic and Mediterranean Sea. *Geophys. Res. Lett.* **2007**, *34*, L18604. [CrossRef]

36. Gomis, D.; Ruiz, S.; Sotillo, M.G.; Álvarez-Fanjul, E.; Terradas, J. Low frequency Mediterranean sea level variability: The contribution of atmospheric pressure and wind. *Glob. Planet. Chang.* **2008**, *63*, 215–229. [CrossRef]
37. Tsimplis, M.N.; Baker, T.F. Sea level drop in the Mediterranean Sea: An indicator of deep water salinity and temperature changes? *Geophys. Res. Lett.* **2000**, *27*, 1731–1734. [CrossRef]
38. Pinardi, N.; Masetti, E. Variability of the large scale general circulation of the Mediterranean Sea from observations and modelling: A review. *Palaeogeogr. Palaeoclimatol. Palaeoecol.* **2000**, *158*, 153–173. [CrossRef]
39. Calafat, F.M.; Chambers, D.P.; Tsimplis, M.N. Mechanism of decadal sea level variability in the eastern North Atlantic and the Mediterranean Sea. *J. Geophys. Res.* **2012**, *117*, C09022. [CrossRef]
40. Landerer, F.W.; Volkov, D.L. The anatomy of recent large sea level fluctuations in the Mediterranean Sea. *Geophys. Res. Lett.* **2013**, *40*, 553–557. [CrossRef]
41. Tsimplis, M.N.; Raicich, F.; Fenoglio-Marc, L.; Shaw, A.G.P.; Marcos, M.; Somot, S.; Bergamasco, F. Recent developments in understanding sea level rise in the Adriatic coasts. *Phys. Chem. Earth Parts A/B/C* **2012**, *40–41*, 59–71. [CrossRef]
42. Holgate, S.J. On the decadal rates of sea level change during the twentieth century. *Geophys. Res. Lett.* **2007**, *34*, L01602. [CrossRef]
43. Woodworth, P.L.; White, N.J.; Jevrejeva, S.; Holgate, S.J.; Church, J.A.; Gehrels, W.R. Evidence for the accelerations of sea level on multi-decade and century timescales. *Int. J. Climatol.* **2009**, *29*, 777–789. [CrossRef]
44. Lozier, M.S.; Roussenov, V.; Reed, M.S.C.; Williams, R.G. Opposing decadal changes for the North Atlantic Meridional Overturning Circulation. *Nat. Geosci.* **2010**, *3*, 728–734. [CrossRef]
45. Galassi, G.; Spada, G. Linear and non-linear sea-level variations in the Adriatic Sea from tide gauge records (1872–2012). *Ann. Geophys.* **2014**, *57*, P0658. [CrossRef]
46. Lorito, S.; Calabrese, L.; Perini, L.; Cibin, U. Uso del suolo della costa. In *Il Sistema Mare-Costa dell'Emilia-Romagna*; Perini, L., Calabrese, L., Eds.; Edizioni Pendragon: Bologna, Italy, 2010; pp. 109–118.
47. Marsico, A.; Lisco, S.; Lo Presti, V.; Antonioli, F.; Amorosi, A.; Anzidei, M.; Deiana, G.; De Falco, G.; Fontana, A.; Fontolan, G.; et al. Flooding scenario for four Italian coastal plains using three relative sea level rise models. *J. Maps* **2017**, *13*, 961–967. [CrossRef]
48. Perini, L.; Calabrese, L.; Luciani, P.; Olivieri, M.; Galassi, G.; Spada, G. Sea-level rise along the Emilia-Romagna coast (Northern Italy) in 2100: Scenarios and impacts. *Nat. Hazards Earth Syst. Sci.* **2017**, *17*, 2271–2287. [CrossRef]
49. Simoncelli, S.; Fratianni, C.; Pinardi, N.; Grandi, A.; Drudi, M.; Oddo, P.; Dobricic, S. Mediterranean Sea Physical Reanalysis (CMEMS MED-Physics) [Data set]. *Copernic. Monit. Environ. Mar. Serv.* **2019**. [CrossRef]
50. Gambolati, G.; Teatini, P. Numerical analysis of land subsidence due to natural compaction of the Upper Adriatic Sea basin. In *CENAS, Coastline Evolution of the Upper Adriatic Sea due to Sea Level Rise and Natural and Anthropogenic Land Subsidence*; Gambolati, G., Ed.; Kluwer Academic Publishing, Water Science & Technology Library: Norwell, MA, USA, 1998; Volume 28, pp. 103–131.
51. Ferranti, L.; Antonioli, F.; Anzidei, M.; Monaco, C.; Stocchi, P. The timescale and spatial extent of vertical tectonic motions in Italy: Insights from relative sea-level changes studies. *J. Virtual Explor.* **2010**, *36*, 1441–8142. [CrossRef]
52. Antonioli, F.; Anzidei, M.; Lambeck, K.; Auriemma, R.; Gaddi, D.; Furlani, S.; Orrù, P.; Solinas, E.; Gaspari, A.; Karinja, S.; et al. Sea level change in Italy during Holocene from archaeological and geomorphological data. *Quat. Sci. Rev.* **2007**, *26*, 2463–2486. [CrossRef]
53. Antonioli, F.; Ferranti, L.; Fontana, A.; Amorosi, A.; Bondesan, A.; Braitenberg, C.; Dutton, A.; Fontolan, G.; Furlani, S.; Lambeck, K.; et al. Holocene relative sea-level changes and vertical movements along the Italian coastline. *Quat. Int.* **2009**, *206*, 102–133. [CrossRef]
54. Teatini, P.; Ferronato, M.; Gambolati, G.; Bertoni, W.; Gonella, M. A century of land subsidence in Ravenna, Italy. *Environ. Geol.* **2005**, *47*, 831–846. [CrossRef]
55. Aguzzi, M.; Bonsignore, F.; De Nigris, N.; Paccagnella, T.; Romagnoli, C.; Unguendoli, S. *Stato del Litorale Emiliano-Romagnolo al 2012. Erosione e Interventi di Difesa*; I Quaderni di ARPAE: Bologna, Italy, 2016; p. 277. ISBN 978-88-87854-41-1.
56. Pirazzoli, P.A. Secular trends of relative sea-level (RSL) changes indicated by tide-gauge records. *J. Coast. Res.* **1986**, *S11*, 1–26.
57. Aguzzi, M.; Costantino, R.; De Nigris, N.; Morelli, M.; Romagnoli, C.; Unguendoli, S.; Vecchi, E. *Stato del Litorale Emiliano-Romagnolo al 2018. Erosione e Interventi di Difesa*; I Quaderni di ARPAE: Bologna, Italy; p. 259. ISBN 978-88-87854-41-1. in press.
58. Vecchi, E.; Aguzzi, M.; Albertazzi, C.; De Nigris, N.; Gandolfi, S.; Morelli, M.; Tavasci, L. Third beach nourishment project with submarine sands along Emilia-Romagna coast: Geomatic methods and first monitoring results. *Rend. Fis. Acc. Lincei* **2020**, *31*, 79–88. [CrossRef]
59. Montuori, A.; Anderlini, L.; Palano, M.; Albano, M.; Pezzo, G.; Antoncecchi, I.; Chiarabba, C.; Serpelloni, E.; Stramondo, S. Application and analysis of geodetic protocols for monitoring subsidence phenomena along on-shore hydrocarbon reservoirs. *Int. J. Appl. Earth Obs. Geoinf.* **2018**, *69*, 13–26. [CrossRef]
60. Cerenzia, I.; Putero, D.; Bonsignore, F.; Galassi, G.; Olivieri, M.; Spada, G. Historical and recent sea level rise and land subsidence in Marina di Ravenna, northern Italy. *Ann. Geophys.* **2016**, *59*, p0546. [CrossRef]
61. Ciavola, P.; Armaroli, C.; Chiggiato, J.; Valentini, A.; Deserti, M.; Perini, L.; Luciani, P. Impact of storms along the coastline of Emilia-Romagna: The morphological signature on the Ravenna coastline (Italy). *J. Coast. Res.* **2007**, *SI50*, 540–544.
62. Sedrati, M.; Ciavola, P.; Reyns, J.; Armaroli, C.; Sipka, V. Morphodynamics of a Microtidal Protected Beach during Low Wave-energy Conditions. *J. Coast. Res.* **2009**, *SI56*, 198–202.
63. Orlić, M.; Gačić, M.; La Violette, P.E. The currents and circulation of the Adriatic Sea. *Oceanol. Acta* **1992**, *15*, 109–124.

64. Artegiani, A.; Bregant, D.; Paschini, E.; Pinardi, N.; Raicich, F.; Russo, A. The Adriatic Sea general circulation. Part I: Air-sea interactions and water mass structure. *J. Phys. Oceanogr.* **1997**, *14*, 1492–1514. [CrossRef]
65. Artegiani, A.; Paschini, E.; Russo, A.; Bregant, D.; Raicich, F.; Pinardi, N. The Adriatic Sea general circulation. Part II: Baroclinic circulation structure. *J. Phys. Oceanogr.* **1997**, *27*, 1515–1532. [CrossRef]
66. Zore, M. On gradient currents in the Adriatic Sea. *Acta Adriat.* **1956**, *8*, 1–38.
67. Poulain, P.-M. Adriatic Sea surface circulation as derived from drifter data between 1990 and 1999. *J. Mar. Syst.* **2001**, *29*, 3–32. [CrossRef]
68. Fenoglio-Marc, L.; Braitenberg, C.; Turini, L. Sea level variability and trends in the Adriatic Sea in 1993-2008 from tide gauges and satellite altimetry. *Phys. Chem. Earth Parts A/B/C* **2012**, *40–41*, 47–58. [CrossRef]
69. Vignudelli, S.; De Biasio, F.; Scozzari, A.; Zecchetto, S.; Papa, A. Sea Level Trends and Variability in the Adriatic Sea and Around Venice. In *Fiducial Reference Measurements for Altimetry. International Association of Geodesy Symposia*; Mertikas, S., Pail, R., Eds.; Springer: Cham, Switzerland, 2019; Volume 150. [CrossRef]
70. Mohamed, B.; Abdallah, A.M.; Alam El-Din, K.; Nagy, H.; Shaltout, M. Inter-Annual Variability and Trends of Sea Level and Sea Surface Temperature in the Mediterranean Sea over the Last 25 years. *Pure Appl. Geophys.* **2019**, *176*, 3787–3810. [CrossRef]
71. GPS. Available online: https://www.sonel.org/-GPS-.html?lang=en (accessed on 19 August 2020).
72. Devoti, R.; D'Agostino, N.; Serpelloni, E.; Pietrantonio, G.; Riguzzi, F.; Avallone, A.; Cavaliere, A.; Cheloni, D.; Cecere, G.; D'Ambrosio, C.; et al. A Combined Velocity Field of the Mediterranean Region. *Ann. Geophys.* **2017**, *60*, S0215. [CrossRef]
73. Zerbini, S.; Raicich, F.; Prati, C.M.; Bruni, S.; Del Conte, S.; Errico, M.; Santi, E. Sea-level change in the Northern Mediterranean Sea from long-period tide gauge time series. *Earth-Sci. Rev.* **2017**, *167*, 72–87. [CrossRef]
74. Bruni, S.; Zerbini, S.; Raicich, F.; Errico, M. Rescue of the 1873-1922 high and low waters of the Porto Corsini/Marina di Ravenna (northern Adriatic, Italy) tide gauge. *J. Geod.* **2019**, *93*, 1227–1244. [CrossRef]
75. Pellegrinelli, A.; Bencivelli, S.; Lovo, S.; Crocetto, N.; Perfetti, N.; Ricchieri, F.; Russo, P. La stazione Mareografica Integrata di Porto Garibaldi. In Proceedings of the Atti 13a Conferenza Nazionale ASITA, Bari, Italy, 1–4 December 2009; pp. 1565–1570.
76. UNESCO/IOC. Manual on sea-level measurement and interpretation. In *IOC Manuals and Guides*; Intergovernmental Oceanographic Commission of UNESCO: Paris, France, 1985; Volume 14, p. 83.
77. Copernicus – Marine environment monitoring service Website. Available online: https://marine.copernicus.eu/ (accessed on 19 August 2020).
78. Global Climate Observing System (GCOS). Systematic Observation Requirements for Satellite-Based Data Products for Climate (2011 Update)—Supplemental Details to the Satellite-Based Component of the "Implementation Plan for the Global Observing System for Climate in Support of the UNFCCC (2010 update)", GCOS-154 (WMO). Available online: https://library.wmo.int/opac/doc_num.php?explnum_id=3710 (accessed on 19 August 2020).
79. Pascual, A.; Faugere, Y.; Larnicol, G.; Le Traon, P.Y. Improved description of the ocean mesoscale variability by combining four satellite altimeters. *Geophys. Res. Lett.* **2006**, *33*, L02611. [CrossRef]
80. Dibarboure, G.; Pujol, M-I.; Briol, F.; Le Traon, P.-Y.; Larnicol, G.; Picot, N.; Mertz, F.; Escudier, P.; Ablain, M. Jason-2 in DUACS: Updated System Description, First Tandem Results and Impact on Processing and Products. *Mar. Geod.* **2011**, *34*, 214–241. [CrossRef]
81. AVISO altimetry Website. Available online: https://www.aviso.altimetry.fr/ (accessed on 19 August 2020).
82. Wunsch, C.; Stammer, D. Atmospheric loading and the oceanic "inverted barometer" effect. *Rev. Geophys.* **1997**, *35*, 79–107. [CrossRef]
83. Carrere, L.; Lyard, F. Modeling the barotropic response of the global ocean to atmospheric wind and pressure forcing—Comparison with observations. *Geophys. Res. Lett.* **2003**, *30*, 1275. [CrossRef]
84. Copernicus Climate Change Service (C3S) (2017): ERA5: Fifth Generation of ECMWF Atmospheric Reanalyses of the Global Climate. Copernicus Climate Change Service Climate Data Store (CDS). Available online: https://cds.climate.copernicus.eu/cdsapp#!/home (accessed on 19 August 2020).
85. Spada, G.; Galassi, G. New estimates of secular sea level rise from tide gauge data and GIA modelling. *Geophys. J. Int.* **2012**, *191*, 1067–1094. [CrossRef]
86. Harris, C.R.; Millman, K.J.; van der Walt, S.J.; Gommers, R.; Virtanen, P.; Cournapeau, D.; Wieser, E.; Taylor, J.; Berg, S.; Smith, N.J.; et al. Array programming with NumPy. *Nature* **2020**, *585*, 357–362. [CrossRef]
87. Lomb, N.R. Least-squares frequency analysis of unequally spaced data. *Astrophys. Space Sci.* **1976**, *39*, 447–462. [CrossRef]
88. Scargle, J.D. Studies in astronomical time series analysis. *II—Statistical aspects of spectral analysis of unevenly spaced data." Astrophys. J.* **1982**, *263*, 835–853.
89. Ruf, T. The Lomb-Scargle Periodogram in Biological Rhythm Research: Analysis of Incomplete and Unequally Spaced time series. *Biol. Rhythm Res.* **1999**, *30*, 178–201. [CrossRef]
90. R Core Team. *R: A Language and Environment for Statistical Computing*; R Foundation for Statistical Computing: Vienna, Austria, 2020; Available online: https://www.R-project.org/ (accessed on 19 August 2020).
91. Huang, N.E.; Shen, Z.; Long, S.R.; Wu, M.C.; Shih, H.H.; Zheng, Q.; Yen, N.-C.; Tung, C.C.; Liu, H.H. The empirical mode decomposition and the Hilbert spectrum for nonlinear and non-stationary time series analysis. *Proc. R. Soc. Lond. Ser. A Math. Phys. Eng. Sci.* **1998**, *454*, 903–995. [CrossRef]

92. Loudet, L. Application of Empirical Mode Decomposition to the Detection of Sudden Ionospheric Disturbances by Monitoring the Signal of a Distant Very Low Frequency Transmitter. Creative Commons Version. 2009. Available online: https://sidstation.loudet.org/emd-en.xhtml (accessed on 19 August 2020).
93. Chambers, J.M. Linear models. In *Statistical Models in S*; Chambers, J.M., Hastie, T.J., Eds.; Wadsworth & Brooks/Cole: Pacific Grove, CA, USA, 1992.
94. Hollander, M.; Wolfe, D.A. Kendall and Spearman tests. In *Nonparametric Statistical Methods*; Wiley & Sons: Hoboken, NJ, USA, 1973; pp. 185–194.
95. Sea Level Research Group, University of Colorado. Available online: http://sealevel.colorado.edu (accessed on 19 August 2020).
96. Meyssignac, B.; Calafat, F.M.; Somot, S.; Rupolo, V.; Stocchi, P.; Cazenave, A. Two-dimensional reconstruction of the Mediterranean sea level over 1970-2006 from tide gauge data and regional ocean circulation model outputs. *Glob. Planet. Chang.* **2011**, *77*, 49–61. [CrossRef]
97. Vilibić, I.; Šepić, J.; Pasarić, M.; Orlić, M. The Adriatic Sea: A Long-Standing Laboratory for Sea Level Studies. *Pure Appl. Geophys.* **2017**, *174*, 3765–3811. [CrossRef]
98. Klein, M.; Lichter, M. Statistical analysis of recent Mediterranean Sea-Level data. *Geomorphology* **2009**, *107*, 3–9. [CrossRef]
99. Pasarić, M.; Orlić, M. Response of the Adriatic Sea Level to the planetary-scale atmospheric forcing. In *Sea Level Changes-Determination and Effects, Geophysical Monograph*; Woodworth, P.L., Ed.; American Geophysical Union: Washington, DC, USA, 1992; Volume 69, pp. 29–39.
100. Bonaduce, A.; Pinardi, N.; Oddo, P.; Spada, G.; Larnicol, G. Sea-level variability in the Mediterranean Sea from altimetry and tide gauges. *Clim. Dyn.* **2016**, *47*, 2851–2866. [CrossRef]
101. Tsimplis, M.N.; Woodworth, P.L. The global distribution of the seasonal sea level cycle calculated from coastal tide gauge data. *J. Geophys. Res.* **1994**, *99*, 16031–16039. [CrossRef]
102. Oddo, P.; Bonaduce, A.; Pinardi, N.; Guarnieri, A. Sensitivity of the Mediterranean sea level to atmospheric pressure and free surface elevation numerical formulation in NEMO. *Geosci. Model Dev.* **2014**, *7*, 3001–3015. [CrossRef]
103. Tsimplis, M.N.; Calafat, F.M.; Marcos, M.; Jordà, G.; Gomis, D.; Fenoglio-Marc, L.; Struglia, M.V.; Josey, S.; Chambers, D.P. The effect of the NAO on sea level and on mass changes in the Mediterranean Sea. *J. Geophys. Res. Oceans* **2013**, *118*, 944–952. [CrossRef]
104. Taylor, J.R. *An Introduction to Error Analysis: The Study of Uncertainties in Physical Measurements*; University Science Books: Mill Valley, CA, USA, 1997; p. 327.
105. Masina, M.; Lamberti, A. A nonstationary analysis for the Northern Adriatic extreme sea levels. *J. Geophys. Res. Oceans* **2013**, *118*, 3999–4016. [CrossRef]
106. Antonioli, F.; Anzidei, M.; Amorosi, A.; Lo Presti, V.; Mastronuzzi, G.; Deiana, G.; De Falco, G.; Fontana, A.; Fontolan, G.; Lisco, S.; et al. Sea-level rise and potential drowning of the Italian coastal plains: Flooding risk scenarios for 2100. *Quat. Sci. Rev.* **2017**, *158*, 29–43. [CrossRef]
107. Peltier, W.R.; Tushingham, A.M. Global sea level rise and the greenhouse effect—Might they be connected? *Science* **1989**, *244*, 806–810. [CrossRef] [PubMed]
108. Prandi, P.; Cazenave, A.; Becker, M. Is coastal mean sea level rising faster than the global mean? A comparison between tide gauges and satellite altimetry over 1993-2007. *Geophys. Res. Lett.* **2009**, *36*, L05602. [CrossRef]
109. Carminati, E.; Di Donato, G. Separating natural and anthropogenic vertical movements in fast subsiding areas: The Po plain (N. Italy) case. *Geophys. Res. Lett.* **1999**, *26*, 2291–2294. [CrossRef]
110. Zerbini, S.; (Department of Physics and Astronomy, University of Bologna, Bologna, Emilia-Romagna, Italy). Personal communication, 2020.
111. ARPAE. *Rilievo Della Subsidenza Nella Pianura Emiliano-Romagnola—Seconda Fase. Relazione Finale*; ARPAE: Bologna, Italy, 2018; p. 105.
112. Benedetti, L.; Tapponnier, P.; King, G.C.P.; Meyer, B.; Manighetti, I. Growth folding and active thrusting in the Montello region, Veneto, northern Italy. *J. Geophys. Res. Solid Earth* **2000**, *105*, 739–766. [CrossRef]
113. Fenoglio-Marc, L.; Dietz, C.; Groten, E. Vertical land motion in the Mediterranean Sea from altimetry and tide gauge stations. *Mar. Geod.* **2004**, *27*, 683–701. [CrossRef]
114. Garcia, D.; Vigo, I.; Chao, B.F.; Martinez, M.C. Vertical crustal motion along the Mediterranean and Black Sea coast derived from ocean altimetry and tide gauge data. *Pure Appl. Geophys.* **2007**, *64*, 851–863. [CrossRef]
115. Wöppelmann, G.; Marcos, M. Coastal sea level rise in southern Europe and the nonclimate contribution of vertical land motion. *J. Geophys. Res.* **2012**, *117*, C01007. [CrossRef]
116. Nerem, R.S.; Mitchum, G.T. Estimates of vertical crustal motion derived from differences of TOPEX/POSEIDON and tide gauge sea level measurements. *Geophys. Res. Lett.* **2002**, *29*, 1934–1938. [CrossRef]
117. Shum, C.; Kuo, C.; Mitrovica, J.X. Glacial Isostatic Adjustment in the Great Lakes region inferred by tide gauges and satellite altimetry. Available online: https://ui.adsabs.harvard.edu/abs/2002AGUSM.U42A..14S/abstract (accessed on 19 August 2020).
118. Larsen, C.F.; Echelmeyer, K.A.; Freymueller, J.T.; Motyka, R.J. Tide gauge records of uplift along the northern Pacific-North American plate boundary, 1937 to 2001. *J. Geophys. Res.* **2003**, *108*, 2216–2231. [CrossRef]
119. Aoki, Y.; Scholz, C.H. Vertical deformation of the Japanese islands, 1996-1999. *J. Geophys. Res.* **2003**, *108*, 2257–2269. [CrossRef]

120. Kuo, C.Y.; Shum, C.; Braun, A.; Mitrovica, J.X. Vertical crustal motion determined by satellite altimetry and tide gauge data in Fennoscandia. *Geophys. Res. Lett.* **2004**, *31*, L01608. [CrossRef]
121. Ray, R.; Beckley, B.; Lemoine, F. Vertical crustal motion derived from satellite altimetry and tide gauges, and comparison with DORIS measurements. *Adv. Space Res.* **2010**, *45*, 1510–1522. [CrossRef]
122. Santamarìa-Gomez, A.; Gravelle, M.; Wöppelmann, G. Long-term vertical land motion from double-differenced tide gauge and satellite altimetry data. *J. Geod.* **2014**, *88*, 207–222. [CrossRef]
123. Kleinherenbrink, M.; Riva, R.; Frederikse, T. A comparison of methods to estimate vertical land motion trends from GNSS and altimetry at tide gauge stations. *Ocean Sci.* **2018**, *14*, 187–204. [CrossRef]
124. Watson, P.J. An Assessment of the Utility of Satellite Altimetry and Tide Gauge Data (ALT-TG) as a Proxy for Estimating Vertical Land Motion. *J. Coast. Res.* **2019**, *35*, 1131–1144. [CrossRef]
125. Hamlington, B.D.; Frederikse, T.; Nerem, R.S.; Fasullo, J.T.; Adhikari, S. Investigating the Acceleration of Regional Sea Level Rise During the Satellite Altimeter Era. *Geophys. Res. Lett.* **2020**, *47*, e2019GL086528. [CrossRef]
126. Fasullo, J.T.; Nerem, R.S.; Hamlington, B. Is the detection of accelerated sea level rise imminent? *Sci. Rep.* **2016**, 31245. [CrossRef]
127. Cazenave, A.; Cabanes, C.; Dominh, K.; Mangiarotti, S. Recent sea level change in the Mediterranean Sea revealed by Topex/Poseidon satellite altimetry. *Geophys. Res. Lett.* **2001**, *28*, 1607–1610. [CrossRef]
128. Fenoglio-Marc, L. Analysis and representation of regional sea-level variability from altimetry and atmospheric-oceanic data. *Geophys. J. Int.* **2001**, *145*, 1–18. [CrossRef]
129. Vigo, I.; García, D.; Chao, B.F. Change of sea level trend in Mediterranean and Black Seas. *J. Mar. Res.* **2005**, *63*, 1085–1100. [CrossRef]
130. Criado-Aldeanueva, F.; Del Río, J.; Vera, J.G.-L. Steric and mass-induced Mediterranean sea level trends from 14 years of altimetry data. *Glob. Planet. Chang.* **2008**, *60*, 563–575. [CrossRef]
131. Woodworth, P. A search for accelerations in records of European mean sea level. *Int. J. Climatol.* **1990**, *10*, 129–143. [CrossRef]
132. Douglas, B.C. Global sea level rise. *J. Geophys. Res. Oceans* **1991**, *96*, 6981–6992. [CrossRef]
133. Jevrejeva, S.; Grinsted, A.; Moore, J.C.; Holgate, S. Nonlinear trends and multiyear cycles in sea level records. *J. Geophys. Res.* **2006**, *111*, C09012. [CrossRef]
134. Meloni, M.; Bouffard, J.; Doglioli, A.M.; Petrenko, A.A.; Valladeau, G. Toward science-oriented validations of coastal altimetry: Application to the Ligurian Sea. *Remote Sens. Environ.* **2019**, *224*, 275–288. [CrossRef]
135. Poitevin, C.; Wöppelmann, G.; Raucoules, D.; Le Cozannet, G.; Marcos, M.; Testut, L. Vertical land motion and relative sea level changes along the coastline of Brest (France) from combined space-borne geodetic methods. *Remote Sens. Environ.* **2019**, *222*, 275–285. [CrossRef]
136. De Biasio, F.; Baldin, G.; Vignudelli, S. Revisiting Vertical Land Motion and Sea Level Trends in the Northeastern Adriatic Sea Using Satellite Altimetry and Tide Gauge Data. *J. Mar. Sci. Eng.* **2020**, *8*, 949. [CrossRef]
137. Zanchettin, D.; Bruni, S.; Raicich, F.; Lionello, P.; Adloff, F.; Androsov, A.; Antonioli, F.; Artale, V.; Carminati, E.; Ferrarin, C.; et al. Review article: Sea-level rise in Venice: Historic and future trends. *Nat. Hazards Earth Syst. Sci. Discuss.* **2020**. [CrossRef]

3.2 Manuscript II

Title:

Evidence and Implications of Hydrological and Climatic Change in the Reno and Lamone River Basins and Related Coastal Areas (Emilia–Romagna, Northern Italy) over the Last Century

Authors:

Matteo Meli (Department of Biological, Geological and Environmental Sciences (BiGeA), University of Bologna, Bologna, Italy)

Claudia Romagnoli (Department of Biological, Geological and Environmental Sciences (BiGeA), University of Bologna, Bologna, Italy)

Status:

Published in *Water (2022), vol. 14, 2650.* https://doi.org/10.3390/w14172650

Overview:

In this paper, the linear and non–linear evolution of environmental–climatic parameters for both the Reno and Lamone river basins have been analyzed by considering river discharge, rainfall, and air temperature datasets, representative of the river basins over the last century. The main goal of the analysis is to better understand the implications of the hydrological and climatic variations occurring over the river basins and reflecting at the coast.

Open question:

How natural and anthropogenic footprints impacted dynamics of the catchment areas and, indirectly, the coast?

water

MDPI

Article

Evidence and Implications of Hydrological and Climatic Change in the Reno and Lamone River Basins and Related Coastal Areas (Emilia-Romagna, Northern Italy) over the Last Century

Matteo Meli * and Claudia Romagnoli

Department of Biological, Geological and Environmental Sciences, University of Bologna, 40126 Bologna, Italy
* Correspondence: matteo.meli7@unibo.it

Abstract: Climate change and human activities have consequences on coastal areas as they affect hydrological processes in the related river basins. The riverine sediment supply to the beaches of the Emilia-Romagna coast, a highly urbanized area with high economic and naturalistic value, has been heavily impacted by human activities throughout the catchment, reducing solid transport to the coast and increasing the threat of coastal erosion and flooding. Despite the introduction of safeguard policies in the early 1980s and the consequent stoppage of such activities, the expected return in solid transport has not yet been reflected at the coast. To better understand the various processes acting at the river basin scale, we utilized empirical mode decomposition to analyze the variability in different parameters (river discharge, rainfall, air temperature, and sea level) from the headwaters to the coast of the Reno and Lamone rivers over the last century. The anthropogenic footprint, linked to the large-scale dimming/brightening phenomenon, is visible in the long-term trends. Moreover, natural signals with variable periodicity are evident and partially correlated with two major climate modes (North Atlantic Oscillation and Atlantic Multidecadal Oscillation). The coupled interactions among these processes, combined with the changes in land use and evapotranspiration during the last century, have resulted in the prolonged scarcity of river sediment supply and a long-term trend of erosion of the coastal area.

Keywords: climate change; human impact; riverine sediment supply; sea level rise; land-use change

Citation: Meli, M.; Romagnoli, C. Evidence and Implications of Hydrological and Climatic Change in the Reno and Lamone River Basins and Related Coastal Areas (Emilia-Romagna, Northern Italy) over the Last Century. *Water* **2022**, *14*, 2650. https://doi.org/10.3390/w14172650

Academic Editors: Qianfeng Wang, Haijun Deng and Jinshi Jian

Received: 21 July 2022
Accepted: 25 August 2022
Published: 28 August 2022

1. Introduction

Riverine sediment discharge, the foremost feeding source for low-elevation coastal zones (LECZ) [1,2], has declined drastically worldwide over the last century (e.g., [3–8]) and will likely continue to decline [9,10]. The amount and role of sediment supplies at the coast varies with the local climate, geological setting, and degree of human impact within each catchment area [11–13]. LECZs worldwide have reached a critical tipping point, shifting from a natural pseudo-stable state since the Holocene to a state controlled by human dynamics [14] owing to land use modifications throughout their catchment areas [15,16]. Furthermore, rising sea levels and other climate-driven effects are expected to exacerbate such impacts on LECZs [17]. Despite climate-driven modifications remaining influential, they may locally be of secondary importance [18] since human effects may more heavily interact with hydrological processes. Anthropogenic modifications over catchment areas, together with the hydrological and climatic changes, and their related connection with atmospheric dynamics, should be thus taken into account in order to better understand which processes are most likely to drive the evolution of coastal areas.

The Emilia-Romagna (ER) coast is a 130 km long LECZ south of the Po River Delta, Northern Italy, facing the northern Adriatic Sea (Figure 1a), which has undergone severe

anthropization since the 1950s [19]. Increased subsidence due to underground fluid exploitation [20–23], land reclamation, and the widespread use of coastal defense structures [24–26] have affected the ER coastal plain, making it sensitive to floods [27]. Furthermore, the heavy, anthropogenically driven reduction in sediment delivery by rivers (mainly due to sediment digging and river regulation), mostly between the 1940s and 1980s, has led to generalized erosion and shoreline retreat [28–30]. Although safeguard policies for riverbed excavation, introduced by the ER regional government during the early 1980s, were expected to gradually reverse this, only the amount of suspended material has slowly increased, whereas fluvial bedload has decreased [31,32]. Granulometric analysis on samples collected since the 1970s in the submerged beach of the ER coast, at or below 3 m depth, has shown a generalized overall decrease in grain size until the present day [33–36]. Indeed, a recovery in bedload sediment supply has not yet occurred since the introduction of the safeguard policies; thus, most of the ER shoreline has become threatened by erosion and flooding [34]. Previous analyses have been conducted over the regional scale in order to better elucidate the hydrological, environmental, and climatic evolution of the area, finding a significant decrease in river discharge [37] and indicating that sediments are currently not being transferred downstream as they were previously. While a clear increase in air temperature has also been observed for the last 70 years (e.g., [38]), trends in rainfall have been found to be statistically significant only at certain locations [39–41], highlighting a great spatial variability for this parameter. This effect has primarily been linked to the frequencies of diverse weather regimes which, locally, have led to differentiation in both total annual rainfall amount and its variability through time [42]. Generally speaking, significant/non-significant decreases in rainfall are a matter of debate on both the Italian [43–46] and Mediterranean scales [47,48], for which the contrast has been mainly attributed to the length of the time interval considered in the analysis [45].

In this study, the Reno and Lamone river basins (Figure 1a), which feed an approximately 20 km stretch of the ER coast between the Porto Garibaldi and Porto Corsini harbors (Figure 1b), have been considered. The Reno River, with a length of 210 km and a basin area of approximately 4630 km^2, is the main river of the ER region after the Po River, and the sixth nationwide in terms of basin size. It drains both mountains and plains and is joined by many tributaries from the Apennines and artificial channels in the plains (Figure 1c). The basin of the Lamone River (approximately 520 km^2, Figure 1a) is much smaller than the Reno River basin; nevertheless, its sediment supply also provides an input for the coastal budget of this area. Coastal prograding at the mouth of the Reno River during the early 20th century was previously associated with a sustained sediment supply [33], whereas from the late 1930s onward, progressive erosion has occurred [34]. The coastal areas of these river basins and adjacent wetlands (the Comacchio Valleys and the Bellocchio marsh; Figure 1b), represent a significant economic and naturalistic resource (Ramsar Convention site); however, these areas are among the most threatened by shoreline retreat and flooding along the Mediterranean and European coasts [49]. Furthermore, these coasts are significantly impacted by economic activities that cause land subsidence, such as gas exploitation by ENI (Ente Nazionale Idrocarburi) in the "Dosso degli Angeli" reservoir (Figure 1b) [50].

In this paper, the linear and nonlinear evolution of environmental-climatic parameters for both river basins have been analyzed by considering river discharge, rainfall, and air temperature datasets, representative of the river basins over the last century. The main goal of the study is to better understand the implications of the hydrological and climatic variations occurring over the river basins and at the coast. According to Preciso et al. [37], the Reno River catchment no longer represents the primary sediment source for the coast, primarily because of reforestation within the catchment since the 1950s. Moreover, in several Mediterranean locations, changes in land use, together with increased evapotranspiration and soil erosion control measures, have reduced runoff, and thus, sediment supply [51–54]. Due to this, land use changes and evapotranspiration datasets were also taken into account in our analyses in order to obtain a more holistic view of the changes occurring throughout the catchment areas. Moreover, the local sea level, here affected by both natural and

anthropogenic components (see [55,56] for details), was considered, as it is a critical factor in coastal evolution.

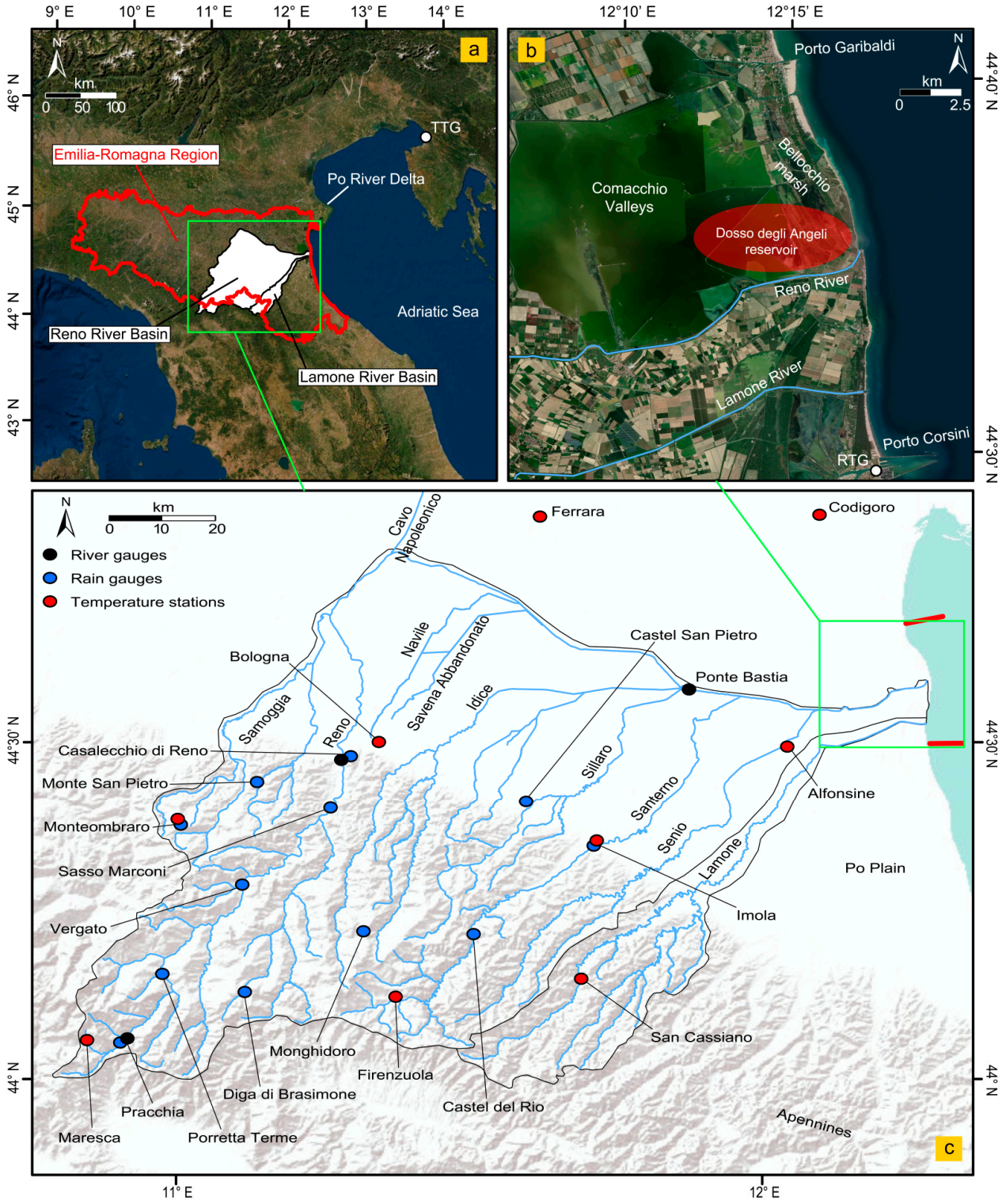

Figure 1. (**a**) Location of the Reno and Lamone river basins in the Emilia-Romagna region, Northern Italy. TTG: Trieste tide gauge; (**b**) the coastal portion of the river basins. RTG: Marina di Ravenna tide gauge; (**c**) detailed map of the Reno and Lamone river basins and tributaries, with position of gauges and stations used in this study.

In detail, this study addresses the following questions: (1) How have anthropogenic and natural signals acted on hydrological processes at the river-basin scale, from the headwater to the coast, over the last century? (2) Why, despite safeguards for river basin management, has the solid river supply to coastal sites not yet recovered? (3) How have climate change and anthropogenic footprints affected sea-level changes in the studied LECZ?

2. Materials and Methods

2.1. Data

The average monthly river discharge, rainfall, and air temperature data were obtained from the Dext3r-SIMC platform [57] and the annals of the National Hydrological Service [58]. Only long-term data within both the river basins were obtained, in order to consider a wider, historical view of the surface processes. Furthermore, liquid transport time series were reconstructed from three selected river gauges (Figure 1c); however, these datasets contained gaps (Figure 2). To rebuild a representative time series, thereby increasing the signal-to-noise ratio, data from the twelve longest and more complete individual rain gauges (out of a total of 92 stations available throughout the two basins) were considered and stacked. Although these datasets were affected by a common gap in the year 1924, minor gaps in each time series were filled using records from the closest station (excluded from the analysis) within 10 km after careful comparison of the overlapping data. To further examine rainfall variability, the number of wet days ($\geq$1 mm/day) were also considered. The minimum and maximum temperatures were used to produce a monthly climatological assessment of the river basins. Additionally, a stacked curve was computed to achieve a basin-representative climate time series that considered data from nine stations (Figure 1c).

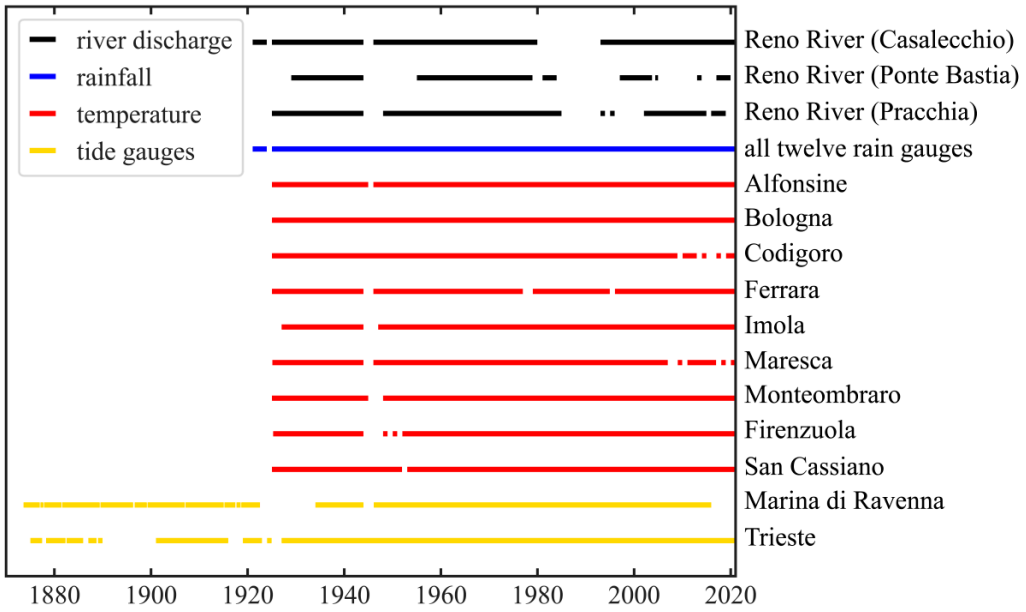

Figure 2. Duration of the considered records.

The relative sea level data (RSL, which measures the sea level with respect to a benchmark on land) were obtained from the Marina di Ravenna tide gauge (RTG; Figure 1b), which is currently managed by ISPRA (Istituto Superiore per la Protezione e la Ricerca Ambientale). The gauge has recorded data since 1873, with a gap from 1922 to 1933 and discontinuities since 2016 (Figure 2); hence, data after 2015 were discarded. The RTG time series was assembled using data from various sources (1873–1979 and 2001–2016 from the Permanent Service for Mean Sea Level (PSMSL) data bank [59,60]; 1971–2001 from Romagnoli et al. [61], and homogenized considering data overlaps and following Bruni et al. [56]).

River discharge, rainfall, temperature, and RTG time series were compared with three climate indices, namely the North Atlantic Oscillation (NAO), Atlantic Multidecadal Oscillation (AMO), and Western Mediterranean Oscillation (WeMO). The NAO is among the most significant modes of climate variability in the Northern Hemisphere, with seasonally fluctuating manifestations, especially during the boreal winter [62,63]. The winter (December–March) station-based NAO dataset was used; this represents the normalized sea-level pressure between Lisbon (Portugal) and Stykkishólmur (Iceland) since 1864, by the National Centers for Environmental Prediction/National Center for Atmospheric Research [64], based on Hurrell et al. [63]. The AMO [65] is another prominent climate variability mode in the Northern Hemisphere, defined by variability in sea surface temperature (SST) in the North Atlantic Ocean and characterized by a dominant periodicity of approximately 60–70 years. The AMO is the area-weighted average SST (between 0° and 70° N) with the linear trend removed. The annual AMO index, available since 1856, was provided by the National Oceanic and Atmospheric Administration/Physical Sciences Division [66]. The WeMO index [67] is defined as a dipole structure formed (in its positive phase) by an anticyclone over the Azores and a depression over north-western Italy; its index is the result of the difference between the standardized values of surface atmospheric pressure in San Fernando (Spain) and Padua (Italy). In this study, we also accounted for the WeMO since it is considered by some authors more significant than the NAO to explain rainfall anomalies over the north-western Mediterranean (e.g., [68] and references within).

The Standardized Precipitation Evapotranspiration Index (SPEI) [69] was used for long-term drought analysis (1921–2019). The SPEI allows for the identification of drought severity using its length and intensity at various timescales, considering the effects of both temperature and precipitation. This index combines the strength of the multi-temporal Standardized Precipitation Index [70] and the sensitivity of the Palmer Drought Severity Index [71]. The Global SPEI database [72] used in this study covers the globe at a spatial resolution of 0.5 degrees and offers timescales from 1 to 48 months. The potential evapotranspiration in the SPEI database is based on the FAO-56 Penman-Monteith method [73]. Despite its coarser spatial resolution with respect to local datasets, the SPEI has been adopted as it has been thoroughly validated by several authors (e.g., [74–81]) to reveal moisture anomalies for environmental and agricultural applications. Since our study primarily considers the long-term (decadal to centennial) alternation of drought and wet conditions rather than short-term (monthly) events, the 48 month-average time series have been used. The Bologna grid cell was considered as representative of the Lamone and Reno river basins because the variability between adjacent cells at this spatial scale was negligible.

Snow cover percentage over the period 1950–2022 was obtained from the ERA5-Land reanalysis dataset [82–84] and limited to the area under analysis. This parameter represents the fraction (0–100%) of the grid cell occupied by snow and is provided with a spatial resolution of 0.1 × 0.1 degrees.

Land use was evaluated using land use maps for 1976, 1994, 2003, 2008, 2014, and 2017, produced by the GIS and Statistic Service of the ER Region [85]. These maps were developed utilizing aerial photography and are characterized by their minimal detectable area: 0.375 (1976), 1.56 (1994 and 2003), and 0.16 (2008, 2014, and 2017) hectares. The land use for these products was mapped using the Corine Land Cover legend until level three.

2.2. Methods

All datasets in this study were homogenized into monthly means. The time series were plotted using a 1-year moving average low-pass filter to highlight the interannual variability. Modified non-parametric Mann-Kendall (MK) tests [86–88] were performed to assess temporal trends (statistically significant at the 95% confidence interval). MK analysis was implemented using the Theil-Sen estimator [89,90] to evaluate linear trends. This method is insensitive to outliers and more accurate than simple linear regression [91]. To

account for serial autocorrelation and properly estimate trend-related errors, the procedure described in Zervas [92] has been followed.

Considering the stacked rainfall time series and the monthly sum of wet days, the Simple Daily Intensity Index (SDII), which is the ratio of total rainfall to the number of wet days, was computed based on Frich et al. [93]. Only the SDII values above the 95th and 99th percentiles were considered.

For RSL analysis, several authors have addressed the removal or assessment of vertical crustal movements (VLM) from tide gauge data [55,94–97]. Optimally, VLM contributions can be distinguished by Global Navigation Satellite System monitoring of tide gauge data [98]; however, this began in the late 1990s [99,100]. To remove the VLM components, the RTG time series was subtracted from the Trieste Tide Gauge (TTG; location in Figure 1a) dataset (data 1875–2021 from the PSMSL archive); from this, a locally weighted polynomial regression was created and subsequently removed from the original RTG datasets. This procedure relies on the assumption that TTG location is considered a relatively stable area in terms of vertical land movements, with a weak uplift in the range of a few tenths of mm·year^{-1} or negligible (e.g., [101–106]).

To assess nonlinear and non-stationary signals, empirical mode decomposition (EMD) [107] was applied to decompose monthly mean river discharge, rainfall, air temperature, and sea level into finite empirical orthogonal intrinsic mode functions (IMFs). Each IMF describes cyclic variations, though not necessarily constant phases and amplitudes, representative of the oscillating mode from the highest to the lowest frequency. The lasting, non-oscillatory mode is the residual (RES), usually associated with the long-term trend of the signal, which is typically monotonic and provides information about the reliability of the linear model for nonperiodic components. Previous studies have employed EMD to correlate nonlinear variations among different phenomena [108–114]; moreover, it is well suited for analyzing non-stationary time series.

The non-parametric Kendall rank correlation was employed to examine statistical relationships for NAO, AMO, and WeMO with our time series. This method has significantly smaller gross error sensitivity and asymptotic variance than Spearman rho or Pearson r and provides significantly more accurate p-values [115]. To evaluate autocorrelation, the time series were linearly detrended, and their effective sample size, based on the lag-1 autocorrelation coefficient, was considered [116,117]. The statistical significance of the correlation results was set at 95% CI.

Periodic signals were characterized by computing Lomb-Scargle periodograms [118,119] for each time series and both the NAO and AMO indices, providing a description of the overall frequencies. The periodograms were confined to the standard normalized power interval 0–1, according to Baluev [120], and limited to >4 years to focus on low-frequency signals.

In the land use analysis, only polygons within the Reno and Lamone river basins were considered. A further subdivision was made between the polygons within the alluvial plain and Apennine portions of the maps to highlight the various changes between the two sectors.

3. Results

3.1. Long-Term Linear Analysis

MK tests on all three river gauge stations indicated a statistically significant decrease in river liquid discharge (Figures 3a and A1) over the last century. The Casalecchio di Reno time series, which is the most complete, showed a decrease of -0.18 ± 0.08 m^3/s·year^{-1} during 1921–2021 (Figure 3a). This station was more reliable than that at Ponte Bastia (Figure 1c) since, although the latter could depict the behavior of the lower Reno River basin, it was affected by massive anthropogenic contamination, mainly due to the Cavo Napoleonico (Figure 1c), one of the most significant hydraulic structures in the Po Plain, whose function since the late 1960s has been that of diverting the Reno River water into the Po River during floods and vice versa during drought periods. The river gauge at Pracchia also provides a nearly complete time series of the Reno River runoff (Figure 2).

Despite its location in the high Apennine and the relatively limited drainage area upstream, a significant, slight decrease in river discharge occurred. In terms of seasonality (by considering the sole Casalecchio di Reno time series) the monthly mean data show clear and significant decreasing trends, with the lowest discharge values during summer (namely June, July, and August), marked decrease trends for both winter (December, January, and February) and autumn (September, October, and November), and a stronger decrease during spring (March, April, and May) (Figure A2a).

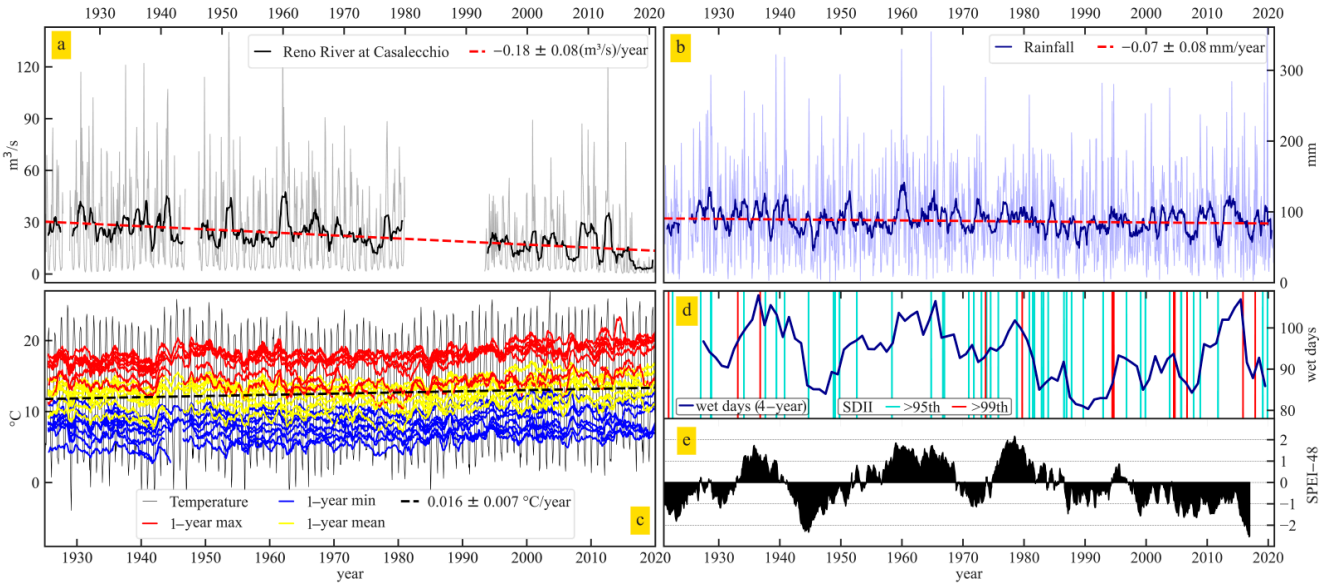

Figure 3. (**a**) Reno River discharge at the Casalecchio river gauge and (**b**) the stacked rainfall time series, both with 1-year low-pass filter time series (solid black and blue lines, respectively) and trend estimates (dashed red lines); (**c**) the stacked temperature time series (black), its trend estimate (dashed black line), and the 1-year moving average time series of max (red), mean (yellow) and min (blue) temperatures observed at the nine stations in this study; (**d**) the number of wet days filtered with a 4-year moving window (solid dark-blue line) and the SDII, showing only instances above the 95th (light blue) and 99th (red) percentiles; (**e**) the 48-month SPEI time series for the study site.

The stacked monthly rainfall time series (Figure 3b) showed a negative but not significant trend (-0.07 ± 0.08 mm·year^{-1}); the same was true for most of the individual rain gauges (Figure A3). Seasonality within the rainfall stacked curve shows the same behavior as that described by Pavan et al. [40], with the minimum values observed during summer and the maximum in autumn (Figure A2b); however, only the other two seasons (winter and spring), comparable in terms of both the amount of precipitation and trends, denote a significant decreasing trend.

The monthly mean temperature trends over the Reno and Lamone river basins during the last century almost all showed statistically significant increases (Figure A4). The stacked temperature curve (Figure 3c) shows a statistically significant increase of 0.016 ± 0.007 °C·year^{-1}, which corresponds to a warming of over 1.5 °C during the last century. The variability of temperature highlights an increasing and significant trend for all seasons (Figure A2c). During autumn, however, the trend is very slight, while stronger warming for the last century is observed in winter. Monthly mean temperatures ranged from 9 to over 14 °C at the highest station in the Apennines (Maresca) and urban areas in the plains (Bologna, Ferrara, and Imola), respectively, showing thermal variability due to both elevation and urbanization. Moreover, the latter has caused an urban heat island effect, which affects local and regional air temperatures near densely settled areas [121]; its main impact is a large increase in nighttime temperatures [122]. In addition, the local topography and land use have led to large variability in temperature, with the minimum (5.5 °C at Maresca) and maximum (18.6 °C at Bologna) averages differing by over 13 °C.

However, grouping datasets from similar geographic contexts allows for a gross assessment of the variability induced by land use and local topography. Long-term minimum and maximum averages from the Apennine datasets were 0.2 and 2.4 °C lower than those from the rural plains, respectively. In contrast, maximum averages in the rural plains were not substantially different from those in urban areas (0.16 °C), whereas minimum averages were approximately 1.6 °C higher in urban areas.

The four-year low-pass filtered time series of wet days in Figure 3d shows a nonlinear, cyclic pattern, with minima during the 1920s, 1940s, and the early 1980s–2010. However, the >95th and >99th percentile values of the SDII do not give a clear pattern throughout the century; rather, they suggest an intensification of their occurrence, beginning in the 1970s.

Figure 3e shows the evolution of the SPEI during 1921–2019 in 48-month intervals. Paulo et al. [123] categorized the SPEI drought classes as non-drought (greater than −0.5), mild (−0.5 to −1), moderate (−1.5 to −1), severe (−1.5 to 2), and extreme (less than −2) conditions. In our data, moist and dry periods fluctuated throughout the century, in agreement with the wet days (Figure 3d); however, the wet periods have declined in recent decades. Since the 1980s, drought conditions have been increasingly persistent. Furthermore, extreme drought conditions only occurred during the 1940s and recently.

Trends in ground snow cover percentage (Figure A2d) over the area under study denote a marked and significant decrease in winter (-0.58 ± 0.18 %·year^{-1}) over the period 1950–2022, corresponding to a decrease in the winter snow surface of about 63% in the last 72 years; no significant trends emerged from both autumn and spring.

RSL data from the RTG time series (Figure 4a) clearly indicates a higher rate of sea-level rise during 1940–1980, compared to the prior and subsequent periods. This behavior witnesses the well-known subsidence phenomena due to local human activities (exploitation of gas and water from the underground) which overlapped with the natural land subsidence of the area [124,125]. However, subsidence has slowed significantly since the 1980s, mainly due to safeguarding policies introduced by the regional administration. Accounting for the TTG time series (Figure 4b) as a stable reference at the century scale, Zerbini et al. [126] evaluated the natural subsidence at the RTG site at around 1.88 mm·year^{-1}, by considering the period prior to the start of the mining activity (1873–1922); this value is in agreement with previous geological investigations [127–129] and with the first portion of the TTG-RTG time series of Figure 4c. The estimated trend of the RTG time series (1875–2016), detrended for VLMs (Figure 4d) is 1.3 ± 0.2 mm·year^{-1}, which is comparable with the TTG estimate of 1.33 ± 0.17 mm·year^{-1} (1875–2021).

3.2. Nonlinear Signal

The EMD-decomposed time series of river discharge, rainfall, and temperature are shown in Figure 5a–c respectively, along with the sea level time series from the corrected RTG (Figure 5d). EMD decomposition produced seven IMFs for each of these four time series; however, to focus on long-term variability, only the lowest frequency IMFs (IMF4, IMF5, and IMF6) and RES were considered.

The RES component in river discharge was not perfectly linear but decreased over time; this decrease was 90% and 190% greater during 1993–2021 compared to that during 1950–1980 and 1921–1950, respectively. The RES in both rainfall and temperature show non-monotonic behavior, suggesting the presence of cycles longer than the time series themselves. In detail, rainfall decreased during 1950–2000 but otherwise increased. In contrast, temperature has increased since the 1920s; although it dropped slightly during the 1960s and 1970s, it has strongly increased since the 1980s. Conversely, the RES in sea level consistently increased over the last 140 years. RES trends (Table 1) were statistically significant in all cases, even for rainfall, in contrast to the original time series (see Section 4.1).

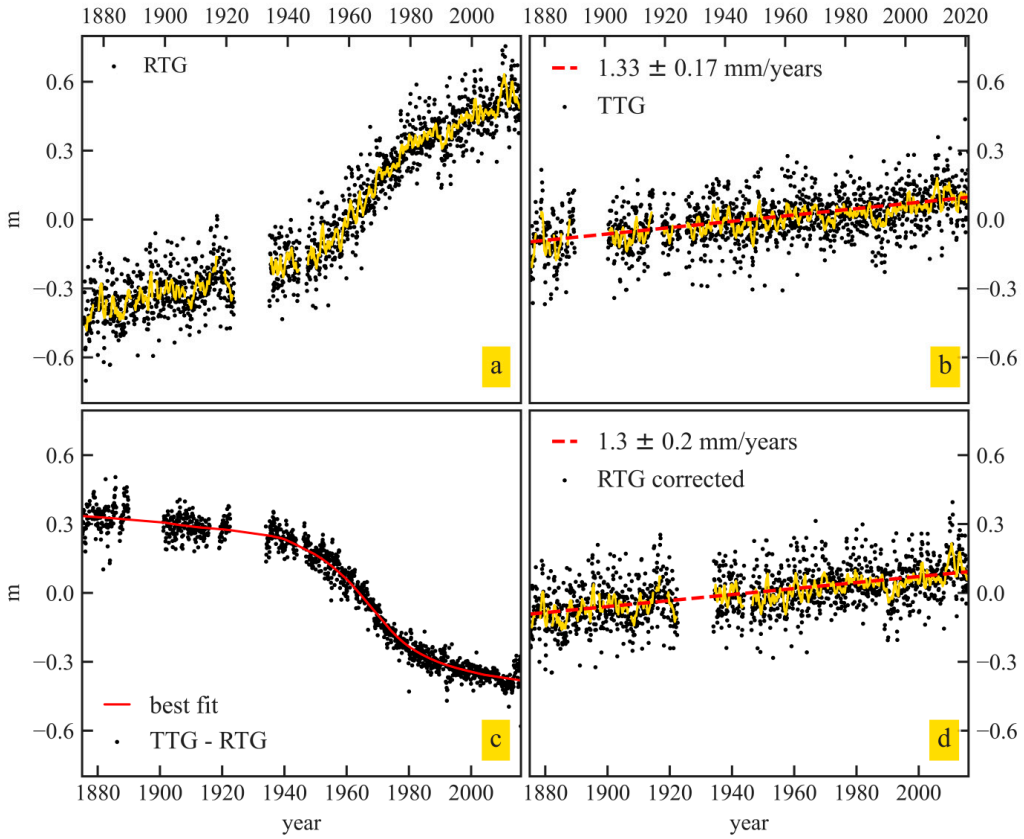

Figure 4. (**a**) RSL recorded at the Marina di Ravenna tide gauge (RTG, 1873–2016) and related 1-year moving window time series (yellow line); (**b**) the TTG, 1875–2021), related trend estimate (dashed red line), and 1-year moving average time series (yellow line); (**c**) the difference between the TTG and RTG time series with the best fit (solid red) line; (**d**) the RTG time series corrected for vertical land movements, long-term trend estimate (red dashed line), and 1-year moving average curve (yellow line).

The time series compared with the NAO and AMO climate indices (Figure 5e,f) show significant (95% CI) negative correlations of NAO phases with river discharge, rainfall, and sea level of −0.31, −0.16, and −0.34, respectively. In contrast, air temperature was positively correlated with both NAO (0.26) and AMO (0.21) fluctuations, and the sea level correlated with the AMO (0.14) index. However, only the air temperature-NAO correlation was statistically significant at the 95% CI, while the correlations with the AMO index become significant only if the 90% CI is considered. No correlations were found between the AMO with either river discharge or rainfall, nor was the WeMO index with any variable considered. Since no correlation was found on any annual time series representative of this area, the latter is not further discussed in this paper.

Several periodicities "contaminate" the time series, as detected by the LSP analysis (Table 2). Most are common to all the datasets, albeit with different values. Periodicities of 4–5 and 8–9 years were detected in all the time series and are dominant within the IMF4 of rainfall and temperature and the IMF4 of sea level, respectively (Figure 5). Additionally, an approximately 6-year periodicity, which is dominant in the IMF4 of river discharge, is not present in the temperature and sea level. At lower frequencies, only the approximately 12-year period is common among all the time series, while periods of 10–11, approximately 14, and 16–17 years are dominant within IMF5 of rainfall, river discharge and temperature, and sea level, respectively. A periodicity of 22–23 years is common to all time series (dominant in the IMF6 of river discharge and temperature) when considering >20 years, whereas in rainfall and sea level, a powerful periodicity of approximately 40 years characterizes IMF6. Furthermore, two periodicities prevail at the longest wavelength: 53–56 years for

river discharge and temperature, and approximately 67 years for sea level. All these periodicities occur in the NAO and AMO time series (Table 2), often with values common to both indices, and fluctuate in phase or anti-phase (as described above) with the IMFs of all the decomposed time series.

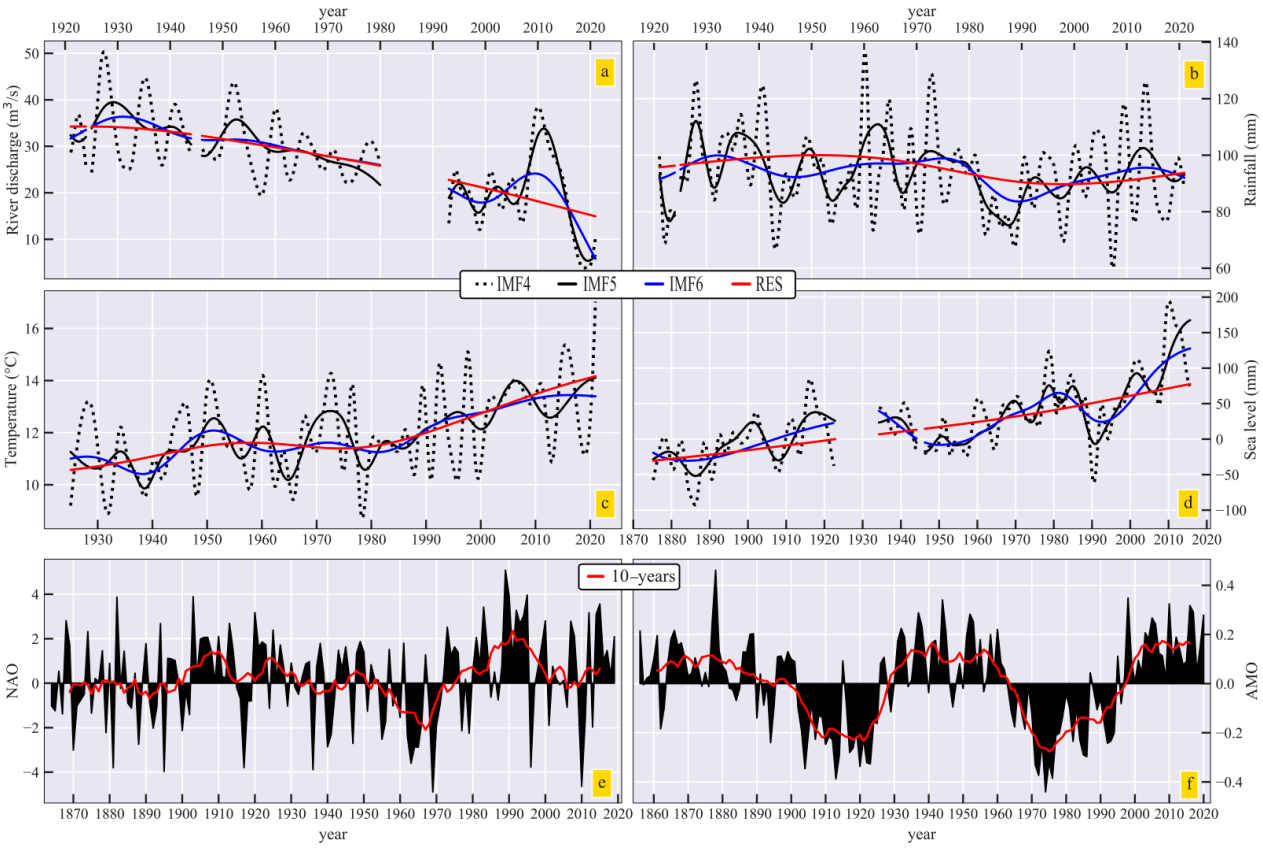

Figure 5. The IMFs and RES curves for river discharge (**a**), rainfall (**b**), temperature (**c**) and sea level (**d**), from the EMD analysis; the winter NAO (**e**) and AMO (**f**) indices time series, with a 10-year filter.

Table 1. Datasets considered in this study and related residual trends.

Station	Variable	Residual Rate (*·Year^{-1})	Period
Casalecchio di Reno (Reno River)	River discharge (m^3/s)	-0.202 ± 0.002	1921–2021
		-0.101 ± 0.004	1921–1950
		-0.190 ± 0.001	1950–1980
		-0.268 ± 0.002	1993–2021
Stacked rainfall	Rainfall(mm)	-0.101 ± 0.005	1921–2021
		0.157 ± 0.004	1921–1950
		-0.263 ± 0.005	1950–2000
		0.200 ± 0.006	2000–2021
Stacked temperature	Temperature (°C)	0.032 ± 0.002	1925–2021
		0.040 ± 0.001	1925–1950
		-0.007 ± 0.001	1950–1980
		0.071 ± 0.001	1980–2021
Marina di Ravenna (VLM corrected)	Sea level (mm)	0.786 ± 0.008	1875–2016

Note: * symbol: unit of measurement of the specific variable.

Table 2. Most evident periodicities that affect the variables considered in this study, and their related Standard Normalized Power (Snp, according to Baluev [120]). Indications in parentheses for some periodicities highlight their dominance within a specific IMF.

Variable	Period	Snp
NAO	4–5	0.041
	~6	0.042
	7–8	0.087
	8–9	0.023
	~12	0.012
	~14	0.022
	16–17	0.011
	22–23	0.04
	37–40	0.04
AMO	4–5	0.015
	~6	0.018
	7–8	0.025
	8–9	0.05
	10–11	0.047
	16–17	0.018
	20–22	0.012
	~67	0.5
River discharge	4–5	0.056
	~6 (IMF 4)	0.073
	8–9	0.037
	10–11	0.072
	~12	0.068
	~14 (IMF 5)	0.058
	16–17	0.028
	22–23 (IMF 6)	0.056
	33–35	0.052
	53–56	0.097
Rainfall	4–5 (IMF 4)	0.094
	~6	0.038
	8–9	0.035
	10–11 (IMF 5)	0.052
	~12	0.027
	16–17	0.019
	23–26	0.021
	38–41 (IMF 6)	0.061

Table 2. *Cont.*

Variable	Period	Snp
Temperature	4–5 (IMF 4)	0.04
	8–9	0.03
	~12	0.042
	~14 (IMF 5)	0.06
	16–17	0.02
	22–23 (IMF 6)	0.07
	30–33	0.022
	53–56	0.19
Sea level	4–5	0.039
	8–9 (IMF 4)	0.043
	10–11	0.02
	~12	0.038
	~14	0.076
	16–17 (IMF 5)	0.079
	22–23	0.06
	28–30	0.13
	40–42 (IMF 6)	0.29
	~67	0.16

3.3. Land Use Changes

Recent land use changes within the Reno and Lamone River basins were categorized using the first level of the Corine Land Cover code as artificial areas, agricultural areas, forests and semi-natural areas, wetlands, and water bodies (see also Heymann et al. [130]). The land use changes in the Apennines for both basins (Figure 6) highlight that agricultural areas have been replaced since the 1970s, mainly by forests and semi-natural areas (approximately 70%) and some artificial surfaces (30%). Recent reforestation in the upper ER river basins has been driven by the migration of rural populations to urban areas and consequent cropland abandonment [32,34].

Trends in the plain sector have been nearly constant since the second postwar period, when the landscape began changing, following a rapid shift from a largely peasant economy to an industrial and touristic economy [131,132]. This has caused a gradual reduction in agricultural areas and intensive urban sprawl. This "uncontrolled spread of towns and villages into undeveloped areas" [133] has increased soil sealing due to impermeable artificial materials, which are considered the largest issue for pervasive soil degradation [134]. Moreover, the area of sealed soils (excluding areas such as gardens, urban wastelands, and parks) has increased by approximately 123% since 1976. Thus, sealed surfaces accounted for approximately 83% of the total artificial areas in all six analyzed maps. Figure 6 shows that forests and wetlands represent very little of the land use in the plains, which is a consequence of human activities beginning with progressive deforestation by the Romans during the first century B.C. and land reclamation of swamps and salt marshes, begun in the 1800s and completed in 1964. Finally, the slight increase in water bodies in the plains was primarily due to progressive increases in artificial basins (over 120%) and, to a lesser extent, in waterways and irrigation canals (approximately 45% increase).

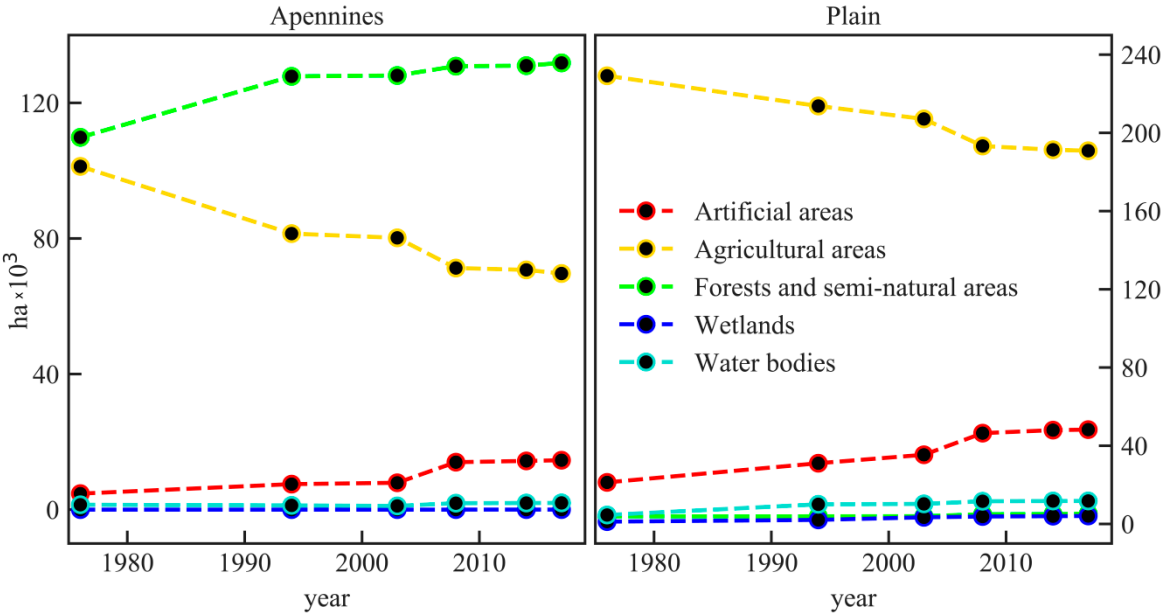

Figure 6. Land use changes (in hectares) within the Reno and Lamone river basins since 1976, for the Apennines (**left panel**) and alluvial plain (**right panel**).

4. Discussion

4.1. Climatic and Hydrological Variability Induced by the Anthropogenic Dimming/Brightening Phenomenon

Surface water runoff has decreased in several areas of the ER region in recent decades [135]. Local water scarcity has been driven by the onset of persistent drought conditions, which began in the 1980s and have worsened, as also suggested by the SPEI (Figure 3e); conditions are projected to further deteriorate over the next decades [136,137].

In our analysis, air temperature (Figure 3c) showed an increasing trend over the last century, as previously observed throughout the ER region by Antolini et al. [38]. However, the RES curve of temperature (Figure 5c) showed an increase from the 1920s to 1950s, a generally stable (or slight cooling) period until the late 1970s, and rapid warming thereafter. This general behavior in temperature, as previously observed throughout Italy [138–140], Europe [141,142], and worldwide [143], has been linked to a dimming/brightening phenomenon [144,145] from surface solar radiation (SSR) changes over the last century [146,147] driven by anthropogenic air pollution, which altered the transparency of the atmosphere [148–150]. The marked change around 1980 led to a "global warming-type drought" [151,152]; its effects on water evaporation and local temperature have been further accentuated by the presence of artificial surfaces.

Despite the lack of statistical significance (Figure A3), the decrease in rainfall over the last century over large portions of the ER was mainly attributed to a decrease in spring and winter rainfall [38–40,153,154], as confirmed by our analysis (Figure A2b). However, when the oscillations are removed, a significant decrease and non-monotonic behavior are visible (Figure 5b). The latter is likely due to the anthropogenic dimming/brightening process described above, as any change in SSR leads to large modifications in the water cycle [155,156]. Wild [157] have found evidence of concurrent decreases in rainfall and SSR from the 1950s to 1980s across the Northern Hemisphere, followed by rainfall intensification from the 1980s onward because of subsequent brightening and increased evapotranspiration [158]. This is consistent with our results, although rainfall resumed long after the 1980s (Figure 5b). This may be due to climatological moisture divergence over the Mediterranean, which transports water vapor outside the region; therefore, moisture does not fully translate to regional increases in rainfall [159–161]. Moreover, this phenomenon is likely connected to a possible increase in rainfall extremes [161,162], as also suggested by the increase in the >95% SDII values from the 1970s (Figure 3d). This could be strictly linked to the concordant

reduction in rainy days, and in this case, not necessarily associated to a substantial decrease in rainfall totals. It can be argued that, following this decline in the 1970s, the amount of total monthly rainfall has not changed considerably (Figures 3b and 5b), and therefore falls in a shorter time.

4.2. Anthropogenic Influences at the River-Basin Scale

The river discharge time series in this study shows a significant decreasing trend since the 1920s (Figures 3a and A1), in agreement with Preciso et al. [37]. Unfortunately, data on bedload materials are lacking, and the relationship between them and river flow discharge cannot be verified [32]. As stated in Section 1, the Reno catchment no longer represents the primary sediment source for the coast, primarily because of reforestation in the catchment since the 1950s [37]. This was confirmed by our analysis (Figure 6); increased forest cover represents the prevailing land use change in the Apennines portion of both basins (see [163]), which likely influenced the reduction in discharge and sediment production. The decrease in discharge showed a negative acceleration in the RES curve (Figure 5a) during 1950–1980, compared to the previous 30 years, which is due to the influence of both river regulation and reforestation, as pastures, shrubs, and crops, consume much less water than forests [164–166]. However, the huge decrease during the following years (1980–2021; Table 1 and Section 4.2) cannot be attributed to river regulation. First, the increase in reforested areas has remained constant, although it has slowed since the mid-1990s. Second, the notable increase in temperature since the 1980s (Figure 5c) has significantly increased the atmospheric evaporative demand and led to persistent local drought conditions (Figure 3e), which, coupled with evapotranspiration, may have driven further declines in discharge. The non-monotonic variation in rainfall (Figure 5b) also contributed to the decreased river discharge since the 1950s; however, its significant but slight changes played a secondary role to the above processes. Furthermore, another consequence of the increasing temperatures may be the decreasing extent of snow cover and number of days with snow present on the Italian peninsula [41] and throughout the Northern Hemisphere [167] over the last century, especially since the late 1970s. Declining snow cover extent throughout the upper catchment areas during winter (Figure A2d) could be a further driver of the reduced river discharge by weakening or even depriving the fluvial systems of water supplied by snowmelt [168,169]. The decline in snow cover extent throughout the upper portion of the studied catchments area can be ascribed as the main driver for the deterioration in spring trends of river discharge (Figure A2a), by weakening, or even depriving, the fluvial systems of the water supply due to the melting of snow.

Once eroded, soil particles can undergo transportation-deposition cycles throughout their travel downstream and either remain within the basin or outflow from it. Thus, processes throughout the plains, usually of anthropogenic origin, are crucial for sediment supply. Our analysis noted that agricultural areas are substantially decreasing in the plains of both basins (Figure 6) and are being replaced by artificial surfaces and, to a lesser extent, water bodies. The increase in the latter, despite the small area, may have significantly influenced discharge by withholding water from the system. Artificial basins (+120% during 1976–2017) and irrigation channels (+45%) have been continuously implemented throughout the plains to satisfy increasing water demand. Intensive groundwater withdrawals in these areas, mainly for industrial and domestic needs [170], also contributed significantly to the decreased discharge, as over-exploitation of aquifers weakens (and often prevents) natural river recharge from the aquifers. The increased temperatures and UHI effect also directly influence the evaporative processes and water demand for both agriculture and domestic needs in the plains. These processes have been magnified during recent decades owing to urban sprawl, the increase in artificial surfaces (Figure 6), and soil sealing (+123% during 1976–2017). The latter reduces and sometimes prevents water infiltration into soils and, therefore, aquifer recharge, increasing both water scarcity and dependence on irrigation and artificial reservoirs [171].

4.3. Natural Contributions from Coupled Ocean/Atmosphere Processes

The NAO influences the weather and hydrology by controlling the wind intensity and direction and the interactions among air masses over much of Europe, and the AMO influences several hydroclimatic variables, including Mediterranean air temperature (e.g., [172–175]). Additionally, the sea level in the Mediterranean is influenced by the NAO, which drives atmospheric sea-level pressure changes [63,176] and the net water flux at Gibraltar by directly altering wind and oceanic circulation near the strait [177,178] and indirectly by impacting regional river runoff, evaporation, and rainfall [179]. Moreover, the AMO influences the SST and sea evaporation [174,179].

Previous studies have found significant correlations between the NAO and Mediterranean surface air temperatures [62,174,180–183]. Our findings of a positive correlation between temperature and AMO cyclicity (Table 2) agree; however, they cannot be confirmed because of the statistical non-significance of the correlation at the 95% CI. Mariotti and Dell'Aquila [174] have also found no correlation between the AMO variability and rainfall over the Mediterranean; our study confirms this apparent lack of influence.

Several authors have found significant negative correlations between rainfall and NAO over Southern Europe and the Mediterranean, with the positive phases of the NAO linked to drier conditions and vice versa [62,63,139,159,181,184,185]. Generally, positive and negative NAO phases decrease and increase rainfall, respectively, over Southern Europe through anomalous behavior of the Atlantic westerlies [184,186], thereby severely impacting regional hydrological cycles [159]. This is reflected by river discharge variability, as indicated by our analysis, which shows a significant negative correlation between NAO phases and river runoff (Figure 5a,e). Negative correlations between river discharge and NAO have been found throughout Europe [187–190]. However, López-Moreno et al. [191] note that, unlike rainfall, river discharge is characterized by a nonlinear response of short, but intense, discharge anomalies during negative NAO phases and persistent, but weaker, anomalies during positive phases. The same authors highlight that during positive NAO years, surface runoff and aquifer recharge are severely reduced, whereas during negative NAO years, river basins receive more rainfall, leading to soil saturation and rapid rainfall transfer to runoff. Positive anomalies, such as the strong peak observed in river discharge in 2010 (Figure 5a), may be a consequence of the negative NAO phase that occurred around 2010, which might have left a record in the river basins and coastal systems. Granulometric analysis performed by ARPAE (Agenzia Regionale per la Prevenzione, l'Ambiente e l'Energia—Emilia Romagna) on samples collected in 2012 in the submerged beach of the studied coastal tract [25] showed larger grain sizes than those from later [36] or prior [33–35] regional sampling. Excluding the possible effects of local interventions (i.e., beach replenishment) [36], these variations in grain size may be related to the large, positive anomaly in river discharge that occurred in 2010. This natural anomaly could have momentarily strengthened the solids' contribution to the coast by enhancing the ability of rivers to carry coarser sediment across the submerged beach through the river mouth bypassing and subsequent redistribution by longshore currents. Thus, the generalized increase in grain size observed in the studied coastal stretch and elsewhere in the nearshore ER coast in 2012 could have been associated with this short-term event, which temporarily disrupted the tendency towards gradually finer and weaker sediment supply observed in recent decades.

At the ER coast, persistent sea-level rise (Figure 5d), periodically altered by various cyclicities, inevitably impacted shoreline evolution. The large positive sea-level anomaly shown in the IMF4 in Figure 5d, has also been observed in previous studies throughout the Mediterranean [178,192,193] and has been attributed to a strongly negative NAO [194]. The dominant periodicity observed in sea-level fluctuations was approximately 8–9 years, which is comparable to the approximately 10-year periodicity found by Bonaduce et al. [112]. Additionally, Galassi and Spada [111] associated the 2010 sea-level anomalies with the coincidence of both negative NAO and positive AMO phases, which has a periodicity of approximately 20 years.

Since the 1990s, sea level has risen rapidly throughout the Mediterranean, which has been linked to increased SST [195], mostly controlled by increasing air temperatures. This also happened during the early 20th century, the other major period of constant rise in global sea and air temperatures [196]. The sea level oscillations at the RTG during these periods are described by IMF6 (Figure 5d), which has a dominant periodicity of approximately 40 years (Table 2). Indeed, major sea-level changes at the RTG over the last 140 years (excluding the effects of local VLMs) were described by multiple phases of acceleration, during the early 20th century, the 1970s–1980s, and 1990s to mid-2000s. Moreover, this behavior is highly phase-correlated with the rainfall IMF6 (Figure 5b), which is also characterized by a similarly dominant periodicity. The NAO may be the driver of this process, because it has a similar periodicity (approximately 37–40 years) and a good negative correlation with both sea level and rainfall. For the same study area, Meli et al. [114] noticed a slight negative acceleration in sea level change since the mid-2000s and attributed it to the possible presence of periodic signals at periods longer than the 26-year period they considered. Therefore, this recent change in the local sea level trend could be associated with the above periodicities, as the final portion of the sea-level IMF6 denotes a temporally concordant, progressive flattening of the rising trend that began in the early 1990s.

5. Conclusions

The environmental and climatic data considered in this study provide a holistic view of the hydrological and climatic processes that have affected the Reno and Lamone river basins of the ER coastal areas in Northern Italy over the last century. The analysis provided responses to the questions posed in Section 1.

- The anthropogenic footprint, attributed to effects such as land use changes and the large-scale anthropogenic dimming/brightening phenomenon, acting at both the river basin and regional-to-global scales, profoundly impacts the catchment dynamics by driving long-term, nonlinear trends, upon which natural oscillations are superimposed. Interactions with major climate modes, in fact, affect the signals over various periodicities. Both positive and negative correlations among some of the studied parameters and the main climatic indexes (NAO, AMO, WeMo) are evidenced;
- The marked negative acceleration in river discharge provides an indication of the lack of recovery in terms of sediment supply to the coast, despite safeguard policies introduced by the ER regional administration in the early 1980s. This decline resulted from river regulation and land use changes during 1950–1980 and related implications. Moreover, since the 1980s, local air temperatures have increased significantly, leading to persistent drought conditions contributing to the drastic reduction in river discharge. However, periodic natural signals can significantly restore the river discharge, as observed during the strongly negative NAO event in 2010;
- Persistent sea-level rise has affected the coastal site under study over the last 140 years. Apart from the extremely high rates during the 1950s–1980s due to anthropogenic-induced land subsidence, sea level is periodically amplified or reduced by natural fluctuations, such as that observed in 2010, and lower frequency fluctuations in the local sea level, as during the early 20th century, 1970s–1980s, and 1990s to mid-2000s. This nonlinear behavior, locally enhanced by subsidence that overwhelms the river sediment inputs, notably impacted the ER coast and may continue to do so.

Overall, the interconnection found between various climatic, hydrological, and anthropogenic processes with individual nonlinear behaviors illustrates the need for a holistic approach when considering complex environments such as LECZs and heavily anthropized areas. Expanded observation and monitoring at the scale of entire river basins is necessary to better understand the natural and anthropogenic influences on coastal behavior. This approach should be thoroughly considered in coastal management and in adaptation strategies, especially when facing a changing climate and increased vulnerability in the most threatened environments, such as LECZs.

Author Contributions: Conceptualization, M.M. and C.R.; methodology, M.M.; formal analysis, M.M.; investigation, M.M. and C.R.; data curation, M.M.; writing—original draft preparation, M.M. and C.R; writing—review and editing, M.M. and C.R.; visualization, M.M.; supervision, C.R. All authors have read and agreed to the published version of the manuscript.

Funding: This research received no external funding. Ph.D. fellowship of M.M. is financed through the Strategic Development Project of the BiGeA Department, University of Bologna.

Data Availability Statement: Not applicable.

Acknowledgments: The authors would like to thank Nunzio De Nigris, Maurizio Morelli, and Margherita Aguzzi from ARPAE (*Agenzia Regionale per la Prevenzione, l'Ambiente e l'Energia—Emilia Romagna*) for making coastal data available. We thank Giovanni Liguori for helpful feedback on technical aspects, Erica and Anna Visibelli for valuable help on Python codes, Marco Olivieri for his help on the EMD analysis and Victor Malagon Santos for his valuable suggestions on an earlier version of this paper. Three anonymous reviewers are acknowledged for their fruitful comments and suggestions that helped improving the paper. This work was carried out in the framework of the Ph.D. course in *Future Earth, Climate Change and Societal Challenges (University of Bologna)*.

Conflicts of Interest: The authors declare no conflict of interest.

Appendix A

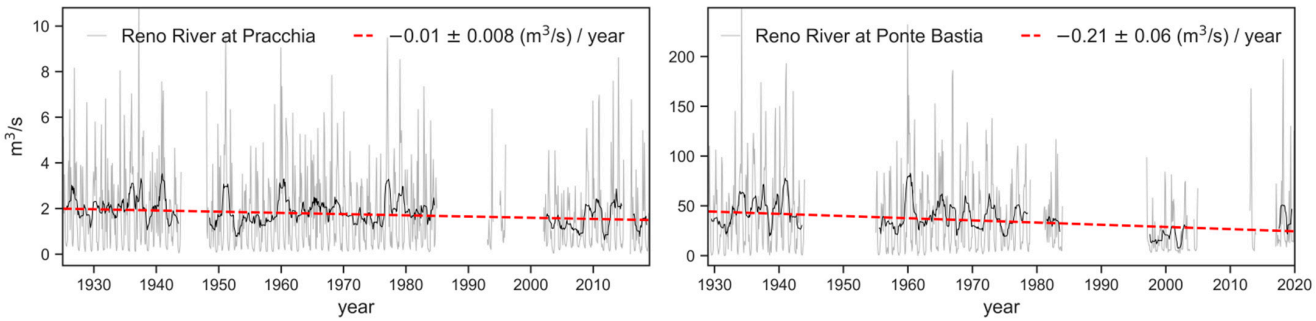

Figure A1. Historical time series of Reno River discharge, and related linear trends, at Pracchia and Ponte Bastia (for locations see Figure 1).

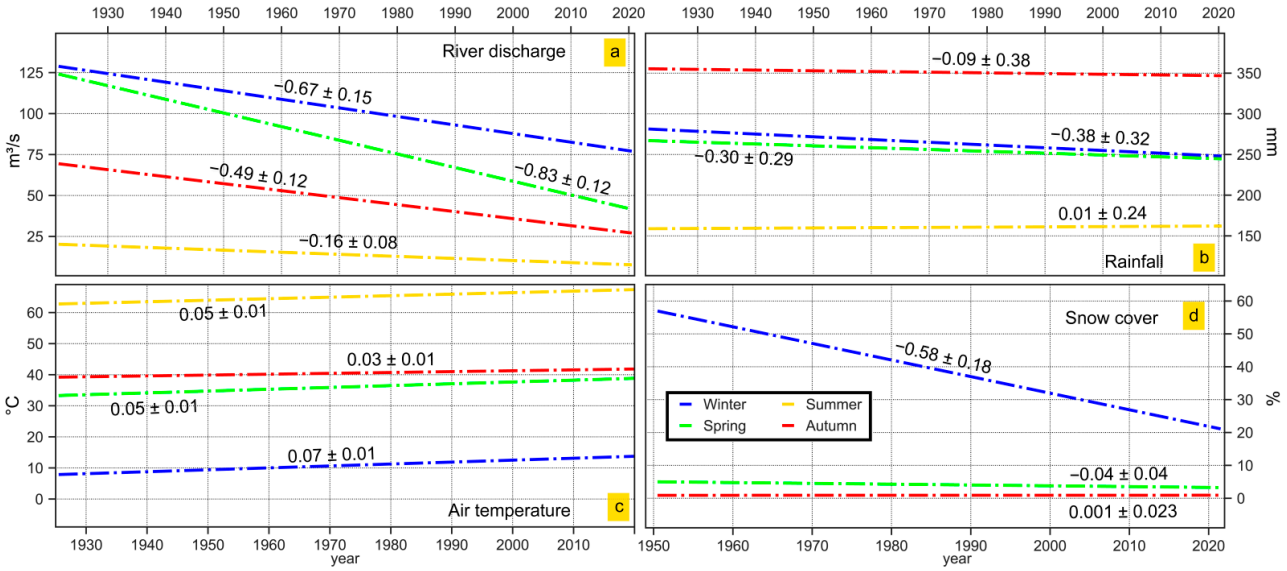

Figure A2. The seasonal trends computed for river discharge (**a**), rainfall (**b**), air temperature (**c**), and snow cover (**d**).

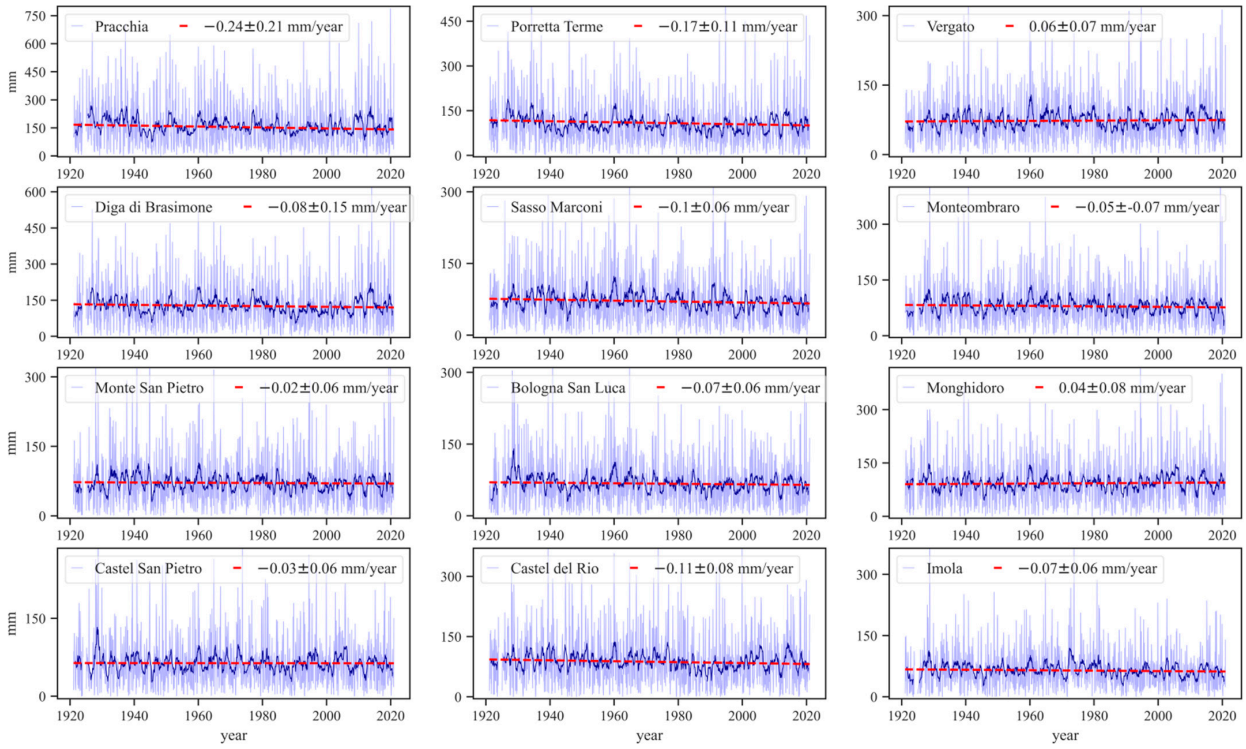

Figure A3. Rainfall time series, and related linear trends, for the twelve rain gauge stations considered in this work (see Figure 1 for locations).

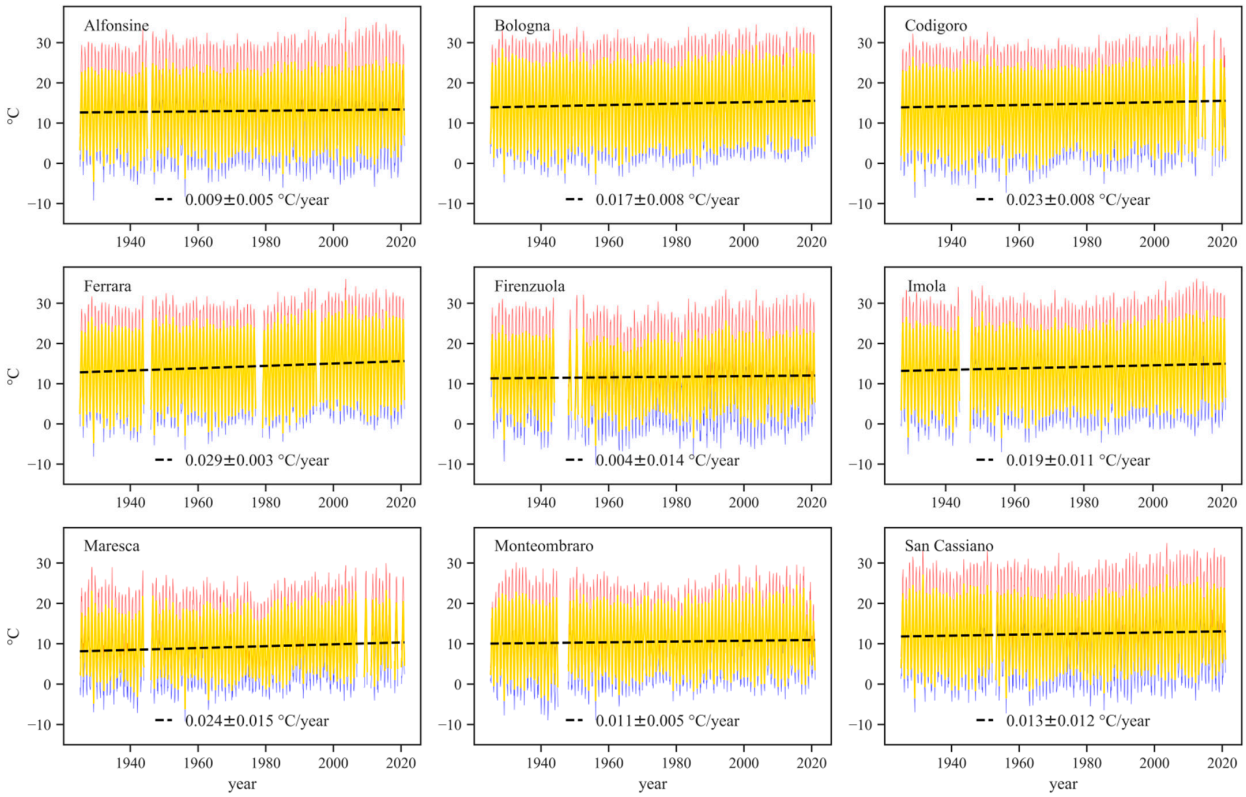

Figure A4. Monthly maximum (red), minimum (blue), and mean (yellow) temperature time series, with estimated linear trends (black dashed line computed over the monthly mean) for the nine stations considered in this work.

References

1. Nicholls, R.J.; Wong, P.P.; Burkett, V.; Codignotto, J.; Hay, J.; McLean, R.; Ragoonaden, S.; Woodroffe, C.D. Coastal systems and low-lying areas. In *Climate Change 2007: Impacts, Adaptation and Vulnerability. Contribution of Working Group II to the Fourth Assessment Report of the Intergovernmental Panel on Climate Change*; Parry, M.L., Canziani, O.F., Palutikof, J.P., Van Der Linden, P., Hanson, C.E., Eds.; Cambridge University Press: Cambridge, UK, 2007; pp. 315–357.
2. Syvitski, J.; Kettner, A.; Overeem, I.; Hutton, E.; Hannon, M.; Brakenridge, G.R.; Day, J.; Vörösmarty, C.; Saito, Y.; Giosan, L.; et al. Sinking deltas due to human activities. *Nat. Geosci.* **2009**, *2*, 681–686. [CrossRef]
3. Llorens, P.; Queralt, I.; Plana, F.; Gallart, F. Studying solute and particulate sediment transfer in a small Mediterranean mountainous catchment subject to land abandonment. *Earth Surf. Process. Landf.* **1997**, *22*, 1027–1035. [CrossRef]
4. Syvitski, J.P.M.; Harvey, N.; Wolanski, E.; Burnett, W.C.; Perillo, G.M.E.; Gornitz, V.; Arthurton, R.K.; Bokuniewicz, H.; Campbell, J.W.; Cooper, L.; et al. Dynamics of the coastal zone. In *Coastal Fluxes in the Anthropocene*; Crossland, C.J., Kremer, H.H., Lindeboom, H., Marshall Crossland, J.I., Le Tissier, M.D.A., Eds.; Springer: Berlin/Heidelberg, Germany, 2005; pp. 39–94.
5. Walling, D.E. Human impact on land-ocean sediment transfer by the world's rivers. *Geomorphology* **2006**, *79*, 192–216. [CrossRef]
6. Syvitski, J.P.M.; Kettner, A. Sediment flux and the Anthropocene. *Phil. Trans. R. Soc. A* **2011**, *369*, 957–975. [CrossRef]
7. Weston, N.B. Declining Sediments and Rising Seas: An Unfortunate Convergence for Tidal Wetlands. *Estuaries Coasts* **2014**, *37*, 1–23. [CrossRef]
8. Buendia, C.; Bussi, G.; Tuset, J.; Vericat, D.; Sabater, S.; Palau, A.; Batalla, R.J. Effects of afforestation on runoff and sediment load in an upland Mediterranean catchment. *Sci. Total Environ.* **2016**, *540*, 144–157. [CrossRef]
9. Zarfl, C.; Lumsdon, A.E.; Berlekamp, J.; Tydecks, L.; Tockner, K. A global boom in hydropower dam construction. *Aquat. Sci.* **2015**, *77*, 161–170. [CrossRef]
10. Dunn, F.E.; Darby, S.E.; Nicholls, R.J.; Cohen, S.; Zarfl, C.; Fekete, B.M. Projections of declining fluvial sediment delivery to major deltas worldwide in response to climate change and anthropogenic stress. *Environ. Res. Lett.* **2019**, *14*, 084034. [CrossRef]
11. Milliman, J.D. Delivery and fate of fluvial water and sediment to the sea: A marine geologist's view of European rivers. *Sci. Mar.* **2001**, *65*, 121–132. [CrossRef]
12. Vörösmarty, C.J.; Meybeck, M.; Fekete, B.; Sharma, K.; Green, P.; Syvitski, J.P.M. Anthropogenic sediment retention: Major global impact from registered river impoundments. *Glob. Planet. Chang.* **2003**, *39*, 169–190. [CrossRef]
13. Syvitski, J.P.M.; Vörösmarty, C.J.; Kettner, A.J.; Green, P. Impact of humans on the flux of terrestrial sediment to the Global Coastal Ocean. *Science* **2005**, *308*, 376–380. [CrossRef] [PubMed]
14. Tessler, Z.D.; Vörösmarty, C.J.; Grossberg, M.; Gladkova, I.; Aizenman, H.; Syvitski, J.P.M.; Foufoula-Georgiou, E. Profiling risk and sustainability in coastal deltas of the world. *Science* **2015**, *349*, 638–643. [CrossRef] [PubMed]
15. Milliman, J.D.; Syvitski, J.P.M. Geomorphic/tectonic control of sediment discharge to the ocean: The importance of small mountainous rivers. *J. Geol.* **1992**, *100*, 525–544. [CrossRef]
16. Darby, S.E.; Hackney, C.R.; Leyland, J.; Kummu, M.; Lauri, H.; Parson, D.R.; Best, J.L.; Nicholas, A.P.; Aalto, R. Fluvial sediment supply to a mega-delta reduced by shifting tropical-cyclone activity. *Nature* **2016**, *539*, 276–279. [CrossRef]
17. Fox-Kemper, B.; Hewitt, H.T.; Xiao, C.; Aðalgeirsdóttir, G.; Drijfhout, S.S.; Edwards, T.L.; Golledge, N.R.; Hemer, M.; Kopp, R.E.; Krinner, G.; et al. Ocean, Cryosphere and Sea Level Change. In *Climate Change 2021: The Physical Science Basis. Contribution of Working Group I to the Sixth Assessment Report of the Intergovernmental Panel on Climate Change*; Masson-Delmotte, V., Zhai, P., Pirani, A., Connors, S.L., Péan, C., Berger, S., Caud, N., Chen, Y., Goldfarb, L., Gomis, M.I., et al., Eds.; Cambridge University Press: Cambridge, UK; New York, NY, USA, 2021; pp. 1211–1362.
18. Darby, S.E.; Dunn, F.E.; Nicholls, R.J.; Rahman, M.; Riddy, L. A first look at the influence of anthropogenic climate change on the future delivery of fluvial sediment to the Ganges-Brahmaputra-Meghna delta. *Environ. Sci. Process. Impact* **2015**, *17*, 1587–1600. [CrossRef]
19. Lorito, S.; Calabrese, L.; Perini, L.; Cibin, U. Uso del suolo della costa. In *Il Sistema Mare-Costa dell'Emilia-Romagna*; Perini, L., Calabrese, L., Eds.; Edizioni Pendragon: Bologna, Italy, 2010; pp. 109–118.
20. Carbognin, L.; Gatto, P.; Mozzi, G. Case history no.9.15: Ravenna, Italy. In *Guidebook to Studies of Land Subsidence due to Ground-Water Withdrawal*; Poland, J.F., Ed.; UNESCO: Paris, France, 1984; pp. 291–305.
21. Bertoni, W.; Brighenti, G.; Gambolati, G.; Ricceri, G.; Vullermin, F. Land subsidence due to gas production in the on- and off-shore natural gas fields of the Ravenna area, Italy. In Proceedings of the 5th International Symposium on Land Subsidence, The Hague, The Netherlands, 16–20 October 1995.
22. Gambolati, G.; Teatini, P.; Tomasi, L.; Gonella, M. Coastline regression of the Romagna Region, Italy, due to sea level rise and natural and anthropogenic land subsidence. *Water Resour. Res.* **1999**, *35*, 163–184. [CrossRef]
23. Teatini, P.; Ferronato, M.; Gambolati, G.; Bertoni, W.; Gonella, M. A century of land subsidence in Ravenna, Italy. *Environ. Geol.* **2005**, *47*, 831–846. [CrossRef]
24. Elfrink, B.; Christensen, E.D.; Broker, I. Coastal morphodynamics in subsiding areas. In *CENAS: Coastline Evolution of the Upper Adriatic Sea Due to Sea Level Rise and Natural and Anthropogenic Land Subsidence*; Gambolati, G., Ed.; Kluwer Academic Publishers: Dordrecht, The Netherlands, 1998; pp. 235–270.
25. Aguzzi, M.; Bonsignore, F.; De Nigris, N.; Morelli, M.; Paccagnella, T.; Romagnoli, V.; Unguendoli, S. *Stato del Litorale Emiliano-Romagnolo al 2012. Erosione e Interventi di Difesa*; Arpae Emilia-Romagna: Bologna, Italy, 2016; p. 230.

26. Billi, P.; Salemi, E.; Preciso, E.; Ciavola, P.; Armaroli, C. Field measurement of bedload in a sand-bed river supplying a sediment starving beach. *Z. Für Geomorphol.* **2017**, *61*, 207–223. [CrossRef]
27. Antonioli, F.; Anzidei, M.; Amorosi, A.; Lo Presti, V.; Mastronuzzi, G.; Deiana, G.; De Falco, G.; Fontana, A.; Fontolan, G.; Lisco, S.; et al. Sea-level rise and potential drowning of the Italian coastal plains: Flooding risk scenarios for 2100. *Quat. Sci. Rev.* **2017**, *158*, 29–43. [CrossRef]
28. Dal Cin, R. I litorali del delta del Po e alle foci dell'Adige e del Brenta: Caratteri tessiturali e dispersione dei sedimenti, cause dell'arretramento e previsioni sull'evoluzione futura. *Boll. Soc. Geol. Ital.* **1983**, *102*, 9–56.
29. Simeoni, U.; Bondesan, M. The role and responsibility of man in the evolution of the Adriatic alluvial coasts of Italy. In *Transformations and Evolution of the Mediterranean Coastline*; Briand, F., Maldonado, A., Eds.; Musée Océanographique: Monaco-Ville, Monaco, 1997; pp. 111–132.
30. Preti, M.; De Nigris, N.; Morelli, M.; Monti, M.; Bonsignore, F.; Aguzzi, M. *Stato del Litorale Emiliano-Romagnolo All'anno 2007 e Piano Decennale di Gestione*; Arpa Emilia-Romagna: Bologna, Italy, 2008.
31. Ente Regionale per le Politiche Ambientali (IDROSER). *Il Trasporto Solido Fluviale Nei Bacini Tributari Dell'Adriatico. Regione Emilia-Romagna, Piano Progettuale per la Difesa della Costa Emiliano-Romagnola*; Regione Emilia-Romagna: Bologna, Italy, 1983; p. 429.
32. Agenzia Regionale per la Protezione Ambientale (ARPA). *Stato Del Litorale Emiliano-Romagnolo All'anno 2000*; Arpa Emilia-Romagna: Bologna, Italy, 2002.
33. Bondesan, M.; Calderoni, G.; Dal Cin, R. Il litorale delle province di Ferrara e Ravenna (Alto Adriatico); evoluzione morfologica e distribuzione dei sedimenti. *Bol. Soc. Geol. Ital.* **1978**, *97*, 247–287.
34. Ente Regionale per le Politiche Ambientali (IDROSER). *Progetto di Piano per la Difesa dal Mare e la Riqualificazione Ambientale del Litorale della Regione Emilia-Romagna, Relazione Generale*; Regione Emilia-Romagna: Bologna, Italy, 1996; p. 365.
35. Simeoni, U.; Atzeni, P.; Bonora, N.; Borasio, E.; Del Grande, C.; Gabbianelli, G.; Gonella, M.; Tessari, U.; Valpreda, E.; Zamariolo, A. Integrated Management Study of Comacchio Coast (Italy). *J. Coast. Res.* **2002**, *36*, 686–693. [CrossRef]
36. Aguzzi, M.; Costantino, R.; De Nigris, N.; Morelli, M.; Romagnoli, C.; Unguendoli, S.; Vecchi, E. *Stato del Litorale Emiliano-Romagnolo al 2018. Erosione e Interventi di Difesa*; Arpae Emilia-Romagna: Bologna, Italy, 2020; p. 222.
37. Preciso, E.; Salemi, E.; Billi, P. Land use changes, torrent control works and sediment mining: Effect on channel morphology and sediment flux, case study of the Reno River (Northern Italy). *Hydrol. Processes* **2012**, *26*, 1134–1148. [CrossRef]
38. Antolini, G.; Auteri, L.; Pavan, V.; Tomei, F.; Tomozeiu, R.; Marletto, V. A daily high-resolution gridded climatic data set for Emilia-Romagna, Italy, during 1961–2010. *Int. J. Clim.* **2016**, *36*, 1970–1986. [CrossRef]
39. Pavan, V.; Tomozeiu, R.; Cacciamani, C.; Di Lorenzo, M. Daily precipitation observations over Emilia-Romagna: Mean values and extremes. *Int. J. Climatol.* **2008**, *28*, 2065–2079. [CrossRef]
40. Pavan, V.; Antolini, G.; Barbiero, R.; Berni, N.; Brunier, F.; Cacciamani, C.; Cagnati, A.; Cazzuli, O.; Cicogna, A.; De Luigi, C.; et al. High resolution climate precipitation analysis for north-central Italy, 1961–2015. *Clim. Dyn.* **2019**, *52*, 3435–3453. [CrossRef]
41. Fioravanti, G.; Piervitali, E.; Desiato, F.; Perconti, W.; Fraschetti, P. *Variazioni e Tendenze Degli Estremi di Temperature e Precipitazione in Italia*; ISPRA: Roma, Italy, 2013; p. 60.
42. Cacciamani, C.; Nanni, S.; Tibaldi, S. Mesoclimatology of winter temperature and precipitation in the Po Valley of Northern Italy. *Int. J. Climatol.* **1994**, *14*, 777–814. [CrossRef]
43. Brunetti, M.; Maugeri, M.; Monti, F.; Nanni, T. Temperature and precipitation variability in Italy in the last two centuries from homogenized instrumental time series. *Int. J. Climatol.* **2006**, *26*, 345–381. [CrossRef]
44. Desiato, F.; Fioravanti, G.; Fraschetti, P.; Piervitali, E.; Pavan, V. *Gli Indicatori del Clima in Italia nel 2014*; ISPRA: Roma, Italy, 2015.
45. Billi, P.; Fazzini, M. Global change and river flow in Italy. *Glob. Planet. Chang.* **2017**, *155*, 234–246. [CrossRef]
46. Toreti, A.; Fioravanti, G.; Perconti, W.; Desiato, F. Annual and seasonal precipitation over Italy from 1961 to 2006. *Int. J. Climatol.* **2009**, *29*, 1976–1987. [CrossRef]
47. Trenberth, K.E.; Jones, P.D.; Ambenje, P.; Bojariu, R.; Easterling, D.; Klein Tank, A.; Parker, D.; Rahimzadeh, F.; Renwick, J.A.; Rusticucci, M.; et al. Observations: Surface and atmospheric climate change. In *Climate Change 2007: The Physical Science Basis, Contribution of Working Group I to the Fourth Assessment Report of the IPCC*; Solomon, S., Qin, D., Manning, M., Chen, Z., Marquis, M., Averyt, K.B., Tignor, M., Miller, H.L., Eds.; Cambridge University Press: Cambridge, UK, 2007.
48. Norrant, C.; Douguedroit, A. Monthly and daily precipitation trends in the Mediterranean (1950–2000). *Theor. Appl. Climatol.* **2006**, *83*, 89–106. [CrossRef]
49. Eurosion. *Living with Coastal Erosion in Europe: A Guide to Coastal Erosion Management Practices in Europe: Lessons Learned. A Case Study of Marina di Ravenna and Lido Adriano*; Directorate General Environment European Commission: Brussels, Belgium, 2004.
50. Comerci, V.; Vittori, E. The Need for a Standardized Methodology for Quantitative Assessment of Natural and Anthropogenic Land Subsidence: The Agosta (Italy) Gas Field Case. *Remote Sens.* **2019**, *11*, 1178. [CrossRef]
51. Lasanta, T.; Beguería, S.; García-Ruiz, J.M. Geomorphic and hydrological effects of traditional shifting agriculture in a Mediterranean mountain, Central Spanish Pyrenees. *Mt. Res. Dev.* **2006**, *26*, 146–152. [CrossRef]
52. Falcucci, A.; Maiorano, L.; Boitani, L. Changes in land-use/land-cover patterns in Italy and their implications for biodiversity conservation. *Landsc. Ecol.* **2007**, *22*, 617–631. [CrossRef]
53. Béjar, M.; Vericat, D.; Batalla, R.J.; Gibbins, C.N. Variation in flow and suspended sediment transport in a montane river affected by hydropeaking and instream mining. *Geomorphology* **2018**, *310*, 69–83. [CrossRef]

54. Spalevic, V.; Barovic, G.; Vujacic, D.; Curovic, M.; Behzadfar, M.; Djurovic, N.; Dudic, B.; Billi, P. The Impact of Land Use Changes on Soil Erosion in the River Basin of Miocki Potok, Montenegro. *Water* **2020**, *12*, 2973. [CrossRef]
55. Zerbini, S.; Raicich, F.; Prati, C.M.; Bruni, S.; Del Conte, S.; Errico, M.; Santi, E. Sea-level change in the Northern Mediterranean Sea from long-period tide gauge time series. *Earth Sci. Rev.* **2017**, *167*, 72–87. [CrossRef]
56. Bruni, S.; Zerbini, S.; Raicich, F.; Errico, M. Rescue of the 1873-1922 high and low waters of the Porto Corsini/Marina di Ravenna (northern Adriatic, Italy) tide gauge. *J. Geod.* **2019**, *93*, 1227–1244. [CrossRef]
57. Dext3r-SIMC Platform. Available online: https://simc.arpae.it/dext3r/ (accessed on 19 April 2021).
58. Arpae Website. Available online: www.arpae.it (accessed on 12 February 2021).
59. Holgate, S.J.; Matthews, A.; Woodworth, P.L.; Rickards, L.J.; Tamisiea, M.E.; Bradshaw, E.; Foden, P.R.; Gordon, K.M.; Jevrejeva, S.; Pugh, J. New Data System and Products at the Permanent Service for Mean Sea Level. *J. Coast. Res.* **2013**, *29*, 493–504. [CrossRef]
60. PSMSL Website. Available online: http://www.psmsl.org/data/obtaining/ (accessed on 3 January 2022).
61. Romagnoli, C.; Zerbini, S.; Raicich, F.; Richter, B.; Lago, L.; Domenichini, D.; Thomsen, I. Sea level variations from tide gauges and GPS in the Northern Adriatic. In Proceedings of the EGS XXVII General Assembly, Nice, France, 21–26 April 2002.
62. Hurrell, J.W.; van Loon, H. Decadal variations in climate associated with the north Atlantic oscillation. *Clim. Chang.* **1997**, *36*, 301–326. [CrossRef]
63. Hurrell, J.W.; Kushnir, Y.; Ottersen, G.; Visbeck, M. An Overview of the North Atlantic Oscillation. In *The North Atlantic Oscillation: Climatic Significance and Environmental Impact*; Hurrell, J.W., Kushnir, Y., Ottersen, G., Visbeck, M., Eds.; American Geophysical Union: Washington, DC, USA, 2003. [CrossRef]
64. NCAR Website. Available online: https://climatedataguide.ucar.edu/climate-data/hurrell-north-atlantic-oscillation-nao-index-station-based (accessed on 14 March 2021).
65. Kerr, R.A. A North Atlantic Climate Pacemaker for the Centuries. *Science* **2000**, *288*, 1984–1985. [CrossRef] [PubMed]
66. NOAA/PSD Website. Available online: https://psl.noaa.gov/data/timeseries/AMO/ (accessed on 14 March 2021).
67. Universitat de Barcelona Website. Available online: http://www.ub.edu/gc/wemo/ (accessed on 29 June 2022).
68. Lopez-Bustins, J.A.; Lemus-Canovas, M. The influence of the Western Mediterranean Oscillation upon the spatio-temporal variability of precipitation over Catalonia (northeastern of the Iberian Peninsula). *Atmos. Res.* **2020**, *236*, 104819. [CrossRef]
69. Vicente-Serrano, S.M.; Begueria, S.; López-Moreno, J.I. A multiscalar drought index sensitive to global warming: The standardized precipitation evapotranspiration index. *J. Clim.* **2010**, *23*, 1696–1718. [CrossRef]
70. McKee, T.B.; Doesken, N.J.; Kleist, J. The relationship of drought frequency and duration to time scales. In Proceedings of the 8th Conference on Applied Climatology, Anaheim, CA, USA, 17–22 January 1993.
71. Palmer, W.C. *Meteorological Drought*; U.S. Government Printing Office: Washington, DC, USA, 1965.
72. CSIC Website. Available online: https://spei.csic.es/database.html (accessed on 18 April 2021).
73. Allen, R.G.; Pereira, L.S.; Raes, D.; Smith, M. *Crop Evapotranspiration—Guidelines for Computing Crop Water Requirements—FAO Irrigation and Drainage Paper 56*; FAO: Rome, Italy, 1998.
74. Wang, K.; Li, Z.; Cribb, M. Estimation of evaporative fraction from a combination of day and night land surface temperatures and NDVI: A new method to determine the Priestley–Taylor parameter. *Remote Sens. Environ.* **2006**, *102*, 293–305. [CrossRef]
75. Vicente-Serrano, S.M.; Beguería, S.; Lorenzo-Lacruz, J.; Camarero, J.J.; López-Moreno, J.I.; Azorin-Molina, C.; Revuelto, J.; Morán-Tejeda, E.; Sanchez-Lorenzo, A. Performance of Drought Indices for Ecological, Agricultural, and Hydrological Applications. *Earth Interact.* **2012**, *16*, 1–27. [CrossRef]
76. McEvoy, D.J.; Huntington, J.L.; Abatzoglou, J.T.; Edwards, L.M. An Evaluation of Multiscalar Drought Indices in Nevada and Eastern California. *Earth Interact.* **2012**, *16*, 1–18. [CrossRef]
77. Zipper, S.C.; Qiu, J.; Kucharik, C.J. Drought effects on US maize and soybean production: Spatiotemporal patterns and historical changes. *Environ. Res. Lett.* **2016**, *11*, 094021. [CrossRef]
78. Chen, T.; Xia, G.; Liu, T.; Chen, W.; Chi, D. Assessment of drought impact on main cereal crops using a standardized precipitation evapotranspiration index in Liaoning Province, China. *Sustainability* **2016**, *8*, 1069. [CrossRef]
79. Zhang, Q.; Kong, D.; Singh, V.P.; Shi, P. Response of vegetation to different time-scales drought across China: Spatiotemporal patterns, causes and implications. *Glob. Planet. Chang.* **2017**, *152*, 1–11. [CrossRef]
80. Páscoa, P.; Gouveia, C.M.; Russo, A.; Trigo, R.M. The role of drought on wheat yield interannual variability in the Iberian Peninsula from 1929 to 2012. *Int. J. Biometeorol.* **2017**, *61*, 439–451. [CrossRef]
81. Labudová, L.; Labuda, M.; Takáč, A. Comparison of SPI and SPEI applicability for drought impact assessment on crop production in the Danubian lowland and the east Slovakian lowland. *Theor. Appl. Climatol.* **2017**, *128*, 491–506. [CrossRef]
82. Muñoz Sabater, J. ERA5-Land Monthly Averaged Data from 1981 to Present. Copernicus Climate Change Service (C3S) Climate Data Store (CDS). Available online: https://cds.climate.copernicus.eu/cdsapp#!/dataset/10.24381/cds.68d2bb30?tab=overview (accessed on 10 July 2022).
83. Muñoz Sabater, J. ERA5-Land Monthly Averaged Data from 1950 to 1980. Copernicus Climate Change Service (C3S) Climate Data Store (CDS). Available online: https://cds.climate.copernicus.eu/cdsapp#!/dataset/10.24381/cds.68d2bb30?tab=overview (accessed on 10 July 2022).
84. C3S Website. Available online: https://cds.climate.copernicus.eu/cdsapp#!/dataset/reanalysis-era5-land-monthly-means?tab=overview (accessed on 10 July 2022).
85. Emilia-Romagna Region Website. Available online: https://geoportale.regione.emilia-romagna.it/ (accessed on 4 March 2021).

86. Mann, H.B. Non-parametric tests against trend. *Econometrica* **1945**, *13*, 163–171. [CrossRef]
87. Kendall, M.G. *Rank Correlation Methods*, 4th ed.; Charles Griffin: London, UK, 1975.
88. Hamed, K.H.; Rao, A.R. A modified Mann-Kendall trend test for autocorrelated data. *J. Hydrol.* **1998**, *204*, 182–196. [CrossRef]
89. Theil, H. *A Rank-Invariant Method of Linear and Polynomial Regression Analysis*; Nederl. Akad. Wetensch., Proc.; Springer: Berlin/Heidelberg, Germany, 1950.
90. Sen, P.K. Estimates of the Regression Coefficient Based on Kendall's Tau. *J. Am. Stat. Assoc.* **1968**, *63*, 1379–1389. [CrossRef]
91. Wilcox, R.R. *Theil–Sen Estimator, Fundamentals of Modern Statistical Methods: Substantially Improving Power and Accuracy*; Springer: New York, NY, USA, 2001.
92. Zervas, C.E. Sea level variations of the United States, 1854–1999. In *NOAA Technical Report NOS CO-OPS 36*; U.S. Department of Commerce; National Oceanic and Atmospheric Administration; National Ocean Service: Silver Spring, MD, USA, 2011.
93. Frich, P.; Alexander, L.V.; Della-Marta, P.; Gleason, B.; Haylock, M.; Klein Tank, A.M.G.; Peterson, T. Observed coherent changes in climatic extremes during the second half of the twentieth century. *Clim. Res.* **2002**, *19*, 193–212. [CrossRef]
94. Tsimplis, M.N.; Raicich, F.; Fenoglio-Marc, L.; Shaw, A.G.P.; Marcos, M.; Somot, S.; Bergamasco, F. Recent developments in understanding sea level rise in the Adriatic coasts. *Phys. Chem. Earth Parts A/B/C* **2012**, *40–41*, 59–71. [CrossRef]
95. Wöppelmann, G.; Marcos, M. Vertical land motion as a key to understanding sea level change and variability. *Rev. Geophys.* **2016**, *54*, 64–92. [CrossRef]
96. Watson, P.J. An Assessment of the Utility of Satellite Altimetry and Tide Gauge Data (ALT-TG) as a Proxy for Estimating Vertical Land Motion. *J. Coast. Res.* **2019**, *35*, 1131–1144. [CrossRef]
97. Oelsmann, J.; Passaro, M.; Dettmering, D.; Schwatke, C.; Sánchez, L.; Seitz, F. The zone of influence: Matching sea level variability from coastal altimetry and tide gauges for vertical land motion estimation. *Ocean Sci.* **2021**, *17*, 35–57. [CrossRef]
98. Santamaría-Gómez, A.; Gravelle, M.; Collilieux, X.; Guichard, M.; Martín Míguez, B.; Tipahaneau, P.; Wöppelmann, G. Mitigating the effects of vertical land motion in tide gauge records using a state-of-the-art GPS velocity field. *Glob. Planet. Chang.* **2012**, *98–99*, 6–17. [CrossRef]
99. Zerbini, S.; Plag, H.-P.; Baker, T.; Becker, M.; Billiris, H.; Bürki, B.; Kahle, H.-G.; Marson, I.; Pezzoli, L.; Richter, B.; et al. Sea level in the Mediterranean: A first step towards separating crustal movements and absolute sea-level variations. *Glob. Planet. Chang.* **1996**, *14*, 1–48. [CrossRef]
100. Bouin, M.-N.; Wöppelmann, G. Land motion estimates from GPS at tide gauges: A geophysical evaluation. *Geophys. J. Int.* **2010**, *180*, 193–209. [CrossRef]
101. Carbognin, L.; Teatini, P.; Tosi, L. The impact of relative sea level rise on the Northern Adriatic Sea coast, Italy. In *Management of Natural Resources, Sustainable Development and Ecological Hazards II*; Brebbia, C.A., Jovanovic, N., Tiezzi, E., Eds.; WIT Press: Southampton, UK, 2009.
102. Furlani, S.; Biolchi, S.; Cucchi, F.; Antonioli, F.; Busetti, M.; Melis, R. Tectonic effects on Late Holocene sea level changes in the Gulf of Trieste (NE Adriatic Sea, Italy). *Quat. Int.* **2011**, *232*, 144–157. [CrossRef]
103. Farolfi, G.; Del Ventisette, C. Contemporary crustal velocity field in Alpine Mediterranean area of Italy from new geodetic data. *GPS Solut.* **2016**, *20*, 715–722. [CrossRef]
104. Vacchi, M.; Marriner, N.; Morhange, C.; Spada, G.; Fontana, A.; Rovere, A. Multiproxy assessment of Holocene relative sea-level changes in the western Mediterranean: Sea-level variability and improvements in the definition of the isostatic signal. *Earth Sci. Rev.* **2016**, *155*, 172–197. [CrossRef]
105. Vilibić, I.; Šepić, J.; Pasarić, M.; Orlić, M. The Adriatic Sea: A long-standing laboratory for sea level studies. *Pure Appl. Geophys.* **2017**, *174*, 3765–3811. [CrossRef]
106. Sánchez, L.; Völksen, C.; Sokolov, A.; Arenz, H.; Seitz, F. Presentday surface deformation of the Alpine region inferred from geodetic techniques, *Earth Syst. Sci. Data* **2018**, *10*, 1503–1526.
107. Huang, N.E.; Shen, Z.; Long, S.R.; Wu, M.C.; Shih, H.H.; Zheng, Q.; Yen, N.-C.; Tung, C.C.; Liu, H.H. The empirical mode decomposition and the Hilbert spectrum for nonlinear and non-stationary time series analysis. *Proc. R. Soc. Lond. A* **1998**, *45*, 903–995. [CrossRef]
108. Ezer, T.; Corlett, W.B. Is sea level rise accelerating in the Chesapeake Bay? A demonstration of a novel new approach for analyzing sea level data. *Geophys. Res. Lett.* **2012**, *39*, L19605. [CrossRef]
109. Ezer, T.; Atkinson, L.P.; Corlett, W.B.; Blanco, J.L. Gulf Stream's induced sea level rise and variability along the US mid-Atlantic coast. *J. Geophys. Res. Oceans* **2013**, *118*, 685–697. [CrossRef]
110. Spada, G.; Galassi, G.; Olivieri, M. A study of the longest tide gauge sea-level record in Greenland (Nuuk/Godthab, 1958–2002). *Glob. Planet. Chang.* **2014**, *118*, 42–51. [CrossRef]
111. Galassi, G.; Spada, G. Linear and non-linear sea-level variations in the Adriatic Sea from tide gauge records (1872–2012). *Ann. Geophys.* **2014**, *57*, P0658. [CrossRef]
112. Bonaduce, A.; Pinardi, N.; Oddo, P.; Spada, G.; Larnicol, G. Sea-level variability in the Mediterranean Sea from altimetry and tide gauges. *Clim. Dyn.* **2016**, *47*, 2851–2866. [CrossRef]
113. Vecchio, A.; Anzidei, M.; Serpelloni, E.; Florindo, F. Natural Variability and Vertical Land Motion Contributions in the Mediterranean Sea-Level Records over the Last Two Centuries and Projections for 2100. *Water* **2019**, *11*, 1480. [CrossRef]
114. Meli, M.; Olivieri, M.; Romagnoli, C. Sea-Level Change along the Emilia-Romagna Coast from Tide Gauge and Satellite Altimetry. *Remote Sens.* **2021**, *13*, 97. [CrossRef]

115. Croux, C.; Dehon, C. Influence function of the Spearman and Kendall correlation measures. *Stat. Methods Appl.* **2010**, *19*, 497–515. [CrossRef]
116. Bartlett, M.S. Some aspects of the time-correlation problem in regard to tests of significance. *J. R. Stat. Soc.* **1935**, *98*, 536–543. [CrossRef]
117. Santer, B.D.; Wigley, T.M.L.; Boyle, J.S.; Gaffen, D.J.; Hnilo, J.J.; Nychka, D.; Parker, D.E.; Taylor, K.E. Statistical significance of trends and trend differences in layer-average atmospheric temperature time series. *J. Geophys. Res.* **2000**, *105*, 7337–7356. [CrossRef]
118. Lomb, N.R. Least-squares frequency analysis of unequally spaced data. *Astrophys. Space Sci.* **1976**, *39*, 447–462. [CrossRef]
119. Scargle, J.D. Studies in astronomical time series analysis. II—Statistical aspects of spectral analysis of unevenly spaced data. *Astrophys. J.* **1982**, *263*, 835–853. [CrossRef]
120. Baluev, R.V. Assessing the statistical significance of periodogram peaks. *Mon. Not. R. Astron. Soc.* **2008**, *385*, 1279–1285. [CrossRef]
121. Oke, T.R. The energetic basis of the urban heat island. *Q. J. R. Meteorol. Soc.* **1982**, *108*, 1–24. [CrossRef]
122. Swaid, H. Nocturnal variation of air-surface temperature gradients for typical urban and rural surfaces. *Atmos. Environ. Part B Urban Atmos.* **1991**, *25*, 333–341. [CrossRef]
123. Paulo, A.A.; Rosa, R.D.; Pereira, L.S. Climate trends and behaviour of drought indices based on precipitation and evapotranspiration in Portugal. *Nat. Haz. Earth Syst. Sci.* **2012**, *12*, 1481–1491. [CrossRef]
124. Gatto, P.; Carbognin, L. The Lagoon of Venice: Natural environmental trend and man-induced modification. *Hydrol. Sci. J.* **1981**, *26*, 379–391. [CrossRef]
125. Tosi, L.; Teatini, P.; Strozzi, T.; Carbognin, L.; Brancolini, G.; Rizzetto, F. Ground surface dynamics in the northern Adriatic coastland over the last two decades. *Rend. Fis. Acc. Lincei* **2010**, *21*, 115–129. [CrossRef]
126. Zerbini, S.; Bruni, S.; Raicich, F. Tide gauge data archaeology provides natural subsidence rates along the coasts of the Po Plain and of the Veneto–Friuli Plain, Italy. *Geophys. J. Int.* **2021**, *225*, 253–260. [CrossRef]
127. Gambolati, G.; Teatini, P. Numerical analysis of land subsidence due to natural compaction of the upper Adriatic Sea Basin. In *CENAS: Coastline Evolution of the Upper Adriatic Sea Due to Sea Level Rise and Natural and Anthropogenic Land Subsidence*; Gambolati, G., Ed.; Springer: Berlin/Heidelberg, Germany, 1998.
128. Carminati, E.; Doglioni, C.; Scrocca, D. Apennines subduction-related subsidence of Venice (Italy). *Geophys. Res. Lett.* **2003**, *30*, 1717. [CrossRef]
129. Antonioli, F.; Ferranti, L.; Fontana, A.; Amorosi, A.; Bondesan, A.; Braitenberg, C.; Dutton, A.; Fontolan, G.; Furlani, S.; Lambeck, K.; et al. Holocene relative sea-level changes and vertical movements along the Italian and Istrian coastlines. *Quat. Int.* **2009**, *206*, 102–133. [CrossRef]
130. Heymann, Y.; Steenmans, C.; Croisille, G.; Bossard, M. *CORINE Land Cover. Technical Guide*; Office for Official Publications of European Communities: Luxembourg, 1994.
131. Foley, J.A.; Defries, R.; Asner, G.P.; Barford, C.; Bonan, G.; Carpenter, S.R.; Chapin, F.S.; Coe, M.T.; Daily, G.C.; Gibbs, H.K.; et al. Global consequences of land use. *Science* **2005**, *309*, 570–574. [CrossRef]
132. Blondel, J. The 'design' of Mediterranean landscapes: A millennial story of humans and ecological systems during the historic period. *Hum. Ecol.* **2006**, *34*, 713–729. [CrossRef]
133. Federal Office for the Environment (FOEN). *Urban Sprawl in Europe*; Publications Office of the European Union: Luxembourg, 2016.
134. Scalenghe, R.; Marsan, F.A. The anthropogenic sealing of soils in urban areas. *Landsc. Urban Plan.* **2009**, *90*, 1–10. [CrossRef]
135. Agenzia Regionale per la Protezione Ambientale (ARPA). *Annuario Regionale dei Dati Ambientali*; ARPA: Bologna, Italy, 2010.
136. Todaro, V.; D'Oria, M.; Secci, D.; Zanini, A.; Tanda, M.G. Climate Change over the Mediterranean Region: Local Temperature and Precipitation Variations at Five Pilot Sites. *Water* **2022**, *14*, 2499. [CrossRef]
137. Mariotti, A.; Zeng, N.; Yoon, J.; Artale, V.; Navarra, A.; Alpert, P.; Li, L.Z.X. Mediterranean water cycle changes: Transition to drier 21st century conditions in observations and CMIP3 simulations. *Environ. Res. Lett.* **2008**, *3*, 044001. [CrossRef]
138. Maugeri, M.; Nanni, T. Surface Air Temperature Variations in Italy: Recent Trends and an Update to 1993. *Theor. Appl. Climatol.* **1998**, *61*, 191–196. [CrossRef]
139. Brunetti, M.; Maugeri, M.; Nanni, T. Variations of Temperature and Precipitation in Italy from 1866 to 1995. *Theor. Appl. Climatol.* **2000**, *65*, 165–174. [CrossRef]
140. Toreti, A.; Desiato, F. Temperature trend over Italy from 1961 to 2004. *Theor. Appl. Climatol.* **2008**, *91*, 51–58. [CrossRef]
141. Balling, R.C., Jr.; Vose, R.S.; Weber, G.-R. Analysis of long-term European temperature records: 1751–1995. *Clim. Res.* **1998**, *10*, 193–200. [CrossRef]
142. Klein Tank, A.M.G.; Wijngaard, J.B.; Koennen, G.P.; Boehm, R.; Demaree, G.; Gocheva, A.; Mileta, M.; Pashiardis, S.; Hejkrlik, L.; Kern-Hansen, C.; et al. Daily dataset of 20th-century surface air temperature and precipitation series for the European Climate Assessment. *Int. J. Climatol.* **2002**, *22*, 1441–1453. [CrossRef]
143. Jones, P.D.; Parker, D.E.; Osborn, T.J.; Briffa, K.R. *Global and Hemisphere Temperature Anomalies Land and Marine Instrumental Records*; ESS-DIVE Repository; Carbon Dioxide Information Analysis Center (CDIAC); Oak Ridge National Laboratory (ORNL): Oak Ridge, TN, USA, 2005.
144. Stanhill, G.; Cohen, S. Global dimming: A review of the evidence for a widespread and significant reduction in global radiation with discussion of its probable causes and possible agricultural consequences. *Agric. For. Meteor.* **2001**, *107*, 255–278. [CrossRef]

145. Wild, M.; Gilgen, H.; Roesch, A.; Ohmura, A.; Long, C.N.; Dutton, E.G.; Forgan, B.; Kallis, A.; Russak, V.; Tsvetkov, A. From Dimming to Brightening: Decadal Changes in Solar Radiation at Earth's Surface. *Science* **2005**, *308*, 847–850. [CrossRef] [PubMed]
146. Kvalevåg, M.M.; Myrhe, G. Human impact on direct and diffuse solar radiation during the industrial era. *J. Clim.* **2007**, *20*, 4874–4883. [CrossRef]
147. Kim, D.Y.; Ramanathan, V. Solar radiation budget and radiative forcing due to aerosols and clouds. *J. Geophys. Res.* **2008**, *113*, D02203. [CrossRef]
148. Ruckstuhl, C.; Philipona, R.; Behrens, K.; Coen, M.C.; Dürr, B.; Heimo, A.; Mätzler, C.; Nyeki, S.; Ohmura, A.; Vuilleumier, L.; et al. Aerosol and cloud effects on solar brightening and the recent rapid warming. *Geophys. Res. Lett.* **2008**, *35*, L12708. [CrossRef]
149. Streets, D.G.; Yan, F.; Chin, M.; Diehl, T.; Mahowald, N.; Schultz, M.; Wild, M.; Wu, Y.; Yu, C. Anthropogenic and natural contributions to regional trends in aerosol optical depth, 1980-2006. *J. Geophys. Res. Atmos.* **2009**, *114*, D00D18. [CrossRef]
150. Wang, K.C.; Dickinson, R.E.; Liang, S.L. Clear sky visibility has decreased over land globally from 1973 to 2007. *Science* **2009**, *323*, 1468–1470. [CrossRef]
151. Breshears, D.D.; Cobb, N.S.; Rich, P.M.; Price, K.P.; Allen, C.D.; Balice, R.G.; Romme, W.H.; Kastens, J.H.; Floyd, M.L.; Belnap, J.; et al. Regional vegetation die-off in response to global-change-type drought. *Proc. Nat. Acad. Sci. USA* **2005**, *102*, 15144–15148. [CrossRef]
152. Adams, H.D.; Guardiola-Claramonte, M.; Barron-Gafford, G.A.; Villegas, J.C.; Breshears, D.D.; Zou, C.B.; Troch, P.A.; Huxman, E. Temperature sensitivity of drought-induced tree mortality portends increased regional die-off under global-change-type drought. *Proc. Nat. Acad. Sci. USA* **2009**, *106*, 7063–7066. [CrossRef]
153. Tomozeiu. R.; Busuioc, A.; Marletto, V.; Zinoni, F.; Cacciamani, C. Detection of changes in the summer precipitation time series of the region Emilia-Romagna, Italy. *Theor. Appl. Climatol.* **2000**, *67*, 193–200. [CrossRef]
154. Crespi, A.; Brunetti, M.; Lentini, G.; Maugeri, M. 1961–1990 high resolution monthly precipitation climatologies for Italy. *Int. J. Climatol.* **2018**, *38*, 878–895. [CrossRef]
155. Ramanathan, V.; Crutzen, P.J.; Jiehl, J.T.; Rosenfeld, D. Aerosols, climate, and the hydrological cycle. *Science* **2001**, *294*, 2119–2124. [CrossRef] [PubMed]
156. Wild, M.; Liepert, B. The Earth radiation balance as driver of the global hydrological cycle. *Environ. Res. Lett.* **2010**, *5*, 025003. [CrossRef]
157. Wild, M. Enlightening Global Dimming and Brightening. *Bull. Am. Meteor. Soc.* **2012**, *93*, 27–37. [CrossRef]
158. Wild, M. Global dimming and brightening: A review. *J. Geophys. Res.* **2009**, *114*, D00D16. [CrossRef]
159. Mariotti, A.; Struglia, M.V.; Zeng, N.; Lau, K.-M. The Hydrological Cycle in the Mediterranean Region and Implications for the Water Budget of the Mediterranean Sea. *J. Clim.* **2002**, *15*, 1674–1690. [CrossRef]
160. Seager, R.; Liu, H.; Henderson, N.; Simpson, I.; Kelley, C.; Shaw, T.; Kushnir, Y.; Ting, M. Causes of increasing aridification of the Mediterranean region in response to rising greenhouse gases. *J. Clim.* **2014**, *27*, 4655–4676. [CrossRef]
161. Mariotti, A.; Pan, Y.; Zeng, N.; Alessandri, A. Long-term climate change in the Mediterranean region in the midst of decadal variability. *Clim. Dyn.* **2015**, *44*, 1437–1456. [CrossRef]
162. Toreti, A.; Naveau, P.; Zampieri, M.; Schindler, A.; Scoccimarro, E.; Xoplaki, E.; Dijkstra, H.A.; Gualdi, S.; Luterbacher, J. Projections of global changes in precipitation extremes from Coupled Model Intercomparison Project Phase 5 Models. *Geophys. Res. Lett.* **2013**, *40*, 4887–4892. [CrossRef]
163. Benini, L.; Bandini, V.; Marazza, D.; Contin, A. Assessment of land use changes through an indicator-based approach: A case study from the Lamone river basin in Northern Italy. *Ecol. Indic.* **2010**, *10*, 4–14. [CrossRef]
164. Scanlon, B.R.; Jolly, I.; Sophocleous, M.; Zhang, L. Global impacts of conversion from natural to agricultural ecosystems on water resources: Quantity versus quality. *Water Resour. Res.* **2007**, *43*, W03437. [CrossRef]
165. Filoso, S.; Bezerra, M.O.; Weiss, K.C.B.; Palmer, M.A. Impacts of forest restoration on water yield: A systematic review. *PLoS ONE* **2017**, *12*, e0183210. [CrossRef] [PubMed]
166. Teuling, A.J.; de Badts, E.; Jansen, F.A.; Fuchs, R.; Buitink, J.; van Dijke, A.J.; Sterling, S. Climate change, re-/afforestation, and urbanisation impacts on evapotranspiration and streamflow in Europe. *Hydrol. Earth Syst. Sci.* **2019**, *23*, 3631–3652. [CrossRef]
167. Milner, A.M.; Khamis, K.; Battin, T.J.; Brittain, J.E.; Barrand, N.E.; Füreder, L.; Cauvy-Fraunié, S.; Gíslason, G.M.; Jacobsen, D.; Hannah, D.M.; et al. Glacier shrinkage driving global changes in downstream systems. *Proc. Nat. Acad. Sci. USA* **2017**, *114*, 9770–9778. [CrossRef]
168. López-Moreno, J.I.; García-Ruiz, J.M.; Beniston, M. Environmental change and water management in the Pyrenees. Facts and future perspectives for Mediterranean mountains. *Glob. Planet. Chang.* **2008**, *66*, 300–312. [CrossRef]
169. García-Ruiz, J.M.; López-Moreno, J.I.; Vicente-Serrano, S.M.; Lasanta-Martínez, T.; Beguería, S. Mediterranean water resources in a global change scenario. *Earth Sci. Rev.* **2011**, *105*, 121–139. [CrossRef]
170. Istituto Nazionale di Statistica (ISTAT), 2010. Censimento Agricoltura 2010. Database. Available online: http://dati-censimentoagricoltura.istat.it/ (accessed on 7 September 2021).
171. European Commission. *Guidelines on Best Practice to Limit, Mitigate or Compensate Soil Sealing*; Publications Office of the European Union: Luxembourg, 2012.
172. Kingston, D.G.; Lawler, D.M.; McGregor, G.R. Linkages between atmospheric circulation, climate and streamflow in the northern North Atlantic: Research prospects. *Prog. Phys. Geogr.* **2006**, *30*, 143–174. [CrossRef]

173. Marullo, S.; Artale, V.; Santoleri, R. The SST multi-decadal variability in the Atlantic- Mediterranean region and its relation to AMO. *J. Clim.* **2011**, *24*, 4385–4401. [CrossRef]
174. Mariotti, A.; Dell'Aquila, A. Decadal climate variability in the Mediterranean region: Roles of large-scale forcings and regional processes. *Clim. Dyn.* **2012**, *38*, 1129–1145. [CrossRef]
175. Börgel, F.; Frauen, C.; Neumann, T.; Markus Meier, H.E. The Atlantic Multidecadal Oscillation controls the impact of the North Atlantic Oscillation on North European climate. *Environ. Res. Lett.* **2020**, *15*, 104025. [CrossRef]
176. Tsimplis, M.N.; Josey, S.A. Forcing of the Mediterranean Sea by atmospheric oscillations over the North Atlantic. *Geophys. Res. Lett.* **2001**, *28*, 803–806. [CrossRef]
177. Menemenlis, D.; Fukumori, J.; Lee, T. Atlantic to Mediterranean Sea Level Difference Driven by Winds near Gibraltar Strait. *J. Phys. Oceanogr.* **2007**, *37*, 359–376. [CrossRef]
178. Tsimplis, M.N.; Calafat, F.M.; Marcos, M.; Jordà, G.; Gomis, D.; Fenoglio-Marc, L.; Struglia, M.V.; Josey, S.A.; Chambers, D.P. The effect of the NAO on sea level and on mass changes in the Mediterranean Sea. *J. Geophys. Res.* **2013**, *118*, 944–952. [CrossRef]
179. Fenoglio-Marc, L.; Mariotti, A.; Sannino, G.; Meyssignac, B.; Carillo, A.; Struglia, M.V.; Rixen, M. Decadal variability of net water flux at the Mediterranean Sea Gibraltar Strait. *Glob. Planet. Chang.* **2013**, *100*, 1–10. [CrossRef]
180. Della-Marta, P.M.; Luterbacher, J.; von Weissenfluh, H.; Xoplaki, E.; Brunet, M.; Wanner, H. Summer heat waves over western Europe 1880-2003, their relationship to large-scale forcings and predictability. *Clim. Dyn.* **2007**, *29*, 251–275. [CrossRef]
181. López-Moreno, J.I.; Vicente-Serrano, S.M.; Morán-Tejeda, E.; Lorenzo-Lacruz, J.; Kenawy, A.; Beniston, M. Effects of the North Atlantic Oscillation (NAO) on combined temperature and precipitation winter modes in the Mediterranean mountains: Observed relationship and projections for the 21st century. *Glob. Planet. Chang.* **2011**, *77*, 62–76. [CrossRef]
182. Rust, H.W.; Richling, A.; Bissolli, P.; Ulbrich, U. Linking teleconnection patterns to European temperature—a multiple linear regression model. *Meteorol. Z.* **2015**, *24*, 411–423. [CrossRef]
183. Di Bacco, M.; Scorzini, A.R. Recent changes in temperature extremes across the north-eastern region of Italy and their relationship with large-scale circulation. *Clim. Res.* **2020**, *81*, 167–185. [CrossRef]
184. Hurrell, J.W. Decadal trends in the North-Atlantic Oscillation: Regional temperatures and precipitation. *Science* **1995**, *269*, 676–679. [CrossRef]
185. Xoplaki, E.; González-Rouco, J.F.; Luterbacher, J.; Wanner, H. Wet season Mediterranean precipitation variability: Influence of large-scale dynamics and trends. *Clim. Dyn.* **2004**, *23*, 63–78. [CrossRef]
186. Serreze, M.C.; Carse, F.; Barry, R.G.; Rogers, J.C. Icelandic low cyclone activity: Climatological features, linkages with the NAO, and relationships with recent changes in the Northern Hemisphere circulation. *J. Clim.* **1997**, *10*, 453–464. [CrossRef]
187. Cullen, H.M.; Kaplan, A.; Arkin, P.; Demenocal, P.B. Impact of the North Atlantic Oscillation on Middle Eastern climate and streamflow. *Clim. Chang.* **2002**, *55*, 315–338. [CrossRef]
188. Struglia, M.V.; Mariotti, A.; Filograsso, A. River discharge into the Mediterranean Sea: Climatology and aspects of the observed variability. *J. Clim.* **2004**, *17*, 4740–4751. [CrossRef]
189. Trigo, R.M.; Pozo-Vasquez, D.; Osborn, T.J.; Castro-Diez, Y.; Gamiz-Fortis, S.; Esteban-Parra, M.J. North Atlantic Oscillation influence on precipitation, river flow and water resources in the Iberian Peninsula. *Int. J. Climatol.* **2004**, *24*, 925–944. [CrossRef]
190. Rimbu, N.; Boroneant, C.; Buta, C.; Dima, M. Decadal variability of the Danube River flow in the lower basin and its relation with the North Atlantic Oscillation. *Int. J. Climatol.* **2006**, *22*, 1169–1179. [CrossRef]
191. López-Moreno, J.I.; Beguería, S.; Vicente-Serrano, S.M.; García-Ruiz, J.M. Influence of the North Atlantic Oscillation on water resources in central Iberia: Precipitation, streamflow anomalies, and reservoir management strategies. *Water Resour. Res.* **2007**, *43*, W09411. [CrossRef]
192. Calafat, F.; Chambers, D.; Tsimplis, M. Mechanism of decadal sea level variability in the eastern North Atlantic and the Mediterranean Sea. *J. Geophys. Res. Oceans* **2012**, *117*, C9. [CrossRef]
193. Mohamed, B.; Abdallah, A.M.; El-Din, K.A.; Nagy, H.; Shaltout, M. Inter-Annual Variability and Trends of Sea Level and Sea Surface Temperature in the Mediterranean Sea over the Last 25 years. *Pure Appl. Geophys.* **2019**, *176*, 3787–3810. [CrossRef]
194. Landerer, F.W.; Volkov, D.L. The anatomy of recent large sea level fluctuations in the Mediterranean Sea. *Geophys. Re. Lett.* **2013**, *40*, 553–557. [CrossRef]
195. Cazenave, A.; Cabanes, C.; Dominh, K.; Mangiarotti, S. Recent sea level changes in the Mediterranean Sea revealed by TOPEX/POSEIDON satellite altimetry. *Geophys. Res. Lett.* **2001**, *28*, 1607–1610. [CrossRef]
196. Jones, P.D.; Osborn, T.J.; Briffa, K.R.; Folland, C.K.; Horton, E.B.; Alexander, L.V.; Parker, D.E.; Rayner, N.A. Adjusting for sampling density in grid box land and ocean surface temperature time series. *J. Geophys. Res.* **2001**, *106*, 3371–3380. [CrossRef]

3.3 Manuscript III

Title:

Sea–level trend variability in the Mediterranean during the 1993–2019 period

Authors:

Matteo Meli (Department of Biological, Geological and Environmental Sciences (BiGeA), University of Bologna, Bologna, Italy)

Carolina M. L. Camargo (Royal Netherlands Institute for Sea Research (NIOZ), Department of Estuarine and Delta Systems, Yerseke, the Netherlands and Delft University of Technology, Department of Geoscience and Remote Sensing, Delft, the Netherlands)

Marco Olivieri (Istituto Nazionale di Geofisica e Vulcanologia (INGV), Bologna, Italy)

Aimée B. A. Slangen (Royal Netherlands Institute for Sea Research (NIOZ), Department of Estuarine and Delta Systems, Yerseke, the Netherlands)

Claudia Romagnoli (Department of Biological, Geological and Environmental Sciences (BiGeA), University of Bologna, Bologna, Italy)

Status:

Published in *Frontiers in Marine Science: Physical Oceanography (2023), vol. 10, 1150488.*

`https://doi.org/10.3389/fmars.2023.1150488`

Overview:

This analysis deals with the main variability of sea–level trends across the Mediterranean Sea and its sub–basins, observed from altimetry (geocentric sea level) and investigates the related contributions of changes in water temperature (thermosteric effect) and salinity (halosteric effect), which together account for the steric component of sea level.

Open question:

What is the main variability of sea–level trends in the Mediterranean Sea?

frontiers | Frontiers in Marine Science

TYPE Original Research
PUBLISHED 30 March 2023
DOI 10.3389/fmars.2023.1150488

OPEN ACCESS

EDITED BY
Şükrü Beşiktepe,
Dokuz Eylül University, Türkiye

REVIEWED BY
Hazem Nagy,
Alexandria University, Egypt
William Llovel,
UMR6523 Laboratoire d'Oceanographie Physique et Spatiale (LOPS), France

*CORRESPONDENCE
Matteo Meli
matteo.meli7@unibo.it

SPECIALTY SECTION
This article was submitted to Physical Oceanography, a section of the journal Frontiers in Marine Science

RECEIVED 24 January 2023
ACCEPTED 15 March 2023
PUBLISHED 30 March 2023

CITATION
Meli M, Camargo CML, Olivieri M, Slangen ABA and Romagnoli C (2023) Sea-level trend variability in the Mediterranean during the 1993–2019 period. *Front. Mar. Sci.* 10:1150488. doi: 10.3389/fmars.2023.1150488

Sea-level trend variability in the Mediterranean during the 1993–2019 period

Matteo Meli [1]*, Carolina M. L. Camargo [2,3], Marco Olivieri [4], Aimée B. A. Slangen [2] and Claudia Romagnoli [1]

[1]Department of Biological, Geological and Environmental Sciences, University of Bologna, Bologna, Italy, [2]Department of Estuarine and Delta Systems, Royal Netherlands Institute for Sea Research (NIOZ), Yerseke, Netherlands, [3]Department of Geoscience and Remote Sensing, Delft University of Technology, Delft, Netherlands, [4]Istituto Nazionale di Geofisica e Vulcanologia (INGV), Sezione di Bologna, Bologna, Italy

Sea-level change is one of the most concerning climate change and global warming consequences, especially impacting coastal societies and environments. The spatial and temporal variability of sea level is neither linear nor globally uniform, especially in semi-enclosed basins such as the Mediterranean Sea, which is considered a hot spot regarding expected impacts related to climate change. This study investigates sea-level trends and their variability over the Mediterranean Sea from 1993 to 2019. We use gridded sea-level anomaly products from satellite altimetry for the total observed sea level, whereas ocean temperature and salinity profiles from reanalysis were used to compute the thermosteric and halosteric effects, respectively, and the steric component of the sea level. We perform a statistical change point detection to assess the spatial and temporal significance of each trend change. The linear trend provides a clear indication of the non-steric effects as the dominant drivers over the entire period at the Mediterranean Sea scale, except for the Levantine and Aegean sub-basins, where the steric component explains the majority of the sea-level trend. The main changes in sea-level trends are detected around 1997, 2006, 2010, and 2016, associated with Northern Ionian Gyre reversal episodes, which changed the thermohaline properties and water mass redistribution over the sub-basins.

KEYWORDS

Mediterranean Sea, sea-level change, satellite altimetry, steric component, thermosteric and halosteric effects, trend variability, sub-basins scale variability

1 Introduction

Sea-level change observations have been considered one of the key aspects of climate change reconstruction over the last few decades because of their interconnection with all other climate indicators, such as atmospheric temperature. Therefore, global mean sea-level assessment has been one of the main objectives of different studies in the past few decades (Fox-Kemper et al., 2021).

Global mean sea-level change is determined by mass addition, driven by continental ice melting and changes in land water storage, and the steric effect that is driven by changes in water column density induced by salinity (negligible at the global scale) and thermal fluctuations (Levitus et al., 2012; Fox-Kemper et al., 2021). However, sea-level change at the global scale is far from uniform, and on a regional to local scale it can vary greatly from global mean rates (e.g., Stammer et al., 2013; Jevrejeva et al., 2014; Slangen et al., 2014). For instance, sea-level trends in the Mediterranean differ from global mean sea-level trends, mainly because of its semi-enclosed conditions (Pinardi et al., 2014), and can even differ from the values observed in the nearby Atlantic Ocean (Tsimplis and Baker, 2000). Sea level in the Mediterranean has changed with a rate of 2.5 ± 0.4 mm/yr from 1993 to 2017 (Mohamed et al., 2019a), compared to a global mean rate of 3.2 ± 0.4 mm/yr for a similar period (Fox-Kemper et al., 2021). Additionally, within the Mediterranean, sea-level trends can differ from the basin mean (Bonaduce et al., 2016; Mohamed et al., 2019a; Calafat et al., 2022) due to non-linear local oceanographic processes (Vera et al., 2009).

Because of the many low-lying densely inhabited coastal areas, the Mediterranean Sea has been classified as one of the most susceptible climate change zones worldwide (Giorgi, 2006). Sea-level rise and related future projections (IPCC, 2021) may significantly impact coastal populations and activities, strengthening climate-related concerns and prompting a better understanding of processes from a global to a regional and local scale. Furthermore, the low elevation may significantly exacerbate sea-level rise at several coastal locations throughout the Mediterranean Sea, due to the local vertical land motion processes. These are caused by a combination of natural factors such as the compaction of alluvial sediments and volcanic-tectonic activity, as well as anthropogenic factors including the extraction of underground fluids (Gambolati and Teatini, 1998; Syvitski et al., 2009). These processes can cause land subsidence and amplify the effects of rising sea levels in these regions (García et al., 2007; Wöppelmann and Marcos, 2012; Mohamed et al., 2019b). Thus, there is a need to understand sea level change at the scale of the Mediterranean Sea.

This study focuses on sea-level variations in the Mediterranean Sea region (Figure 1A) to elucidate the large variability that occurred at both regional and sub-basin scales over the period 1993-2019. Most of the previous studies of the Mediterranean focus on trends either at the basin scale or in a specific region. Hence, there is a gap in understanding the changes in sea level variability over the Mediterranean at a sub-basin scale, likely driven by internal processes within the domain and masked by averaging at larger scales. In this framework, this study analyzes the main variability of sea-level trends observed from altimetry (total sea level) and the related contributions of changes in water temperature (thermosteric effect) and salinity (halosteric effect), which together account for the steric component across the Mediterranean Sea and its sub-basins. The significance of the variability observed in sea-level trends is then discussed at different spatiotemporal scales.

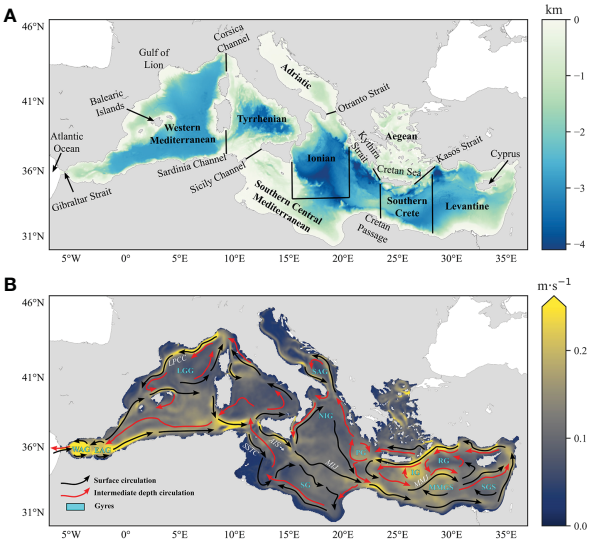

FIGURE 1
(A) Bathymetry of the Mediterranean Sea with regionalization of sub-basins (bold) and related borders. **(B)** Schematic representation of the surface (black arrows) and intermediate depth (red arrows) circulation in the Mediterranean Sea, superimposed on the map of 1993-2019 time-mean current velocities at 15 m depth. Both the bathymetry and current velocities are computed from the Mediterranean Sea Physics Reanalysis dataset (MEDSEA_MULTIYEAR_PHY_006_004). The labels of currents are in italics white, while gyres are in bold cyan. Acronyms: AIS, Atlantic Ionian Stream; AMC, Asia Minor Current; EAG, Eastern Alboran Gyre; EIC, Eastern Ionian Current; IG, Ierapetra Gyre; LGG, Gulf of Lion Gyre; LPCC, Liguro-Provencal-Catalan Current; MIJ, Mid-Ionian Jet; MMGS, Mersa Matruh Gyre System; MMJ, Mid-Mediterranean Jet; NIG, Northern Ionian Gyre; PG, Pelops Gyre; RG, Rhodes Gyre; SAG, Southern Adriatic Gyre; SG, Sirte Gyre; SGS; Shikmona Gyre System; SSTC, Sicily Strait Tunisian Current; WAG, Western Alboran Gyre.

1.1 General settings of the Mediterranean Sea

The Mediterranean Sea is a semi-enclosed, mid-latitude sea connected to the North Atlantic Ocean by the Gibraltar Strait (Figure 1A), where the exchange of water, heat, and salt occurs (Pinardi et al., 2015). The bathymetry of the basin (Figure 1A) varies significantly around the 1500 m average, ranging from a few tens of meters of depth (e.g., Northern Adriatic and Southern Central Mediterranean) to more than 4000 m depth (Tyrrhenian and Ionian) (Miramontes et al., 2022 and references therein).

The Mediterranean Sea can be divided into different sub-basins as (from west to east) the Western Mediterranean, Tyrrhenian, Ionian, Southern Central Mediterranean, Southern Crete, Levantine, and two marginal seas, Adriatic and Aegean (Figure 1A). The Western Mediterranean is connected from the Tyrrhenian by the Sardinia and Corsica channels, while the Tyrrhenian is connected from the Southern Central Mediterranean by the Sicily Channel (Figure 1A). Furthermore, the Southern Central Mediterranean is connected towards the east to the Southern Crete through the Cretan Passage (Figure 1A), whereas the connection/division with the Ionian is not purely based

on straits or passages but following variations in local bathymetry and oceanographic processes. Therefore, the latter can also be defined as a separation criterion in the case of Southern Crete and Levantine (Figure 1A). Finally, the Adriatic is connected to the Ionian by the Otranto Strait, whereas the Aegean is connected from the rest by the Kythira and Kasos straits (Figure 1A). Furthermore, to avoid confusion among the terms used in this study, we also define WMed and EMed as the macro-portions of the Mediterranean west and east of the Sicily Channel, respectively.

The Mediterranean receives ocean water from the Atlantic Ocean to compensate for a persistent surface water loss, mainly driven by evaporation (owing to the increase in sea surface temperature) and a persistent freshwater deficit (Romanou et al., 2010; Pastor et al., 2018), leading to basin-wide salinification (Grodsky et al., 2019). Excess evaporation over precipitation, especially in the EMed, forms high-salinity waters that drive and maintain the thermohaline circulation in the Mediterranean Sea through a large salinity contrast that forms between the Levantine waters and the inflowing waters at Gibraltar (Robinson et al., 2001), which contrasts with the thermohaline circulation outside the Mediterranean, dominated by divergences in heat content.

Deep-water masses are distinct between the WMed and EMed because of the occurrence of the Sicily Channel sill (Figure 1A). The WMed and EMed deep waters are formed in the Gulf of Lion (Figure 1A) and the Adriatic, respectively. Deep waters can also form in the Rhodes Gyre (RG, Figure 1B), namely the Levantine Intermediate Water (LIW; see Pinardi et al., 2015 and references therein). The key event for EMed circulation, linked to a yet not fully understood chain of oceanic, hydrological, and atmospheric interactions, was the migration of dense water formation from the Adriatic to the southern Aegean that occurred from the late eighties to the early nineties (Roether et al., 1996; Roether et al., 2014). This shift is known as the Eastern Mediterranean Transient (EMT; Roether et al., 1996; Malanotte-Rizzoli et al., 1999; Theocharis et al., 1999). It was a prolonged stepped process that culminated in 1997 with the so-called Northern Ionian Reversal phenomenon (Pinardi et al., 2015), that is, the shift of the Northern Ionian Gyre (NIG, Figure 1B) from the anticyclonic circulation mode to cyclonic circulation (Civitarese et al., 2010). This phenomenon has been reported multiple times over the last decades (Malanotte-Rizzoli et al., 1997; Pinardi et al., 1997; Malanotte-Rizzoli et al., 1999; Larnicol et al., 2002; Borzelli et al., 2009; Gačić et al., 2010; Gačić et al., 2011; Poulain et al., 2012; Menna et al., 2019; von Schuckmann et al., 2019), with the surface circulation oscillating from cyclonic to anticyclonic around 1987, 2006 and 2017 and vice-versa around 1997 and 2011.

This suggests that circulation reversal is a recurrent phenomenon that occurs on a quasi-decadal time scale in the EMed (or Ionian Sea region). However, there is a lack of consensus regarding the causes of the upper layer circulation pattern changes in the Ionian (see also Chiggiato et al., 2023). Some studies attributed it to internally driven processes (Pisacane et al., 2006; Borzelli et al., 2009; Gačić et al., 2010; Gačić et al., 2011; Gačić et al., 2014; Theocharis et al., 2014; Reale et al., 2016; Reale et al., 2017; Grodsky et al., 2019), while others indicated wind forcing as a possible mechanism (Korres et al., 2000; Demirov and Pinardi, 2002; Nagy et al., 2019). Regardless of the drivers, reversal events strongly impact the formation and distribution of water masses and influence local thermohaline properties throughout the Mediterranean sub-basins (von Schuckmann et al., 2019).

1.2 The ocean circulation in the Mediterranean Sea

Circulation in the Mediterranean (see Pinardi et al., 2015 for an extensive review) reflects its complexity, in which the northern regions are mainly characterized by cyclonic gyres, whereas anticyclonic gyres and eddy-dominated flow fields are predominant in the southern regions (Figure 1B), except for the northern Ionian Sea (Pinardi et al., 2015). Two types of circulation cells co-exist: a basinwide thermohaline circulation, driven mainly by the east-west salinity contrast between the Atlantic Water (AW) and the LIW, which is mainly limited to the surface and intermediate layers, and a deep circulation controlled by the north-south temperature gradient, where the driving mechanisms are winter air-sea heat losses and vertical convection (Gačić et al., 2014). Generally, the Mediterranean Sea is characterized by high salinity, temperature, and density, where net evaporation exceeds precipitation (Tanhua et al., 2013). This drives an anti-estuarine circulation at the Strait of Gibraltar (Figure 1A), where the incoming AW moves mainly eastward (Figure 1B) in the upper 50–100 m layer (Pinardi et al., 2015), overlying the LIW. As the AW moves east, it transforms into a warmer and saltier water mass due to wind-induced evaporation, in the Levantine (Lascaratos et al., 1993).

The circulation of the Mediterranean Sea is composed of several currents and gyres, as detailed in this paragraph (Figure 1B). The AW enters the WMed at Gibraltar, it meanders around the two anticyclonic western and eastern Alboran gyres (WAG and EAG; Heburn and La Violette, 1990) and then separates into two distinct currents, the first mainly flows towards the east (Millot, 1985; Ayoub et al., 1998) while the second flows northward towards the Balearic Islands and then towards east, along the southern boundary of the Gulf of Lion gyre (LGG; Madec et al., 1991; Pinardi et al., 2006). Simultaneously, the northern border of the cyclonic LGG is intensified by the Liguro–Provencal–Catalan Current (LPCC; Pinardi et al., 2006), which flows back to the Balearic Islands towards the southwest. In the Sardinia Channel, the different current merges and then split further into three branches (Beranger et al., 2004; Pinardi et al., 2006): one flowing towards the Tyrrhenian, whereas the other two branches enter the Sicily Channel, hence the EMed, forming the Atlantic Ionian Stream (AIS; Robinson et al., 1999) and Sicily Strait Tunisian Current (SSTC; Lermusiaux and Robinson, 2001; Onken et al., 2003).

In the central EMed, the SSTC flows along the southern coast of the south-central Mediterranean sub-basin, turning first northward and then eastward around the anticyclonic Sirte Gyre (SG; Pinardi et al., 2006). The most prominent oceanographic feature in the Ionian is represented by the NIG, which is characterized by a quasi-decadal reversal of the vorticity, from cyclonic to anticyclonic and vice-versa (see Section 1.1), capable of strongly impacting the

circulation at the sub-basin scale and beyond, especially by influencing the AW path by shifting the AIS position (Malanotte-Rizzoli et al., 1997; Menna et al., 2019). During the cyclonic state, the AIS is mainly prolonged toward the east, conveying AW directly to the Cretan passage through the shortest route by an intense current defined as Mid-Ionian Jet (MIJ; Robinson et al., 2001; Gačić et al., 2011; Bessières et al., 2013; Gačić et al., 2014). During anticyclonic phases, the AIS is primarily deflected towards north-east, meandering the northern Ionian and partially entering the Adriatic (Vilibić et al., 2012) and the Southern Adriatic Gyre (SAG; Artegiani et al., 1997) *via* the Otranto Strait, and then flowing south towards the Levantine, flanking the Pelops Gyre (PG; Robinson et al., 1992). In this configuration, the AW flows towards the Levantine are greatly reduced owing to the weakening of the MIJ (Gačić et al., 2011), whereas the thermohaline properties of the eastern EMed changes due to the longer path of the AW to reach the Cretan Passage (Gačić et al., 2014).

Once the AIS reaches the eastern EMed, passing through the Cretan Passage, it forms a broad current which flows along the North African coasts; part of it, branches the Mid-Mediterranean Jet (MMJ; Golnaraghi and Robinson, 1994). The MMJ is represented by a free open ocean jet meandering first between the Ierapetra Gyre (IG; Robinson et al., 1991), the Rhodes Gyre (RG; Milliff and Robinson, 1992), and the Mersa Matruh Gyre System (MMGS), then partially between Cyprus (Figure 1A) and the Shikmona Gyre System (SGS; Hecht et al., 1988).

As stated above, the Levantine represents the LIW area of formation, primarily in the RG, which is representative of the intermediate depth circulation in the Mediterranean Sea (Figure 1B) as the average currents between 200 and 300 m depth (Pinardi et al., 2015), flowing in the opposite direction of the AW and eventually exiting Gibraltar (Pinardi and Masetti, 2000). Over the eastern EMed, the circulation of the intermediate depth (Figure 1B) is consistent with the surface (Pinardi et al., 2015). Exiting the Cretan Passage and Kythira Strait, the LIW branches into three streams (Pinardi et al., 2015): the first turns east towards the Levantine, the second southward to the SG, and the third towards the Adriatic. The latter is influenced by the NIG, which strongly enhances (reduces) the flux during cyclonic (anticyclonic) phases (see also Menna et al., 2019), whereas the branch that joins the SG arises as the preferred path of the LIW westward (Pinardi et al., 2015). In the WMed, part of the LIW enters the Western Mediterranean through the Sardinia Channel and directly reaches Gibraltar (Puillat et al., 2006), while the other part flows cyclonically along the Tyrrhenian border and finally exits across the Corsica Channel (Figure 1B). The latter, before reaching Gibraltar, flows cyclonically around the LGG, playing a critical role in dense water formation (Pinardi et al., 2023).

1.3 Sea level in the Mediterranean Sea

According to Pinardi et al. (2014), five terms contribute to the mean sea level change when limited areas of the world ocean are considered, such as the semi-enclosed Mediterranean Sea: (i) the mass fluxes at the open boundaries, accounting for the net volume transport at Gibraltar that alters the mass in the domain; (ii) the net changes linked to the loss or addition of water by surface processes (driven by processes such as evaporation, precipitation, and river runoff within the domain); (iii) the density changes induced by salinity changes (halosteric effect); (iv) the density changes induced by changes in heat flux (thermosteric effect); and (v) the density advection term. The latter, however, is several orders of magnitude smaller than the other four terms, and thus can be considered negligible (Pinardi et al., 2014). The first two terms are defined as incompressible terms that, for simplicity, can be referred to as the mass component. The combined variability of the thermosteric and halosteric effects is referred to as the steric component. The latter fluctuates periodically around zero and is superimposed on the mass component characterized by a yearly and seasonal imbalance between terms (i) and (ii), giving rise to the regional mean sea-level tendency (Pinardi et al., 2014).

The mass component is considered the dominant contributor to the mean sea-level trend in the Mediterranean Sea (Calafat et al., 2010; Pinardi et al., 2014), while the steric component accounts for approximately 20% of the total variance (Calafat et al., 2012). This contrasts with the steric influence at the global scale, which explains approximately 50%–70% of the total sea level variability (Storto et al., 2019). However, there are large differences across the Mediterranean. For instance in the Aegean and Levantine the steric component explains approximately 52% (Mohamed and Skliris, 2022), mainly due to the thermosteric effect (Vera et al., 2009). A direct relationship between sea surface temperature and sea level in the Mediterranean has been demonstrated in previous studies (Cazenave et al., 2001; Cazenave et al., 2002; Fenoglio-Marc, 2002), highlighting a continuous and positive trend associated with sea surface temperature from 1992 to 1999 and for all sub-basins, except for the Ionian.

Large-scale climatic modes also influence long-term and inter-annual variability of the Mediterranean sea level (Vigo et al., 2011; Calafat et al., 2012; Landerer and Volkov, 2013; Tsimplis et al., 2013), such as the North Atlantic Oscillation (NAO) and the Atlantic Multidecadal Oscillation (AMO). For example, NAO positive and negative phases influence precipitation, air temperature, and sea level from local (Meli et al., 2021; Meli and Romagnoli, 2022; Romagnoli et al., 2022) to European scales (Mariotti and Dell'Aquila, 2012; Criado-Aldeanueva and Soto-Navarro, 2020). In particular, the NAO drives atmospheric sea-level pressure changes in the Mediterranean (Tsimplis and Josey, 2001) and alters wind and oceanic circulation near Gibraltar, influencing the net water flux exchange with the Atlantic Ocean (Menemenlis et al., 2007; Tsimplis et al., 2013). Instead, the AMO significantly correlates with heat and salt content (Iona et al., 2018), influencing sea surface temperature and evaporation (Marullo et al., 2011). However, the role of these large climatic modes, despite their importance on the Mediterranean variability at a multidecadal time scale (Calafat et al., 2022), has a limited effect on the quasi-decadal time scale variability (Menna et al., 2022) and is not fully appreciated when short time series are considered (as in the case of satellite altimetry).

Moreover, the sea-level trend can be considerably influenced at regional scale by the contribution of glacial isostatic adjustment

(GIA), the gravitational, rotational, and deformation (GRD) effects, and the dynamic component of sea level, induced by the lateral mass transport. In the Mediterranean Sea the GIA contribution is relatively small (-0.3 mm/yr, Melini and Spada, 2019), while the GRD effects contributed by about 1.5 ± 0.2 mm/yr over the period 2000-2018 (Calafat et al., 2022). For simplicity, all these terms, plus the contribution of large-scale modes and the mass component, from hereon is referred to as the "non-steric effects".

Strong differences in sea-level trends at the sub-basin scale are a well-known aspect of the Mediterranean (Bonaduce et al., 2016; Skliris et al., 2018; Mohamed et al., 2019a), in which variability and complexity arise from thermohaline changes and local circulation (Menna et al., 2012; Mauri et al., 2019; Menna et al., 2019; Menna et al., 2021; Poulain et al., 2021). For instance, the Ionian has in general a negative sea-level trend (Cazenave et al., 2002; Fenoglio-Marc, 2002), in contrast to other sub-basins, primarily because of complexities and changes in the local circulation pattern (Malanotte-Rizzoli et al., 1997; Pinardi et al., 1997; Malanotte-Rizzoli et al., 1999).

Regarding non-linearity in sea-level trends, an abrupt change was observed around 1999, leading to a loss of correlation between sea surface temperature and sea level after that year (Vigo et al., 2005). Furthermore, the Ionian began to be characterized by a rising trend after 1998, which was attributed to the switch of surface circulation from anticyclonic to cyclonic (Gačić et al., 2010) after the relaxation of the EMT (Vera et al., 2009, see also Section 1.1). After that period and since the early 2000s, a non-linear behavior has been observed in sea-level trends, where a rising condition peaked in 2003, followed by a drop until 2009 (Vigo et al., 2011).

2 Materials and methods

2.1 Data

Gridded daily mean sea-level anomalies (SLA) at 1/8°x1/8° spatial resolution over the Mediterranean Sea for 1993–2019 were obtained from the Copernicus Climate Change Service (C3S). The dataset was delivered by the DUACS altimeter production system, which includes data from several altimetry missions, but always merging a steady number (two) of altimetry measurements at the same time. This procedure avoids introducing biases and provides stability and homogeneity of the record over the entire period, which is crucial for climate applications and long-term evolutionary analyses (Legeais et al., 2021). All standard corrections (e.g., signal refraction passing through the atmosphere, sea state bias, instrumental drift, and dynamic atmospheric correction) were applied to the dataset (for details, see Taburet et al., 2019).

Monthly average temperature and salinity vertical profiles were obtained from the Mediterranean Sea Physics Reanalysis dataset (Escudier et al., 2020), distributed by the Copernicus Marine Environment Monitoring Service (CMEMS; available at the url: https://marine.copernicus.eu/). This dataset covers the period 1987–2020, and it has a spatial grid resolution of 1/24°x1/24° and 141 vertical levels (unevenly spaced). The physical dynamics of the Mediterranean Sea are modeled using an Ocean General Circulation Model (OGCM) that is based on the Nucleus for European Modelling of the Ocean (NEMO) code (Madec et al., 2017). This numerical model is used to solve the primitive equations of motion that describe the movement of water in the Mediterranean Sea. The water balance is computed using the difference between evaporation, derived from latent heat flux data, and the combination of precipitation and rivers runoff, derived from various datasets (Escudier et al., 2021 and references therein). The connection with the Marmara Sea is modeled as a river (Kourafalou and Barbopoulos, 2003), while the exchanges at Gibraltar are resolved by extending the model into the north-east Atlantic Ocean. Temperature and salinity observations are assimilated into the system through the OceanVar data assimilation scheme (Dobricic and Pinardi, 2008), which includes *in-situ* vertical profiles from the Argo profiling floats, CTDs, and XBTs from SeaDataNet (https://www.seadatanet.org/) and CMEMS (INSITU_GLO_NRT_OBSERVATIONS_013_030) database. Details of this reanalysis dataset are discussed in Escudier et al. (2021).

2.2 Methods

To cope with the large oceanographic and bathymetric variability characterizing the Mediterranean Sea, the time series analysis at the sub-basin scale was made by following the same partitioning (Figure 1A) outlined by Carillo et al. (2012) and Galassi and Spada (2014). The C3S altimetry observations were corrected for GIA using the geoid height estimates (dGeoid) from the ICE-6G_C (VM5a) model (Argus et al., 2014; Peltier et al., 2015), was applied to the C3S altimetry observations as a correction for the GIA effect. Furthermore, to account for the altimeter instrumental drift that influences the accuracy and uncertainty of the records between 1993 and 1998 (Watson et al., 2015; Beckley et al., 2017; Dieng et al., 2017), a TOPEX-A instrumental drift correction (WCRP Global Sea Level Budget Group, 2018), derived from altimetry and tide gauge global comparisons, was added to the C3S sea-level datasets. Although this correction is computed for the global mean sea level, it can also be used at a regional or local scale as the best available estimate. This is still preferable to not correcting at all, given that the regional variation of the instrumental drift is currently unknown.

The Thermodynamic Equation of Seawater (TEOS-10, McDougall and Barker, 2011) was used as the equation of state to compute the steric sea-level component, following Camargo et al. (2020). The steric (η_s) computation is based on the vertical integration of density anomalies from the maximum local depth (-H) to the water surface (0), following Gill and Niller (1973) and Tomczak and Godfrey (2003):

$$\eta_s = -\frac{1}{\rho_0}\int_{-H}^{0}\rho' dz$$

where ρ' and ρ_0 are the local and reference density anomalies, respectively. The former is a function of temperature and salinity variations retrieved from the reanalysis dataset (see Section 2.1).

Before computing steric anomalies, potential temperature and practical salinity values are converted to conservative temperature and absolute salinity (McDougall and Barker, 2011; McDougall et al., 2012). In addition, the thermosteric and halosteric effects were also computed and analyzed individually to better appreciate the influence and evolution of both effects.

Due to the different temporal coverage of the datasets, we restricted the analyses to the common period from January 1993 to December 2019. Daily time series were converted into monthly and annual means. Moreover, the mean seasonal cycle was removed from all the monthly mean time series. To ensure a full comparability between the datasets, the steric, thermosteric, and halosteric datasets were regridded from 1/24° to 1/8°, i.e. the resolution of the altimetry data, using the First-Order Conservative Remapping method (Jones, 1999), which is implemented in the Climate Data Operators software.

A non-parametric Mann–Kendall test (Mann, 1945; Kendall, 1975), modified for autocorrelated data (Hamed and Rao, 1998), was performed to assess the statistical significance of trends at the 95% confidence interval. The Mann-Kendall test was implemented with the non-parametric Theil–Sen estimator (Theil, 1950; Sen, 1968) to evaluate the preferred slope from the simple linear regression computed for each time series. The resulting preferred slope was assumed to be a constant trend (or rate) of the time series over the selected period. Associated error is determined from the distribution of values. In principle this can be not normal and lead to a not symmetric associated error bar. To ease the reading and result interpretation, we assign a conservative symmetric error by choosing the largest one.

In this analysis, the Binary Segmentation algorithm (Scott and Knott, 1974; Sen and Srivastava, 1975) was used to search for the unknown epoch of change points in the altimetry monthly time series (de-seasoned, TOPEX-A and GIA corrected). This is among the most-competitive methods for change point analysis (Cho and Fryzlewicz, 2015; Rice and Zhang, 2022). The algorithm uses a cost function, namely the Radial Basis function (Harchaoui and Cappé, 2007), to search for the preferred epoch at which the change point should be set. Then it uses the change point to split the time series in two sub-series and it iterates the change point search process until a predefined stopping criterion (here defined as the max change point number equal to three) is reached (Truong et al., 2020). Figure 2A show the detection of change points on a single time series. The Radial Basis Function was preferred since it belongs to the kernel-based methods and it is suitable for performing change point detection in a non-parametric setting (Harchaoui and Cappé, 2007); this model is particularly useful when the change points are suspected to be irregularly distributed in the time series (Killick et al., 2012; Truong et al., 2020). Offsets were not present in the considered dataset.

The detected change points (three for each time series) were then aggregated at the basin scale, to create a cumulative distribution (Figure 2B). The occurrence of a change point cannot be precisely attributed to a single moment in time, as it may be influenced by a variety of processes that induce a spatially and temporally varying response in sea level. As a consequence, only distributions exceeding the 75th percentile were considered and selected (represented by black bars in Figure 2B), accompanied by their respective reference medians (indicated by hatched vertical red lines in Figure 2A). Each median, accompanied by an arbitrary error margin of ± 1 year (depicted as a red shaded area in Figure 2B), provided an effective means of clustering the major distributions into four distinct groups, which were centered around the years

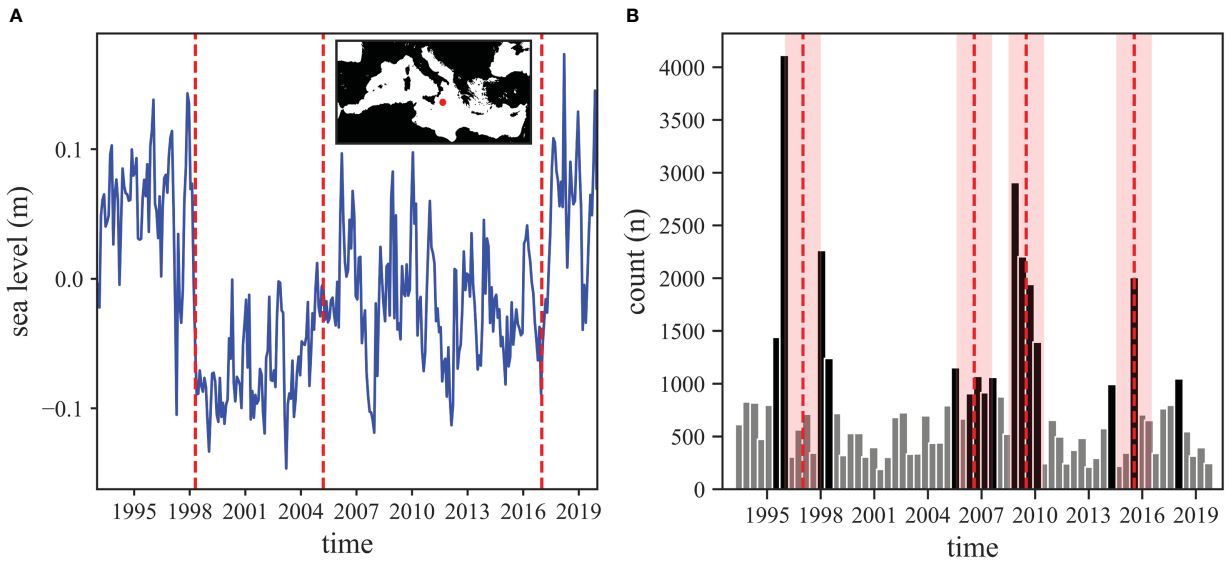

FIGURE 2
Left panel **(A)** shows one sample of monthly mean sea level time series from the Ionian region (marked by the red dot in the inset map. Red hatched lines mark the three most likely change point detected by the algorithm described in Section 2.2. The right panel **(B)** displays the cumulative distribution (grey bars) for the whole set change points detected in altimetry monthly time series throughout the Mediterranean Sea. Black bars mark the subset of distributions exceeding the 75th percentile. For each selected distribution, the median (hatched red lines) defines the selected change point while an arbitrary error of ± 1 year (shaded in red) was introduced to account for potential uncertainties in the analysis.

1997, 2006, 2010, and 2016. The two distributions localized around 2014 and 2018 were excluded from this clustering, as their proximity to the 2016 cluster makes them unusable for the analysis.

To properly account for autocorrelation and clean the signal from interannual variability, the time series were converted into annual means and the modified Theil-Sen estimator was used to calculate trends and errors for each sub-series. Subsequently, the statistical significance (at the 95% confidence interval) of each change point was evaluated for each time series by applying a Fisher F-test to the Chow statistics (Chow, 1960; Winer, 1962; Olivieri and Spada, 2013).

3 Results and discussion

3.1 Linear trend analysis

Figure 3A shows a large spatial variability of the rate of sea-level rise derived from satellite altimetry (total sea level) for the period 1993–2019, confirming observations by Bonaduce et al. (2016), despite the different time windows. The highest positive rates (from ca. 3 to 4 mm/yr and above) are observed over the Aegean and Levantine, especially in regions where recurring gyres and eddies in the circulation are present (PG, MMGS, and SGS in Figure 1B). Conversely, negative rates (down to over -4 mm/yr) are observed in some portions of the Ionian, corresponding to the NIG and along the MIJ, and largely in the Southern Crete along the MMJ and IG; the latter represents the area with the largest negative rate observed throughout the Mediterranean Sea. At the Mediterranean basin scale, the average sea-level trend is 2.1 ± 0.5 mm/yr (95% confidence interval), comparable with Mohamed et al. (2019a). However, long-term linear trends of total sea-level change at the sub-basin scale (see also Section3.2) confirm the variability observed in Figure 3A as the consequence of local processes. In detail, values of 1.8 ± 0.6, 2.1 ± 0.8, and 2.5 ± 0.6 mm/yr are observed for the Western Mediterranean, Southern Central Mediterranean, and Tyrrhenian, respectively. Higher trends (albeit comparable within the ranges) are observed for the Adriatic (2.6 ± 0.8 mm/yr), Levantine (2.6 ± 0.9 mm/yr), and Aegean (3.1 ± 1.0 mm/yr), consistent with Mohamed and Skliris (2022), who found an average rate of 3.23 ± 0.61 mm/yr for the eastern EMed over the same period. Conversely, trends for the Ionian (1.6 ± 1.6 mm/yr) and Southern Crete (0.3 ± 1.3 mm/yr) are non-significant.

The significance of the rate obtained from the trend analysis is considered by plotting the spatial distribution of the statistics at the 95% confidence interval (CI) in Figure 3A. Dots represent regions where the null hypothesis cannot be rejected, that is, the significance of the resulting rate cannot be statistically confirmed. This can be associated with a null rate and significant changes in the time series that diverge from the linear model. Notably, these time series have no significant trend clusters in specific sectors of the Mediterranean Sea, suggesting that it cannot be the consequence of a random process but, conversely, related to local dynamics, such as the influence of gyres/eddies or currents. In detail, a lack of significance in the Western Mediterranean is observed for sea-level trend from altimetry in the EAG-Balearic Islands area (hereafter refer to Figure 1 for location). A very large portion of the Ionian also denotes weak or non-significant rates, especially in conformity with the NIG, AIS, and along MIJ. When moving toward the east, a lack of significance is observed in correspondence with the PG, in a large part of Southern Crete, and a spot within the SGS. However, the significance in the IG is noteworthy, representing the only statistically significant negative rate in the entire Mediterranean Sea from 1993 to 2019.

Steric sea-level trends (Figure 3B) also show wide spatial variability, described by a progressive increase from west to east.

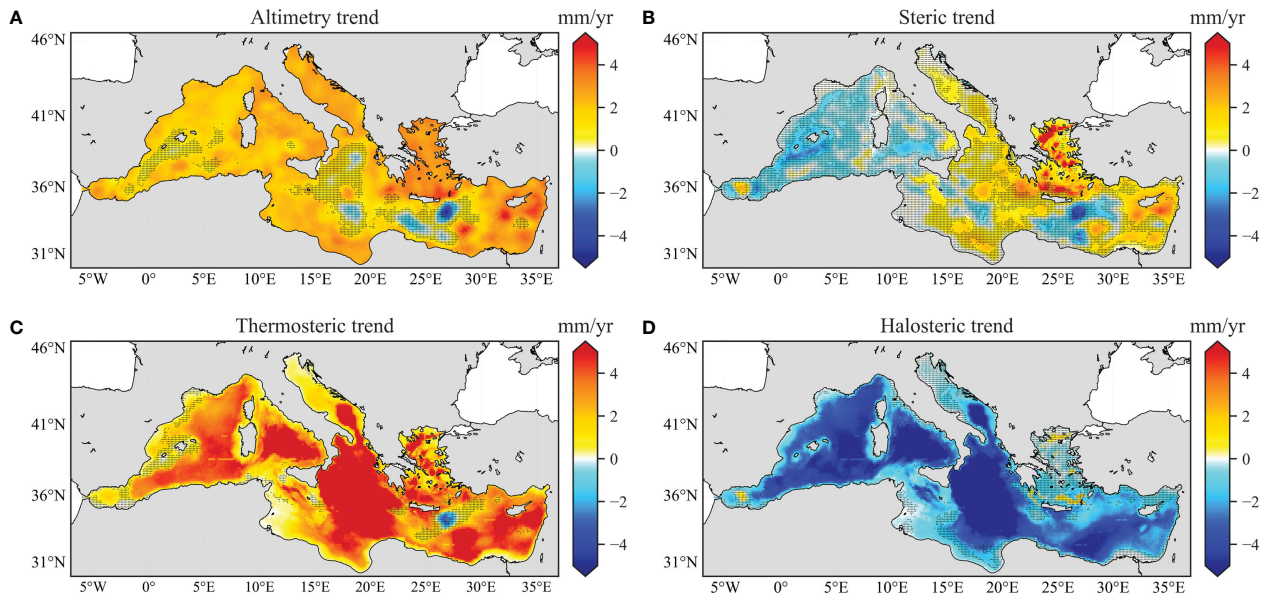

FIGURE 3
Trends of total sea level **(A)**, steric **(B)**, thermosteric **(C)**, and halosteric **(D)** components, computed over the satellite altimetry era (1993–2019). Black dots mark areas in which the trend is non-significant (95% CI).

General negative trends are observed throughout the WMed, except for WAG. A behavior similar to altimetric trends is observed in the Ionian, where low values are aligned along the AIS and MIJ. Weak positive values characterized the Adriatic, whereas the Aegean shows higher positive trends linked to the steric component of the entire Mediterranean Sea. As for altimetry, steric trends in the Levantine and Southern Crete can be split into positive and negative trends, respectively, and negative trends are shown along the MMJ, with the most prominent (down to -4.5 mm/yr) at the IG.

The statistical significance of the steric component trends (Figure 3B) tends to be absent throughout the Mediterranean Sea, characterized by an average non-significant rate of 0.3 ± 0.6 mm/yr. While almost all sub-basins show a non-significant steric sea-level trend, the presence of significant trends denotes a patchy pattern. A few exceptions are the Aegean (2.1 ± 1.3 mm/yr), Levantine (1.1 ± 1.0 mm/yr), and Southern Central Mediterranean (1.0 ± 0.8 mm/yr), in which the average spatial trends are significant, albeit spatially uneven. These values denote an influence of the steric component on the total sea-level change of approximately 68, 42, and 48%, respectively, for the three sub-basins, consistent with Mohamed and Skliris (2022), who reported that 52% of the total sea-level change in the eastern EMed was due to steric effects. In this case, the behavior of the three sub-basins is consistent with the global mean, where the steric component accounts for approximately 44% of the total sea-level change over the period 1993-2017 (Storto et al., 2019). In contrast, the steric component in the other sub-basins contributes negatively to the long-term total sea-level trend, except for the Adriatic and Ionian, where it accounted for approximately 15 and 31%, respectively. This highlights how a large part of the long-term sea-level trend within the Mediterranean Sea, except for the eastern EMed, is driven by non-steric effects (ca. 86%). This is consistent with previous studies, who found an influence of the steric component over the Mediterranean of less than 20% and that the mass component becomes the dominant element for regional sea-level trends (Calafat et al., 2010; Calafat et al., 2012; Pinardi et al., 2014).

Thermosteric trends (Figure 3C) are generally positive throughout the domain, with high values (>3–4 mm/yr) observed in the Ionian (5.3 ± 1.0 mm/yr), Tyrrhenian (3.0 ± 0.6 mm/yr), Levantine (3.3 ± 1.1 mm/yr), Southern Central Mediterranean (3.4 ± 0.6 mm/yr), and Aegean (2.8 ± 1.0 mm/yr). The IG is the only region with negative thermosteric values, which contributes to lowering the average rate of the Southern Crete (2.4 ± 1.1 mm/yr). Most of the thermosteric rates over the Mediterranean Sea are statistically significant (average rate of 2.8 ± 0.5 mm/yr), including the IG negative rate, and except for the PG, MMJ-RG alignment, and the EAG-Balearic Islands region. Lower but significant thermosteric trends are observed over the Adriatic (1.9 ± 0.6 mm/yr) and Western Mediterranean (2.0 ± 0.6 mm/yr).

In contrast, the halosteric effect (Figure 3D) is characterized by negative trends (increasing water column salinity, leading to an increase in sea water density and related volume reduction) in all sub-basins, with some small spots showing a weakly positive trend in the Aegean and WAG. At the sub-basin scale, the Aegean shows a not statistically significant trend of -0.6 ± 0.9 mm/yr, whereas the Adriatic (-1.5 ± 0.5 mm/yr), Southern Central Mediterranean (-2.4 ± 0.5 mm/yr), Tyrrhenian (-2.5 ± 0.7 mm/yr), and Levantine (-2.0 ± 0.8 mm/yr) have a significant negative trend. Generally, halosteric trends contribute negatively to the total altimetric sea level across almost the entire Mediterranean Sea (-2.5 ± 0.3 mm/yr). Stronger negative trend is observed for the Ionian (-4.9 ± 1.3 mm/yr).

Thermosteric trends are often higher than the total sea level trends; however, their overall contribution to the steric component is strongly influenced and lowered by the negative contribution of the halosteric effect. The opposite contributions of these two effects have been observed throughout the eastern EMed (Mohamed and Skliris, 2022) and the North Atlantic Ocean (Storto et al., 2019). This opposite effect is the direct outcome of the progressive regional increase in water temperature and salinity (Romanou et al., 2010; Pastor et al., 2018; Skliris et al., 2018; Grodsky et al., 2019; Mohamed et al., 2019a; Pisano et al., 2020; Menna et al., 2022). Additionally, this opposite behavior is the cause of the generalized non-significance of the steric component over the entire Mediterranean Sea, as the two opposite effects almost cancel each other out (Passaro and Seitz, 2010). This highlights the extent to which the halosteric effect is influential within semi-enclosed basins at mid-latitudes, conversely to the global ocean where the thermosteric effect represents the dominant driver of steric component variability (Robinson et al., 2001; IPCC, 2021).

3.2 Mediterranean sea-level inflections

Following the four change point clusters detected (1997, 2006, 2010, and 2016), each of the variables are reanalyzed for the sub-periods (1993-1997, 1997-2006, 2006-2010, 2010-2016, 2016-2019). Figure 4 shows the spatial difference that characterizes each point of the grid for each variable considered (i.e., total sea level from altimetry, steric component, thermosteric, and halosteric effects) between two different sub-periods separated by a selected change point that acts as a pivotal point in the time series. A positive (negative) value suggests an acceleration (deceleration) in sea-level change at a specific location. This could also reflect a sign variation, namely from negative to positive or vice versa, or just an increase or decrease in the observed rate. For each of the four change points, both the complete map of the trend changes (to have an overview and intensity of the process) and the map with only the statistically significant trend changes at 95% CI, as determined through the Chow test (see Section 2.2), are shown. The latter means that any points which change of trend is considered statistically valid, and thus better represented by a bilinear model rather than by the simple linear model. From hereon, for simplicity, the term "inflection" is defined as a change in rate, positive or negative, occurring in a time series in a specific pivotal year.

On the other hand, Figure 5 shows the temporal evolution, with related significant inflections, of the variables considered at the sub-basins scale. The time series of average annual mean sea level from altimetry for the entire Mediterranean Sea (Figure 5A, solid black line) highlights how the sea level is rising, unlike the steric component (dashed yellow line), which shows a weak and an overall non-significant positive trend, consistent with the map in

10.3389/fmars.2023.1150488

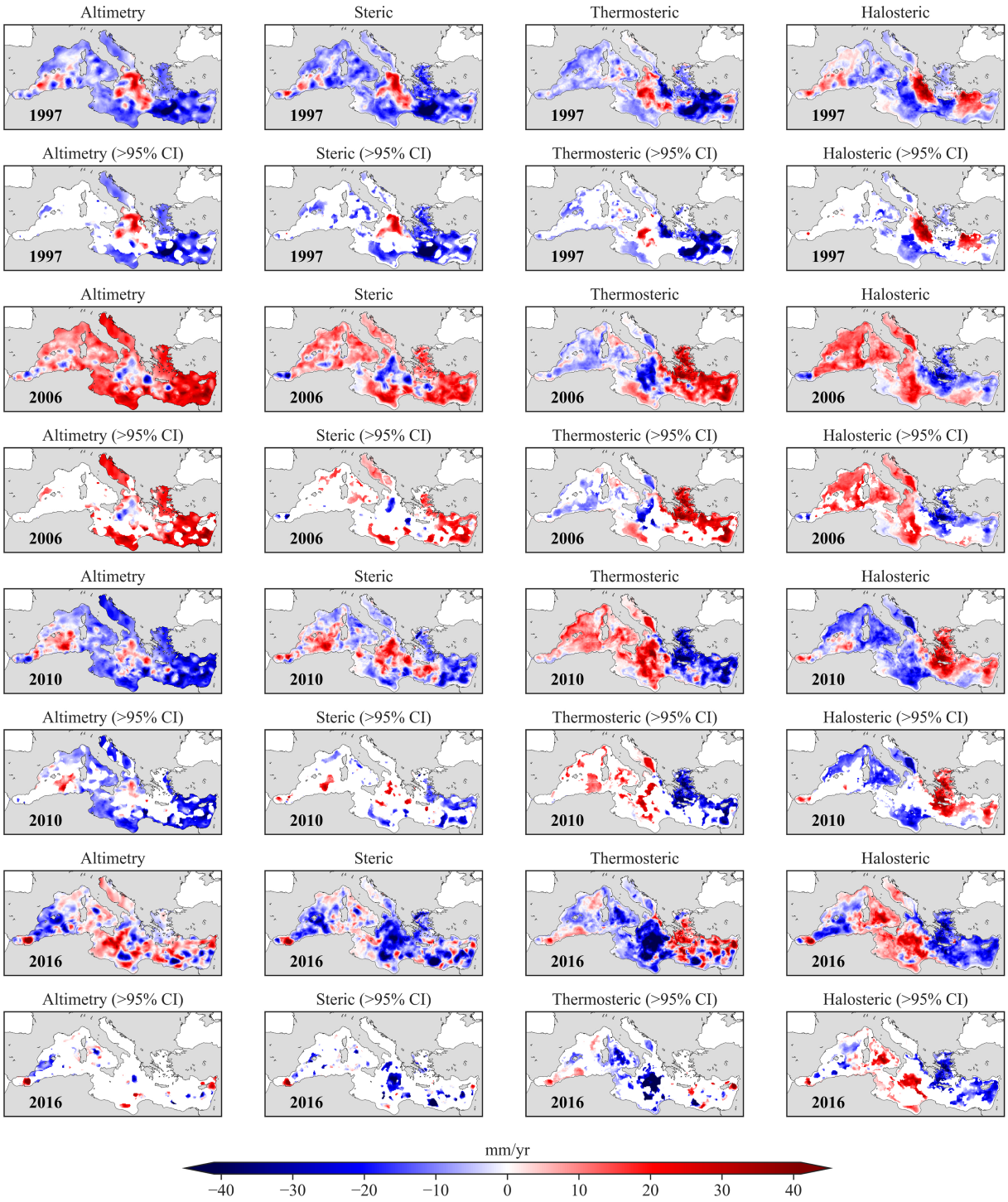

FIGURE 4
Rate variations from yearly mean time series for each of the four years (1997, 2006, 2010, and 2016) resulting from the change point analysis for (from left to right column) the total observed sea level from altimetry, steric component, and thermosteric and halosteric effects. Each inflection of trends is shown both overall, at the scale of the Mediterranean basin, and only in those sectors where the statistically significant (>95% CI) change of trend occurred. Positive (negative) inflections are shown in reddish (bluish) colors, corresponding to increased (decreased) sea-level trends at a specific location after the given year (statement in bold in the lower left corner of the maps).

Figure 3B. Opposite trends of thermosteric and halosteric components (red dotted and blue dash-dotted lines, respectively) over the Mediterranean Sea denote considerable rising and decreasing trends, respectively (see also Figures 3C, D).

3.2.1 The 1997 inflection

The spatial distribution of the 1997 inflection shows a marked bimodal behavior at the basin scale (Figure 4) with positive inflection over a large portion of the Ionian and negative values

10.3389/fmars.2023.1150488

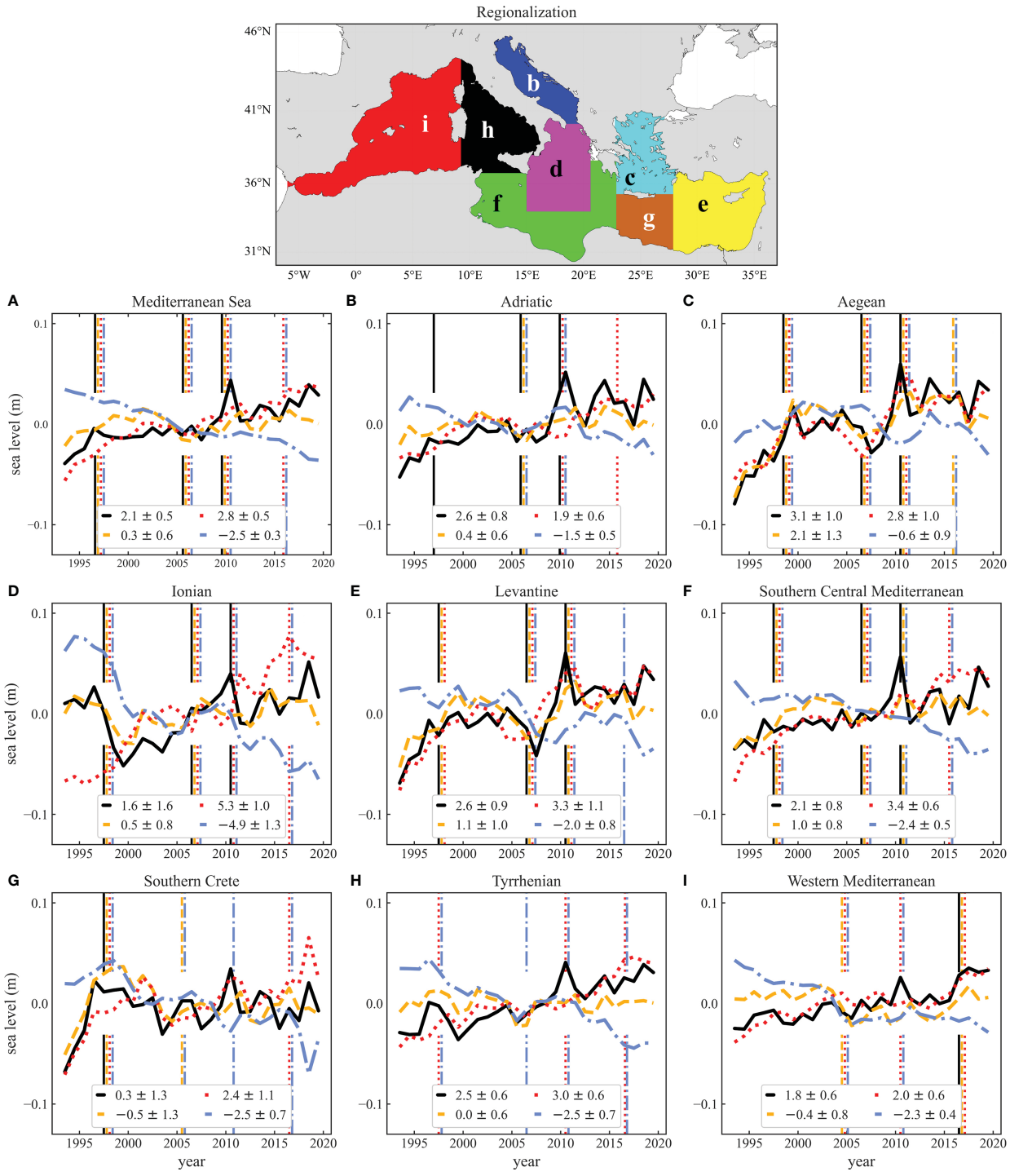

FIGURE 5
Annual sea level time series from altimetry (black solid line), steric (dashed yellow), thermosteric (dotted red), and halosteric (dash-dotted blue) components over different spatial scales (see also map at the top of figure): Mediterranean Sea **(A)**, Adriatic Sea **(B)**, Aegean Sea **(C)**, Ionian Sea **(D)**, Levantine Basin **(E)**, Southern Central Mediterranean **(F)**, Southern Crete **(G)**, Tyrrhenian Sea **(H)** and Western Mediterranean Basin **(I)**. Vertical lines denote significant changepoint in the related component (same color and line style) at a specific time. Trends refer to the period 1993–2019.

that characterize most of the EMed. The WMed is characterized by non-uniform behavior. Considering the entire Mediterranean basin, an average negative inflection of ca. -6.9 mm/yr occurs between 1993–1997 and 1997–2006. Most of the positive inflections over the Ionian (Figure 5D) and negative ones in the Aegean (Figure 5C), Southern Crete (Figure 5G), Levantine (Figure 5E), and Adriatic (Figure 5B) are statistically significant (see also Figure 4). Furthermore, part of the Southern Central Mediterranean also has significant negative inflections. Changes in the steric trends in 1997 show a large similarity to altimetry regarding spatial

distribution and statistical significance; indeed, the steric negative inflection at the scale of the Mediterranean Sea is -6.7 mm/yr, in agreement with the altimetric value.

Both thermosteric and halosteric effects show a positive inflection in a large part of the Ionian, albeit not overlapping but characterizing opposing sectors, that is, south-west for the thermosteric and northeast for the halosteric, with the latter almost entirely significant. In contrast, inflection owing to the thermosteric element, apart from the Ionian, shows negative values for the entire Mediterranean Sea, with large areas of significant inflection in the Levantine. Similarly, the halosteric inflection denotes areas with a significant change in trend: positive values, besides the eastern Ionian, characterize large parts of the Levantine and Western Mediterranean regions, while the negative ones are particularly relevant in the Southern Central Mediterranean. The thermosteric effect inflection at the Mediterranean scale accounts for approximately 97% of the steric component inflection, whereas the remaining 3% is attributable to the halosteric effect.

The time series representative of the Ionian (Figure 5D) denotes a unique non-linear behavior in the altimetry, with an abrupt and significant positive inflection around 1997 for all variables. The 1997 positive inflection that characterizes the Ionian, for total and steric components, represents a direct consequence of the switch of NIG from anticyclonic to cyclonic circulation after EMT relaxation (Vera et al., 2009; Gačić et al., 2010). The total sea level in the Ionian is therefore characterized by a long-term rising trend when only data from 1997 are considered (see also Vera et al., 2009), and the strong inflection that occurred in 1997 is the cause of the lack of significance in the Ionian trend over the period 1993-2019 (observed in Figure 3A).

According to Vigo et al. (2005), the changes of state in the thermohaline circulation in this phase led to a 'breathing' oscillation, possibly linked to an in-phase cooling/heating of the whole Mediterranean Sea or a loss/addiction process of water mass; this is also observed in this study for total and steric 1997 inflections across the whole EMed (Figure 4), where all sub-basins trends move up and down in phase, reaching a peak-to-peak amplitude of approximately 10 cm. Conversely, no significant inflections arise in the WMed (Figures 4, 5H, I), confirming the observations of Vigo et al. (2005).

The shift to a cyclonic phase led to the reinforcement of the AW flux along the MIJ towards the Levantine, thus diluting the surface waters and modifying the thermohaline properties of the latter (Gačić et al., 2011; Gačić et al., 2014), possibly becoming fresher and cooler. During the cyclonic phase, the AW reaches Levantine, traveling eastward directly from the Sicily Channel. The related consequences can be observed in Figure 4, where significant 1997 inflections in Levantine are negative for the thermosteric effect (water contraction due to lower temperature) and positive for the halosteric effect (water expansion due to lower salinity), especially in the RG. The latter represents the area of the main formation of the LIW (Pinardi et al., 2015 and references therein) which then flows westward through the Cretan Passage and Cretan Sea (entering and exiting the Kasos and Kithira straits, respectively), which explains the generalized, significant positive (negative) inflection that characterizes the eastern Ionian (Figure 4), where fresher (cooler) waters were carried toward the northwest along the LIW path. Conversely, the thermosteric effect provides a significant positive inflection along the western flank of the Ionian, ascribed to the replacement of the AW masses (deflected toward the northern Ionian during the previous anticyclonic phase) with those from the Levantine, with a long period to heat up and are relatively warmer than the AW that directly enters the Sicily Channel. This also influenced the Adriatic water properties, especially at the SAG, where relatively saltier waters from the Levantine replaced the AW, which had previously arrived directly from the Sicily Channel during the anticyclonic phase (see also Gačić et al., 2013). For the Adriatic, however, a significant negative inflection is observed in the altimetry, which cannot be explained by the steric component (Figures 4, 5B). It can be argued that the altimetry inflection was caused by the reduction of the AW mass amount entering the Otranto Strait after the cyclonic regime was established. However, the influence of internal processes (e.g., river discharge) within the sub-basin during this phase cannot be excluded.

Finally, the effect observed in the Southern Central Mediterranean was mainly linked to the salinization of the area around the SG, leading to a significant negative inflection, ascribed to the southward path of the LIW (Figure 1B), that is, the preferred path towards the Sicily Channel (Pinardi et al., 2015), which joins the SG and flows along the Gulf of Sirte shelf break and eventually exits the EMed (Sparnocchia et al., 1999; Pinardi et al., 2006). As the salinity of the SG area during cyclonic phases generally increases, it suggests that the intermediate depth waters flowing towards the Sicily Channel (see also Schroeder et al., 2017) drive the steric sea-level change over this area, despite the presence of AW that flows along the SSTC at the surface.

3.2.2 The 2006 inflection

Considering the change point occurrence in 2006, the inflections on the altimetric rate are again distributed according to a well-defined pattern, consistent with the steric component. In detail, a relatively bimodal behavior is shown, similar to the 1997 inflection but showing the opposite phase condition, with the Ionian characterized by negative values, in contrast to all the other regions that showed positive values (Figure 4). In addition, statistical significance is found for altimetry, corresponding with the NIG for negative values and large portions of the EMed for positive values. Overall, this inflection at the Mediterranean scale led to a generalized positive change of sea-level trend of approximately 11 mm/yr, with about 50% explained by the steric trend inflection, which reached 5.5 mm/yr.

The thermosteric and halosteric inflections show a generalized behavior of opposite signs. The distribution of significance for the two effects shows different patterns, with the thermosteric significance limited to some specific areas, while the halosteric one covers a large portion of the Mediterranean Sea. Furthermore, the halosteric effect at this stage explains approximately 31% of the steric component variability; hence, it has a greater influence than the case of the 1997 inflection. Specifically, for the 2006 inflection, a marked and homogeneous opposite behavior of thermosteric and halosteric effects is shown in the WMed.

The inflection detected in 2006 might be the response of sea level to the switch of the NIG to an anticyclonic from a cyclonic state. Cyclonic circulation, established around 1997, shifted again to anticyclonic circulation in 2006 (Gačić et al., 2014). The onset of an opposite behavior in NIG circulation led to a further breathing oscillation throughout the EMed, with all sub-basins moving up and down in the reversed phase for 1997. The peak-to-peak amplitude for this inflection point decreased about 1 cm in comparison to the previous inflection, reaching values of approximately 9 cm for both the altimetry and steric components.

The shift to anticyclonic NIG circulation also led to opposite inflections of thermosteric and halosteric sea-level trends (Figure 4) for 2006. During this phase, the western Ionian interior was replenished by the colder and fresher AW that mainly advected northward (Robinson et al., 1999), entering the Adriatic, affecting the sea surface temperature and salinity. The halosteric provides a significant (positive) inflection throughout the whole sub-basin, decreasing the water density in the whole Adriatic, thus driving a positive steric inflection. However, it is not strong enough to fully explain the marked, significant positive inflection observed in the altimetry over the Adriatic, suggesting that an opposite mechanism, with respect to 1997, impacted the sub-basin.

A possible mechanism could be a greater replenishment of AW masses, which directly entered the Otranto Strait in the anticyclonic context. The direct AW flow towards the Cretan Passage was greatly reduced owing to the absence (or drastic weakening) of the MIJ caused by the anticyclonic Ionian meander (Gačić et al., 2011). This state led to a generalized freshening of the Southern Central Mediterranean (driving the halosteric trend change), as the portion of AW not deflected northward branched into the SSTC and SG (Lermusiaux and Robinson, 2001; Onken et al., 2003). Thus, we can hypothesize that, during this phase, surface circulation is the dominant driver of steric changes. Furthermore, this state also led to salinization and warming of the Levantine because of the longer pathway of the AW reaching the eastern EMed (Manca, 2000).

As observed for the 1997 inflection, significant changes occurred around RG, influencing (this time with a negative halosteric inflection) the formation of the LIW. A lower dilution context increased the LIW salinity, leading to Aegean salinification with the LIW passing through the Cretan Sea and eastern Ionian (Theocharis et al., 1999). However, the significant positive inflection of the thermosteric effect in the Aegean and Levantine regions, caused by the sea surface temperature increase during this phase, seems to be the main driver of the inflection observed in the steric component.

The observations on the WMed time series (Figures 5H, I) and the spatial distribution of significant inflections (Figure 4) show negative and positive inflections for thermosteric and halosteric effects, respectively. The 2006 inflection is not reflected in the altimetric signal over the WMed and, in the Western Mediterranean, seems to start earlier, around 2004. This could be linked to the Western Mediterranean Transition (WMT, Roether et al., 1996), that was linked to a thermohaline anomaly that occurred around 2004–2005 and spread throughout the WMed, inducing freshening and cooling in the deep and intermediate layers (Schroeder et al., 2010; Zunino et al., 2012; Schroeder et al., 2016). This agrees with our observations in Figure 4, especially with the generalized positive, significant inflection in the halosteric effect.

3.2.3 The 2010 inflection

For the 2010 inflection, a well-defined bimodal behavior of the sea-level trend is also observed, and a good agreement between the altimetry and steric component regarding spatial variability (Figure 4). The main pattern is very similar (but with a more patchy distribution) to that observed for the 1997 inflection when the same type of reversal (i.e., from anticyclonic to cyclonic) in the NIG circulation occurred (Gačić et al., 2014). In detail, positive values characterize the Ionian, whereas generalized negative values are representative of the entire remaining EMed. Conversely, in WMed, the pattern appears randomly distributed but with a more substantial positive value. Most of the Mediterranean shows significant inflections in altimetry, especially in areas with negative values, almost the entire Adriatic, Levantine, and Southern Central Mediterranean. Positive significance emerges only corresponding to the NIG, PG, and over part of the Western Mediterranean region. The 2010 inflection, at the scale of the Mediterranean Sea, provides an average negative value of approximately -8.9 mm/yr, which is lower but similar to the 1997 inflection. In this case, the steric inflection is weaker than the variation observed in the total sea level, reaching about -1.6 mm/yr. The peak-to-peak amplitude remains the same as in 2006 for the altimetry and steric components, with a value of approximately 9 cm. Conversely, the contribution of the non-steric effects to the 2010 inflection seems to increase again (ca. -7.3 mm/yr) but negatively, enhancing the effect of the steric component on the total sea level. Regarding the steric component influence, the thermosteric effect accounts for approximately 68% of the average 2010 steric inflection, similar to that observed in 2006.

A similar behavior to the 1997 of thermosteric and halosteric effects is shown in 2010 in the EMed, while major differences arose in the Adriatic and Aegean, showing some significant inflections with opposite signs than 1997. In detail, the same sea water freshening in the RG area occurred, influencing the LIW properties, which propagated westward through the Cretan Passage and Cretan Sea and eventually changed the salinity of the eastern Ionian and Aegean. The latter, different from 1997, seems to have been impacted entirely by the freshening, while cooling, similar to 1997, is observed. In the Adriatic, the inflections of both effects are noticeable and more marked in 2010 than in 1997, with significant warming and salinization owing to the replacement of the AW (directly entering during the previous anticyclonic phase) with the waters coming from the Levantine. More prominent than in 1997, the generalized negative inflection observed in the altimetry over the Adriatic cannot be ascribed to the steric component, reinforcing the hypothesis advanced in Section 3.2.1 regarding the decrease in the intake of AW masses during the cyclonic phases. Thus, in 2010, as well as for 1997 and 2006 (Figures 4, 5B), for the Adriatic, the significant inflections may have been mainly driven by the non-steric effects as a consequence of the differential contribution of AW masses during NIG shifts.

3.2.4 The 2016 inflection

The 2016 inflection, in contrast to the others previously analyzed, does not provide the same defined pattern throughout the Mediterranean Sea (Figure 4). Instead, it provides a patchy

pattern linked to local gyres and complexities at the sub-basin scale and information about a significant positive inflection in the westernmost portion of the WMed. Despite this detected inflection being close to the subsequent NIG reversal (from cyclonic to anticyclonic), which occurred around 2017 (von Schuckmann et al., 2019), another significant shift (also in this case from cyclonic to anticyclonic) occurred in 2012, probably linked to the extremely cold winter that affected the Adriatic during the same year (Bensi et al., 2013; Mihanović et al., 2013; Gačić et al., 2014), but quickly restored to cyclonic conditions in 2013. This brief reversal episode may have influenced the sea level and the formation of the breathing oscillation, as observed previously. However, further analyses with different time-resolution datasets are required to prove this hypothesis. Furthermore, it should be considered that, in this case, the upper limit of the split series is the end of the time series themselves; therefore, to properly evaluate the effect of the 2016 change point (likely related to the last NIG reversal), it would require considering the entire time interval until the next shift.

At the Mediterranean Sea scale, the 2016 inflection provides an average value of 0 mm/yr, which contrasts with the steric component that is ca. -5.6 mm/yr, of which about 52% is explained by the halosteric effect. This suggests that the impact of the halosteric effect has been further amplified, and that the non-steric elements have positively contributed by approximately 5.6 mm/yr to balance the total sea level budget, as observed in the 2006 inflection. Moreover, similarities with the 2006 inflection can also be observed in the thermosteric and halosteric effects, especially in the EMed (Figure 4).

The significant inflection observed in the Western Mediterranean in 2016 for altimetry (Figure 4) represents the only change point observed in the total sea level throughout the WMed over the period under analysis (Figure 5I), possibly driven by the steric component and, in detail, by the thermosteric effect. This phenomenon can also be linked to the WMT footprint, as suggested by Schroeder et al. (2016) and Naranjo et al. (2017), with a strong acceleration in temperature and salinity trends after 2013 (consistent with the observation in Figure 5I), driven by the Western Mediterranean deep-water formation and flowing out of the Gibraltar Strait.

4 Summary and conclusions

When considering linear modeling, the distribution of sea-level trends across the entire Mediterranean basin (Figure 3A) shows a large spatial variability since 1993, consistent with previous studies (Bonaduce et al., 2016; Mohamed et al., 2019a). Zones of non-significance in the total sea level trend from altimetry (Figure 3A) reflect areas of critical passages of different water masses with related complex circulation at surface and intermediate depths, as in the case of the EAG-Balearic Islands sector, Southern Central Mediterranean, and Southern Crete. Also, the Ionian lacked a significant trend over the whole period; however, it becomes significant when analyzed only since 1997 (as previously observed by Vera et al., 2009), thus the lack of significance in the long-term trend is caused by the abrupt change point within the time series (Figure 5D). Conversely, the lack of significance in the Southern Crete (Figures 3A, 5G) is not due to inflections of opposite signs, which may affect the long-term trend, but this sub-basin is linked to a substantial absence of a trend. This also probably reflects regionalization, as Southern Crete comprehends the Cretan Passage and the IG, which strongly influences sea level. However, a large positive trend before 1997 characterizes all the time series within the sub-basin, denoting a different behavior for 1997–2019. This could be linked to the final phase of the EMT and the restoration of thermohaline cell circulation of the EMed in 1999 (Manca et al., 2003), with the consequent restitution of the pre-EMT situation (Vigo et al., 2005). As for the Southern Crete, the absence of trend in the western WMed is probably linked to the complexity of the area, with incoming AW and outflowing LIW waters heavily impacting sea level.

The steric component, contrary to the global mean sea-level change (Storto et al., 2019), generally slightly affect the total long-term sea-level trend (Figure 3B) in the Mediterranean Sea, which is dominated by the contribution of the non-steric effects explaining approximately 80% of the total variance, consistent with previous studies (Calafat et al., 2010; Calafat et al., 2012; Pinardi et al., 2014). However, at the sub-basin scale, the steric component can explain a substantial part of the total sea-level variance, for instance in the Aegean (68%), Southern Central Mediterranean (48%), and Levantine (42%), consistent with Mohamed and Skliris (2022). Regarding long-term trends, the steric component in the other sub-basins proved to be non-significant (Figures 3B, 5), as well as the halosteric component in the Aegean (Figures 3D, 5C), which is linked to the progressive presence of significant inflections with opposite signs along the time series, resulting in an irregular oscillation around zero through time. Furthermore, the weak contribution of the steric component to the total sea level is linked to the opposite evolution of the thermosteric (water expansion owing to increasing ocean temperature) and halosteric (water contraction owing to increasing salinity) effects (Figures 3C, D), which cancel each other out in almost all sub-basins.

Four main change points in the total sea-level trend arose from our analysis over 1993–2019 (Figure 2B), occurring around 1997, 2006, 2010, and 2016. These matched perfectly with the occurrence of NIG reversal episodes in the Ionian (von Schuckmann et al., 2019; Menna et al., 2022), where the surface circulation switched from anticyclonic to cyclonic (1997 and 2011) and vice-versa (2006 and 2017). These changes strongly impacted the water mass redistribution and thermohaline circulation throughout the EMed (Vigo et al., 2005; Gačić et al., 2010), thus affecting the sea level and generating a significant inflection in trends, as previously observed in 1998 (Vera et al., 2009). Generally, all sub-basins within the EMed move up and down in phases (Figure 4), leading to a breathing oscillation (Vigo et al., 2005), where the Ionian behaves the opposite way to the other sub-basins. This behavior can also be observed for the steric component, similar to the total sea level inflections. Accordingly, variations in the steric component seem to be the main cause of breathing oscillations observed in the total sea level, thus driving this variability at the sub-basin and Mediterranean Sea scales which emerge from quasi-decadal trend

changes. This is also supported by the 2016 inflection observations, where the bimodal breathing oscillation was not detected in the steric component, and therefore not in the total sea level. However, this inflection cannot be accurately assessed, both because the time series end in December 2019 and because a brief NIG shift that occurred around 2012 could have influenced the evolution of the phenomenon.

The contribution of the steric and non-steric components to the total sea level inflections change over time at the Mediterranean Sea scale. For example, in 1997, a negative inflection of -6.9 and -6.7 mm/yr was observed for the total sea level and steric component, respectively, then in 2006, positive inflections of 11 (total) and 5.5 (steric) mm/yr, whereas in 2010 negative inflections again of approximately -8.9 (total) and -1.6 (steric) mm/yr were observed. Unlike the previous events, the steric and non-steric effects in 2016 were found to contribute with opposing signs, with the steric component exhibiting a negative inflection of approximately -5.6 mm/yr and the non-steric component contributing positively (5.6 mm/yr) to the total sea level (as observed for the same type of NIG reversal in 2006). Some changes within the steric component properties were also observed for each reversal episode, with the thermosteric (halosteric) effect explaining approximately 97% (3%) of the steric variability in 1997, 69% (31%) in 2006, 68% (32%) in 2010, and 48% (52%) in 2016. Finally, the peak-to-peak amplitude of each breathing oscillation is consistent with each NIG reversal (ca. 9-10 cm), at least over the altimetric era, for the total sea level and steric component.

The residual contribution attributed to the non-steric effects increased over time, from approximately 2% in 1997 to 50% in 2006, 80% in 2010, and again 50% in 2016. Furthermore, the contribution of the halosteric effect has increased over time, balancing out the thermosteric contribution; this could have had an impact on the contribution of the steric component over time, as the contrast between thermosteric and halosteric effects gradually led to a cancellation of the steric variability. The 1997 inflection was strongly influenced by the steric and thermosteric effects, while a singular behavior can be observed in the EMed time series for this period (Figure 5). Therefore, it is possible that the concurrent effect of NIG reversal and EMT relaxation, which occurred around 1997, is the cause of the divergence of 1997 inflection and the subsequent inflections. However, EMT (as well as WMT) might be a non-recurrent phenomenon occurring at time scales longer than the decadal (Gačić et al., 2013; Roether et al., 2014), in contrast to NIG reversal episodes that appear to be cyclical at a quasi-decadal time scale (Gačić et al., 2010). The stronger contribution of the non-steric effects observed in 2010, instead, may be linked to an anomalously low NAO index that, in the winter of 2010, led to an average increase in the Mediterranean sea level of about 12 cm (Tsimplis et al., 2013). The extent of the phenomenon, however, was found to be variable among the sub-basins (see Bonaduce et al., 2016).

The individual thermosteric and halosteric effects allow the observation of the main variability occurring at the sub-basin scale, the main driver that modifies the steric component. Each breathing oscillation underlies variations in thermohaline properties and water mass redistribution at the sub-basin scale over the EMed owing to NIG reversal episodes. Switches to cyclonic NIG phases (1997, 2011) led to relative freshening and cooling of Levantine water while shifting to an anticyclonic phase (2006 and 2017) to salinization and warming, thereby impacting LIW properties in both cases. Changes in LIW properties are then reflected throughout the EMed sub-basins by flowing westward and changing the thermohaline properties of the intermediate depth layer. The thermosteric effect seems to be the main driver of the Levantine and Aegean steric variability. In contrast, the halosteric effect in the Adriatic and Southern Central Mediterranean contributes similarly to the steric variability of the Ionian, albeit influencing different portions of the sub-basin. The simultaneous opposite changes in both effects in some inflections led to annulment; thus, no significant steric inflections were generated in these cases. However, the steric inflection in the Adriatic, usually limited to the SAG area, cannot explain the significant inflections achieved from altimetry over the whole sub-basin. This suggests that the water mass redistribution, linked to the NIG, could be the dominant driver for this sub-basin, in which sea-level trends increase (decrease) during cyclonic (anticyclonic) phases due to the intake (lack) of AW flowing directly from the Sicily Channel.

The only significant inflection observed for total sea level in 2016 arose in the Western Mediterranean (Figure 5I), specifically in the EAG-Balearic Islands (Figure 4), where a positive jump was observed in altimetry, steric, and thermosteric trends. This variation is limited to the WMed and is probably linked to the WMT footprint, as it also occurred around 2004 over the same sub-basins (namely the Tyrrhenian and the Western Mediterranean).

This study highlights how non-linearity of sea-level trends within the Mediterranean Sea occurs due to oceanographic processes at the sub-basin scale, which is also reflected at the basin scale. Critical dynamic effects such as the NIG reversal phenomenon in the Ionian, which occurs at a quasi-decadal cyclicity, significantly affect the sea-level trends, especially in the EMed. This suggests that for the Mediterranean Sea, sea-level time series should be analyzed carefully, paying attention to both regionalization and to the fact that the processes acting in a given location reflect a chain of changes that have taken place elsewhere. Furthermore, sea-level projections in the Mediterranean Sea should take into account the existence of this non-linearity, which acts differentially between the sub-basins and significantly impacts the trend in the short and medium term. Future works should look further into the non-steric effects, in order to better understand which, and if, other processes could play an important role in driving the sea-level trend changes. Additionally, inflections on the steric component could also be evaluated separately for the surface and intermediate depths, thus better attributing sea-level trend changes to a specific process at the sub-basin scale.

Data availability statement

The raw data supporting the conclusions of this article will be made available by the authors, without undue reservation.

Author contributions

MO and MM contributed to conception and design of the study. CR supervised the work. CC performed the computation of the datasets. MM performed the analyses and wrote the first draft of the manuscript. AS, CC, CR, and MO contributed to manuscript revision. All authors contributed to the article and approved the submitted version.

Funding

This study has been partly developed in the framework of the MACMAP project funded by Istituto Nazionale di Geofisica e Vulcanologia (Environment Department), and partly by BiGeA funding, RFO project (CR).

Acknowledgments

The authors would like to thank Giorgio Spada, Marco Zavatarelli and Nadia Pinardi for their valuable suggestions on an earlier version of this paper. This work was carried out in the framework of the Ph.D. course in *Future Earth, Climate Change and Societal Challenges* (University of Bologna), and facilitated by a research visit to the NIOZ Royal Netherlands Institute of Sea Research (Yerseke, the Netherlands). The authors express their gratitude to Hazem Nagy and William Llovel whose valuable revisions significantly enhanced the quality of this work.

Conflict of interest

The authors declare that the research was conducted in the absence of any commercial or financial relationships that could be construed as a potential conflict of interest.

Publisher's note

References

Argus, D. F., Peltier, W. R., Drummond, R., and Moore, A. W. (2014). The Antarctica component of postglacial rebound model ICE-6G_C (VM5a) based upon GPS positioning, exposure age dating of ice thickness, and relative sea level histories. *Geophys. J. Int.* 198, 537–563. doi: 10.1093/gji/ggu140

Artegiani, A., Paschini, E., Russo, A., Bregant, D., Raicich, F., and Pinardi, N. (1997). The Adriatic Sea general circulation. part II: Baroclinic circulation structure. *J. Phys. Oceanogr.* 27, 1515–1532. doi: 10.1175/1520-0485(1997)027<1515:TASGCP>2.0.CO;2

Ayoub, N., Le Traon, P.-Y., and De Mey, P. (1998). A description of the Mediterranean surface variable circulation from combined ERS-1 and TOPEX/POSEIDON altimetric data. *J. Mar. Syst.* 18, 3–40. doi: 10.1016/S0924-7963(98)80004-3

Beckley, B. D., Callahan, P. S., Hancock, D. W., Mitchum, G. T., and Ray, R. D. (2017). On the "cal-mode" correction to TOPEX satellite altimetry and its effect on the global mean sea level time series. *J. Geophys. Res.: Oceans* 122, 8371–8384. doi: 10.1002/2017JC013090

Bensi, M., Cardin, V., Rubino, A., Notarstefano, G., and Poulain, P. M. (2013). Effects of winter convection on the deep layer of the southern Adriatic Sea in 2012. *J. Geophys. Res. Oceans* 118, 6064–6075. doi: 10.1002/2013JC009432

Beranger, K., Mortier, L., Gasparini, G. P., Gervasio, L., Astraldi, M., and Crepon, M. (2004). The dynamics of the Sicily strait: a comprehensive study from observations and models. *Deep Sea Res. Part II: Topical Stud. Oceanogr.* 51, 411–440. doi: 10.1016/j.dsr2.2003.08.004

Bessières, L., Rio, M. H., Dufau, C., Boone, C., and Pujol, M. I. (2013). Ocean state indicators from MyOcean altimeter products. *Ocean Sci.* 9, 545–560. doi: 10.5194/os-9-545-2013

Bonaduce, A., Pinardi, N., Oddo, P., Spada, G., and Larnicol, G. (2016). Sea-Level variability in the Mediterranean Sea from altimetry and tide gauges. *Clim. Dyn.* 47, 2851–2866. doi: 10.1007/s00382-016-3001-2

Borzelli, G. L. E., Gačić, M., Cardin, V., and Civitarese, G. (2009). Eastern Mediterranean Transient and reversal of the Ionian Sea circulation. *Geophys. Res. Lett.* 36, L15108. doi: 10.1029/2009GL039261

C3S Copernicus Climate change service. In: *Satellite altimetry data*. Available at: https://climate.copernicus.eu/ (Accessed Aug 19, 2022).

Calafat, F. M., Chambers, D. P., and Tsimplis, M. N. (2012). Mechanism of decadal sea level variability in the eastern north Atlantic and the Mediterranean Sea. *J. Geophys. Res.* 117, C09022. doi: 10.1029/2012JC008285

Calafat, F. M., Frederikse, T., and Horsburgh, K. (2022). The sources of Sea-level changes in the Mediterranean Sea since 1960. *J. Geophys. Res. Oceans* 127, e2022JC019061. doi: 10.1029/2022JC019061

Calafat, F. M., Marcos, M., and Gomis, D. (2010). Mass contribution to the Mediterranean Sea level variability for the period 1948-2000. *Glob. Planet. Change* 73, 193–201. doi: 10.1016/j.gloplacha.2010.06.002

Camargo, C. M. L., Riva, R. E. M., Hermans, T. H. J., and Slangen, A. B. A. (2020). Exploring sources of uncertainty in steric Sea-level change estimates. *J. Geophys. Res. Oceans* 125, 1–18. doi: 10.1029/2020JC016551

Carillo, A., Sannino, G., Artale, V., Ruti, P., Calmanti, S., and Dell'Aquila, A. (2012). Steric sea level rise over the Mediterranean Sea: present climate and scenario simulations. *Clim. Dyn.* 39, 2167–2184. doi: 10.1007/s00382-012-1369-1

Cazenave, A., Bonnefond, P., Mercier, F., Dominh, K., and Toumazou, V. (2002). Sea Level variations in the Mediterranean Sea and black Sea from satellite altimetry and tide gauges. *Glob. Planet. Change* 34, 59–86. doi: 10.1016/S0921-8181(02)00106-6

Cazenave, A., Cabanes, C., Dominh, K., and Mangiarotti, S. (2001). Recent sea level change in the Mediterranean Sea revealed by Topex/Poseidon satellite altimetry. *Geophys. Res. Lett.* 28, 1607–1610. doi: 10.1029/2000GL012628

Chiggiato, J., Artale, V., Durrieu de Madron, X., Schroeder, K., Taupier-Letage, I., Velaoras, D., et al. (2023). "Chapter 9 - Recent changes in the Mediterranean Sea," in *Oceanography of the Mediterranean Sea*. Eds. K. Schroeder and J. Chiggiato (Elsevier), 289–334. doi: 10.1016/B978-0-12-823692-5.00008-X

Cho, H., and Fryzlewicz, P. (2015). Multiple-change-point detection for high dimensional time series *via* sparsified binary segmentation. *J. R. Stat. Soc. Ser. B* 77, 475–507. doi: 10.1111/rssb.12079

Chow, G. C. (1960). Tests of equality between sets of coefficients in two linear regressions. *Econometrica* 28, 591–605. doi: 10.2307/1910133

Civitarese, G., Gačić, M., Eusebi Borzelli, G. L., and Lipizer, M. (2010). On the impact of the bimodal oscillating system (BiOS) on the biogeochemistry and biology of the Adriatic and Ionian seas (eastern Mediterranean). *Biogeosciences* 7, 3987–3997. doi: 10.5194/bg-7-3987-2010

CMEMS Copernicus Marine service. In: *Mediterranean Reanalysis dataset*. Available at: https://marine.copernicus.eu/ (Accessed Aug 19, 2022).

Criado-Aldeanueva, F., and Soto-Navarro, J. (2020). Climatic indices over the Mediterranean Sea: A review. *Appl. Sci.* 10, 5790. doi: 10.3390/app10175790

Demirov, E., and Pinardi, N. (2002). Simulation of the Mediterranean circulation from 1979 to 1993 model simulations: Part II. energetics of variability. *J. Mar. Syst.* 33, 23–50. doi: 10.1016/S0924-7963(02)00051-9

Dieng, H. B., Cazenave, A., Meyssignac, B., and Ablain, M. (2017). New estimate of the current rate of sea level rise from a sea level budget approach. *Geophys. Res. Lett.* 44, 3744–3751. doi: 10.1002/2017GL073308

Dobricic, S., and Pinardi, N. (2008). An oceanographic three-dimensional variational data assimilation scheme. *Ocean Model.* 22, 89–105. doi: 10.1016/j.ocemod.2008.01.004

Escudier, R., Clementi, E., Cipollone, A., Pistoia, J., Drudi, M., Grandi, A., et al. (2021). A high resolution reanalysis for the Mediterranean Sea. *Front. In Earth Sci.* 9. doi: 10.3389/feart.2021.702285

Escudier, R., Clementi, E., Omar, M., Cipollone, A., Pistoia, J., Aydogdu, A., et al. (2020). Mediterranean Sea Physical reanalysis (CMEMS MED-currents) (Version 1) *Data set. Copernicus Monit. Environ. Mar. Service (CMEMS)*. doi: 10.25423/CMCC/MEDSEA_MULTIYEAR_PHY_006_004_E3R1

Fenoglio-Marc, L. (2002). Long-term sea level change in the Mediterranean Sea from multi-satellite altimetry and tide gauges. *Phys. Chem. Earth* 27, 1419–1431. doi: 10.1016/S1474-7065(02)00084-0

Fox-Kemper, B., Hewitt, H. T., Xiao, C., Aðalgeirsdóttir, G., Drijfhout, S. S., Edwards, T. L., et al. (2021). "Ocean, cryosphere and Sea level change," in *Climate change 2021: The physical science basis. contribution of working group I to the sixth assessment report of the intergovernmental panel on climate change*. Eds. V. Masson-Delmotte, P. Zhai, A. Pirani, S. L. Connors, C. Péan, S. Berger, N. Caud, Y. Chen, L. Goldfarb, M. I. Gomis, M. Huang, K. Leitzell, E. Lonnoy, J. B. R. Matthews, T. K. Maycock, T. Waterfield, O. Yelekçi, R. Yu and B. Zhou (Cambridge, United Kingdom and New York, NY, USA: Cambridge University Press), 1211–1362. doi: 10.1017/9781009157896.011

Gačić, M., Civitarese, G., Eusebi Borzelli, G. L., Kovačević, V., Poulain, P.-M., Theocharis, A., et al. (2011). On the relationship between the decadal oscillations of the northern Ionian Sea and the salinity distributions in the Eastern Mediterranean. *J. Geophys. Res.* 116, C12002. doi: 10.1029/2011JC007280

Gačić, M., Civitarese, G., Kovačević, V., Ursella, L., Bensi, M., Menna, M., et al. (2014). Extreme winter 2012 in the Adriatic: an example of climatic effect on the BiOS rhythm. *Ocean Sci.* 10, 513–522. doi: 10.5194/os-10-513-2014

Gačić, M., Eusebi Borzelli, G. L., Civitarese, G., Cardin, V., and Yari, S. (2010). Can internal processes sustain reversal of the ocean upper circulation? the Ionian Sea example. *Geophys. Res. Lett.* 37. doi: 10.1029/2010GL043216

Gačić, M., Schroeder, K., Civitarese, G., Cosoli, S., Vetrano, A., and Eusebi Borzelli, G. L. (2013). Salinity in the Sicily channel corroborates the role of the Adriatic-Ionian bimodal oscillating system (BiOS) in shaping the decadal variability of the Mediterranean overturning circulation. *Ocean Sci.* 9, 83–90. doi: 10.5194/os-9-83-2013

Galassi, G., and Spada, G. (2014). Sea-Level rise in the Mediterranean Sea by 2050: Roles of terrestrial ice melt, steric effects and glacial isostatic adjustment. *Glob. Planet. Change* 123, 55–66. doi: 10.1016/j.gloplacha.2014.10.007

Gambolati, G., and Teatini, P. (1998). "Numerical analysis of land subsidence due to natural compaction of the upper Adriatic Sea basin," in *CENAS, coastline evolution of the upper Adriatic Sea due to Sea level rise and natural and anthropogenic land subsidence*, vol. 28 . Ed. G. Gambolati (Norwell, MA, USA: Kluwer Academic Publishing, Water Science & Technology Library), 103–131.

García, D., Vigo, I., Chao, B. F., and Martínez, M. C. (2007). Vertical crustal motion along the Mediterranean and black Sea coast derived from ocean altimetry and tide gauge data. *Pure Appl. Geophys.* 164, 851–863. doi: 10.1007/s00024-007-0193-8

Gill, A. E., and Niller, P. P. (1973). The theory of the seasonal variability in the ocean. *Deep Sea Res. Oceanogr. Abstract* 20, 141–177. doi: 10.1016/0011-7471(73)90049-1

Giorgi, F. (2006). Climate change hot-spots. *Geophys. Res. Lett.* 33, L08707. doi: 10.1029/2006GL025734

Golnaraghi, M., and Robinson, A. R. (1994). "Dynamical studies of the Eastern Mediterranean circulation," in *Ocean processes in climate dynamics: Global and Mediterranean examples, NATO science series c*, vol. 419 . Eds. P. Malanotte-Rizzoli and A. R. Robinson (Springer, Dordrecht: Kluwer Academic Publishers), 437.

Grodsky, S. A., Reul, N., Bentamy, A., Vandemark, D., and Guimbard, S. (2019). Eastern Mediterranean Salinification observed in satellite salinity from SMAP mission. *J. Mar. Syst.* 198, 103190. doi: 10.1016/j.jmarsys.2019.103190

Hamed, K. H., and Rao, A. R. (1998). A modified Mann-Kendall trend test for autocorrelated data. *J. Hydrol.* 204, 182–196. doi: 10.1016/S0022-1694(97)00125-X

Harchaoui, Z., and Cappé, O. (2007). "Retrospective mutiple change-point estimation with kernels," in *IEEE/SP 14th workshop on statistical signal processing*, vol. 2007. (Madison, WI, USA: IEEE), 768–772. doi: 10.1109/SSP.2007.4301363

Heburn, G. W., and La Violette, P. E. (1990). Variations in the structure of the anticyclonic gyres found in the alboran Sea. *J. Geophys. Res.* 95, 1599–1613. doi: 10.1029/JC095iC02p01599

Hecht, A., Pinardi, N., and Robinson, A. R. (1988). Currents, water masses, eddies and jets in the Mediterranean levantine basin. *J. Phys. Oceanogr.* 18, 1320–1353. doi: 10.1175/1520-0485(1988)018<1320:CWMEAJ>2.0.CO;2

Iona, A., Theodorou, A., Sofianos, S., Watelet, S., Troupin, C., and Beckers, J. M. (2018). Mediterranean Sea climatic indices: Monitoring long-term variability and climate changes. *Earth Syst. Sci. Data* 10, 1829–1842. doi: 10.5194/essd-10-1829-2018

IPCC (2021). "Climate change 2021," in *The physical science basis. contribution of working group I to the sixth assessment report of the intergovernmental panel on climate change*. Eds. V. Masson-Delmotte, P. Zhai, A. Pirani, S. L. Connors, C. Péan, S. Berger, N. Caud, Y. Chen, L. Goldfarb, M. I. Gomis, M. Huang, K. Leitzell, E. Lonnoy, J. B. R. Matthews, T. K. Maycock, T. Waterfield, O. Yelekçi, R. Yu and X. X. X. B. Zhou (Cambridge, United Kingdom and New York, NY, USA: Cambridge University Press). doi: 10.1017/9781009157896

Jones, P. W. (1999). First- and second-order conservative remapping schemes for grids in spherical coordinates. *Monthly Weather Rev.* 127, 2204–2210. doi: 10.1175/1520-0493(1999)127<2204:FASOCR>2.0.CO;2

Jevrejeva, S., Moore, J. C., Grinsted, A., Matthews, A. P., and Spada, G. (2014). Trends and acceleration in global and regional sea levels since 1807. *Glob. Planet. Change* 113, 11–22. doi: 10.1016/j.gloplacha.2013.12.004

Kendall, M. G. (1975). *Rank correlation methods. 4th ed.* Ed. C. Griffin (London, UK: Charles Griffin).

Killick, R., Fearnhead, P., and Eckley, I. (2012). Optimal detection of changepoints with a linear computational cost. *J. Amer. Stat. Assoc.* 107, 1590–1598. doi: 10.1080/01621459.2012.737745

Korres, G., Pinardi, N., and Lascaratos, A. (2000). The ocean response to low frequency inter-annual atmospheric variability in the Mediterranean sea. part, i. sensitivity experiments and energy analysis. *J. Clim.* 13, 705–731. doi: 10.1175/1520-0442(2000)013<0705:TORTLF>2.0.CO;2

Kourafalou, V. H., and Barbopoulos, K. (2003). High resolution simulations on the north Aegean Sea seasonal circulation. *Ann. Geophys.* 21, 251–265. doi: 10.5194/angeo-21-251-2003

Landerer, F. W., and Volkov, D. L. (2013). The anatomy of recent large sea level fluctuations in the Mediterranean Sea. *Geophys. Res. Lett.* 40, 553–557. doi: 10.1002/grl.50140

Larnicol, G., Ayoub, N., and Le Traon, P. Y. (2002). Major changes in Mediterranean Sea level variability from 7 years of TOPEX/Poseidon and ERS-1/2 data. *J. Mar. Syst.* 33–34, 63–89. doi: 10.1016/S0924-7963(02)00053-2

Lascaratos, A., Williams, R. G., and Tragou, E. (1993). A mixed-layer study of the formation of levantine intermediate water. *J. Geophys. Res.* 98, 14739–14749. doi: 10.1029/93JC00912

Legeais, J., Meyssignac, B., Faugère, Y., Guerou, A., Ablain, M., Pujol, M.-I., et al. (2021). Copernicus Sea Level space observations: A basis for assessing mitigation and developing adaptation strategies to Sea level rise. *Front. Mar. Sci.* 8. doi: 10.3389/fmars.2021.704721

Lermusiaux, P., and Robinson, A. (2001). Features of dominant mesoscale variability, circulation patterns and dynamics in the strait of Sicily. *Deep Sea Res. Part I: Oceanogr. Res. Pap.* 48, 1953–1997. doi: 10.1016/S0967-0637(00)00114-X

Levitus, S., Antonov, J. I., Boyer, T. P., Baranova, O. K., Garcia, H. E., Locarnini, R. A., et al. (2012). World ocean heat content and thermosteric sea level change (0–2000 m), 1955–2010. *Geophys. Res. Lett.* 39, L10603. doi: 10.1029/2012GL051106

Madec, G., Bourdallé-Badie, R., Bouttier, P.-A., Bricaud, C., Bruciaferri, D., Calvert, D., et al. (2017). *NEMO ocean engine* (Paris, France: Notes du Pôle de modélisation de l \'Institut Pierre-Simon Laplace (IPSL). doi: 10.5281/zenodo.1472492

Madec, G., Delecluse, P., Crepon, M., and Chartier, M. (1991). A three-dimensional numerical study of deep-water formation in the northwestern Mediterranean Sea. *J. Phys. Oceanogr.* 21, 1349–1371. doi: 10.1175/1520-0485(1991)021<1349:ATDNSO>2.0.CO;2

Malanotte-Rizzoli, P., Manca, B. B., D'Alcalà, R., Theocharis, A., Bergamasco, A., Bregant, D., et al. (1997). A synthesis of the Ionian Sea hydrography, circulation and water mass pathways during POEM-phase I. *Prog. Oceanogr.* 39, 153–204. doi: 10.1016/S0079-6611(97)00013-X

Malanotte-Rizzoli, P., Manca, B. B., Ribera d'Alcalà, M., Theocharis, A., Brenner, S., Budillon, G., et al. (1999). The eastern Mediterranean in the 80s and in the 90s: The big transition in the intermediate and deep circulations. *Dyn. Atmos. Oceans* 29, 365–395. doi: 10.1016/S0377-0265(99)00011-1

Manca, B. B. (2000). "Recent changes in dynamics of the eastern Mediterranean affecting the water characteristics of the adjacent basins," in *The Eastern Mediterranean climatic transient: Its origin, evolution and impact on the ecosystem*, vol. 10 . Ed. F. Briand (Monaco: CIESM Workshop Ser.), 27–31. Mediter. Sci. Comm., Monaco.

Manca, B. B., Budillon, G., Scarazzato, P., and Ursella, L. (2003). Evolution of dynamics in the eastern Mediterranean affecting water mass structures and properties in the Ionian and Adriatic seas. *J. Geophys. Res. Oceans* 108, 8102. doi: 10.1029/2002JC001664

Mann, H. B. (1945). Non-parametric tests against trend. *Econometrica* 13, 163–171. doi: 10.2307/1907187

Mariotti, A., and Dell'Aquila, A. (2012). Decadal climate variability in the Mediterranean region: Roles of large-scale forcings and regional processes. *Clim. Dyn.* 38, 1129–1145. doi: 10.1007/s00382-011-1056-7

Marullo, S., Artale, V., and Santoleri, R. (2011). The SST multidecadal variability in the Atlantic-Mediterranean region and its relation to AMO. *J. Climate* 24, 4385–4401. doi: 10.1175/2011JCLI3884.1

Mauri, E., Sitz, L., Gerin, R., Poulain, P.-M., Hayes, D., and Gildor, H. (2019). On the variability of the circulation and water mass properties in the Eastern levantine Sea between September 2016–august 2017. *Water* 11, 1741. doi: 10.3390/w11091741

McDougall, T. J., and Barker, P. M. (2011) *Getting started with TEOS-10 and the Gibbs seawater oceanographic toolbox*. Available at: http://www.teos-10.org/pubs/Getting_Started.pdf.

McDougall, T. J., Jackett, D. R., Millero, F. J., Pawlowicz, R., and Barker, P. M. (2012). A global algorithm for estimating absolute salinity. *Ocean Sci.* 8, 1123–1134. doi: 10.5194/os-8-1123-2012

Meli, M., Olivieri, M., and Romagnoli, C. (2021). Sea-Level change along the Emilia-romagna coast from tide gauge and satellite altimetry. *Remote Sens.* 13, 97. doi: 10.3390/rs13010097

Meli, M., and Romagnoli, C. (2022). Evidence and implications of hydrological and climatic change in the Reno and lamone river basins and related coastal areas (Emilia-romagna, northern Italy) over the last century. *Water* 14, 2650. doi: 10.3390/w14172650

Melini, D., and Spada, G. (2019). Some remarks on glacial isostatic adjustment modelling uncertainties. *Geophys. J. Int.* 218, 401–413. doi: 10.1093/gji/ggz158

Menemenlis, D., Fukumori, I., and Lee, T. (2007). Atlantic To Mediterranean Sea level difference driven by winds near Gibraltar strait. *J. Phys. Oceanogr.* 37, 359–376. doi: 10.1175/JPO3015.1

Menna, M., Gačić, M., Martellucci, R., Notarstefano, G., Fedele, G., Mauri, E., et al. (2022). Climatic, decadal, and interannual variability in the upper layer of the Mediterranean Sea using remotely sensed and in-situ data. *Remote Sens.* 14, 1322. doi: 10.3390/rs14061322

Menna, M., Gerin, R., Notarstefano, G., Mauri, E., Bussani, A., Pacciaroni, M., et al. (2021). On the circulation and thermohaline properties of the Eastern Mediterranean Sea. *Front. Mar. Sci.* 8. doi: 10.3389/fmars.2021.671469

Menna, M., Poulain, P.-M., Zodiatis, G., and Gertman, I. (2012). On the surface circulation of the levantine sub-basin derived from Lagrangian drifters and satellite altimetry data. *Deep-Sea Res. Part I* 65, 46–58. doi: 10.1016/j.dsr.2012.02.008

Menna, M., Reyes-Suarez, N. C., Civitarese, G., Gačić, M., Poulain, P.-M., and Rubino, A. (2019). Decadal variations of circulation in the central Mediterranean and its interactions with the mesoscale gyres. *Deep Sea Res. Part II Top. Stud. Oceanogr.* 164, 14–24. doi: 10.1016/j.dsr2.2019.02.004

Mihanović, H., Vilibić, I., Carniel, S., Tudor, M., Russo, A., Bergamasco, A., et al. (2013). Exceptional dense water formation on the Adriatic shelf in the winter of 2012. *Ocean Sci.* 9, 561–572. doi: 10.5194/os-9-561-2013

Milliff, R. F., and Robinson, A. R. (1992). Structure and dynamics of the rhodes gyre system and dynamical interpolation for estimates of the mesoscale variability. *J. Phys. Oceanogr.* 22, 317–337. doi: 10.1175/1520-0485(1992)022<0317:SADOTR>2.0.CO;2

Millot, C. (1985). Some features of the Algerian current. *J. Geophys. Res.* 90, 7169–7176. doi: 10.1029/JC090iC04p07169

Miramontes, E., Déverchère, J., Pellegrini, C., and Chiarella, D. (2022). "Mediterranean Sea Evolution and present-day physiography," in *Oceanography of the Mediterranean Sea*. Eds. K. Schroeder and J. Chiggiato (Elsevier), 13–39.

Mohamed, B., Abdallah, A. M., Alam El-Din, K., Nagy, H., and Shaltout, M. (2019a). Inter-annual variability and trends of Sea level and Sea surface temperature in the Mediterranean Sea over the last 25 years. *Pure Appl. Geophys.* 176, 3787–3810. doi: 10.1007/s00024-019-02156-w

Mohamed, B., Mohamed, A., Alam El-Din, K., Nagy, H., and Elsherbiny, A. (2019b). Sea Level changes and vertical land motion from altimetry and tide gauges in the southern levantine basin. *J. Geodyn.* 128, 1–10. doi: 10.1016/j.jog.2019.05.007

Mohamed, B., and Skliris, N. (2022). Steric and atmospheric contributions to interannual sea level variability in the eastern Mediterranean sea over 1993-2019. *Oceanologia* 64, 50–62. doi: 10.1016/j.oceano.2021.09.001

Nagy, H., Di-Lorenzo, E., and El-Gindy, A. (2019). The impact of climate change on circulation patterns in the Eastern Mediterranean Sea upper layer using med-ROMS model. *Prog. Oceanogr.* 175, 226–244. doi: 10.1016/j.pocean.2019.04.012

Naranjo, C., García-Lafuente, J., Sammartino, S., Sánchez-Garrido, J. C., Sánchez-Leal, R. , and Jesús Bellanco, M. (2017). Recent changes, (2004-2016) of temperature and salinity in the Mediterranean outflow. *Geophys. Res. Lett.* 44, 5665–5672. doi: 10.1002/2017GL072615

Olivieri, M., and Spada, G. (2013). Intermittent sea-level acceleration. *Glob. Planet. Change* 109, 64–72. doi: 10.1016/j.gloplacha.2013.08.004

Onken, R., Robinson, A. R., Lermusiaux, P. F. J., Haley, P. J., and Anderson, L. A. (2003). Data-driven simulations of synoptic circulation and transports in the Tunisia-Sardinia-Sicily region. *J. Geophys. Res.: Oceans* 108, 8123. doi: 10.1029/2002JC001348

Passaro, M., and Seitz, F. (2010). Steric sea level variations in the central-eastern Mediterranean Sea from argo observations. *Bollettino di Geofisica Teorica Applicata* 52, 131–147.

Pastor, F., Valiente, J. A. , and Palau, J. L. (2018). Sea Surface temperature in the Mediterranean: Trends and spatial patterns, (1982–2016). *Pure Appl. Geophys.* 175, 4017–4029. doi: 10.1007/s00024-017-1739-z

Peltier, W. R., Argus, D. F., and Drummond, R. (2015). Space geodesy constrains ice age terminal deglaciation: The global ICE-6G-C (VM5a) model. *J. Geophys. Res. Solid Earth* 120, 450–487. doi: 10.1002/2014JB011176

Pinardi, N., Bonaduce, A., Navarra, A., Dobricic, S., and Oddo, P. (2014). The mean Sea level equation and its application to the Mediterranean Sea. *J. Clim.* 27, 442–447. doi: 10.1175/JCLI-D-13-00139.1

Pinardi, N., Korres, G., Lascaratos, A., Roussenov, V., and Stanev, E. (1997). Numerical simulation of the interannual variability of the Mediterranean Sea upper ocean circulation. *Geophys. Res. Lett.* 24, 425–428. doi: 10.1029/96GL03952

Pinardi, N., and Masetti, E. (2000). Variability of the large scale general circulation of the Mediterranean Sea from observations and modelling: a review. *Palaeogeogr. Palaeoclimatol. Palaeoecol.* 158, 153–173. doi: 10.1016/S0031-0182(00)00048-1

Pinardi, N., Zavatarelli, M., Adani, M., Coppini, G., Fratianni, C., Oddo, P., et al. (2015). Mediterranean Sea Large-scale low-frequency ocean variability and water mass formation rates from 1987 to 2007: A retrospective analysis. *Prog. Oceanogr.* 132, 318–332. doi: 10.1016/j.pocean.2013.11.003

Pinardi, N., Zavatarelli, M., Arneri, E., Crise, A., and Ravaioli, M. (2006). "The physical, sedimentary and ecological structure and variability of shelf areas in the Mediterranean Sea," in *THE GLOBAL the global coastal ocean: Interdisciplinary regional studies and syntheses*, vol. 14 . Eds. A. Robinson and K. Brink (Cambridge, MA, USA: Harvard University Press, The Sea). (Chapter 32).

Pinardi, N., Estournel, C., Cessi, P., Escudier, R., and Lyubartsev, V. (2023). "Chapter 7 - dense and deep water formation processes and Mediterranean overturning circulationOceanography of the Mediterranean Sea,". Eds. K. Schroeder and J. Chiggiato (Elsevier), 209–261. doi: 10.1016/B978-0-12-823692-5.00009-1

Pisacane, G., Artale, V., Calmanti, S., and Rupolo, V. (2006). Decadal oscillations in the Mediterranean Sea: a result of the overturning circulation variability in the eastern basin? *Clim. Res.* 31, 257–271. doi: 10.3354/cr031257

Pisano, A., Marullo, S., Artale, V., Falcini, F., Yang, C., Leonelli, F. E., et al. (2020). New evidence of Mediterranean climate change and variability from Sea surface temperature observations. *Remote Sens.* 12, 132. doi: 10.3390/rs12010132

Poulain, P. M., Centurioni, L., Özgökmen, T., Tarry, D., Pascual, A., Ruiz, S., et al. (2021). On the structure and kinematics of an Algerian eddy in the southwestern Mediterranean Sea. *Remote Sens.* 13, 3039. doi: 10.3390/rs13153039

Poulain, P.-M., Menna, M., and Mauri, E. (2012). Surface geostrophic circulation of the Mediterranean Sea derived from drifter and satellite altimeter data. *J. Phys. Oceanogr.* 42, 973–990. doi: 10.1175/JPO-D-11-0159.1

Puillat, I., Sorgente, R., Ribotti, A., Natale, S., and Echevin, V. (2006). Westward Branching of LIW induced by Algerian anticyclonic eddies close to the sardinian slope. *Chem. Ecol.* 22, S293–S305. doi: 10.1080/02757540600670760

Reale, M., Crise, A., Farneti, R., and Mosetti, R. (2016). A process study of the Adriatic-Ionian system baroclinic dynamics. *J. Geophys. Res. Oceans* 121, 5872–5887. doi: 10.1002/2016JC011763

Reale, M., Salon, S., Crise, A., Farneti, R., Mosetti, R., and Sannino, G. (2017). Unexpected covariant behavior of the Aegean and Ionian seas in the period 1987-2008 by means of a nondimensional Sea surface height index. *J. Geophys. Res. Oceans* 122, 8020–8033. doi: 10.1002/2017JC012983

Rice, G., and Zhang, C. (2022). Consistency of binary segmentation for multiple change-point estimation with functional data. *Stat Probability Lett.* 180, 109228. doi: 10.1016/j.spl.2021.109228

Robinson, A. R., Malanotte-Rizzoli, P., Hecht, A., Michelato, A., Roether, W., Theocharis, A., et al. (1992). General circulation of the Eastern Mediterranean. *Earth-Science Rev.* 32, 285–309. doi: 10.1016/0012-8252(92)90002-B

Robinson, A. R., Golnaraghi, M., Leslie, W. G., Artegiani, A., Hecht, A., Lazzoni, E., et al. (1991). The eastern Mediterranean general circulation: features, structure and variability. *Dynamics Atmospheres Oceans* 15, 215–240. doi: 10.1016/0377-0265(91)90021-7

Robinson, A. R., Leslie, W. G., Theocharis, A., and Lscaratos, A. (2001). "Mediterranean Sea Circulation," in *Encyclopedia of ocean sciences*. Ed. J. H. Steele (Academic Press), 1689–1705. doi: 10.1006/rwos.2001.0376

Robinson, A. R., Sellschopp, J., Warn-Varnas, A., Leslie, W. G., Lozano, C. J., Haley, P. J.Jr., et al. (1999). The Atlantic Ionian stream. *J. Mar. Syst.* 20, 129–156. doi: 10.1016/S0924-7963(98)00079-7

Roether, W., Klein, B., and Hainbucher, D. (2014). "The Eastern Mediterranean transient: Evidence for similar events previously? in geophysical monograph series, 202, AGU (American geophysical union)," in *The Mediterranean Sea: Temporal variability and spatial patterns* (Washington, USA: Wiley), 75–83. doi: 10.1002/9781118847572.ch6

Roether, W., Manca, B. B., Klein, B., Bregant, D., Georgopoulos, D., Beitzel, V., et al. (1996). Recent changes in eastern Mediterranean deep waters. *Science* 271, 333–335. doi: 10.1126/science.271.5247.333

Romagnoli, C., Bosman, A., Casalbore, D., Anzidei, M., Doumaz, F., Bonaventura, F., et al. (2022). Coastal erosion and flooding threaten low-lying coastal tracts at lipari (Aeolian islands, Italy). *Remote Sens.* 14, 2960. doi: 10.3390/rs14132960

Romanou, A., Tselioudis, G., Zerefos, C. S., Clayson, C.-A. J., Curry, A., and Andersson, A. (2010). Evaporation-precipitation variability over the Mediterranean and the black seas from satellite and reanalysis estimates. *J. Clim.* 23, 5268–5287. doi: 10.1175/2010JCLI3525.1

Schroeder, K., Chiggiato, J., Bryden, H. L., Borghini, M., and Ismail, S. B. (2016). Abrupt climate shift in the western Mediterranean Sea. *Sci. Rep.* 6, 23009. doi: 10.1038/srep23009

Schroeder, K., Chiggiato, J., Josey, S. A., Borghini, M., Aracri, S., and Sparnocchia, S. (2017). Rapid response to climate change in a marginal sea. *Sci. Rep.* 7, 4065. doi: 10.1038/s41598-017-04455-5

Schroeder, K., Josey, S. A., Herrmann, M., Grignon, L., Gasparini, G. P., and Bryden, H. L. (2010). Abrupt warming and salting of the Western Mediterranean deep water after 2005: Atmospheric forcings and lateral advection. *J. Geophys. Res.* 115, C08029. doi: 10.1029/2009JC005749

Scott, A. J., and Knott, M. (1974). A cluster analysis method for grouping means in the analysis of variance. *Biometrics* 30, 507–512. doi: 10.2307/2529204

Sen, P. K. (1968). Estimates of the regression coefficient based on kendall's tau. *J. Am. Stat. Assoc.* 63, 1379–1389. doi: 10.1080/01621459.1968.10480934

Sen, A., and Srivastava, M. S. (1975). On tests for detecting change in mean. *Ann. Stat* 3, 98–108. doi: 10.1214/aos/1176343001

Skliris, N., Zika, J. D., Herold, L., Josey, S. A., and Marsh, R. (2018). Mediterranean Sea water budget long-term trend inferred from salinity observations. *Clim. Dyn.* 51, 2857–2876. doi: 10.1007/s00382-017-4053-7

Slangen, A. B. A., van de Wal, R. S. W., Wada, Y. , and Vermeersen, L. L. A. (2014). Comparing tide gauge observations to regional patterns of sea-level change, (1961-2003). *Earth Syst. Dynam.* 5, 243–255. doi: 10.5194/esd-5-243-2014

Sparnocchia, S., Gasparini, G. P., Astraldi, M., Borghini, M., and Pistek, P. (1999). Dynamics and mixing of the Eastern Mediterranean outflow in the tyrrhenian basin. *J. Mar. Syst.* 20, 301–317. doi: 10.1016/S0924-7963(98)00088-8

Stammer, D., Cazenave, A., Ponte, R. M., and Tamisiea, M. E. (2013). "Causes for contemporary regional sea level changes," in *Annual review of marine science, annual reviews*, vol. 5 . Eds. C. A. Carlson and S. J. Giovannoni (CA, USA: Palo Alto), 21–46.

Storto, A., Bonaduce, A., Feng, X., and Yang, C. (2019). Steric sea level changes from ocean reanalyses at global and regional scales. *Water* 11, 1987. doi: 10.3390/w11101987

Syvitski, J., Kettner, A., Overeem, I., Hutton, E., Hannon, M., Brakenridge, G. R., et al. (2009). Sinking deltas due to human activities. *Nat. Geosci.* 2, 681–686. doi: 10.1038/ngeo629

Taburet, G., Sanchez-Roman, A., Ballarotta, M., Pujol, M.-I., Legeais, J.-F., Fournier, F., et al. (2019). DUACS DT2018: 25 years of reprocessed sea level altimetry products. *Ocean Sci.* 15, 1207–1224. doi: 10.5194/os-15-1207-2019

Tanhua, T., Hainbucher, D., Schroeder, K., Cardin, V., Álvarez, M., and Civitarese, G. (2013). The Mediterranean Sea system: a review and an introduction to the special issue. *Ocean Sci.* 9, 789–803. doi: 10.5194/os-9-789-2013

Theil, H. (1950). *A rank-invariant method of linear and polynomial regression analysis* Vol. 1950 (Berlin/Heidelberg, Germany: Nederl. Akad. Wetensch., Proc. Springer).

Theocharis, A., Nittis, K., Kontoyiannis, H., Papageoirgiou, E., and Balopoulos, E. (1999). Climatic changes in the Aegean Sea influence the eastern Mediterranean thermohaline circulation, (1986–1997). *Geophys. Res. Lett.* 26, 1617–1620. doi: 10.1029/1999GL900320

Theocharis, A., Krokos, G., Velaoras, D., and Korres, G. (2014). An internal mechanism driving the alternation of the eastern mediterranean dense/deep water sources. *Mediterr. Sea: Temporal Variab. Spatial Patterns* 113–137. doi: 10.1002/9781118847572.ch8

Tomczak, M., and Godfrey, J. S. (2003). "Temperature, salinity, density and oceanic pressure field," in *Regional oceanography: An introduction* (Delhi: Daya Publishing House), 15–28.

Truong, C., Oudre, L., and Vayatis, N. (2020). Selective review of offline change point detection methods. *Signal Process.* 167, 107299. doi: 10.1016/j.sigpro.2019.107299

Tsimplis, M. N., and Baker, T. F. (2000). Sea Level drop in the Mediterranean Sea: An indicator of deep water salinity and temperature changes? *Geophys. Res. Lett.* 27, 1731–1734. doi: 10.1029/1999GL007004

Tsimplis, M. N., Calafat, F. M., Marcos, M., Jordà, G., Gomis, D., Fenoglio-Marc, L., et al. (2013). The effect of the NAO on sea level and on mass changes in the Mediterranean Sea. *J. Geophys. Res. Oceans* 118, 944–952. doi: 10.1002/jgrc.20078

Tsimplis, M. N., and Josey, S. A. (2001). Forcing of the Mediterranean Sea by atmospheric oscillations over the north Atlantic. *Geophys. Res. Lett.* 28, 803–806. doi: 10.1029/2000GL012098

Vera, J. D. R., Criado-Aldeanueva, F., García-Lafuente, J., and Soto-Navarro, F. J. (2009). A new insight on the decreasing sea level trend over the Ionian basin in the last decades. *Global Planetary Change* 68, 232–235. doi: 10.1016/j.gloplacha.2009.04.002

Vigo, I., García, D., and Chao, B. F. (2005). Change of sea level trend in Mediterranean and black seas. *J. Mar. Res.* 63, 1085–1100. doi: 10.1357/002224005775247607

Vigo, M. I., Sánchez-Reales, J. M., Trottini, M., and Chao, B. F. (2011). Mediterranean Sea Level variations: Analysis of the satellite altimetric data 1992–2008. *J. Geodynamics* 52, 271–278. doi: 10.1016/j.jog.2011.02.002

Vilibić, I., Matijević, S., Šepić, J., and Kušpilić, G. (2012). Changes in the Adriatic oceanographic properties induced by the Eastern Mediterranean transient. *Biogeosciences* 9, 2085–2097. doi: 10.5194/bg-9-2085-2012

von Schuckmann, K., Le Traon, P. Y., Smith, N., Pascual, A., Djavidnia, S., Gattuso, J. P., et al. (2019). Copernicus Marine service ocean state report. *J. Oper. Oceanogr.* 12 (3), S1–S123. doi: 10.1080/1755876X.2019.1633075

Watson, C. S., White, N. J., Church, J. A., King, M. A., Burgette, R. J., and Legresy, B. (2015). Unabated global mean sea-level rise over the satellite altimeter era. *Nat. Clim. Change* 5, 565–568. doi: 10.1038/nclimate2635

WCRP Global Sea Level Budget Group (2018). Global sea-level budget 1993–present. *Earth Syst. Sci. Data* 10, 1551–1590. doi: 10.5194/essd-10-1551-2018

Winer, B. J. (1962). *Statistical principles in experimental design* (NewYork, NY, US: McGraw-Hill Book Company).

Wöppelmann, G., and Marcos, M. (2012). Coastal sea level rise in southern Europe and the nonclimate contribution of vertical land motion. *J. Geophys. Res.* 117, C01007. doi: 10.1029/2011JC007469

Zunino, P., Schroeder, K., Vargas-Yáñez, M., Gasparini, G. P., Coppola, L., García-Martínez, M. C., et al. (2012). Effects of the Western Mediterranean transition on the resident water masses: Pure warming, pure freshening and pure heaving. *J. Mar. Syst.* 96-96, 15–23. doi: 10.1016/j.jmarsys.2012.01.011

4 Conclusions and Outlook

This thesis offers a multidisciplinary contribution to the understanding of sea–level change at different spatiotemporal scales. In particular, it focused on variations in RSL at the coastal scale, how natural and anthropogenic footprints impacted catchment areas, thus the riverine sediment supply to the coast, and on the main variability of geocentric sea level, and related steric component, at the regional scale. To reach this goal, the project concentrated on three different spatiotemporal perspectives, from the Emilia–Romagna coast (Section 3.1), up to the Reno and Lamone river basins (Section 3.2), and the Mediterranean Sea (Section 3.3).

The first step involved the local RSL assessment at the scale of the Emilia–Romagna coast during the period 1993–2019, to quantify the long–term linear rate and the differential control induced by subsidence along the coast (Meli et al., 2021). The analysis provided an answer to the research question: *How sea level has changed at the Emilia–Romagna coastal scale as resulting from different observative approaches?* Despite the short overlap between SA time series and data provided by three local TGs, a generalized high correlation coefficient arise among RSL and ASL time series, with lower correspondences mostly associated to the effect of local VLM. Data from altimetry showed that the ASL is coherent along the coast over the satellite altimetry era, providing a linear rate of 2.8 $\pm$ 0.5 mm·year^{-1} and a negative acceleration of -0.3 $\pm$ 0.1 mm·year^{-2}. The former is smaller but comparable with the GMSL average for the same time frame (3.3 $\pm$ 0.5 mm·year^{-1}), while the latter contrasts with the ongoing, albeit debated, positive GMSL acceleration (0.084 $\pm$ 0.025 mm·year^{-2}, according to Nerem et al. (2018)). The found negative acceleration could be the consequence of local scale and short–lived phenomena, climatological events, or multidecadal oscillations, only partially sampled by the available data. Our interpretation puts this phenomenon in the broader context of the Mediterranean Sea in which a marked spatiotemporal variability of sea–level trend has been observed. The non–linearity of local sea–level trend could be also confirmed by the presence of different, significant periodicities within the signal.

The second step of this research focused on the climatic and hydrological processes that have affected the Lamone and Reno river basins of the ER Region and the related

coastal area over the last century (Meli and Romagnoli, 2022). The holistic approach considered for the analysis took into account different climatic and environmental parameters, providing an answer to the research question: *How natural and anthropogenic footprints impacted dynamics of the catchment areas and, indirectly, the coast?* The large–scale anthropogenic dimming/brightening phenomenon (Wild et al., 2005; Wild, 2009), that act at both the global–to–regional and river basin scale, and local land–use changes turned out to be the main drivers of the observed long–term, non–linear trends within the catchment area. However, the influence of natural oscillations, despite of secondary importance, still have an impact on all environmental and climatic parameters considered. Indeed, interactions with major climatic modes (e.g., NAO and AMO) can significantly modify the signals over various periodicities. A substantial negative acceleration in river discharge supports a lack of recovery in terms of sediment delivery to the coast, despite safeguard policies introduced by the ER regional administration in the early 1980s. The drastic reduction in river discharge and sediment supply was driven first by river regulation and land–use changes, mainly from 1950s to 1980s, then, since the 1980s, by the dramatic local air temperature rise, resulting in protracted drought conditions. Furthermore, over the last 140 years, the small coastal portion under consideration (Figure 7, Section 2.2) has been influenced by persistent sea–level rise (1.3 ± 0.2 mm·year^{-1}), periodically reduced or amplified by natural fluctuations at high–frequency (e.g., observed in 2010) and low–frequency (observed in the early twentieth century, 1970s–1980s, and 1990s to mid–2000s) fluctuations.

At last, the third step of this project aimed at shedding light on the main variability of sea–level trends across the Mediterranean Sea (Meli et al., 2023). The related scientific question, i.e. *What is the main variability of sea–level trends in the Mediterranean Sea?*, has been answered. A statistical analysis performed on the total sea level observed from altimetry provided an indication of four main changes occurred in sea–level trends during the satellite era (1993–2019). These have been detected around 1997, 2006, 2010 and 2016. These change points appear to have occurred in correspondence with the quasi–decadal Ionian surface circulation reversal episodes (Gačić et al., 2013; Menna et al., 2019), thus suggesting that observed changes in sea–level trends are directly driven by modification of

thermohaline circulation and mass redistribution. This process mostly impacts the whole Eastern Mediterranean Sea (i.e., excluding the Western Mediterranean and Tyrrhenian sub–basins, Figure 9), leading to a sort of breathing oscillation mode (Vigo et al., 2005) with the sub–basins moving up and down in phase. In detail, a switch from anticyclonic to cyclonic (and vice versa) mode in the northern Ionian circulation led to a significant positive (negative) change of sea–level trend throughout the Ionian Sea, while a concurrent negative (positive) variation is observed for all other sub–basins. The same behavior is observed also for the steric component but with different magnitude in time with respect to the total sea level; this suggests that only part of these changes in sea–level trends can be explained as a consequence of the steric variability, and that non–steric effects (e.g., the mass component) always gave their contribute.

Some aspects related to the main question of this work (**Which is the sea–level variability for the Emilia–Romagna coastal area in the framework of the Mediterranean Sea?**) have been originally addressed, leading to a better comprehension of different processes and their interaction. ASL along the ER has risen with a rate of 2.8 ± 0.5 mm·year^{-1} and 1.3 ± 0.2 mm·year^{-1} over the periods 1993–2019 and 1875–2016, respectively. However, significant non–linearities influenced the signal at different frequencies. These are probably driven, at both the inter–annual and multi–decadal time scales, by coupled atmosphere-ocean interactions, also occurring outside the Mediterranean basin, mainly linked to the influence of the NAO (see Manuscript I and II), while, at the quasi–decadal time scale, by changes in the surface circulation of the nearby Ionian sub–basin (see Manuscript III). The main differences that arise between the ASL and RSL at the coastal scale are inevitably linked to the influence of VLMs, of both natural and anthropogenic origin, that differentially contribute at any location. According to the existing literature (ARPA, 2002; Preti et al., 2008; Aguzzi et al., 2016, 2020), the subsidence trend of the whole coastal plain has generally decreased over the last two decades; however, this study highlighted the fact that local VLMs may differ from the general trend, and therefore there is the need to assess RSL case by case.

This study also provided information about one of the major contributor to the shoreline evolution in terms of erosion/accretion, although not considered in the sea–

level equation, represented by the riverine sediment supply to the coast (see Manuscript II). Analysis on catchment dynamics showed that the anthropogenic influence over the last century, acting at different spatial scale for different processes, drove the long–term changes of several parameters. This partly explains the lack of recovery in the sediment supply, despite the introduction of safeguard policies in the early 1980s by the ER regional administration.

Answering to the sub–questions and the related analyses, nevertheless, opens new questions, as new evidences emerged. Future works should provide coastal plain VLMs at high resolution and their non–linear components. This would lead to more accurate local RSL estimates and a widespread view of the extent of the anthropogenic impact. In terms of sea–level projections at the local scale, there is the need to better clarify the origin of the non–linear, multi–decadal oscillations observed in local ASL over the last 140 years, since failure to consider these would lead to unreliable future estimates. Furthermore, it is necessary to better understand the influence of quasi–decadal oceanographic changes on sea level at the sub–basin scale, quantifying the differential impact of all sea–level components over time. The absence of this consideration could lead to critical issues in terms of studying sea–level projections in the near–term for the Mediterranean Sea, and might be essential when testing the validity of projections computed from regional or global models that may not be able to capture this type of local, sub–basinal variability.

References

Ablain, M., Legeais, F. F., Prandi, P., Fenoglio-Marc, L., Marcos, M., Benveniste, J., and Cazenave, A. (2017). Satellite altimetry based sea level at global and regional scales. *Surveys in Geophysics*, 38:9–33.

Ablain, M., Meyssignac, B., Zawadzki, L., Jugier, R., Ribes, A., Spada, G., Benveniste, J., Cazenave, A., and Picot, N. (2019). Uncertainty in satellite estimates of global mean sealevel changes, trend and acceleration. *Earth System Science Data*, 11:1189–1202.

Aguzzi, M., Bonsignore, F., De Nigris, N., Morelli, M., Paccagnella, T., Romagnoli, C., and Unguendoli, S. (2016). *Stato del Litorale Emiliano- Romagnolo al 2012. Erosione e Interventi di Difesa*. Arpae Emilia-Romagna, Bologna, Italy.

Aguzzi, M., Costantino, R., De Nigris, N., Morelli, M., Romagnoli, C., Unguendoli, S., and Vecchi, E. (2020). *Stato del Litorale Emiliano-Romagnolo al 2018. Erosione e Interventi di Difesa*. Arpae Emilia-Romagna, Bologna, Italy.

Amorosi, A. M. L. C., Fusco, F., Pasini, G., and Fiorini, F. (1999). Glacio-eustatic control of continental-shallow marine cyclicity from late quaternary deposits of the south-eastern po plain (northern italy). *Quaternary Research*, 52:1–13.

Andersen, O. B. and Scharroo, R. (2011). Range and geophysical corrections in coastal regions: and implications for mean sea surface determination. In Vignudelli, S., Kostianoy, A., Cipollini, P., and Benveniste, J., editors, *Coastal Altimetry*, pages 103–146. Springer, Berlin, Germany.

Antonioli, F., Anzidei, M., Amorosi, A., Presti, V. L., Mastronuzzi, G., Deiana, G., Falco, G. D., Fontana, A., Fontolan, G., Lisco, S., Marsico, A., Moretti, M., Orrù, P. E., Sannino, G. M., Serpelloni, E., and Vecchio, A. (2017). Sea-level rise and potential drowning of the italian coastal plains: Flooding risk scenarios for 2100. *Quaternary Science Reviews*, 158:29–43.

Armaroli, C., Ciavola, P., Perini, L., Calabrese, L., Lorito, S., Valentini, A., and Masina, M. (2012). Critical storm thresholds for significant morphological changes and damage along the emilia-romagna coastline, italy. *Geomorphology*, 143-144:34–51.

ARPA (2002). *Stato Del Litorale Emiliano-Romagnolo All'anno 2000*. Arpa Emilia-Romagna, Bologna, Italy.

Bamber, J., Riva, R. E. M., Vermeersen, B. L. A., and Brocq, A. M. L. (2009). Reassessment of the potential sea-level rise from a collapse of the west antarctic ice sheet. *Science*, pages 901–903.

Bilbao, R. F., Gregory, J. M., and Nathaelle, B. (2015). Analysis of the regional pattern of sea level change due to ocean dynamics and density change for 1993–2099 in observations and cmip5 aogcms. *Climate Dynamics*, 45:2647–2666.

Billi, P., Salemi, E., Preciso, E., Ciavola, P., and Armaroli, C. (2017). Field measurement of bedload in a sand-bed river supplying a sediment starving beach. *Zeitschrift für Geomorphologie*, 61:207–223.

Bird, E. C. F. (1987). The modern prevalence of beach erosion. *Mar. Pollut.*, 18(4):151–157.

Birol, F., Léger, F., Passaro, M., Cazenave, A., Niño, F., Calafat, F., Shaw, A., Legeais, J.-F., Gouzenes, Y., Schwatke, C., and Benveniste, J. (2021). The x-track/ales multi-mission processing system: New advances in altimetry towards the coast. *Advances in Space Research*, 67(8):2398–2415.

Bonaduce, A., Pinardi, N., Oddo, P., Spada, G., and Larnicol, G. (2016). Sea-level variability in the mediterranean sea from altimetry and tide gauges. *Climate Dynamics*, 47:2851–2866.

Bondesan, M., Calderoni, G., and Cin, R. D. (1978). Il litorale delle province di ferrara e ravenna (alto adriatico); evoluzione morfologica e distribuzione dei sedimenti. *Bollettino della Società Geologica Italiana*, 97:247–287.

Bouin, M. N. and Wöppelmann, G. (2010). Land motion estimates from gps at tide gauges: a geophysical evaluation. *Geophysical Journal International*, 180(1):193–209.

Brown, G. S. (1977). The average impulse response of a rough surface and its applications. *IEEE Trans. Antennas Propag.*, 25:67–74.

Buendia, C., Bussi, G., Tuset, J., Vericat, D., Sabater, S., Palau, A., and Batalla, R. (2016). Effects of afforestation on runoff and sediment load in an upland mediterranean catchment. *Science of The Total Environment*, 540:144–157.

Calafat, F. M., Chambers, D. P., and Tsimplis, M. N. (2012). Mechanism of decadal sea level variability in the eastern north atlantic and the mediterranean sea. *Journal of Geophysical Research*, 117:C09022.

Calafat, F. M., Marcos, M., and Gomis, D. (2010). Mass contribution to the mediterranean sea level variability for the period 1948-2000. *Global and Planetary Change*, 73:193–201.

Carbognin, L., Gatto, P., and Mozzi, G. (1984). Case history no.9.15: Ravenna, italy. In Poland, J. F., editor, *Guidebook to Studies of Land Subsidence due to Ground-Water Withdrawal*, pages 291–305. UNESCO, Paris, France.

Carrere, L. and Lyard, F. (2003). Modeling the barotropic response of the global ocean to atmospheric wind and pressure forcing - comparison with observations. *Geophysical Research Letters*, 30(6):1275.

Cazenave, A., Bonnefond, P., Mercier, F., Dominh, K., and Toumazou, V. (2002). Sea level variations in the mediterranean sea and black sea from satellite altimetry and tide gauges. *Global and Planetary Change*, 34:59–86.

Cazenave, A., Cabanes, C., Dominh, K., and Mangiarotti, S. (2001). Recent sea level change in the mediterranean sea revealed by topex/poseidon satellite altimetry. *Geophysical Research Letters*, 28:1607–1610.

Chao, B. F., Wu, Y. H., and Li, Y. S. (2008). Impact of artificial reservoir water impoundment on global sea level. *Science*, 320:212–214.

Chelton, D. B. and McCabe, P. J. (1985). A review of satellite altimeter measurement of sea surface wind speed: With a proposed new algorithm. *Journal of Geophysical Research*, 90:4707–4720.

Chelton, D. B., Ries, J. C., Haines, B. J., Fu, L. L., and Callahan, P. S. (2001). Satellite altimetry. In Fu, L.-L. and Cazenave, A., editors, *Satellite Altimetry and Earth Sciences:*

A Handbook of Techniques and Applications, volume 69, pages 1–131. Int. Geophys. Series. Academic Press, San Diego, CA, USA.

Church, J. A., Clark, P. U., Cazenave, A., Gregory, J. M., Jevrejeva, S., Levermann, A., Merrifield, M. A., Milne, G. A., Nerem, R. S., Nunn, P. D., Payne, A., Pfeffer, W., Stammer, D., and Unnikrishnan, A. (2013). Sea level change. In Stocker, T. F., Qin, D., Plattner, G.-K., Tignor, M., Allen, S. K., Boschung, J., Nauels, A., Xia, Y., Bex, V., and Midgley, P. M., editors, *Climate Change 2013: The Physical Science Basis, Contribution of Working Group I to the Fifth Assessment Report of the Intergovernmental Panel on Climate Change*, pages 1139–1216. Cambridge University Press, Cambridge, UK.

Church, J. A., Roemmich, D., Domingues, C. M., Willis, J. K., White, N. J., Gilson, J. E., Stammer, D., Köhl, A., Chambers, D. P., Landerer, F. W., Marotzke, J., Gregory, J. M., Suzuki, T., Cazenave, A., and Traon, P.-Y. L. (2010). Ocean temperature and salinity contributions to global and regional sea-level change. In Church, J. A., Woodworth, P. L., Aarup, T., and Wilson, W. S., editors, *Understanding Sea-Level Rise and Variability*, chapter 6, pages 143–176. Wiley-Blackwell, Hoboken, NJ, USA.

Church, J. A. and White, N. J. (2011). Sea-level rise from the late 19th to the early 21st century. *Surveys in Geophysics*, 32(4-5):585–602.

Ciavola, P., Armaroli, C., Chiggiato, J., Valentini, A., Deserti, M., Perini, L., and Luciani, P. (2007). Impact of storms along the coastline of emilia-romagna: The morphological signature on the ravenna coastline (italy). *Journal of Coastal Research*, SI50:540–544.

Cipollini, P., Calafat, F. M., Jevrejeva, J., Melet, A., and Prandi, P. (2017). Monitoring sea level in the coastal zone with satellite altimetry and tide gauges. *Surveys in Geophysics*, 38:33–57.

Comerci, V. and Vittori, E. (2019). The need for a standardized methodology for quantitative assessment of natural and anthropogenic land subsidence: The agosta (italy) gas field case. *Remote Sensing*, 11(10):1178.

Correggiari, A., Cattaneo, A., and Trincardi, F. (2005). The modern po delta system: Lobe switching and asymmetric prodelta growth. *Marine Geology*, 222-223:49–74.

Couhert, A., Cerri, L., Legeais, J.-F., Ablain, M., Zelensky, N. P., Haines, B. J., Lemoine, F. G., Bertiger, W. I., Desai, S. D., and Otten, M. (2015). Towards the 1 mm/yr stability of the radial orbit error at regional scales. *Advances in Space Research*, 55:2–23.

Crespi, A., Brunetti, M., Lentini, G., and Maugeri, M. (2018). 1961–1990 high-resolution monthly precipitation climatologies for italy. *International Journal of Climatology*, 38(2):878–895.

Dangendorf, S., Hay, C., Calafat, F., Marcos, M., Piecuch, C. G., Berk, K., and Jürgen, J. (2019). Persistent acceleration in global sea-level rise since the 1960s. *Nature Climate Change*, 9:705–710.

Darby, S. E., Dunn, F. E., Nicholls, R. J., Rahman, M., and Riddy, L. (2015). A first look at the influence of anthropogenic climate change on the future delivery of fluvial sediment to the ganges–brahmaputra–meghna delta. *Environmental Sciences: Processes & Impacts*, 17:1587–1600.

Darby, S. E., Hackney, C. R., Leyland, J., Kummu, M., Lauri, H., Parsons, D. R., Best, J. L., Nicholas, A. P., and Aalto, R. (2016). Fluvial sediment supply to a mega-delta reduced by shifting tropical-cyclone activity. *Nature*, 539:276–279.

Dorandeu, J. and Traon, P.-Y. L. (1999). Effects of global mean atmospheric pressure variations on mean sea level changes from topex/poseidon. *J. Atmos. Oceanic Tech.*, 16:1279–1283.

Douglas, B. C. (1991). Global sea level rise. *Journal of Geophysical Research*, 96(C4):6981–6992.

Douglas, B. C. (1997). Global sea rise: A redetermination. *Surveys in Geophysics*, 18:279–292.

Douglas, B. C. (2001). Sea level change in the era of the recording tide gauge. In Douglas, B. C., Kearney, M., and Leatherman, S., editors, *Sea Level Rise: History and Consequences*, pages 37–64. Academic Press, San Diego, CA, USA.

Dunn, F. E., Darby, S. E., Nicholls, R. J., Cohen, S., Zarfl, C., and Fekete, B. M. (2019). Projections of declining fluvial sediment delivery to major deltas worldwide in response to climate change and anthropogenic stress. *Environmental Research Letters*, 14(8):084034.

Durack, P. J. and Wijffels, S. E. (2010). Fifty-year trends in global ocean salinities and their relationship to broad-scale warming. *Journal of Climate*, 23.

Elfrink, B., Christensen, E. D., and Broker, I. (1998). Coastal morphodynamics in subsiding areas. In Gambolati, G., editor, *CENAS: Coastline Evolution of the Upper Adriatic Sea Due to Sea Level Rise and Natural and Anthropogenic Land Subsidence*, pages 235–270. Kluwer Academic Publishers, Dordrecht, The Netherlands.

Farrell, W. E. and Clark, J. A. (1976). On postglacial sea level. *Geophysical Journal International*, 46(3):647–667.

Fedele, G., Mauri, E., Notarstefano, G., and Poulain, P.-M. (2021). Characterization of the atlantic water and levantine intermediate water in the mediterranean sea using argo float data. *Ocean Sci.*, 18:129–149.

Fenoglio-Marc, L. (2002). Long-term sea level change in the mediterranean sea from multi-satellite altimetry and tide gauges. *Phys. Chem. Earth*, 27:1419–1431.

Fernandes, M., Làzaro, C., Ablain, M., and Pires, N. (2015). Improved wet path delays for all esa and reference altimetric missions. *Remote Sensing of Environment*, 169:50–74.

Fox-Kemper, B., Hewitt, H. T., Xiao, C., Aðalgeirsdóttir, G., Drijfhout, S. S., Edwards, T. L., Golledge, N. R., Hemer, M., Kopp, R. E., Krinner, G., Mix, A., Notz, D., Nowicki, S., Nurhati, I. S., Ruiz, L., Sallée, J.-B., Slangen, A. B. A., and Yu, Y. (2021). Ocean, cryosphere and sea level change. In Masson-Delmotte, V., Zhai, P., Pirani, A., Connors, S. L., Péan, C., Berger, S., Caud, N., Chen, Y., Goldfarb, L., Gomis, M. I.,

Huang, M., Leitzell, K., Lonnoy, E., Matthews, J. B. R., Maycock, T. K., Waterfield, T., Yelekçi, O., Yu, R., and Zhou, B., editors, *Climate Change 2021: The Physical Science Basis. Contribution of Working Group I to the Sixth Assessment Report of the Intergovernmental Panel on Climate Change*, pages 1211–1362. Cambridge University Press, Cambridge, United Kingdom and New York, NY, USA.

Frederikse, T., Landered, F., Caron, L., Adhikari, S., Parkes, D., Humphrey, V. W., Dangendorf, S., Hogarth, P., Zanna, L., Cheng, L., and Wu, Y.-H. (2020). The causes of sea-level rise since 1900. *Nature*, 584:393–397.

Fukumori, I., Raghunath, R., and Fu, L. (1998). Nature of global large-scale sea level variability in relation to atmospheric forcing: A modeling study. *Journal of Geophysical Research*, 103:0148–0227.

Gaeta, M. G., Bonaldo, D., Samaras, A. G., Carniel, S., and Archetti, R. (2018). Coupled wave-2d hydrodynamics modeling at the reno river mouth (italy) under climate change scenarios. *Water*, 10(10):1380.

Galassi, G. and Spada, G. (2014). Sea-level rise in the mediterranean sea by 2050: Roles of terrestrial ice melt, steric effects and glacial isostatic adjustment. *Global and Planetary Change*, 123:55–66.

Gambolati, G., Teatini, P., Tomasi, L., and Gonella, M. (1999). Coastline regression of the romagna region, italy, due to sea level rise and natural and anthropogenic land subsidence. *Water Resources Research*, 35:163–184.

Gačić, M., Schroeder, K., Civitarese, G., Cosoli, S., Vetrano, A., and Borzelli, G. L. E. (2013). Salinity in the sicily channel corroborates the role of the adriatic-ionian bimodal oscillating system (bios) in shaping the decadal variability of the mediterranean overturning circulation. *Ocean Sci.*, 9:83–90.

Gregory, J. M., Griffies, S. M., Hughes, C. W., Lowe, J., Church, J. A., Fukimori, I., Gomez, N., Kopp, R., Landered, F., Cozannet, G. L., Ponte, R. M., Stammer, D., Tamisiea, M. E., and van de Wal, R. S. W. (2019). Concepts and terminology for

sea level: Mean, variability and change, both local and global. *Surveys in Geophysics*, 40:1251–1289.

Grodsky, S., Reul, N., Bentamy, A., Vandemark, D., and Guimbard, S. (2019). Eastern mediterranean salinification observed in satellite salinity from smap mission. *Journal of Marine Systems*, 198:103190.

Gröger, M. and Plag, H.-P. (1993). Estimations of a global sea level trend: limitations from the structure of the psmsl global sea level data set. *Global and Planetary Change*, 8(3):161–179.

Holgate, S. J., Matthews, A., Woodworth, P. L., Rickards, L. J., Tamisiea, M. E., Bradshaw, E., Foden, P. R., Gordon, K. M., Jevrejeva, S., and Pugh, J. (2013). New data systems and products at the permanent service for mean sea level. *Journal of Coastal Research*, 29(3):493–504.

IDROSER (1983). *Il Trasporto Solido Fluviale Nei Bacini Tributari Dell'Adriatico. Regione Emilia-Romagna, Piano Progettuale per la Difesa della Costa Emiliano-Romagnola*. Regione Emilia-Romagna.

IDROSER (1996). *Progetto di Piano per la Difesa dal Mare e la Riqualificazione Ambientale del Litorale della Regione Emilia-Romagna, Relazione Generale*. Regione Emilia-Romagna, Bologna, Italy.

Imel, D. (1994). Evaluation of the topex/poseidon dual-frequency ionosphere correction. *Journal of Geophysical Research*, 99.

Iona, A., Theodorou, A., Sofianos, S., Watelet, S., Troupin, C., and Beckers, J. M. (2018). Mediterranean sea climatic indices: Monitoring long-term variability and climate changes. *Earth Syst. Sci. Data*, 10:1829–1842.

IPCC (2021). Climate change 2021. In Masson-Delmotte, V., Zhai, P., Pirani, A., Connors, S., Péan, C., Berger, S., Caud, N., Chen, Y., Goldfarb, L., Gomis, M., Huang, M., Leitzell, K., Lonnoy, E., Matthews, J., Maycock, T., Waterfield, T., Yelekçi, O., Yu, R., , and Zhou, B., editors, *The Physical Science Basis. Contribution of Working Group*

I to the Sixth Assessment Report of the Intergovernmental Panel on Climate Change. Cambridge University Press, Cambridge, UK and New York, USA.

Ivins, E. R. (2009). Ice sheet stability and sea level. *Science*, 324:888–889.

Joughin, I. and Alley, R. B. (2011). Stability of the west antarctic ice sheet in a warming world. *Nature Geosci.*, 4(8):506–513.

Keihm, S. J., Janssen, M. A., and Ruf, C. S. (1995). Topex/poseidon microwave radiometer (tmr): Iii. wet tropospheric range correction algorithm and pre-launch error budget. *IEEE Trans. Geosci. Rem. Sens.*, 33:147–161.

King, M. A., Keshin, M., Whitehouse, P. L., Thomas, I. D., Milne, G., and Riva, R. E. M. (2012). Regional biases in absolute sea-level estimates from tide gauge data due to residual unmodeled vertical land movement. *Geophysical Research Letters*, 39:L14604.

Kopp, R. E., Kemp, A. C., Bittermann, K., Horton, B. P., Donnelly, J. P., Gehrels, W. R., Hay, C. C., Mitrovica, J. X., Morrow, E. D., and Rahmstorf, S. (2016). Temperature-driven global sea-level variability in the common era. *Proceedings of the National Academy of Sciences*, 113(11):E1434–E1441.

Lambeck, K., Rouby, H., Purcell, A., Sun, Y., and Sambridge, M. (2014). Sea level and global ice volumes from the last glacial maximum to the holocene. *Proceedings of the National Academy of Sciences*, 111(43):15296–15303.

Landerer, F. and Volkov, D. L. (2013). The anatomy of recent large sea level fluctuations in the mediterranean sea. *Geophysical Research Letters*, 40:553–557.

Larour, E., Ivins, E., and Adhikari, S. (2017). Should coastal planners have concern over where land ice is melting? *Science Advance*, 3(11).

Lascaratos, A., Williams, R. G., and Tragou, E. (1993). A mixed-layer study of the formation of levantine intermediate water. *Journal of Geophysical Research*, 98:14739–14749.

Le Traon, P., Nadal, F., and Ducet, N. (1998). An improved mapping method of multi-satellite altimeter data. *J. Atmos. Ocean. Technol.*, 15(2):522–534.

Le Traon, P. and Ogor, F. (1998). Ers-1/2 orbit improvement using t/p: The 2 cm challenge. *Journal of Geophysical Research*, 103:8045–8057.

Legeais, J.-F., Ablain, M., Zawadzki, L., Zuo, H., Johannessen, J. A., Scharffenberg, M. G., Fenoglio-Marc, L., Fernandes, M. J., Andersen, O. B., Rudenko, S., Cipollini, P., Quartly, G. D., Passaro, M., Cazenave, A., and Benveniste, J. (2018). An improved and homogeneous altimeter sea level record from the esa climate change initiative. *Earth System Science Data*, 10(1):281–301.

Lemke, P., Ren, J., Alley, R. B., Allison, I., Carrasco, J., Flato, G., Fujii, Y., Kaser, G., Mote, P., Thomas, R. H., and Zhang, T. (2007). Observations: Changes in snow, ice and frozen ground. In Solomon, S., Qin, D., Manning, M., Chen, Z., Marquis, M., Averyt, K. B., Tignor, M., and Miller, H. L., editors, *Climate Change 2007: The Physical Science Basis. Contribution of Working Group I to the Fourth Assessment Report of the Intergovernmental Panel on Climate Change*, pages 337–383. Cambridge University Press, Cambridge, United Kingdom and New York, NY, USA.

Levitus, S., Antonov, J. I., Boyer, T. P., Baranova, O. K., Garcia, H. E., Locarnini, R. A., Mishonov, A. V., Reagan, J. R., Seidov, D., Yarosh, E. S., and Zweng, M. M. (2012). World ocean heat content and thermosteric sea level change (0–2000 m), 1955–2010. *Geophysical Research Letters*, 39(10).

Llorens, P., Queralt, I., Plana, F., and Gallart, F. (1997). Studying solute and particulate sediment transfer in a small mediterranean mountainous catchment subject to land abandonment. *Earth Surface Processes and Landforms*, 22:1027–1035.

Lorbacher, K., Marsland, S. J., Church, J. A., Griffies, S. M., and Stammer, D. (2012). Rapid barotrophic sea-level rise from ice-sheet melting scenarios. *Journal of Geophysical Research*, 117:c06003.

Lorito, S., Calabrese, L., Perini, L., and Cibin, U. (2010). Uso del suolo della costa. In Perini, L. and Calabrese, L., editors, *Il Sistema Mare-Costa dell'Emilia-Romagna*, pages 109–118. Pendragon, Bologna, Italy.

Malanotte-Rizzoli, P., Manca, B. B., d'Alcalà, M. R., Theocharis, A., Brenner, S., Budillon, G., and Ozsoy, E. (1999). The eastern mediterranean in the 80s and in the 90s: The big transition in the intermediate and deep circulations. *Dyn. Atmos. Oceans*, 29:365–395.

Malanotte-Rizzoli, P., Manca, B. B., D'Alcalà, R., Theocharis, A., Bergamasco, A., Bregant, D., Budillon, G., Civitarese, G., Georgopoulos, D., Michelato, A., Sansone, E., Scarazzato, P., and Souvermezoglou, E. (1997). A synthesis of the ionian sea hydrography, circulation and water mass pathways during poem-phase i. *Progress in Oceanography*, 39:153–204.

Marcos, M., Wöppelmann, G., Calafat, F. M., Vacchi, M., and Amores, A. (2023). Chapter 5 - mediterranean sea level. In Schroeder, K. and Chiggiato, J., editors, *Oceanography of the Mediterranean Sea*, pages 125–159. Elsevier.

Marsico, A., Lisco, S., Presti, V. L., Antonioli, F., Amorosi, A., Anzidei, M., Deiana, G., Falco, G. D., Fontana, A., Fontolan, G., Moretti, M., Orrù, P. E., Serpelloni, E., Vecchio, G. M. S. A., and Mastronuzzi, G. (2017). Flooding scenario for four italian coastal plains using three relative sea level rise models. *Journal of Maps*, 13:961–967.

Marullo, S., Artale, V., and Santoleri, R. (2011). The sst multidecadal variability in the atlantic-mediterranean region and its relation to amo. *Journal of Climate*, 24:4385–4401.

Matthäus, W. (1972). On the history of recording tide gauges. *Proceedings of the Royal Society of Edinburgh, Section B: Biological Sciences*, 72:26–34.

Mauri, E., Sitz, L., Gerin, R., Poulain, P.-M., Hayes, D., and Gildor, H. (2019). On the variability of the circulation and water mass properties in the eastern levantine sea between september 2016–august 2017. *Water*, 11:1741.

Meier, M. F., Dyurgerov, M. B., Rick, U. K., O'Neel, S., Pfeffer, W. T., Anderson, R. S., Anderson, S. P., and Glazovsky, A. F. (2007). Glaciers dominate eustatic sea-level rise in the 21st century. *Science*, 317(5841):1064–1067.

Meli, M., Camargo, C. M. L., Olivieri, M., Slangen, A. B. A., and Romagnoli, C. (2023). Sea–level trend variability in the mediterranean during the 1993–2019 period. *Frontiers in Marine Science*, 10:1150488.

Meli, M., Olivieri, M., and Romagnoli, C. (2021). Sea-level change along the emilia-romagna coast from tide gauge and satellite altimetry. *Remote Sensing*, 13:97.

Meli, M. and Romagnoli, C. (2022). Evidence and implications of hydrological and climatic change in the reno and lamone river basins and related coastal areas (emilia-romagna, northern italy) over the last century. *Water*, 14:2650.

Mellor, G. L. and Ezer, T. (1995). Sea level variations induced by heating and cooling: An evaluation of the boussinesq approximation in ocean models. *Journal of Geophysical Research: Oceans*, 100(C10):20565–20577.

Menemenlis, D., Fukumori, I., and Lee, T. (2007). Atlantic to mediterranean sea level difference driven by winds near gibraltar strait. *Journal of Physical Oceanography*, 37:359–376.

Menna, M., Gerin, R., Notarstefano, G., Mauri, E., Bussani, A., Pacciaroni, M., and Poulain, P.-M. (2021). On the circulation and thermohaline properties of the eastern mediterranean sea. *Frontiers in Marine Science*, 8:671469.

Menna, M., Poulain, P.-M., Zodiatis, G., and Gertman, I. (2012). On the surface circulation of the levantine sub-basin derived from lagrangian drifters and satellite altimetry data. *Deep-Sea Research: Part I*, 65:46–58.

Menna, M., Reyes-Suarez, N. C., Civitarese, G., Gačić, M., Poulain, P.-M., and Rubino, A. (2019). Decadal variations of circulation in the central mediterranean and its interactions with the mesoscale gyres. *Deep-Sea Research: Part II Top. Stud. Oceanogr.*, 164:14–24.

Meyssignac, B., Piecuch, C. G., Merchant, C. J., Racault, M.-F., Palanisamy, H., MacIntosh, C., Sathyendranath, S., and Brewin, R. (2017). Causes of the regional variability in observed sea level, sea surface temperature and ocean colour over the period 1993-2011. *Surveys in Geophysics*, 38(1):187–215.

Milliman, J. D. (2001). Delivery and fate of fluvial water and sediment to the sea: A marine geologist's view of european rivers. *Scientia Marina*, 65:121–132.

Milliman, J. D. and Syvitski, J. P. M. (1992). Geomorphic/tectonic control of sediment discharge to the ocean: The importance of small mountainous rivers. *The Journal of Geology*, 100(5):525–544.

Mitchum, G. T. (2000). An improved calibration of satellite altimetric heights using tide gauge sea levels with adjustment for land motion. *Marine Geodesy*, 23:145–166.

Mitrovica, J., Hay, C., Kopp, R., Harig, C., and Latychev, K. (2018). Quantifying the sensitivity of sea level change in coastal localities to the geometry of polar ice mass flux. *Journal of Climate*, 31(9).

Mohamed, B., Abdallah, A. M., El-Din, K. A., Nagy, H., and Shaltout, M. (2019). Interannual variability and trends of sea level and sea surface temperature in the mediterranean sea over the last 25 years. *Pure and Applied Geophysics*, 176:3787–3810.

Mohamed, B. and Skliris, N. (2022). Steric and atmospheric contributions to interannual sea level variability in the eastern mediterranean sea over 1993-2019. *Oceanologia*, 64:50–62.

Nerem, R. S., Beckley, B. D., Fasullo, J. T., Hamlington, B. D., Masters, D., and Mitchum, G. T. (2018). Climate-change–driven accelerated sea-level rise detected in the altimeter era. *Proceedings of the National Academy of Sciences*, 115(9):2022–2025.

Nerem, S. and Mitchum, G. (2001). Observations of sea level change from satellite altimetry. In Douglas, B. K. M. and Leatherman, S., editors, *Sea Level Rise: History and Consequences*, pages 121–164. Academic Press, San Diego, CA, USA.

Neumann, B., Vafeidis, A. T., Zimmermann, J., and Nicholls, R. J. (2015). Future coastal population growth and exposure to sea-level rise and coastal flooding - a global assessment. *PLoS ONE*, 10(3):e0118571.

Ngo-Duc, T., Laval, K., Polcher, J., Lombard, A., and Cazenave, A. (2005). Effects of

land water storage on global mean sea level over the past half century. *Geophysical Research Letters*, 32(9).

Nicholls, R., Wong, P. P., Burkett, V., Codignotto, J., Hay, J., McLean, R., Ragoonaden, S., and Woodroffe, C. D. (2007). Coastal systems and low-lying areas. In Parry, M., Canziani, O., Palutikof, J., Van Der Linden, P., and Hanson, C., editors, *Climate Change 2007: Impacts, Adaptation and Vulnerability. Contribution of Working Group II to the Fourth Assessment Report of the Intergovernmental Panel on Climate Change*, pages 315–357. Cambridge University Press, Cambridge, UK.

Nicholls, R. J., Marinova, N., Lowe, J. A., Brown, S., Vellinga, P., de Gusmão, D., Hinkel, J., and Tol, R. S. J. (2011). Sea-level rise and its possible impacts given a 'beyond 4°c world' in the twenty-first century. *Philosophical Transactions of the Royal Society A: Mathematical, Physical and Engineering Sciences*, 369(1934):161–181.

Oppenheimer, M., Glavovic, B., Hinkel, J., van de Wal, R., Magnan, A., Abd-Elgawad, A., Cai, R., Cifuentes-Jara, M., DeConto, R., Ghosh, T., Hay, J., Isla, F., Marzeion, B., Meyssignac, B., and Sebesvari, Z. (2019). Sea level rise and implications for low-lying islands, coasts and communities. In Portner, H.-O., Roberts, D. C., Masson-Delmotte, V., Zhai, P., Tignor, M., Poloczanska, E., Mintenbeck, K., Alegria, A., Nicolai, M., Okem, A., Petzold, J., Rama, B., and Weyer, N., editors, *IPCC Special Report on the Ocean and Cryosphere in a Changing Climate*, pages 321–445. Cambridge University Press, Cambridge, UK and New York, USA.

Palmer, M. D., Gregory, J. M., Bagge, M., Calvert, D., Hagedoorn, J. M., Howard, T., Klemann, V., Lowe, J. A., Roberts, C. D., Slangen, A. B. A., and Spada, G. (2020). Exploring the drivers of global and local sea-level change over the 21st century and beyond. *Earth's Future*, 8(9):e2019EF001413.

Passaro, M., Cipollini, P., Vignudelli, S., Quartly, G., and Snaith, H. (2014). Ales: a multi-mission subwaveform retracker for coastal and open ocean altimetry. *Remote Sensing of Environment*, 145:173–189.

Pastor, F., Valiente, J. A., and Palau, J. L. (2018). Sea surface temperature in the

mediterranean: Trends and spatial patterns (1982–2016). *Pure and Applied Geophysics*, 175:4017–4029.

Peltier, W., Argus, D., and Drummond, R. (2015). Space geodesy constrains ice age terminal deglaciation: The global ice-6g (vm5a) model. *120*, 1:450–487.

Perini, L., Calabrese, L., Luciani, P., Olivieri, M., Galassi, G., and Spada, G. (2017). Sea-level rise along the emilia-romagna coast (northern italy) in 2100: Scenarios and impacts. *Natural Hazards and Earth System Science*, 17:2271–2287.

Pinardi, N., Bonaduce, A., Navarra, A., Dobricic, S., and Oddo, P. (2014). The mean sea level equation and its application to the mediterranean sea. *Journal of Climate*, 27:442–447.

Pinardi, N., Korres, G., Lascaratos, A., Roussenov, V., and Stanev, E. (1997). Numerical simulation of the interannual variability of the mediterranean sea upper ocean circulation. *Geophysical Research Letters*, 24:425–428.

Pinardi, N., Zavatarelli, M., Adani, M., Coppini, G., Fratianni, C., Oddo, P., Simoncelli, S., Tonani, M., Lyubartsev, V., Dobricic, S., and Bonaduce, A. (2015). Mediterranean sea large-scale low-frequency ocean variability and water mass formation rates from 1987 to 2007: A retrospective analysis. *Progress in Oceanography*, 132:318–332.

Pirazzoli, P. A. (1986). Secular trends of relative sea-level (rsl) changes indicated by tide-gauge records. *Journal of Coastal Research*, s11:1–26.

Ponte, R. M. and Gaspar, P. (1999). Regional analysis of the inverted barometer effect over the global ocean using topex/poseidon data and model results. *Journal of Geophysical Research*, 104(15):587–602.

Poulain, P., Centurioni, L., Özgökmen, T., Tarry, D., Pascual, A., Ruiz, S., Mauri, E., Menna, M., and Notarstefano, G. (2021). On the structure and kinematics of an algerian eddy in the southwestern mediterranean sea. *Remote Sensing*, 13:3039.

Preti, M., De Nigris, N., Morelli, M., Monti, M., Bonsignore, F., and Aguzzi, M. (2008).

Stato del Litorale Emiliano-Romagnolo All'anno 2007 e Piano Decennale di Gestione. Arpa Emilia-Romagna, Bologna, Italy.

PSMSL (2022). Tide gauge data. *http://www.psmsl.org/data/obtaining/*. Last accessed on Dec 29, 2022.

Pugh, D. and Woodworth, P. L. (2014). *Understanding Tides, Surges, Tsunamis and Mean Sea-Level Changes*. Cambridge University Press, Cambridge, UK.

Rhein, M., Rintoul, S. R., Aoki, S., Campos, E., Chambers, D., Feely, R., Gulev, S., Johnson, G. C., Josey, S. A., Kostianoy, A., Mauritzen, C., Roemmich, D., Talley, L. D., and Wang, F. (2013). Observations: Ocean. In Stocker, T., Qin, D., Plattner, G.-K., Tignor, M., Allen, S., Boschung, J., Nauels, A., Xia, Y., Bex, V., and Midgley, P., editors, *Climate Change 2013: The Physical Science Basis. Contribution of Working Group I to the Fifth Assessment Report of the Intergovernmental Panel on Climate Change*. Cambridge University Press, Cambridge, United Kingdom and New York, NY, USA.

Rignot, E., Velicogna, I., van den Broeke, M. R., Monaghan, A., and Lenaerts, J. (2011). Acceleration of the contribution of the greenland and antarctic ice sheets to sea level rise. *Geophysical Research Letters*, 38:L05503.

Robinson, A. R., Leslie, W. G., Theocharis, A., and Lscaratos, A. (2001). Mediterranean sea circulation. In Steele, J. H., editor, *Encyclopedia of Ocean Sciences*, pages 1689–1705. Academic Press.

Romanou, A., Tselioudis, G., Zerefos, C. S., Clayson, C.-A., Curry, A., and Andersson, A. (2010). Evaporation-precipitation variability over the mediterranean and the black seas from satellite and reanalysis estimates. *Journal of Climate*, 23:5268–5287.

Rudenko, S., Otten, M., Visser, P., Scharroo, R., Schone, T., and Esselborn, S. (2012). New improved orbit solutions for the ers-1 and ers-2 satellites. *Advances in Space Research*, 49:1229–1244.

Santamarìa-Gòmez, A., Gravelle, M., Collilieux, X., Guichard, M., Mìguez, B. M., Tiphaneau, P., and Wöppelmann, G. (2012). Mitigating the effects of vertical land

motion in tide gauge records using a state-of-the-art gps velocity field. *Global and Planetary Change*, 98-99:6–17.

Schroeder, K., Chiggiato, J., Josey, S. A., Borghini, M., Aracri, S., and Sparnocchia, S. (2017). Rapid response to climate change in a marginal sea. *Scientific Report*, 7:4065.

Simeoni, U., Tessari, U., Corbau, C., Tosatto, O., Polo, P., and Teatini, P. (2017). Impact of land subsidence due to residual gas production on surficial infrastructures: The dosso degli angeli field study (ravenna, northern italy). *Engineering Geology*, 229:1–12.

Skliris, N., Zika, J. D., Herold, L., Josey, S. A., and Marsh, R. (2018). Mediterranean sea water budget long-term trend inferred from salinity observations. *Climate Dynamics*, 51:2857–2876.

Slangen, A. B. A., Church, J. A., Agosta, C., Fettweis, X., Marzeion, B., and Richter, K. (2016). Anthropogenic forcing dominates global mean sea-level rise since 1970. *Nature Climate Change*, 6:701–705.

Slangen, A. B. A., Meyssignac, B., Agosta, C., Champollion, N., Church, J. A., Fettweis, X., Ligtenberg, S. R. M., Marzeion, B., Melet, A., Palmer, M. D., Richter, K., Roberts, C. D., and Spada, G. (2017). Evaluating model simulations of twentieth-century sea level rise. part i: Global mean sea level change. *Journal of Climate*, 30(21):8539–8563.

Stammer, D., Cazenave, A., Ponte, R. M., and Tamisiea, M. E. (2013). Causes for contemporary regional sea level changes. In Carlson, C. and Giovannoni, S. J., editors, *Annual Review of Marine Science*, pages 21–46. Annual Reviews, Palo Alto, CA, USA.

Storto, A., Bonaduce, A., Feng, X., and Yang, C. (2019). Steric sea level changes from ocean reanalyses at global and regional scales. *Water*, 11:1987.

Syvitski, J. P. M. and Kettner, A. (2011). Sediment flux and the anthropocene. *Philosophical Transactions of the Royal Society A: Mathematical, Physical and Engineering Sciences*, 369(1938):957–975.

Syvitski, J. P. M., Kettner, A. J., Overeem, I., Hutton, E. W. H., Hannon, M. T., Braken-

ridge, G. R., Day, J., Vörösmarty, C., Saito, Y., Giosan, L., and Nicholls, R. J. (2009). Sinking deltas due to human activities. *Nature Geoscience*, 2:681–686.

Syvitski, J. P. M., Vörösmarty, C. J., Kettner, A. J., and Green, P. (2005). Impact of humans on the flux of terrestrial sediment to the global coastal ocean. *Science*, 308(5720):376–380.

Tanhua, T., Hainbucher, D., Schroeder, K., Cardin, V., Álvarez, M., and Civitarese, G. (2013). The mediterranean sea system: a review and an introduction to the special issue. *Ocean Sci.*, 9:789–803.

Tapley, B. D., Ries, J. C., Davis, G. W., Eanes, R. J., Schutz, B. E., Shum, C. K., Watkins, M. M., Marshall, J. A., Nerem, R. S., Putney, B. H., Klosko, S. M., Luthcke, S. B., Pavlis, D., Williamson, R. G., and Zelensky, N. P. (1994). Precision orbit determination for topex/poseidon. *Journal of Geophysical Research*, 99.

Teatini, P., Ferronato, M., Gambolati, G., Bertoni, W., and Gonella, M. (2005). A century of land subsidence in ravenna, italy. *Environmental Geology*, 47:831–846.

Tessler, Z. T., Vörösmarty, C. J., Grossberg, M., Gladkova, I., Aizenman, H., Syvitski, J. P. M., and Foufoula-Georgiou, E. (2015). Profiling risk and sustainability in coastal deltas of the world. *Science*, 349(6248):638–643.

Toreti, A., Fioravanti, G., Perconti, W., and Desiato, F. (2009). Annual and seasonal precipitation over italy from 1961 to 2006. *International Journal of Climatology*, 29(13):1976–1987.

Tran, N., Labroue, S., Philipps, S., Bronner, E., and Picot, N. (2010). Overview and update of the sea state bias corrections for the jason-2, jason-1 and topex missions. *Marine Geodesy*, 33.

Tsimplis, M., Calafat, F. M., Marcos, M., Jordà, G., Gomis, D., Fenoglio-Marc, L., Struglia, M. V., Josey, S., and Chambers, D. P. (2013). The effect of the nao on sea level and on mass changes in the mediterranean sea. *Journal of Geophysical Research: Oceans*, 118:944–952.

Tsimplis, M. N. and Baker, T. F. (2000). Sea level drop in the mediterranean sea: An indicator of deep water salinity and temperature changes? *Geophysical Research Letters*, 27:1731–1734.

Tsimplis, M. N. and Josey, S. A. (2001). Forcing of the mediterranean sea by atmospheric oscillations over the north atlantic. *Geophysical Research Letters*, 28:803–806.

Velicogna, I. (2009). Increasing rates of ice mass loss from the greenland and antarctic ice sheets revealed by grace. *Geophys. Res. Lett.*, 36:L19503.

Vellinga, P. and Leatherman, S. P. (1989). Sea level rise, consequences and policies. *Clim. Change*, 15(1-2):175–189.

Vera, J., Criado-Aldeanueva, F., García-Lafuente, J., and Soto-Navarro, F. J. (2009). A new insight on the decreasing sea level trend over the ionian basin in the last decades. *Global and Planetary Change*, 68:232–235.

Vignudelli, S., Florence, B., Benveniste, J., Fu, L.-L., Picot, N., Raynal, M., and Roinard, H. (2019). Satellite altimetry measurements of sea level in the coastal zone. *Surveys in Geophysics*, 40:1319–1349.

Vigo, I., Garcia, D., and Chao, B. F. (2005). Change of sea level trend in the mediterranean and black seas. *J. Mar. Res.*, 63:1085–1100.

Vigo, M. I., Sánchez-Reales, J. M., Trottini, M., and Chao, B. F. (2011). Mediterranean sea level variations: Analysis of the satellite altimetric data, 1992–2008. *Journal of Geodynamics*, 52:271–278.

Von Schuckmann, K., Traon, P. Y. L., Smith, N., Pascual, A., Djavidnia, S., Gattuso, J. P., Grégoire, M., Nolan, G., Aaboe, S., Aguiar, E., and et al. (2019). Copernicus marine service ocean state report. *J. Oper. Oceanogr.*, 12:s1–s123.

Vörösmarty, C., Meybeck, M., Fekete, B., Sharma, K., Green, P., and Syvitski, J. P. M. (2003). Anthropogenic sediment retention: major global impact from registered river impoundments. *Global and Planetary Change*, 39(1):169–190.

Wada, Y., van Beek, L. P. H., Weiland, F. C. S., Chao, B. F., Wu, Y. H., and Bierkens, M. F. P. (2012). Past and future contribution of global groundwater depletion to sea-level rise. *Geophysical Research Letters*, 39:L09402.

Walling, D. E. (2006). Human impact on land–ocean sediment transfer by the world's rivers. *Geomorphology*, 79(3):192–216.

Weston, N. B. (2014). Declining sediments and rising seas: an unfortunate convergence for tidal wetlands. *Estuaries and Coasts*, 37:1–23.

Whitehouse, P. L. (2018). Glacial isostatic adjustment modelling: historical perspectives, recent advances, and future directions. *Earth Surface Dynamics*, 6(2):401–429.

Wild, M. (2009). Global dimming and brightening: A review. *J. Geophys. Res.*, 114:D00D16.

Wild, M., Gilgen, H., Roesch, A., Ohmura, A., Long, C., Dutton, E., Forgan, B., Kallis, A., Russak, V., and Tsvetkov, A. (2005). From dimming to brightening: Decadal changes in solar radiation at earth's surface. *Science*, 308:847–850.

Woodworth, P., Gehrels, W., and Nerem, R. (2011). Nineteenth and twentieth century changes in sea level. *Oceanography*, 24(2):80–93.

Woodworth, P. L., Wöppelmann, G., Gravelle, M., Marcos, M., and Bingley, R. M. (2017). Why we must tie satellite positioning to tide gauge data. *EOS*, 98:13–15.

Wöppelmann, G., Cozannet, G. L., de Michele, M., Raucoules, D., Cazenave, A., Garcin, M., Hanson, S., Marcos, M., and Santamaria-Gomez, A. (2013). Is land subsidence increasing the exposure to sea level rise in alexandria, egypt? *Geophysical Research Letters*, 40:2953–2957.

Wöppelmann, G., Pouvreau, N., Coulomb, A., Simon, B., and Woodworth, P. (2008). Tide gauge datum continuity at brest since 1711: France's longest sea-level record. *Geophysical Research Letters*, 35:L22605.

Wöppelmann, G. and Marcos, M. (2016). Vertical land motion as a key to understanding sea level change and variability. *Reviews of Geophysics*, 54(1):64–92.

Zarfl, C., Lumsdon, A. E., Berlekamp, J., Tydecks, L., and Tockner, K. (2015). A global boom in hydropower dam construction. *Aquatic Sciences*, 77:161–170.

Zemp, M., Frey, H., Gärtner-Roer, I., Nussbaumer, S. U., Hoelzle, M., Paul, F., W. Haeberli, W., Denzinger, F., Ahlstrøm, A., Andreas, P., Anderson, B., and et al. (2015). Historically unprecedented global glacier decline in the early 21st century. *Journal of Glaciology*, 61(228):745–762.

Zerbini, S., Plag, H.-P., Baker, T., Becker, M., Billiris, H., Burki, B., Kahle, H.-G., Marsone, I., Pezzoli, L., Richter, B., Romagnoli, C., Sztobryn, M., Tomasi, P., Veis, M. T. G., and Verrone, G. (1996). Sea level in the mediterranean: a first step towards separating crustal movements and absolute sea-level variations. *Global and Planetary Change*, 14(1):1–48.

Zerbini, S., Raicich, F., Prati, C. M., Bruni, S., Conte, S. D., Errico, M., and Santi, E. (2017). Sealevel change in the northern mediterranean sea from long-period tide gauge time series. *Earth Science Review*, 167:72–87.

Zerbini, S., Richter, B., Rocca, F., van Dam, T., and Matonti, F. (2007). A combination of space and terrestrial geodetic techniques to monitor land subsidence. case study, the south eastern po plain, italy. *Journal of Geophysical Research*, 112:B05401.